



Electronic-Textile (E-Textile) Electrodes for use in Bioelectrical Impedance Analysis

AUTHOR(S)

Irini Logothetis

PUBLICATION DATE

01-12-2020

HANDLE

[10779/DRO/DU:23918541.v1](https://hdl.handle.net/10779/DRO/DU:23918541.v1)

Downloaded from Deakin University's Figshare repository

Deakin University CRICOS Provider Code: 00113B

Electronic-Textile (E-Textile) Electrodes for use in Bioelectrical Impedance Analysis

by

Irini (Rena) Logothetis
BCompSc(Hons), BEng (Elect.)

Submitted in fulfilment of the requirements for the degree of
Doctor of Philosophy

Institute of Frontier Materials
Deakin University
December, 2020

*Dedicated to
my late father Angelostamatis Logothesis,
and my mother Chrissie Logothesis.*



DEAKIN UNIVERSITY CANDIDATE DECLARATION

I certify the following about the thesis entitled (10 word maximum)

Electronic Textile (E-Textile) Electrodes for use in Bioelectrical Impedance Analysis

submitted for the degree of Doctor of Philosophy

- a. I am the creator of all or part of the whole work(s) (including content and layout) and that where reference is made to the work of others, due acknowledgment is given.
- b. The work(s) are not in any way a violation or infringement of any copyright, trademark, patent, or other rights whatsoever of any person.
- c. That if the work(s) have been commissioned, sponsored or supported by any organisation, I have fulfilled all of the obligations required by such contract or agreement.
- d. That any material in the thesis which has been accepted for a degree or diploma by any university or institution is identified in the text.
- e. All research integrity requirements have been complied with.

'I certify that I am the student named below and that the information provided in the form is correct'

Full Name: Irini Logothetis

Signed:

Signature Redacted by Library

Date: 30 October 2020



**DEAKIN UNIVERSITY
ACCESS TO THESIS - A**

I am the author of the thesis entitled

Electronic Textile (E-Textile) Electrodes for use in Bioelectrical Impedance Analysis

submitted for the degree of

This thesis may be made available for consultation, loan and limited copying in accordance with the Copyright Act 1968.

'I certify that I am the student named below and that the information provided in the form is correct'

Full Name: Irini Logothetis

(Please Print)

Signed:

Signature Redacted by Library

Date: 05 June 2021

AUTHORSHIP STATEMENT

1. Details of publication and executive author

| | | |
|---|--|------------------------------------|
| Title of Publication | | Publication details |
| Embroidered electrodes for bioelectrical impedance analysis: impact of surface area and stitch parameters | | Measurement Science and Technology |
| Name of executive author | School/Institute/Division if based at Deakin; Organisation and address if non-Deakin | Email or phone |
| Irini Logothetis | RMIT University – 264 Plenty Rd Bundoora Melbourne VIC AUS | 0403 560 034 |

2. Inclusion of publication in a thesis

| | | |
|---|-----|---|
| Is it intended to include this publication in a higher degree by research (HDR) thesis? | Yes | If Yes, please complete Section 3 If No, go straight to Section 4. |
|---|-----|---|

3. HDR thesis author's declaration

| | | |
|--|--|--|
| Name of HDR thesis author if different from above. (If the same, write "as above") | School/Institute/Division if based at Deakin | Thesis title |
| As above. | IFM | E-Textile Electrodes for use in Bioelectrical Impedance Analysis |
| If there are multiple authors, give a full description of HDR thesis author's contribution to the publication (for example, how much did you contribute to the conception of the project, the design of methodology or experimental protocol, data collection, analysis, drafting the manuscript, revising it critically for important intellectual content, etc.) | | |
| Contributed to the concept of the study. Completed all experimental design, data collection, results analysis, synthesis of research findings and writing the entire paper. | | |
| <i>I declare that the above is an accurate description of my contribution to this paper, and the contributions of other authors are as described below.</i> | Signature and date | Signature Redacted by Library |

4. Description of all author contributions

| | |
|--------------------------------|--|
| Name and affiliation of author | Contribution(s) (for example, conception of the project, design of methodology or experimental protocol, data collection, analysis, drafting the manuscript, revising it critically for important intellectual content, etc.) |
| Raul Fernandez-Garcia | Contributed to the concept of the project, provided references to assist me in the intellectual content, reviewed and provided feedback to the manuscript. |
| Olga Troynikov | Reviewed and provided feedback to the manuscript. |
| Peter Dabnichki | Reviewed and provided feedback to the manuscript. |
| Elena Pirogova | Reviewed and provided feedback to the manuscript. |
| Ignacio Gil | Contributed to the concept of the project, provided advice on the methodology and experimental protocol to set the basis for the research. Assisted with the analysis and interpretation. Reviewed and provided structure/grammatical feedback to the manuscript. Co-ordinated this study. |

5. Author Declarations

I agree to be named as one of the authors of this work, and confirm:

- i. that I have met the authorship criteria set out in the Deakin University Research Conduct Policy,
- ii. that there are no other authors according to these criteria,
- iii. that the description in Section 4 of my contribution(s) to this publication is accurate,
- iv. that the data on which these findings are based are stored as set out in Section 7 below.

If this work is to form part of an HDR thesis as described in Sections 2 and 3, I further

- v. consent to the incorporation of the publication into the candidate's HDR thesis submitted to Deakin University and, if the higher degree is awarded, the subsequent publication of the thesis by the university (subject to relevant Copyright provisions).

| Name of author | Signature* | Date |
|-----------------------|------------|--------------------------------|
| Raul Fernandez-Garcia | | 18 th November 2020 |
| Olga Troynikov | | |
| Peter Dabnichki | | |
| Elena Pirogova | | |
| Ignacio Gil | | 17 th November 2020 |

Signatures Redacted
by Library

***Note from institute director: I have sought signatures from Olga, Peter and Elena but received no response. In light of the signatures received from the other co-authors and conversations with Deakin supervisors, IFM HDR co-ordinator and Irini, I am satisfied that the author declaration is appropriate and submit my signature below:**

Signature Redacted by Library

Matthew Barnett, Dec 15, 2020

6. Other contributor declarations

I agree to be named as a non-author contributor to this work.

| Name and affiliation of contributor | Contribution | Signature* and date |
|-------------------------------------|--------------|---------------------|
| | | |
| | | |

* If an author or contributor is unavailable or otherwise unable to sign the statement of authorship, the Head of Academic Unit may sign on their behalf, noting the reason for their unavailability, provided there is no evidence to suggest that the person would object to being named as author

7. Data storage

The original data for this project are stored in the following locations. (The locations must be within an appropriate institutional setting. If the executive author is a Deakin staff member and data are stored outside Deakin University, permission for this must be given by the Head of Academic Unit within which the executive author is based.)

| Data format | Storage Location | Date lodged | Name of custodian if other than the executive author |
|-------------|------------------|-------------|--|
| Excel | Figshare | 06.11.20 | |
| Docx | Figshare | 06.11.20 | |

This form must be retained by the executive author, within the school or institute in which they are based.

If the publication is to be included as part of an HDR thesis, a copy of this form must be included in the thesis with the publication.

Digital Thesis Copyright and Access

Deakin University Library



Before completing this form please read the information in the Guidelines

1. Your details

| | | |
|--|--|----------------|
| Family Name: Logothetis | | Title: Ms |
| Given name(s): Irini | | |
| Postal address: 38A Dundas St, Thornbury VIC | | |
| Australia | | Postcode: 3071 |
| Phone: 0403 560 034 | | Fax: |
| Email: rlogothetis82@gmail.com | | |

2. The thesis

| | |
|--|---|
| Faculty: Science, Engineering and Built Environment | School: Institute of Frontier Materials |
| Full name of degree: Doctor of Philosophy | |
| Title of thesis: Electronic Textile (E-Textile) Electrodes for use in Bioelectrical Impedance Analysis | Year submitted: 2020 |

3. Copyright

I have already declared in my thesis that:

- I am the creator of all or part of the whole work(s) (including content and layout).
- The work(s) are not in any way a violation or infringement of any copyright, trademark, patent, or other rights whatsoever of any person.
- That if the work(s) have been commissioned, sponsored or supported by any organisation, that I have fulfilled all of the obligations required by such contract or agreement.

Your copyright

You retain any rights that you had prior to depositing your thesis. (You are free to publish this work or works elsewhere in their present or future versions). You grant to Deakin University Institutional Repository, Deakin Research Online a non-exclusive license to store and/or communicate your thesis on the terms outlined in 5 below.

Other people's copyright

Section(s) of my thesis contain substantial part(s) of third party copyright material¹:

Yes No

I warrant that I have permission to communicate this material online²:

Yes No

¹ Substantial parts of works where you do not own the copyright cannot be communicated online without the permission of the copyright owner. See <http://www.deakin.edu.au/library/opal>

² You have either written permission or permission is given on a website or as part of a purchase agreement.

4. Access to your thesis

Deakin University will make your thesis available online for world-wide access unless you apply to restrict it in one of the following ways.

Restrict online access to the thesis for a defined period of time: ____ months from ____/____/____.

Restrict online access to administrators only, and provide access through a physical version provided by the Library.

Justification for restricting open access must be stated.

Unless you specify otherwise all access will be in accordance with the Copyright Act 1968.

See the [Creative Commons](#) licences for additional options

(<http://creativecommons.org.au/materials/licencesexplainedcontentcreatorsinfopack.pdf>)

I would like a Creative Commons licence to be applied to my thesis

Indicate type of CC licence:

5. Repository Terms (The Repository's Rights and Responsibilities)

The University, through Deakin Research Online (DRO):

- a. May distribute copies of the work(s) (including any abstracts) worldwide, in electronic format via any medium for the lifetime of the repository for the purpose of free access without charge unless you have restricted access in 4 above DRO.
- b. May electronically store, convert or copy the work(s) to ensure their future preservation and accessibility.
- c. May incorporate metadata or documentation into public access catalogues for the work(s).
- d. Shall retain the right to remove the work(s) for professional or administrative reasons, or if they are found to violate the legal rights of any person.
- e. Shall not be under obligation to take legal action on behalf of the depositor or other rights holders in the event of infringement of intellectual property rights or any other right in the material deposited.
- f. Shall not be under obligations to reproduce, transmit, or display the work(s) in the same format or software as that in which it was originally created.

| | |
|---|--------------------------|
| Signature: <div style="border: 1px solid red; border-radius: 10px; padding: 5px; display: inline-block; color: red;">Signature Redacted by Library</div> | Date: 30 October 2020 |
|---|--------------------------|

An electronic signature is acceptable. Alternatively you may print, sign and rescan this access form.

Acknowledgments

Prof. Xungai Wang

Prof. Joselito Razal

Joe Barber

Pip Barber

A/Prof. Derman V. Baryamol

Joe Bratovich

Prof. Peter Dabnichki

A/Prof. Raul Fernandez-Garcia

Dr. Antonio Giardina

A/Prof. Ignacio Gil

Dr. Michael Gilbert

Prof. David Grayden

Huw James

Dr. Sam John

Prof. Kon Mouzakis

Kelly Nikolopoulos

Prof. Elena Pirogova

Cynthia Shankar

Prof. Elias Siores

Prof. Olga Troynikov

Kon Thermos

Prof. Rajesh Vasa

Prof. Savvas Vassiliadis

Ken Wong

Author Publications

1. *Chapter 4 of this thesis is published as:*

I. Logothetis, D. V. Bayramol, I. Gil, P. Dabnichki, E. Pirogova, "Evaluating silver-plated nylon (Ag/PA66) e-textiles for bioelectrical impedance analysis (BIA) application", *Measurement Science and Technology*, vol. 31, no. 07, <https://doi.org/10.1088/1361-6501/ab78c3>.

Chapter 5 of this thesis is published as:

2. I. Logothetis, R. Fernandez-Garcia, O. Troynikov, P. Dabnichki, E. Pirogova, I. Gil, "Embroidered electrodes for bioelectrical impedance analysis: impact of surface area and stitch parameters", *Measurement Science and Technology*, vol. 30, no. 11, 11501. <https://doi.org/10.1088/1361-6501/ab3201>.
3. I. Logothetis, R. Fernandez-Garcia, P. Dabnichki, E. Pirogova, I. Gil, "E-textiles for bioelectrical impedance analysis (BIA)", Australian Biomedical Engineering Conference (ABEC) 2019, ISBN: 978-1-925627-43-5, Melbourne.

Chapter 6 of this thesis is published as:

4. I. Logothetis, I. Gil, Xungai Wang and Joselito Razal, "Comparison of silver-plated nylon (Ag/PA66) e-textile and Ag/AgCl electrodes for bioelectrical impedance analysis (BIA) application", *Biomedical Physics and Engineering Express* vol. 07, no. 03, <https://doi.org/10.1088/2057-1976/abf2a0>.

Abstract

The need for a quantitative method to measure the wound healing process is becoming important as current methodologies are subjective, and misdiagnosis can lead to wounds transitioning into chronic wounds that can potentially lead to amputations. Recently, bioelectrical impedance analysis (BIA) has been adopted into monitoring wounds and the advances in microtechnology research can allow a wearable BIA device to monitor wounds. This creates the need for wearable electrodes that can be integrated into clothing or pressure bandages to allow for stable monitoring.

There are various methods for creating electronic textile (e-textile) electrodes. A quick, simple and relatively low-cost method is creating e-textile electrodes with embroidery. The objective of this thesis is to study and analyse specific parameters of e-textile electrodes that can influence BIA measurements. The parameters studied are associated with research that adapt BIA for monitoring wounds. These factors are adopted to study the performance of e-textile electrodes. E-textile are considered dry electrodes implying they are associated with a polarization impedance.

An embroidery machine provides versatility in the manufacturing process of e-textile electrodes. There are multiple variables that can be easily controlled on the machine to create a desired electrode design. However, there is an uncertainty on how these variables impact the polarization impedance. It has also been demonstrated that the polarization impedance is greatly improved by including an electrolyte layer to dry electrodes. This study presents the drawback of an electrolyte layer. It provides a set of variables that can be adopted to create e-textile electrodes with a minimised polarization impedance.

Given that the electrodes touch the skin, a set of substrates were selected for the e-textile electrodes and tested to observe the influence of any changes in skin conditions, for example skin temperature and perspiration. The parameters found in the study were adopted for the embroidery machine settings on commercially available textiles. To imitate the skin properties, a climatic chamber was used by applying the appropriate settings. The human comfortability factor was also considered in terms of air permeability. A study was also completed to identify whether a reduction in Z_p of the e-textile electrodes can be achieved by changing the shape.

The final study is the application for e-textile electrodes where pork belly was used to emulate the human skin in terms of dielectric properties. By adopting BIA methods to measure the appropriate parameters used to monitor wounds, the e-textile electrodes were tested and compared to common clinical electrodes. Although e-

textile electrodes can be adopted to measure specific BIA parameters, further research is essential in improving their performance.

The key findings in this study indicate that e-textile electrodes in dry form provide stable measurements compared to using e-textile electrodes with a hydrogel layer. However, dry e-textile electrodes are associated with a high Z_p . Increasing the e-textile electrodes surface area, stitch density (spacing) and stitch length decreases the Z_p . Additional reduction in Z_p is evident by fabricating the electrodes in an elliptical shape. This research also indicated that a polyester non-woven textile had a reduced Z_p compared to the commercially available substrates used for this study. This substrate also showed the least variance when tested over a range of temperatures and relative humidity's emulating skin properties; thus, implying that measurements would be least affected when used on skin. Moreover, it was associated with a relatively high air permeability indicating it would be the most ideal in terms of comfort. Adopting the e-textile electrodes to measuring BIA parameters that are commonly used for wounds indicated that they are comparable to Ag/AgCl when measuring the impedance (Z), resistance (R) and open circuit resistance (R_{inf}).

Table of Contents

| | |
|---|----|
| Acknowledgments..... | 1 |
| Author Publications..... | 1 |
| Abstract..... | i |
| Chapter 1..... | 1 |
| Introduction | 1 |
| 1.1 Motivation..... | 1 |
| 1.2 Objectives and key findings..... | 2 |
| 1.3 Thesis Structure..... | 4 |
| Chapter 2..... | 6 |
| Literature Review | 6 |
| 2.1 Skin Structure and Wounds..... | 6 |
| 2.1.1 Skin | 6 |
| 2.1.2 Cells and action potential..... | 6 |
| 2.1.3 Wounds | 7 |
| 2.1.3.1 Types of Wounds..... | 7 |
| 2.1.3.2 Healing Process | 8 |
| 2.1.3.2.1 Haemostasis and inflammatory phase | 8 |
| 2.1.3.2.2 Proliferation phase | 9 |
| 2.1.3.2.3 Remodelling phase | 9 |
| 2.1.4 Skin temperature..... | 10 |
| 2.2 Wound care management..... | 11 |
| 2.2.1 Current clinical wound care management | 11 |
| 2.2.1.1 Clinical forms for wound care management | 12 |
| 2.2.1.2 Limitations..... | 12 |
| 2.2.2 Diagnostic methodologies used to monitor wound healing | 13 |
| 2.2.2.1 Confocal laser scanning microscope (CLSM) | 14 |
| 2.2.2.2 Optical coherence tomography (OCT) and Cross-polarization optical coherence tomography (CP-OCT)..... | 15 |
| 2.2.2.3 Doppler ultrasound and ultrasound | 15 |
| 2.2.2.4 Laser doppler velocimetry and imaging (LDV and LDI)..... | 16 |
| 2.2.2.5 Thermography | 16 |
| 2.2.2.6 Summary and limitations | 16 |
| 2.3 Bioelectrical Impedance Analysis (BIA) | 19 |

| | |
|---|----|
| 2.3 BIA for soft biotissues..... | 19 |
| 2.3.1 Frequency Classifications | 19 |
| 2.3.2 Electrical circuit models | 20 |
| 2.3.3 Cole – Cole model and plot | 24 |
| 2.3.4 Equipment..... | 26 |
| 2.3.5 Bioimpedance analysis on soft tissue damage | 27 |
| 2.3.6 Summary | 40 |
| 2.4 Adaption of electrodes for BIA systems | 40 |
| 2.4.1 BIA systems | 40 |
| 2.4.2 Electrodes..... | 42 |
| 2.4.3 Electrode configuration..... | 42 |
| 2.4.4 Wet and dry electrodes..... | 43 |
| 2.4.4.1 Dry Electrodes | 43 |
| 2.4.4.2 Rigid electrodes..... | 46 |
| 2.4.4.3 Flexible electrodes | 47 |
| 2.4.4.4 E-textiles electrodes..... | 48 |
| 2.4.4.5 Summary and limitations | 52 |
| Chapter 3..... | 54 |
| Equipment, Materials and Methodology | 54 |
| 3.1 E-textile electrode fabrication and testing..... | 54 |
| 3.1.1 Embroidery Machines | 54 |
| 3.1.1.1 Singer Future XL 550 | 54 |
| 3.1.1.2 Brother F440E Embroidery Machine | 54 |
| 3.1.1.3 Software EasyDesign EX and Embrilliance..... | 55 |
| 3.1.2 Electrical Impedance Measurements Equipment for Embroidered E-Textiles (Voltage Drive) | 56 |
| 3.1.2.1 HM8118 LCR Meter (Rohde & Schwarz, Munich, Germany)..... | 56 |
| 3.1.2.2 PM 6306 LCR Meter (Fluke Australia Pty Ltd, New South Wales, Australia) | 56 |
| 3.1.3 Materials for E-Textiles | 57 |
| 3.1.3.1 Substrates - Textiles | 57 |
| 3.1.3.2 Shieldex 117/17 dtex 2ply Thread..... | 57 |
| 3.1.4 Methodology E-Textiles..... | 58 |
| 3.1.4.1 E-textile electrode fabrication..... | 58 |

| | |
|--|----|
| 3.1.4.2 Methodology for measuring polarization impedance..... | 61 |
| 3.2 Comparison of Electrodes | 61 |
| 3.2.1 Electrical Impedance Measurements Equipment for BIA (Current Drive) SFB761 | |
| 3.2.2 Materials for BIA | 62 |
| 3.2.2.1 Ambu WhiteSensor WS Electrodes | 62 |
| 3.2.2.2 Pork Belly..... | 63 |
| 3.2.3 Methodology | 63 |
| 3.2.3.1 Preparation of the pork belly | 63 |
| 3.2.3.2 Incisions..... | 64 |
| 3.2.3.3 Storing of the pork belly..... | 64 |
| 3.2.3.4 Electrode Configuration | 65 |
| 3.2.3.4 Data collection and trend analysis | 66 |
| Chapter 4..... | 67 |
| Fabrication process for e-textile electrodes: impact of the characteristics on Z_p for use with BIA..... | 67 |
| 4.1 Introduction | 67 |
| 4.1.1 Electrode polarization impedance | 67 |
| 4.1.2 Previous research | 68 |
| 4.2 Materials and methods | 70 |
| 4.3 Methodology..... | 71 |
| 4.3.1 Sample Fabrication..... | 71 |
| 4.3.2 Experimental methodology..... | 73 |
| 4.4 Results..... | 74 |
| 4.4.1 Electrodes in dry and wet form..... | 74 |
| 4.4.2 Surface area | 78 |
| 4.4.3 Stitch parameters..... | 79 |
| 4.4.4 Quantity of conductive thread..... | 80 |
| 4.5 Equivalent Circuit Theory | 81 |
| 4.6 Discussion..... | 82 |
| 4.7 Conclusion | 83 |
| Chapter 5..... | 84 |
| Evaluating e-textiles for usability with BIA application..... | 84 |
| 5.1 Introduction | 84 |
| 5.1.1 Skin temperature and perspiration | 86 |

| | |
|--|-----|
| 5.2 Method..... | 87 |
| 5.2.1 The fabrication process | 88 |
| 5.2.2 Experimental protocol..... | 91 |
| 5.3 Results | 93 |
| 5.3.1 Testing in ambient conditions | 93 |
| 5.3.2 Testing using climatic chamber | 94 |
| 5.3.3 Comfort in terms of air permeability | 106 |
| 5.3.4 Evaluation of shape on Z_p | 107 |
| 5.4 Discussion..... | 108 |
| 5.5 Conclusion | 110 |
| Chapter 6..... | 111 |
| Comparison of e-textile and Ag/AgCl electrodes for BIA | 111 |
| 6.1 Introduction | 111 |
| 6.1.1 Electrodes..... | 111 |
| 6.1.2 Methods adapted for monitoring wounds..... | 112 |
| 6.2 Materials and Methodology..... | 115 |
| 6.2.1 Materials | 115 |
| 6.2.2 Methodology | 115 |
| 6.2.2.1 Part A Preliminary Study of Z on Biotissue Under Study (BUS) | 115 |
| 6.2.2.2 Part B Comparison of Ag/AgCl and Ag/PA66 e-textile electrodes..... | 115 |
| 6.2.2.2.1 Compression Sleeve | 116 |
| 6.2.3 Measurements | 117 |
| 6.2.3.1 Part A..... | 117 |
| 6.2.3.2 Part B..... | 118 |
| 6.2.4 Analysis..... | 119 |
| 6.2.4.1 Part A..... | 119 |
| 6.2.4.2 Part B..... | 119 |
| 6.3 Results | 119 |
| 6.3.1 Temperature | 119 |
| 6.3.2 Error of uncertainty..... | 120 |
| 6.3.3 Part A..... | 120 |
| 6.3.4 Part B..... | 125 |
| 6.3.4.1 Electrode Mismatch | 125 |
| 6.3.4.2 Evaluation of Z and R between Ag/Cl and e-textiles | 125 |

| | |
|---|-----|
| 6.3.4.3 Evaluation of X_c between Ag/Cl and e-textiles..... | 133 |
| 6.3.4.4 Evaluation of φ between Ag/Cl and e-textiles..... | 140 |
| 6.3.4.5 Evaluation of R_o between R_{inf} and e-textiles..... | 147 |
| 6.4 Discussion..... | 152 |
| 6.5 Conclusion | 154 |
| Chapter 7..... | 155 |
| Conclusion and Future Work..... | 155 |
| References | 160 |
| Appendices..... | 182 |
| Appendix I | 182 |
| Appendix II | 184 |
| Appendix III | 186 |
| Appendix IV | 188 |
| Appendix V | 190 |
| Appendix VI | 191 |

List of Tables

| | |
|---|-----|
| Table 2.1 Types of Wounds [77]..... | 8 |
| Table 2.2 Summary of wound assessment guidelines. | 12 |
| Table 2.3 Summary of non-invasive diagnostic tools..... | 18 |
| Table 2.4 BIA parameters of SFB7..... | 26 |
| Table 2.5 BIA diagnosis for injuries, muscle gap, oedema, blood flow | 28 |
| Table 2.6 BIA diagnosis for wounds | 36 |
| Table 2.7 Limitations and potential research..... | 53 |
| Table 4.1 Electrode types - stitch and size mapped to convention [47] “© IOP Publishing. Reproduced with permission. All rights reserved.” | 71 |
| Table 4.2 Stitch variables [47]. “© IOP Publishing. Reproduced with permission. All rights reserved.” | 72 |
| Table 4.3 R , XC , Z_p and Z_{pv} for dry e-textile electrode samples [47]. “© IOP Publishing. Reproduced with permission. All rights reserved.” | 77 |
| Table 5.1 Characteristics of selected substrates as a base for the e-textile electrodes [238]. “© IOP Publishing. Reproduced with permission. All rights reserved.” | 89 |
| Table 5.2 Relative difference of Z_p associated to skin properties (Equation 5.3) [238]. “© IOP Publishing. Reproduced with permission. All rights reserved.” | 95 |
| Table 5.3 Linear regressions associated to skin temperature relative to RH (40 - 80%): $y = mx + c$ [238]. “© IOP Publishing. Reproduced with permission. All rights reserved.” | 103 |
| Table 6.1 Pork belly sample for preliminary experiment..... | 115 |
| Table 6.2 Pork belly samples for final experiment..... | 116 |

List of Figures

| | |
|---|----|
| Figure 2.1 Wound healing process, each phase is mapped to current diagnostic methodologies. | 14 |
| Figure 2.2 Current passing through (a) the ICF + ECF (β dispersion) and (b) the ECF (α dispersion) with (c) circuit equivalence of the methodology..... | 20 |
| Figure 2.3 Equivalent circuit models (a) Schwan et al. [144], (b) modified Fricke et al. [141,149] and (c) Gimsa et al. [148]..... | 23 |
| Figure 2.4 Equivalent circuit models (a) Cole-Fricke-Cole [162] and (b) Extended Cole-Fricke-Cole [161] | 24 |
| Figure 2.5 Cole Cole plot. | 25 |
| Figure 2.6 BIA timeline..... | 27 |
| Figure 2.7 Cole Cole plot with hook artefact..... | 41 |
| Figure 2.8 Electrode Configurations (a) tetrapolar and (b) dipolar..... | 42 |
| Figure 2.9 Dry electrodes (a) types of dry electrodes, (b) fabrication methods for flexible and e-textile electrodes and (c) uses of dry electrodes. | 44 |
| Figure 2.10 Mind map of aspects covered for dry electrodes in literature review..... | 44 |
| Figure 2.11 Literature review of dry electrodes in thesis, including: (a) type of electrodes, (b) countries conducting research, (c) journals publishing articles, (d) number of articles relative to year of publication and (e) dry textiles testing methods..... | 45 |
| Figure 3.1 Singer Futura XL 550 | 54 |
| Figure 3.2 Brother F440E Embroidery Machine..... | 55 |
| Figure 3.3 EasyDesign EX with the weave stitch settings on display | 55 |
| Figure 3.4 HM8118 LCR Meter | 56 |
| Figure 3.5 PM 6306 LCR Meter | 57 |
| Figure 3.6 Shieldex 117/17 dtex 2ply Thread..... | 58 |
| Figure 3.7 Shieldex 117/17 dtex 2ply Thread..... | 60 |
| Figure 3.8 ImpediMed SFB7 | 62 |
| Figure 3.9 Ambu WhiteSenor WS Electrodes..... | 62 |

| | |
|--|----|
| Figure 3.10 Pork belly with incision..... | 64 |
| Figure 3.11 Pork belly with a tetrapolar electrode configuration..... | 65 |
| Figure 4.1 Fabrication and experimental process: (a) embroidery setup, (b) sample e-textile electrode prepared with snap, i.e., ball and spiked ring components (c) e-textile electrode with hydrogel pad tested as a wet e-electrodes, and (d) LCR meter with frequency setting 50 kHz [47]. “© IOP Publishing. Reproduced with permission. All rights reserved.” | 72 |
| Figure 4.2 Experimental protocol [47]. “© IOP Publishing. Reproduced with permission. All rights reserved.” | 73 |
| Figure 4.3 Dry wafer measurements of e-textile electrode samples (refer to table 4.2 for conventions) [47]. “© IOP Publishing. Reproduced with permission. All rights reserved.” . | 74 |
| Figure 4.4 Wet wafer measurements of e-textile electrode samples [47]. “© IOP Publishing. Reproduced with permission. All rights reserved.” | 75 |
| Figure 4.5 Z_p for e-textile electrode samples (a) weave and (b) satin stitch dry wafer measurements; (c) weave and (d) satin stitch wet wafer measurements [47]. “© IOP Publishing. Reproduced with permission. All rights reserved.” | 79 |
| Figure 4.6 Influence of length of conductive thread on Z_p for the e-textile electrodes [47]. “© IOP Publishing. Reproduced with permission. All rights reserved.” | 80 |
| Figure 4.7 Equivalent circuit..... | 81 |
| Figure 5.1 Relation of a BIA diagnostic system and associated components with patient: (a) system relating to the monitoring the patient, (b) patient’s physiological parameters that can impact the e-textile electrodes [238]. “© IOP Publishing. Reproduced with permission. All rights reserved.” | 88 |
| Figure 5.2 SEM representation of the selected textile substrates: (a) S1 (b) S2 (c) S3 and (d) S4 [238]. “© IOP Publishing. Reproduced with permission. All rights reserved.” | 90 |
| Figure 5.3 Fabricated e-textile electrodes with selected substrates: (a) cotton plain weave (E1), (b) cotton poplin (E2), (c) cotton velvet (E3) and (d) polyester non-woven felt (E4) [238]. “© IOP Publishing. Reproduced with permission. All rights reserved.” | 91 |
| Figure 5.4 Experimental protocol using climatic chamber [238]. “© IOP Publishing. Reproduced with permission. All rights reserved.” | 93 |
| Figure 5.5 Ambient measurements of Z_p relative to ϵ_r of substrate [238]. “© IOP Publishing. Reproduced with permission. All rights reserved.” | 94 |
| Figure 5.6a-b Impact of temperature and wetness (RH) on Z_p : (a) E1 and (b) E2 [238]. “© IOP Publishing. Reproduced with permission. All rights reserved.” | 96 |

| | |
|--|-----|
| Figure 5.7c-d Impact of temperature and wetness (RH) on Z_p : (c) E3 and (d) E4 [238]. “© IOP Publishing. Reproduced with permission. All rights reserved.” | 97 |
| Figure 5.8a-b Relative change in Z_p associated with temperature: (a) E1 and (b) E2 [238]. “© IOP Publishing. Reproduced with permission. All rights reserved.” | 98 |
| Figure 5.9c-d Relative change in Z_p associated with temperature: (c) E3 and (d) E4 [238]. “© IOP Publishing. Reproduced with permission. All rights reserved.” | 99 |
| Figure 5.10a-b Relative change in Z_p associated to increments of RH: (a) E1 and (b) E2 [238]. “© IOP Publishing. Reproduced with permission. All rights reserved.” | 100 |
| Figure 5.11c-d Relative change in Z_p associated to increments of RH: (c) E3 and (d) E4 [238]. “© IOP Publishing. Reproduced with permission. All rights reserved.” | 101 |
| Figure 5.12a-b Z_p linear regressions associated with skin properties - temperature and wetness RH (40 - 80%): (a) E1 and (b) E2 [238]. “© IOP Publishing. Reproduced with permission. All rights reserved.” | 104 |
| Figure 5.13c-d Z_p linear regressions associated with skin properties - temperature and wetness RH (40 - 80%): (c) E3 and (d) E4 [238]. “© IOP Publishing. Reproduced with permission. All rights reserved.” | 105 |
| Figure 5.14 SEM representations of the e-textile electrodes with various substrates: (a) E1, (b) E2, (c) E3 and (d) E4 [238]. “© IOP Publishing. Reproduced with permission. All rights reserved.” | 107 |
| Figure 5.15 Measuring air permeability for the: (a) substrates and (b) e-textile electrode samples [238]. “© IOP Publishing. Reproduced with permission. All rights reserved.” | 107 |
| Figure 5.16 Comparison of rectangular and elliptical electrodes. | 108 |
| Figure 6.1 Experimental set-up. | 117 |
| Figure 6.2 Adaption of BIA configuration and parameters for monitoring wounds in previous research for the experimental protocol..... | 118 |
| Figure 6.3a-b Trends in intact BUS sample using Ag/AgCl in tetrapolar configuration for (a) Z and R day 1 and (b) Z and R day 2. | 122 |
| Figure 6.4c-d Trends in intact BUS sample using Ag/AgCl in tetrapolar configuration for (c) X_c day 1 and (d) X_c day 2. | 123 |
| Figure 6.5e-f Trends in intact BUS sample using Ag/AgCl in tetrapolar configuration for (e) ϕ day 1 and (f) ϕ day 2. | 124 |
| Figure 6.6 Cole-Cole plot for e-textile electrodes as presented by SFB7. | 125 |

| | |
|---|-----|
| Figure 6.7a-b Z and R ratio relative to time at 3-1000 kHz sweep for electrodes: (a) Ag/AgCl day 1 and (b) day 2..... | 127 |
| Figure 6.8c-d Z and R ratio relative to time at 3-1000 kHz sweep for electrodes: (c) e-textiles day 1 and (d) day 2..... | 128 |
| Figure 6.9a-b Z and R ratio relative to time at 5 kHz for electrodes: (a) Ag/AgCl day 1 and (b) day 2..... | 129 |
| Figure 6.10c-d Z and R ratio relative to time at 5 kHz for electrodes: (c) e-textiles day 1 and (d) day 2. | 130 |
| Figure 6.11a-b Z and R ratio relative to time at 50 kHz for electrodes: (a) Ag/AgCl day 1 and (b) day 2. | 131 |
| Figure 6.12c-d Z and R ratio relative to time at 50 kHz for electrodes: (c) e-textiles day 1 and (d) day 2. | 132 |
| Figure 6.13a-b X_C ratio relative to time at 3-1000 kHz sweep for electrodes: (a) Ag/AgCl day 1 and (b) day 2. | 134 |
| Figure 6.14c-d X_C ratio relative to time at 3-1000 kHz sweep for electrodes: (c) e-textiles day 1 and (d) day 2. | 135 |
| Figure 6.15a-b X_C ratio relative to time at 5 kHz for electrodes: (a) Ag/AgCl day 1 and (b) day 2. | 136 |
| Figure 6.16c-d X_C ratio relative to time at 5 kHz for electrodes: (a) Ag/AgCl day 1, (b) day 2; (c) e-textiles day 1 and (d) day 2. | 137 |
| Figure 6.17a-b X_C ratio relative to time at 50 kHz for electrodes: (a) Ag/AgCl day 1 and (b) day 2..... | 138 |
| Figure 6.18c-d X_C ratio relative to time at 50 kHz for electrodes: (c) e-textiles day 1 and (d) day 2..... | 139 |
| Figure 6.19a-b ϕ ratio relative to time at 3-1000 kHz sweep for electrodes: (a) Ag/AgCl day 1 and (b) day 2. | 141 |
| Figure 6.20c-d ϕ ratio relative to time at 3-1000 kHz sweep for electrodes: (c) e-textiles day 1 and (d) day 2. | 142 |
| Figure 6.21a-b ϕ ratio relative to time at 5 kHz for electrodes: (a) Ag/AgCl day 1 and (b) day 2. | 143 |
| Figure 6.22c-d ϕ ratio relative to time at 5 kHz for electrodes: (c) e-textiles day 1 and (d) day 2..... | 144 |

Figure 6.23a-b ϕ ratio relative to time at 50 kHz for electrodes: (a) Ag/AgCl day 1 and (b) day 2..... 145

Figure 6.24c-d ϕ ratio relative to time at 50 kHz for electrodes: (c) e-textiles day 1 and (d) day 2..... 146

Figure 6.25a-b R_0 ratio relative to time at 3-1000 kHz sweep for electrodes: (a) Ag/AgCl day 1 and (b) day 2. 148

Figure 6.26c-d R_0 ratio relative to time at 3-1000 kHz sweep for electrodes: (c) e-textiles day 1 and (d) day 2. 149

Figure 6.27a-b R_{inf} ratio relative to time at 3-1000 kHz sweep for electrodes: (a) Ag/AgCl day 1 and (b) day 2. 150

Figure 6.28c-d R_{inf} ratio relative to time at 3-1000 kHz sweep for electrodes: (c) e-textiles day 1 and (d) day 2..... 151

Chapter 1

Introduction

1.1 Motivation

Wounds are a growing concern globally [1–4]. Current methodologies are based on visual inspection by medical professions that leads to misdiagnosis and potentially wrong treatment [5–9]. Much research has been directed into monitoring wounds quantitatively [10,11,20–29,12,30–32,13–19]. In addition, with the development of micro-electronics and conductive yarns, these methodologies can be transformed into a wearable device that can be used for long-term monitoring [33].

Recently, researchers have adapted bioelectrical impedance analysis (BIA) to identify methodologies into monitoring wounds [34,35,44–46,36–43]. A current is injected through the biotissue under study (BUS) permitting measurements of its resistive and capacitive properties. Currently, discrete measurements are conducted using common clinical electrodes identified as wet electrodes, specifically Ag/AgCl.

Wet electrodes are typically characterised as non-polarised electrodes [47]. Although they are not ideally non-polarized, the electrolyte ‘gel’ layer associated with wet electrodes substantially reduces the polarization to a magnitude of a few ohms [48]. Thus, allowing the use of the electrodes across a range of systems that operate at different frequencies. However, there are several drawbacks to using wet electrodes in long-term monitoring applications. A simple issue associated with wet electrodes is that preparation of the skin is required prior to placing the electrodes on the patient. In addition, there are issues with the comfort of the patient. Wearing wet electrodes long-term can cause discomfort to the patient in addition to causing skin irritations. However, the main issue is their stability in measurements. Wet electrodes are secured to the patient with the aid of an adhesive layer on the electrode. Therefore, there are two wet layers assisting their performance, the adhesive layer secures the electrode to the skin surface that forms the electrode-skin interface. A gel layer is added to the electrodes in order to minimise the electrode-skin impedance (Z_{es}). However, the dehydration of these layers can cause the electrodes to slowly detach from the patient: thus, losing a signal or causing an electrode-skin impedance mismatch [49,50]. Moreover, the dehydration of the gel layer results in an unstable redox reaction influencing the reliability of measurements [51]. This has led to researchers fabricating dry electrodes to replace wet electrodes for various application [51–59]. However, the study of dry electrodes in various fields indicates that due to their capacitive properties, they possess a polarization impedance (Z_p) that can impact measurements.

With the development of conductive yarn, electronic textile (e-textile) electrodes have been adapted to various systems including, ECG, EEG and EMG's [60–62]. Various methods have been adapted in the production of e-textile electrodes. E-textiles have been fabricated by depositing conductive polymers onto simple textiles using dip-coating, ink-jet and screen printing [63–65]. In addition, conductive threads have been woven or knitted to form e-textile electrodes [66]. However, the conductive polymers age and can induce skin irritation when worn for long periods [63,67]. Moreover, the weaving or knitting of e-textile electrodes can be costly. The application of an electrolyte layer has also been studied in improving the performance of e-textile electrodes, specifically for ECG [63].

The embroidery process allows for a controlled methodology into developing e-textile electrodes to reduce Z_p [47,68]. BIA adapted to monitor wounds operate at significantly higher frequencies (close to a magnitude of 10^3) in comparison ECG, EEG and EMG systems [47]. Thus, a change in the magnitude of Z_p associated to the e-textile electrodes at 50 kHz is expected. A common frequency adapted to monitor skin integrity is about 50 kHz [69]. Moreover, the methodology of monitoring wounds using BIA systems differs from these other systems. Therefore, a study into the comparison of wet electrodes to e-textile electrodes based on these parameters has yet to be undertaken.

Research Questions

- 1) What are the fabrication variables required to reduce Z_p of e-textile electrodes?
- 2) How is Z_p influenced by the e-textile electrode substrates and how do these substrates impact Z_p relative to physiological conditions as the body adopts to comfortable level (via cooling typically associated with changes in body temperature and perspiration)?
- 3) What BIA parameters for using e-textile electrodes can be used to monitor the healing of wounds?

1.2 Objectives and key findings

The primary research objective is to establish a suitable method to fabricating e-textile electrodes to monitor skin integrity using BIA. This study includes the stability of Z_p associated with dry electrodes. In addition, suitable embroidery variables were identified to reduce Z_p associated with dry electrodes, such as the size of the e-textile electrode, the stitch type, stitch spacing (density) and stitch length [47]. An appropriate substrate for the e-textile electrodes was found by testing the impact of temperature and wetness on Z_p ; where the temperature and wetness settings were associated with skin temperature and perspiration [67]. In addition, the influence of a rectangular or elliptical shape on Z_p was compared. By selecting the most

appropriate electrodes based on a low Z_p , their efficacy to wet electrodes (Ag/AgCl) was studied. Thus, identifying the parameters that can be used to monitor wounds with e-textile electrodes for sfBIA and mfBIA.

Knowledge

1. Incorporating a gel layer to dry electrodes reduces the Z_p compared to using the dry electrodes without hydrogel; however, measurements are unstable. This could be due to the dehydration of the hydrogel not present in dry electrodes. Dry electrodes indicated a greater Z_p , as expected although measurements were stable.
2. An increase in (i) surface area, (ii) stitch density (spacing) and (iii) stitch length decreases Z_p . In addition, the selected surface area showed a comparable Z_p for the weave and satin stitch. However, the weave stitch required less conductive thread. Elliptical shaped e-textile electrodes also showed a reduction in Z_p compared to rectangular shaped electrodes. Thus, in this study, the e-textile characteristics determined were:
 - a. Stitch type: Weave
 - b. Dimensions: 40 x 30 mm
 - c. Stitch density: 0.4 mm
 - d. Stitch length: 7 mm
 - e. Shape: elliptical
3. The substrate selection for the e-textile electrodes influences Z_p . This is observed when applying temperature and wetness associated with skin properties to measure Z_p of the e-textile electrodes. Z_p was primarily influenced by the wetness (RH) of the e-textile electrodes which can be associated with a gain in moisture absorption thus resulting in a reduction in Z_p across all substrates. Completing this study, it was observed that the e-textile electrodes fabricated using a polyester non-woven felt substrate are preferred, due to:
 - a. A low Z_p compared to the other substrates in this study
 - b. A linear relationship between Z_p and the skin properties of temperature and relative humidity was observed
 - c. A close to 'zero-slope' was observed indicating a negligible impact on Z_p due to the skin properties applied

- d. Demonstrated a greater air permeability relative to the other substrates; thus, indicating a preference in terms of comfort
4. E-textile electrodes can replace Ag/AgCl electrodes to measure specific BIA parameters used in monitoring the wound healing process; however, there are some limitations.
 - a. Z and R trend for Ag/AgCl and e-textile electrodes were comparable; thus, e-textile electrodes are suitable for these parameters
 - b. X_C and φ demonstrated scattering which impacted R_0 implying e-textile electrodes cannot be used to replace Ag/AgCl electrodes
 - c. R_{inf} showed a decrease in Ag/AgCl and e-textile electrodes
 - d. Z is common in measuring the wound healing process and e-textile electrodes can be used to replace Ag/AgCl

1.3 Thesis Structure

This study is based on the fabrication of e-textile electrodes with the aim of adapting them for use with BIA systems to monitor the wound healing phase over a long-term period. Therefore, an initial study of the polarization impedance Z_p was conducted relative to the fabrication process. The second study focused on selecting an appropriate substrate based on physiological parameters. The selection of an appropriate substrate directed the study into identifying the impact of Z_p of e-textile electrodes based on their shape. This process identified the e-textile electrodes with the lowest Z_p . The final analysis was a comparison of the e-textile electrodes to common clinical electrodes, specifically Ag/AgCl, to identify their efficacy in current BIA methodologies adapted to monitor wounds.

Chapter 2 of the thesis presents a review covering several aspects including: (i) the physiology of skin and wounds, (ii) current clinical methods on wound management, (iii) alternative diagnostic methods to monitor the wound healing process, (iv) BIA and associated models, (v) BIA for soft tissue integrity, including wounds and (vi) dry electrodes. This literature review into BIA methodologies used in monitoring soft tissue is essential in the fabrication process and analysis.

Chapter 3 is a short section on the materials and methodology of this study, including the equipment adapted throughout this project. However, in-depth details of the methodologies are incorporated in the individual chapters.

Chapter 4 presents the fabrication process of the e-textile electrodes and its influence on Z_p . It also presents the benefit of dry electrodes in comparison to the assistance of an electrolyte layer used with dry electrodes. Analysis on Z_p is based on various

embroidery characteristics. This includes the dimensions (size) of the e-textile electrodes which relates to the surface area of the conductive component of the electrodes. Then there are the stitch properties, including stitch type, stitch length and stitch spacing (density). The properties associated with the e-textile electrodes that demonstrated the lowest Z_p were adapted for the remainder of this research.

Chapter 5 focused on selecting a suitable substrate based on a reduced Z_p in addition to the influence of physiological properties on the e-textile electrodes. A climatic chamber was adapted to emulate skin temperature and perspiration. The rate of change in Z_p relative to changes in temperature and RH were analysed for the various substrates. To ensure the physiological comfort of the various fabricated electrodes, they were tested to measure the air permeability. The best performing substrate was then adapted to identify the shape for the final e-textile electrodes.

Chapter 6 presents a comparative study of e-textile electrodes with common clinical Ag/AgCl electrodes based on the parameters adapted to BIA to monitor wounds. By adapting a common methodology used in studies monitoring wounds using BIA, an experimental protocol was set up and a comparison was completed. This study indicates the parameters that can be monitored using e-textile electrodes and the parameters that are affected due to the Z_p of the e-textile electrodes.

Chapter 7 presents the conclusion of this study based on e-textile electrodes and introduces future work in improving the quality of care for wound patients.

Chapter 2

Literature Review

2.1 Skin Structure and Wounds

2.1.1 Skin

The human body consists of four soft biological tissue (biotissue) types; muscle, nervous, connective and epithelial tissue. An epithelial tissue of interest is skin and is the largest sensory organ that is found in the human body. It is made up of tightly woven skin cells and its thickness can vary between 0.5 mm to 8.0 mm. This also depends on the location [70]. It has several layers that are classified into three main categories: (i) epidermis, (ii) dermis and (iii) hypodermis [71–73].

The function of the epidermis is to protect the human body from the outside environment. It has no blood vessels and depends on its connection to the dermis sublayer to receive oxygen and nutrients. It consists predominantly of keratinocyte cells (about 95%) while the other main cells include melanocytes and Langerhans cells [72,73].

The dermis can be interpreted as an integrated system consisting of cellular and acellular matrices providing structure to the skin and necessary for wound healing. This layer of the skin is primarily associated with the skin's mechanical properties specifically its elasticity and tensile strength. In addition, it aids in thermoregulation assisting the body in maintaining its body core and skin temperature. It consists of blood vessels, nerves and lymphatics. In addition, this layer contains many cell types including macrophages, mast cells, fibroblasts, and circulating immune cells that are vital for the wound to heal [72,73].

The hypodermis is the fatty layer that insulates the human body. It is mainly composed of fat-storing cells called adipose tissue. In addition to this, it contains connective tissues, blood vessels and nerves. It also has the ability to store energy supply as a reserve [72,73].

2.1.2 Cells and action potential

Cells are the foundation of the structure and function in the human body. Grouped cells that perform a common function form soft biotissue. All cells contain intracellular fluid (ICF) that is confined by the cell membrane (CM). The cells are suspended in interstitial fluid in the tissue. This fluid together with intravascular fluid contained in the blood plasma, constitute the extracellular fluid (ECF). Soft biotissue is composed of approximately 35% ECF whilst the remaining 65% is ICF [74].

An action potential is the electrical potential of a cell in response to stimulation. This exists across the plasma membrane of the cells. The steady state of the cell is defined by the resting membrane potential and is usually -70 mV. Through an electrical stimulus the membrane potential moves toward a positive cell potential known as depolarization reaching a maximum threshold of about +30 mV before repolarization begins and the potential returns to -70mV. However, it is common for repolarization to exceed the resting membrane potential reaching a potential less than -70mV before returning to its resting protentional, referred to as hyperpolarization [75].

Within the grouped cells of soft tissue, local current flow propagates the action potential of the adjacent membrane. All membranes have an absolute refractory period; thus, the recently depolarized membranes will not depolarize during this recovery period unless a stronger stimulus is applied initiating a new action potential. The membrane capacitance and resistance are responsible for the decrease in charge of the local currents where the threshold cannot be reached after a certain distance. The reduction in membrane capacitance results in the ability to store charge thus increasing the distance travelled. Contrary to this, a higher membrane resistance contributes to distance where a disruption to these cells influences the electrophysiological properties of the biotissue.

2.1.3 Wounds

2.1.3.1 Types of Wounds

Typically, wounds are commonly categorised into open or closed wounds. Open wounds are formed by a disruption to the surface of the skin exposing the underlying tissue. Open wounds can be grouped under: (i) penetrating wounds and (ii) blunt trauma wounds [76–78]. Contrary to this, closed wounds commonly occur from underlying skin etiologies, such as immune, metabolic and neurologic disorders. In this situation, the underlying tissue is not exposed. Ulcers are a special case in which there is an internal aetiology that eventually causes a disruption to the skin. Refer to Table 2.1 for the types of wounds [77].

Table 2.1 Types of Wounds [77]

| Open Wounds | | Closed Wounds | Ulcers |
|--|---------------------|----------------|-----------------------|
| Penetrating Wounds | Blunt Trauma Wounds | | |
| Puncture | Abrasions | Contusions | Diabetic foot ulcer |
| Surgical | Lacerations | Blisters | Venous Ulcer |
| Thermal, chemical, or electrical burns | Skin tears | Seroma | Ulcerative dermatitis |
| Gunshot wounds | | Hematoma | Pressure ulcer |
| Bites and stings | | Crush injuries | |

The extension of disruption to skin relative to the underlying tissues has been classified into four stages. Stage 1 is superficial impacting only the epidermis. Stage 2 causes a disruption to the epidermis and dermis layer. Stage 3 extends to the hypodermis layer (subcutaneous layer) while stage 4 is damage that has reached the muscle and bone [78].

2.1.3.2 Healing Process

A disruption to soft tissue triggers receptors in the body giving rise to the healing process [79], altering the compartment ratio and cell activity. The body has a natural mechanism that controls the process of soft tissue healing through concomitant events. These events complete the healing phase, from anywhere between a few months to years, in acute soft tissue damage [80–85]. Factors disturbing this complex interrelated series of events can cause a delay in healing or evoke morbidity inducing mortality. Haemostasis initiates the process giving way to the inflammatory phase [83]. Achieving haemostasis results in the regeneration process beginning with the proliferation phase and then the remodelling phases. There is no defined beginning or end for the three final phases, rather they function with significant overlap [80,84].

2.1.3.2.1 Haemostasis and inflammatory phase

Haemostasis is a momentary phase activating the clotting cascade triggering platelets and endothelial cells [81]. Vascular spasm and vasoconstriction attenuate the loss of blood; a platelet plug is formed filling the exposed area where coagulation forms a fibrin mesh and the blood solidifies into a clot. At this stage growth factors (i.e., PDGF, TGF, β , EGF, VGF, FGF), also referred to as cytokines, are released activating the MMP enzymes. During this phase extra cellular matrix (ECM) is formed serving as the storage and delivery of cytokines and enzymes. The cytokines and enzymes cross talk through messenger within the cells to promote proliferation and remodelling of soft

tissue [86]. Proceeding, the inflammatory phase builds the prevention of infection and is the most vital phase for the healing process.

Inflammation is identified through an increase of blood flow to the injured area stemming from the build up of oedema through vascular and cellular cascades [81]. The vascular response produces the chemical mediators giving rise to vasodilation and vasopermeability. Thus, resulting in an increased exudate production in the ECF causing tissue oedema, a fluid composed of water and ions. The chemical mediators of the cellular response attract phagocytes to the area eliminating microbial pathogens and necrocytes. The main phagocytes in the cellular response are neutrophils and monocytes. Neutrophils constitute of granular polymorphonuclear leukocytes which are the primary phagocytes in the cellular response. These cells migrate to the injured area within the first hour and are active for the initial 48 hours ingesting the microbial pathogens. Monocytes differentiate into inflammatory (IM) and anti-inflammatory (AM) macrophages that are found in the ECF. IMs are effective about 48-72 hours after the trauma and hold TNF- α and IL-1 β immune factors that phagocytize necrocytes. 72 hours post trauma AMs appear and are believed to hold pro-regenerative factors including TGF- β , VEGF and IL-10 supporting proliferation and remodelling [87–90].

2.1.3.2.2 Proliferation phase

The proliferation phase is driven by the pro-regenerative factors derived from the inflammatory phase about 120 hours post trauma. Growth factors (i.e., TGF- β and PDGF) released from the haemostasis and inflammatory phase stimulate fibroplasia and angiogenesis inducing proliferation [91]. Endothelial cells, produced from the VEGF released in the inflammatory phase, generate neovascularization assisting in the repair of damaged blood cells. These fibroblasts form extracellular matrix proteins. Then they generate fibronectin and collagen aiding in wound contraction which fundamentally assists angiogenesis towards proliferation through MMPs (matrixen) released from the neutrophils. MMPs promote angiogenesis through liberation of VEGF and remodelling of the extracellular matrix (ECM) [92]. Collagens produced by fibroblasts are the essential proteins that strengthen the tissues. This phase further contributes to tissue oedema. The proliferation phase is responsible for re-epithelialisation taking days or weeks for the wound size to reduce and eventually close [93].

2.1.3.2.3 Remodelling phase

Remodelling is primarily the process of refining the collagen and its corresponding ECM. During the deposition of the collagen, it initially produces relatively weak fibrils with random orientation. This eventually regains a structure similar to unwounded tissue inducing tensile strength by replacing Collagen 3 with Collagen 1 [94].

However, long term it can only reach 80% of the potential strength of unwounded tissue [95].

2.1.4 Skin temperature

Autonomic thermoregulation regulates the thermal balance of the human body from the autonomic nervous system that is made up of the hypothalamus. In this process skin acts as an effector and receptor [96,97]. Thermoreceptors found in the skin sense a change in temperature triggering the necessary defence responses. The functionality of skin in thermoregulation remains controversial; it is uncertain whether it acts as a feedforward or feedback control. When the skin is considered as a feedforward system, the thermoregulation process is dependent on the skin temperature. Contrary to this, the skin temperature is dependent on the thermoregulation process when modelled as a feedback system [98].

Many factors influence the skin temperature. These include (i) the environmental temperature, (ii) the body core temperature, (iii) any skin conditions and (iv) the structure found beneath the skin. The underlying soft and hard tissues located beneath the skin is what causes the human body to have different skin temperature recordings relative to the part of the body. For instance, a higher skin temperature is expected over muscles, arteries and active organs; while a lower skin temperature is observed over (i) veins, (ii) organs at rest, (iii) bone or tendons and (iv) protruding parts [99].

A wound disrupts the regular bodily structure and functionality thus altering the skin temperature [100]. In order to fight any infectious agents, including viruses and bacteria, the immune response system of the human body reacts by increasing the body core temperature [101]. This increase in body core temperature affectively causes the skin temperature to increase; thus, the body's response is to produce perspiration to cool the body down. The purpose of perspiration is to assist the body in maintaining its thermophysiological temperature. Another factor is the use of anaesthesia during surgery; this can decrease the body's core temperature causing a reduction in skin temperature of the wound bed and the surrounding area (peri-wound) [96].

A standardised threshold for thermophysiological skin temperature has yet to be defined. In 1936 Bierman [99] suggested a range of skin temperature varying from 33.5 and 36.9 °C. Further research presented lower ranges of 30 – 34 °C [102–104]. The temperature of a healthy wound bed can vary within a 1 – 3 °C margin. A complication in the wound healing process can increase the wound bed temperature up to 4 – 5 °C while post infection temperature changes are minuscule ranging between 0.8 – 1.1 °C [96,105].

2.2 Wound care management

2.2.1 Current clinical wound care management

Wounds Australia is a non-government organisation for wound care and management in Australia. The organisation works with government and industry organisations to provide resources for appropriate wound care management. The 'Standards of Wound Prevention and Management' is an evidence-based document providing a framework of guidelines set by Wounds Australia as a tool aiding clinical practices to develop an assessment procedure, specifically a wound assessment form [106]. The integrity of the biotissue of the wound bed and peri-wound area is continuously monitored by practitioners or nurses [107–110]. By conducting this assessment, the proper treatment is delivered to the patient accordingly. This treatment strongly depends on the condition of the wound as observed and assessed through these guidelines [111–113]. A summary of the guidelines can be found in Table 2.2. Ongoing assessment for criteria I – IV is fundamental for acute and chronic wounds while criteria V relates to chronic wounds.

Table 2.2 Summary of wound assessment guidelines.

| Type | Criteria | Rubric |
|-------------------------------------|-------------------------|--|
| Ongoing assessment | I. Individual | <ul style="list-style-type: none"> • Quality of life • Cognitive ability • Health literacy • General health history • Participation in self-care |
| | II. Risk of wound | <ul style="list-style-type: none"> • Skin damage • Skin colour change • Pressure indexes (i.e., ankle brachial pressure index (ABPI) and/or toe) • Loss of protective sensation • Brachial pressure index (TBPI), and transcutaneous oxygen pressure) |
| | III. Wound | <ul style="list-style-type: none"> • Wound dimensions • Characteristics of wound and peri-wound area • Exudation • Assessment of wound infection • Classification of wound • Pain assessment • Evaluation of wound healing progress |
| | IV. Healing environment | <ul style="list-style-type: none"> • Environmental factors (i.e., Temperature & Humidity) • Hygiene and risk to wound contamination (spread of infection) |
| Diagnosis for delayed wound healing | V. Chronic wounds | <ul style="list-style-type: none"> • Histopathology • Diagnostic Imaging |

2.2.1.1 Clinical forms for wound care management

A study into the development of a wound assessment form provides an indicator into the main observations required to be carried out by practitioners and nurses [114]. A significant portion of the form is based on visual assessment of the wound by practitioners and nurses. A pertinent example is the size of the wound. The practitioner measures the wound size (i.e., width, length and depth) with a disposable ruler, edge tracing or a dipstick swab. There is no standardisation as to the selection of reference points for these measurements; thus, it is subjective to the practitioners practice strategy.

2.2.1.2 Limitations

An advantage to the current clinical wound assessment and management standards is the service provided. Continuous monitoring of an acute wound by a team of practitioners and nurses provides a quality of care service to the patient. However,

this gives rise to certain drawbacks. Primarily, the assessment performed is subjective implying that the assessment completed is (i) subject to inconsistency and (ii) prone to human error resulting in poor prognoses that can lead to a variance in the treatment [115–117]. This can inconsequentially lead to a delay to the acute wound healing process. However, a more critical implication is the mistreatment of the wound resulting in a chronic wound that leads to morbidity, amputation or mortality [115,118–120].

Continuous monitoring of an acute wound impacts the quality of life for a patient. A patient is required to visit a practitioner on a regular basis. This implies that the patient is inconvenienced by travelling to the clinic in addition to the waiting period at the clinic which can disrupt their daily routine. Moreover, the out-of-pocket costs related to the wound healing process can impact the financial aspect of their quality of life, not to mention the burden on government expenditure [121].

It is vital to prevent an acute wound forming into a chronic wound. These problems associated with the subjective current clinical wound assessment and monitoring strategies need to be resolved. To accurately assess the integrity of the biotissue, a quantitative methodology must be adapted. By monitoring the wound objectively, proper treatment can be provided thus reducing the risks associated with poor prognoses.

2.2.2 Diagnostic methodologies used to monitor wound healing

Much research into real-time non-invasive diagnostic methodologies have attributed to the advancement of wound prevention and management. However, a vast amount of this research focuses on chronic wounds. Through a thorough search of literature, it appears that imaging tools are favoured. Figure 2.1 presents the wound healing process with the diagnostic methodologies mapped to the phase in which they are applied.

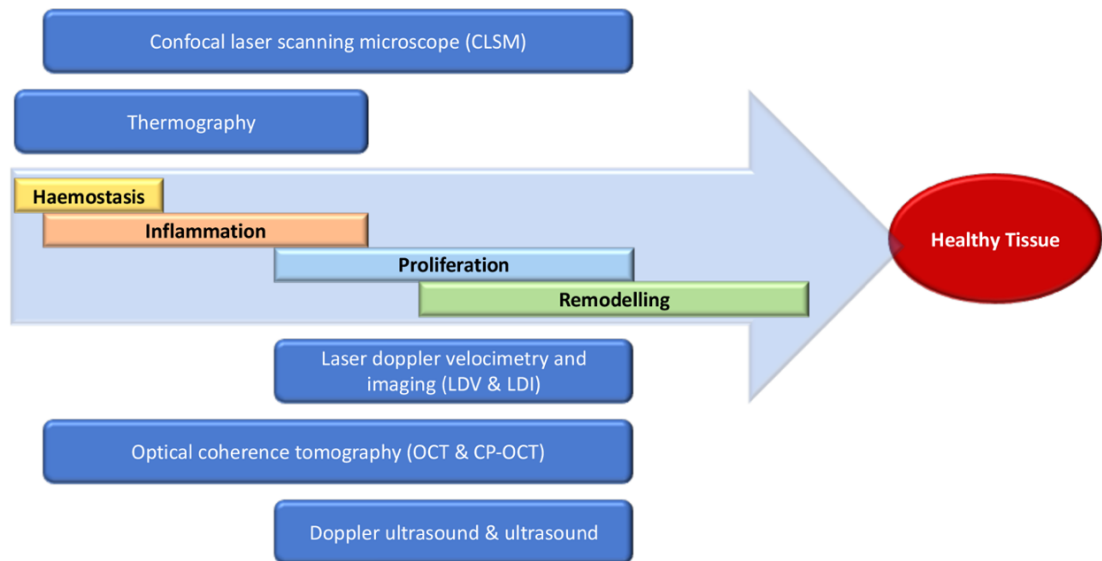


Figure 2.1 Wound healing process, each phase is mapped to current diagnostic methodologies.

2.2.2.1 Confocal laser scanning microscope (CLSM)

The CSLM works by positioning a hand-held device above the wound to produce high-resolution images [10]. By passing a laser beam through a light source aperture and using the focal plane of the objective lens, the beam is focused on the wound. When the beam is focused on the sample, part of the light will return through the objective lens due to the fluorescence of the sample. This is then passed to the detection system that detects the intensity of the light. The detected light may have a low intensity, thus a photomultiplier tube (PMT) detects and amplifies the signal converting it into an electrical signal producing the image [122,123].

This tool has been used for skin tumours (melanoma and nonmelanoma) [10,11] and burns [12,13]. Its high resolution (about 1 μm) [14,15] gives insight into subcellular structures of the epidermis including the cellular, nuclear and tissue structure [16]. In addition, it can be used as a substitute for biopsies in analysing inflammatory infiltrates, tumours and capillaries of the underlying tissue [16]. However, this technology is limited to a small wound size [17], while its depth range is limited to 350–500 μm thus restricted only to the uppermost layer of the dermis [18,19]. In addition, the process of capturing and evaluating a single image is time consuming averaging about 5-15 min [15]. This methodology is also confined for use only by trained medical staff, as a certain amount of knowledge is required in how to read and analyse the image produced from the equipment. Therefore, self-monitoring is not plausible.

2.2.2.2 Optical coherence tomography (OCT) and Cross-polarization optical coherence tomography (CP-OCT)

Optical coherence tomography (OCT) is another non-invasive hand-held, computer assisted imaging diagnostic tool that can be adapted to monitor wounds [20]. It uses a low coherent length of light that is passed through an interferometer dividing it into two separate paths referred to as the reference arm and sample arm. Each individual light relating to these arms are passed through objective lenses in order to reach the focal point. The light of the reference arm is transmitted towards a mirror while the sample arm focuses on the biotissue under study (BUS). The reflected light of the reference arm from the BUS and from the mirror pass through the interferometer where they are combined and passed through to a light detector. The light detector then observes an interference pattern that is produced by the amalgamation of the reference and sample arms resulting in an image [21].

OCT has a high resolution of about 2-15 μm with a depth penetration of about 2-5 mm, thus is limited to the epidermis and dermis layer [20,22,23]. It can identify any disruption between the epidermis and dermis junction, and inflammation. Its penetration depth is also sufficient to identify specific dermal structures including sebaceous, sweat glands and vessels [24]. CP-OCT developed from OCT, can obtain more information on the tissue structure, such as information pertaining to collagen fibres [22]. It is considered a fast, high resolution tool that is low in cost and has been adapted for burns, pressure ulcers and surgical wounds [25,26].

2.2.2.3 Doppler ultrasound and ultrasound

Doppler ultrasound is based on the principles of ultrasound imaging. A high frequency of sound waves is transmitted through the body using a probe. These waves travel through the body until they hit an object or boundary. Some of the waves are reflected to the probe while some continue to pass through the body until they hit another boundary in which they are also reflected. The reflected waves are used to form an image. This image is a representation of the distance of the objects relative to the travel time of the waves (i.e. calculate by speed and density) [124].

A doppler ultrasound is used to measure moving objects including the direction of flow. This is possible by observing the changes in frequency of the reflected waves. It has been adapted to measure the blood flow associated with wounds [27,28]. However, this is also the limiting factor of doppler ultrasound as a diagnostic tool and as such is a feasible explanation to the limited research undertaken in wounds in recent years.

Ultrasound as a diagnostic measures the dimensions of chronic wounds [17,29,30]. In addition, it has been used to measure skin thickness relating to the scar formation

formed in the proliferative phase [17]. However, it has a much lower resolution compared to OCT and CLMS [31]. This could be the explanation to a limited amount of research using ultrasound as a diagnostic methodology for wound healing in recent years.

2.2.2.4 Laser doppler velocimetry and imaging (LDV and LDI)

Laser Doppler has also been adapted to measure the blood flow through the instantaneous velocity. It works by sending a laser beam towards the biotissue under study and collects the reflected laser. A photomultiple tube detects the reflected light converting this energy into electrical energy, specifically current, used to measure the velocity [32].

Even though this technology is limited to blood flow, it has been widely adapted to monitor chronic wounds such as pressure ulcers, venous leg ulcers and burn wounds [125–127]. However, Kairinos et al. in 2014 did a study indicating flawed measuring techniques of LDV when the biotissue under study is compressed [128].

2.2.2.5 Thermography

Thermography uses a lens to focus the infrared radiation emitted by the biotissue. This radiation is scanned and processed by infrared detectors converting and correlating this energy into an equivalent temperature pattern. This is then converted into an electrical signal that undergoes signal processing to convert this information into an image. The emission is a representation relating the various colours displayed to the intensity of the infrared emitted by the biotissue.

Thermography is closely related to chronic wounds, specifically burn wounds and diabetic wounds and ulcers [129–132]. It has also been used to predict the oncoming of pressure ulcers [133]. However, thermography only provides information on the temperature that can be easily influenced by environmental factors and any surgical procedures, such as local anaesthesia which reduced the temperature [96].

2.2.2.6 Summary and limitations

A summary is presented in Table 2.3, where the diagnostic tools have been mapped to the associated research in wound healing. The condition of the wounds that have been monitored are firstly presented (acute/chronic) followed by the wound type. Followed by a list of the observed assessments mapped to the various phases involved in the wound healing process.

CLSM, OCT and thermography are currently the mostly adapted technology in studying the wound healing process; although, previous research into doppler ultrasound and LDV have effectively presented their application in burn wounds. Nevertheless, there are several drawbacks to these technologies. Firstly, these

methodologies require an expert to interpret the image for a diagnosis. In addition, the technology can be complicated and, in some instances, bulky thus making them costly and inconvenient for point-of-care applications. Moreover, the process in capturing the image and making a diagnosis can be slow. In many instances, another drawback is that the methodology simply focuses on the wound bed and peri-wound area. By adapting BIA as a diagnostic tool, the electrical properties of the wound can be analysed. Provided that electrical current flows through the body, there is an increased awareness of the body's physiology and its response to the disruption of the skin integrity. By monitoring the electrical properties from early on, it can be adapted for the prevention of poorly managed acute wounds transforming to chronic wounds. It's ability to monitor real-time electrophysiological properties has drawn much attention into its application as a diagnostic tool for monitoring the integrity of soft biotissue.

Table 2.3 Summary of non-invasive diagnostic tools.

| Non-Invasive Diagnostic Tool | Acute / Chronic | Wound Type | Assessment | Wound Phase |
|---------------------------------------|------------------------|---|--|--|
| Confocal microscopy | Acute and chronic | Burn, superficial and deep dermal skin wounds [10,13,122,123] | Blood flow, skin thickness, oedema, burn depth | Inflammation (vascularization, and formation of keratinocytes), proliferation |
| OCT | Acute and chronic | Burn, diabetic, surgical [20,25,26] | Oedema, skin thickness, scar types, wound size | Inflammation (vascularization), proliferation (re-epithelization, collagen deposition) |
| Doppler ultrasound and ultrasound | Acute and chronic | Burn, surgical, venous leg ulcers [27–30] | Skin thickness, scar types | Proliferation (collagen synthesis) |
| Laser doppler velocimetry and imaging | Chronic | Burn, diabetic, pressure ulcers, vascular pressure ulcers [125–127] | Blood flow | Proliferation (angiogenesis) |
| Thermography | Chronic | Burn, diabetic, pressure ulcers [129–132] | Temperature, oedema, burn depth | Inflammation, proliferation |

2.3 Bioelectrical Impedance Analysis (BIA)

The electrical properties of biological soft tissue are classified into passive responses (bioimpedance) and active responses (bioelectricity). Bioelectrical impedance analysis (BIA) is the measure of the tissue's resisting electric current flow. It is considered passive by cause of the conductive biological tissue responding to an external electrical current. Contrary to this, bioelectricity is active and electricity is conducted from ionic activities in the ICF and ECF [134,135].

Research into BIA for soft tissue is demonstrated using direct current (DC) and alternating current (AC) methodologies. Despite studies proving that DC analysis is efficient, AC is commonly adapted permitting current to flow through the body more easily [136]. Although BIA is commonly used with an AC source, research has proven that a DC source permits detection of inflammation [136]. DC current supplies a unidirectional constant current. For an AC circuit, the variation of the current over time is fed through a sinusoidal waveform thus signifying a switch in polarity including back and forth oscillations based on a frequency. Frequency refers to the number of times the waveform repeats over a time period of one second. For BIA, a discrete frequency is commonly applied namely single frequency BIA (sfBIA) [45,74,137–139]; although, a broad spectrum of frequencies, known as multi frequency (mfBIA) is vital in examining the current path through the ICF and ECF [80] differentiating the regions in soft tissue thus setting the foundation for spectroscopy, tomography, and bioelectrical impedance vector analysis (BIVA).

2.3 BIA for soft tissues

2.3.1 Frequency Classifications

The frequency for BIA is classified into α - β - γ dispersions. This is important in being able to differentiate the regions of soft tissue into three compartments [140]. Below 100 kHz, the frequency range of the α -dispersion is associated with the ECF. With the β -dispersion, frequencies ranging between 100 kHz to 10 MHz, the charge passes through the ICF and ECF; thus, cell health and integrity [141] can be detected. The γ -dispersion relates to a variety of tissues and protein solutions above 1GHz; a subsidiary dispersion effect (δ -dispersion) ranging from about 100 MHz to some GHz refers to polar subgroups of proteins and amino acids [140]. The α - β dispersions are applied to BIA measurements.

For BIA, α -dispersion and β -dispersion are classified as low frequency and high frequency current, respectively. A logarithmic frequency sweep is preferable in mfBIA, this could be due to the correlation of the distribution of frequency points to the occurrence of the largest changes in the dielectric properties [142]. This study indicates that by using a logarithmic scale, the frequency points are distributed

allowing for more points to lie within the frequency regions associated with greater variances in dielectric properties. The salt ions contained in the ICF and ECF give rise to a high conductivity activity in biotissues. In the α -dispersion range, the lipid membrane of cells acts as an insulator allowing the flow of current through the extracellular space resulting in a higher Z due to the lower ratio of ECF in the biotissue (refer to section Cells and action potential). For high frequencies found in the β -dispersion, the current passes the lipid membrane of the cell entering the intracellular space and continues through adjacent cells, passing through ECF and ICF, subsequently lowering Z due to the accumulation of conductive ions in both spaces [143].

To summarise, BIA can provide information on the properties, specifically the integrity, of the plasma membranes and cell volumes through the ECF and ICF in real time establishing non-invasive prognostic information as a diagnosis tool [144]. This information has led to the characterisation of biotissue in terms of electrical circuit modelling providing a more visible understanding of its structure and functionality [140,145–147].

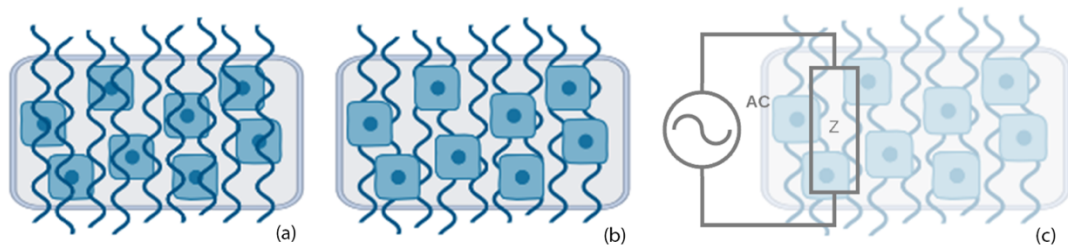


Figure 2.2 Current passing through (a) the ICF + ECF (β dispersion) and (b) the ECF (α dispersion) with (c) circuit equivalence of the methodology.

2.3.2 Electrical circuit models

Impedance is a complex measurement of the resistance of current flow in a conductor based on Ohm's law. Adapting BIA to a BUS, a conductive path is created allowing a charge to continuously move through it. A force initiates this flow of charge, where the force is referred to as the voltage (V) and the flow of charge is the current (I). When the charge flows through a conductor, such as the BUS, it often encounters an opposing force. For a DC circuit this is referred to as the resistance (R) while in an AC circuit this is the impedance (Z). Resistance and impedance are a quantity relative between two points. Ohm's law relates these three measurements depicted in Equation 2.1 and Equation 2.2 for DC and AC circuits, respectively.

$$R = \frac{V}{I} [\Omega],$$

Equation 2.1

$$|Z| = \frac{V}{I} [\Omega]. \quad \text{Equation 2.2}$$

Biotissues and cells can be represented through a collection of electrical components, specifically resistors and capacitors. Resistance measures the opposition of the flow of current through a conductor. A resistor is usually depicted by the geometry of a cylinder, refer to Equation 3.

$$R = \rho \frac{L}{A} [\Omega], \quad \text{Equation 2.3}$$

where: ρ represents the materials resistivity of the cylinder; L , the length; and A , the cross-sectional area.

A capacitor is a component that stores and releases charge. It is composed of two electrical conductors which store the charge and is separated by an insulator (dielectric material). By sending a current through a capacitor, it stores the charge until it is full resulting in the charge being released. A capacitor can be depicted as a cylinder or as a cube and cuboid. A cylindrical capacitor has a core conductive cylindrical plate, wrapped in an insulator and a conductive plate in its outer layer. A cube and cuboid capacitor are simple, consisting of an upper and lower conductive plate separated by an insulator.

A capacitors ability to store an electrical charge is measured in terms of capacitance. The associated capacitance formulae for the cylindrical and cube/cuboid capacitors are described by Equation 2.4 and 2.5, respectively.

$$C = \frac{2\pi\epsilon L}{\ln\left(\frac{r_o}{r_i}\right)} [F], \quad \text{Equation 2.4}$$

where: ϵ is the absolute permittivity of the dielectric material of the cylinder; L , the cylinders length; r_o , the radius measured from the centre of the capacitor (inner conductive plate) to the point where the outer conductive plate begins; and r_i , the radius of the inner conductive plate.

$$C = \epsilon \frac{A}{d} [F], \quad \text{Equation 2.5}$$

where: ϵ is the absolute permittivity of the dielectric material; A , the conductive plates area; and d , the distance in-between the two conductive plates.

For an AC circuit, reactance refers to the opposition of current flow relating to a capacitor and is depicted by Equation 2.6.

$$X_C = \frac{-1}{2\pi f C} [\Omega],$$

Equation 2.6

where f presents the frequency and C is the capacitance.

Fricke et al. [141] were the first to publish work on an electrical model of a biotissue using platinum electrodes for a frequencies between 800 Hz and 4 MHz, associated with the α - β dispersion. They proposed a circuit model for blood based on experimental data on blood in vitro that is commonly adapted in much of the current research. His model is represented by the cell membranes capacitance in series with the ICF resistance, parallel to the resistance of the ECF (Figure 2.3b).

Schwan et al. studied the polarization impedance of electrodes on a biotissue in vitro using a dipolar configuration with platinum electrodes for a frequency range between 0.01 and 100 kHz, correlating to the α -dispersion. From this model, they were able to explain the impact of this phenomenon on the capacitive and resistive properties of biotissue. The capacitive properties of biotissues are at a greater magnitude smaller than the resistive properties; thus, the electrodes polarization impedance greatly impacts the capacitance of the biotissue more than the resistance. Their model depicted a sample biotissue as a simple RC circuit in parallel [144] (Figure 2.3a).

In 1998, Gimsa et al. [148] further developed these models incorporating the frequency behaviour of dielectrophoresis and electrorotation of the β -dispersion (reaching 10 MHz) describing Maxwell-Wagner dispersions. Their model is based on a half model of a cell where the ECF and ICF are separated into branches. There is a branch to represent the ECF while another branch refers to ICF, this model takes into consideration the electrodes in a tetrapolar configuration (Figure 2.3c).

From the first model until now, variances of Fricke et al. [141] and Schwan's [144] models have been presented. Trung et al. [149] proposed that the current passing through the cell membrane was composed of the membrane capacitance in parallel to the cell resistance based on Schwan's model. The ICF is simply presented by a resistance in series to the two boundary RC circuits. This is in parallel to the resistance of the ECF. By simplifying the model, the resistance was considered negligible and this was transposed to Fricke's model. Fricke et al.'s simplified model is often referred to for simplicity and widely adapted to present the biotissues ECF, ICF resistance and cell membrane capacitance [149–153].

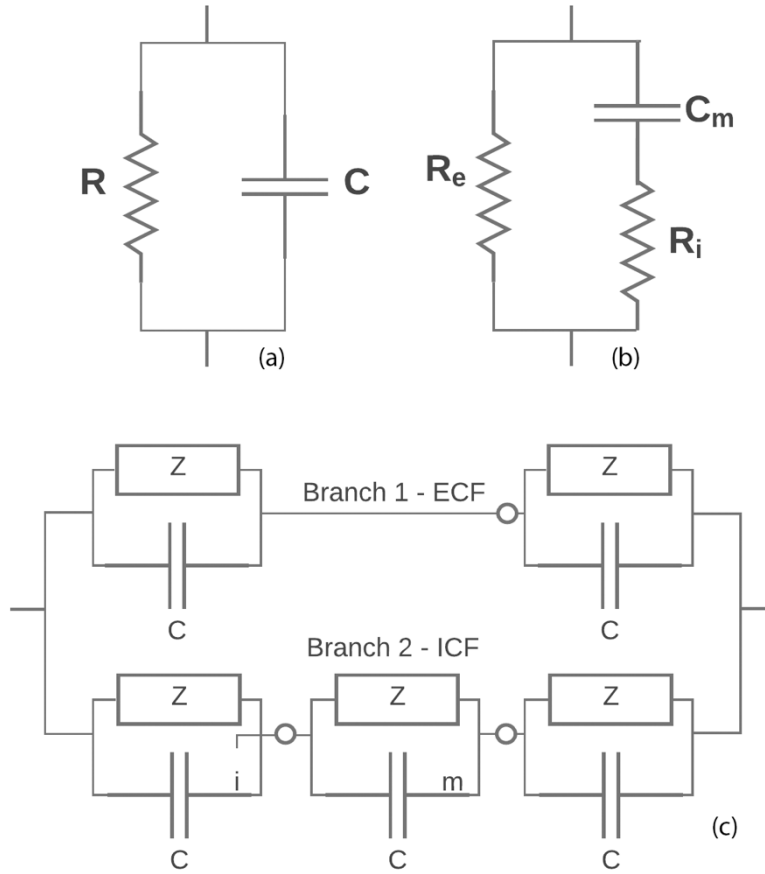


Figure 2.3 Equivalent circuit models (a) Schwan et al. [144], (b) modified Fricke et al. [141,149] and (c) Gimsa et al. [148].

These models represent a flow of electrons travelling through the salt ions in the ICF and ECF. A resistance is identified in the ECF (R_e) in addition to a resistance in the ICF (R_i) in series with a capacitor (C) that represents the capacity of the cell membrane. Through complex mathematical analysis, this can be simplified into an equivalent resistor and capacitor (RC) in series circuit [154].

Mylott et al. deduced the following equations [109]:

$$R_{eff} = \frac{R_e R_i (R_e R_i) + R_e C^2}{(R_e + R_i)^2 + C^2} \quad \text{Equation 2.7}$$

$$X_{Ceff} = \frac{R_e^2 C}{(R_e + R_i)^2 + C^2} \quad \text{Equation 2.8}$$

For the remainder of this paper, R_{eff} and X_{Ceff} will be referred to as R and X_C . Representing the BUS as an RC circuit in series, the impedance (Z) is determined as a total resistance of the two components described mathematically by Equation 2.9. Equation 2.10 represents the phase angle (φ) which is the delay between the electric potential and current waveform. This relates to the cell membrane integrity and the body cell mass. φ strongly correlates to a resistive behaviour if it approaches 0, or a capacitive behaviour if it approaches -90° . A typical RC circuit is characterised as a

complex vector located in the fourth quadrant in the cartesian system. From this vector graph, the relationship between R , X_C , Z and φ can be clearly presented. This provides the basis for the Cole-Cole plot [155].

$$|Z| = \sqrt{R^2 + X_C^2} \quad \text{Equation 2.9}$$

$$\varphi = \tan^{-1} \left(\frac{X_C}{R} \right) \quad \text{Equation 2.10}$$

2.3.3 Cole – Cole model and plot

The circuit derived by Fricke et al. [141] can be transformed into a Cole-Cole equivalent circuit model for a frequency sweep. This is represented in term of the BUS's performance as a short circuit and an open circuit, represented by R_0 and R_{inf} respectively. Typically, this model is represented by a resistance that is equivalent to the difference between R_0 and R_{inf} in parallel with a constant phase element and in series with R_{inf} [156]. The constant phase element represents the non-ideal capacitance of the cell membrane. This model has been adopted to the Fricke model, and is commonly referred to as the Cole-Fricke-Cole model [157–160] (Figure 2.4a).

Lafargue et al. [161] extended the Cole-Cole (Cole-Fricke-Cole) model based on whole body experimental measurements for a frequency ranging between 1 – 250 kHz. This model is depicted by the ICF resistance in series with the cell membrane capacitance in parallel to a node with a resistance in series with an inductor which is parallel to the resistance of the ECF [148]. Comparing the Extended Cole-Fricke-Cole (ECFC) and Cole-Fricke-Cole (CFC) model to the experimental data, the discrepancy was significantly reduced by the ECFC model (Figure 2.4b). Despite this model not accurately representing the experimental data, it was observed that the frequency threshold was reproducible.

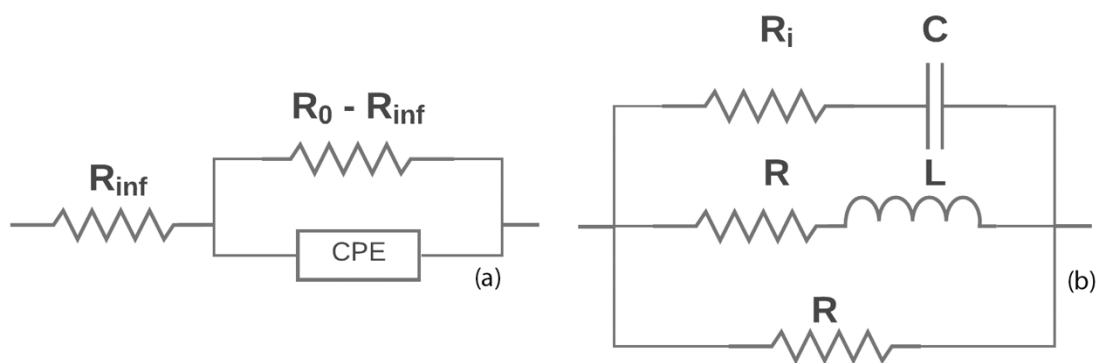


Figure 2.4 Equivalent circuit models (a) Cole-Fricke-Cole [162] and (b) Extended Cole-Fricke-Cole [161] .

The Cole-Cole circuit model is the basis for plotting mfBIA measurements. This plot is named after the model, the Cole-Cole plot and is equivalent to a Nyquist plot, Argand and Wessel diagram. It plots the measured R and X_C on the x and y axis respectively across the frequency sweep from low to high. By plotting R against X_C on a Cole-Cole plot, the characteristic frequency (f_c) can be determined where the maximum reactance occurs [163] relating to the capacitance pole (where the capacitance reaches a maximum). From this, the associated R and X_C for f_c are obtained. Moving across the Cole-Cole plot, R and X_C can be obtained for any frequency. This applies only to mfBIA where a frequency sweep is applied. The advantage of the Cole-Cole plot is that two Bode plots can be visualised on one plot, relating to R and X_C .

From the electrical circuit model representations, the plot is in the fourth quadrant where R is a positive integer and X_C is negative. For simplicity, the Cole-Cole plot is commonly presented in the first quadrant; however, the reactance should be recorded as a negative value [155] as shown in Figure 2.5.

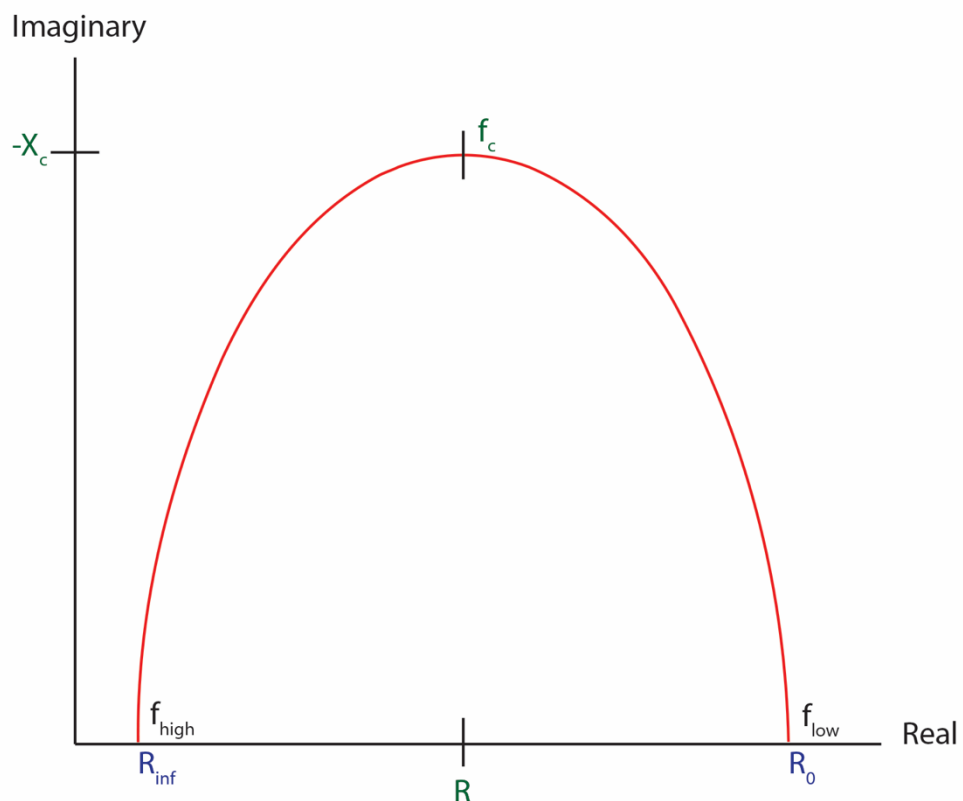


Figure 2.5 Cole Cole plot.

2.3.4 Equipment

Various specialised equipment can be used to measure body impedance. Impedance analysers are commonly adapted in research; however, LCR bridges and potentiostats associated with electronics and the latter electrochemistry can be adapted. Most commercial BIA systems developed for total body weight (TBW) measurements are limited to a single current although they provide more information relating to biotissues. The ImpediMed SFB7 is commonly used for BIA; for use in sfBIA and mfBIA. In mfBIA R and X_C are visualised in a Cole-Cole plot where an algorithm is applied to form a smooth contour fitting these measurements. From this contour the characteristic frequency is located, and its associated parameters are identified, refer to Table 2.4.

Table 2.4 BIA parameters of SFB7

| BIA Parameter | Measurement | Unit |
|---------------|--|----------|
| R | Resistance | Ω |
| X_C | Reactance | Ω |
| f_c | characteristic Frequency | kHz |
| Z | Impedance | Ω |
| φ | Phase Angle | $^\circ$ |
| $R_e (R_0)$ | Extracellular Resistance (Resistance at 0 frequency) | Ω |
| R_{inf} | Resistance at infinity | Ω |
| R_i | Intracellular Resistance | Ω |
| M_C | Membrane Capacitance | pF |
| Rad | Radius | Ω |

Freeborn et al. [164] studied the accuracy of an SFB7 compared to the Keysight E4990A by testing various resistors ranging from 1 to 50 Ω for frequency ranges including: (i) 3 – 10 kHz, (ii) 10 – 100 kHz and (iii) 100 – 1 MHz. For resistors between 10 and 50 Ω , its relative accuracy for the frequency ranges were: (i) 1%, (ii) 1% and (iii) 5%. However, it was concluded that SFB7 is suitable for local BIA applications. In addition, it was shown to be insensitive to temperature ranges from 10 $^\circ\text{C}$ to 35 $^\circ\text{C}$.

2.3.5 Bioimpedance analysis on soft tissue damage

Although a vast amount of research into monitoring soft tissue adapt sfBIA, current research is directed into mfBIA. These two methodologies have been studied as a diagnostic tool to monitor muscle gap and injuries [137–139,165], fractures [166], tissue abnormalities [74,167–169], diseases [134], inflammation [44] and wounds [36,38,40,45,170]. For this review, recent research (dated from 2007 onwards) in BIA for soft tissue integrity was tabulated and presented in Tables 2.5 and 2.6. Table 2.5 presents the research undertaking in monitoring injuries, muscle gap, oedema and blood flow while Table 2.6 is specifically for wounds. Figure 2.6 presents the timeline of when BIA was initially adapted in research where the study of soft tissues began on muscles in 2007.

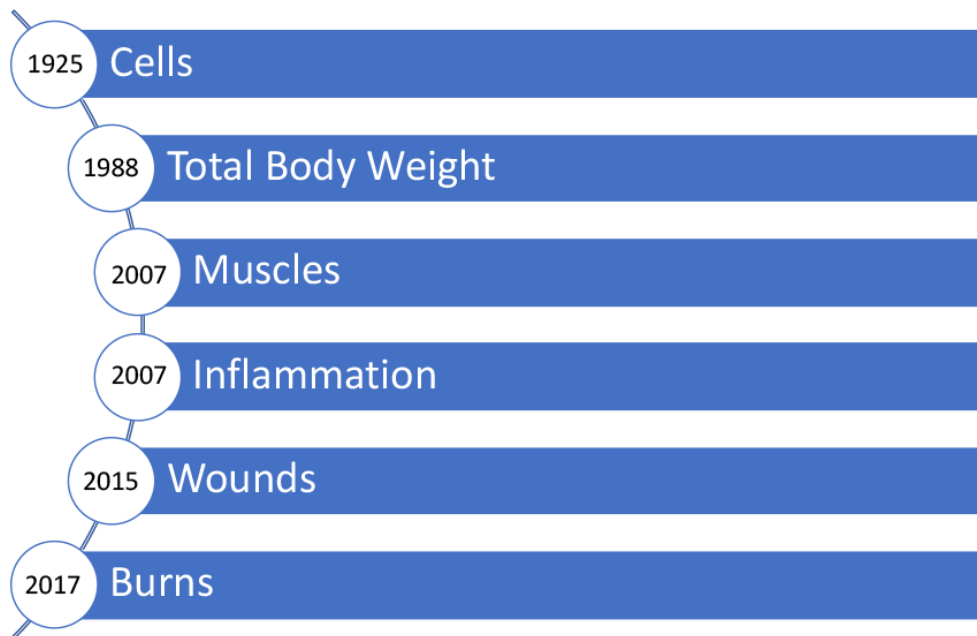


Figure 2.6 BIA timeline.

Table 2.5 BIA diagnosis for injuries, muscle gap, oedema, blood flow

| Author | Bartels, Sorensen and Harrison [163] | King, Clamp, Hutchinson and Moran [44] | Nescolarde, Yanguas, Lukaski, Alomar, Rosell-Ferrer and Rodas [137] | Nescolarde, Yanguas, Lukaski, Alomar, Rosell-Ferrer and Rodas [138] | Nescolarde, Yanguas, Terricabras, Lukaski, Alomar, Rosell-Ferrer and Rodas [139] | Hui and Petrofsky [136] |
|--------------------------------|---|--|--|---|---|---|
| Hypothesis | mfBIA can detect contralateral differences in muscle mass | BIA of the lower limb measuring swelling from an acute ankle fracture | Muscle injury indicates a lower R , X_c and φ in localised BIA relative to the injury severity; analysing return to play (RTP) | Change in BIA parameters, 24 h after muscle injury relative to injury severity diagnosed by objective radiological assessment | Muscle injury severity relating to muscle gap that can measure return to play (RTP) | Determining muscle injury using direct current and microcurrent |
| Subjects | | | | | | |
| i. n | i. 3 (S1-S3) | i. 14 | i. 3 (S1-S3) | i. 21 | i. 22 | i. 34 (healthy n = 24; injured n = 10) |
| ii. Subject Description | ii. Human | ii. Human | ii. Human | ii. Human | ii. Human | healthy n = 14 – blood flow testing; healthy n = 10 – reliability testing; injured n = 10 |
| iii. Anamnesis | iii. S1 healthy; S2 Inflammation of the Achilles tendon in the right leg over a period of 1.5 years; S3 Suffered minor muscle injury in the right leg 2 | iii. Isolated closed ankle fracture sustained in the preceding 5 days with no history of significant swelling, disease, injury, or surgery of either leg | iii. S1 Grade III muscle injury – post trauma caused hematoma requiring surgical drainage and double fasciotomy; S2 Grade II muscle injury - partial detachment of medial head of the calf | iii. 21 muscle injuries: 11 grade I, 8 grade II and 2 grade III | iii. 22 muscle injuries (myotendinous or myofascial): 12 hamstrings, 6 rectus femoris, 3 adductor longus and 1 gastrocnemius Grade II (n = 7): small area of oedema, (<10% | ii. Human iii. Sprained ankle with visible swelling around one ankle only |

| | | | | | | |
|------------------|--------------------------------|---------------|--|----------------|--|---------------|
| | weeks prior to the measurement | | from its common aponeurosis with the soleus, hematoma present in MRI; S3 Grade I muscle injury – strain | | of cross-sectional area (CSA) of the muscle affected and < 5cm of craniocaudal length); no gap | |
| Reference | Uninjured leg | Uninjured leg | Localized BIA was determined at major muscle sites of the lower limb 30 min before a training sessions, 24 h after injury, and during recovery until medical | Uninjured limb | <p>Grade IIa (n = 8): moderate amount of oedema, (10-50% of CSA and 5 – 15 cm of length); with a feather like image and no gap</p> <p>Grade IIb (n = 7): moderate amount of oedema, (10-50% of CSA and 5 – 15 cm of length); with a feather like image and gap</p> | Opposite limb |

| | | | | | | |
|--|---|--|--|---------------------------------------|---------------------------------------|--|
| | | | clearance to return-to-play (RTP) | | | |
| Equipment | ImpediMed SFB7 | BODYSTAT DualScan 2005 | AKERN-Srl BIA-101 | AKERN-Srl BIA-101 | AKERN-Srl BIA-101 | Prototype Zone Finder from Mettler Electronics |
| Current | | | | | | |
| i. Source | i. AC | i. AC | i. AC | i. AC | i. AC | i. DC |
| ii. Current Supply | ii. 250 μ ARMS | ii. | ii. 400 μ ARMS | ii. 400 μ ARMS | ii. 400 μ ARMS | ii. 9 V |
| Frequency | i. mfBIA | i. sfBIA | i. sfBIA | i. sfBIA | i. sfBIA | N/A |
| i. sfBIA / mfBIA | ii. 256 frequencies between 4 kHz and 1000 kHz; detailed analysis was performed at 50kHz (α dispersion) | ii. 5 kHz (α dispersion) and 200 kHz (β dispersion) | ii. 50 kHz (α dispersion) | ii. 50 kHz (α dispersion) | ii. 50 kHz (α dispersion) | |
| ii. Frequency / Frequency Range | | | | | | |
| Electrodes | S1 | | | | | |
| i. Poles | i. Tetrapolar | i. Tetrapolar | i. Tetrapolar | i. Tetrapolar | i. Tetrapolar | i. Dipolar |
| ii. Size | ii. 10 mm \times 25 mm | ii. 5 cm ² | ii. | ii. | ii. | ii. |
| iii. Material | | iii. | iii. Ag/AgCl (3M Red Dot Adult Solid Gel | iii. Ag/AgCl (COVIDIEN Ref. 31050522) | iii. Ag/AgCl (COVIDIEN Ref. 31050522) | iii. Cotton pads soaked with 0.9% saline |

| | | | | | | |
|------------------|--|---|--|---|---|--|
| iv. Placement | iii. Platinum + conductance paste (Ten20, Weaver & Co) | iv. Proximal electrode was placed lateral to the tibial tubercle, with a second placed 7.5 cm distal. The most distal electrode was placed on the dorsum of the foot at the base of the second toe, with the remaining electrode 7.5 cm proximal to this. | Electrode 2239) + Stainless Steel Snap | iv. Voltage sensors (V) placed 5 cm proximally and 5 cm distally from the centre of injury, and the source and sink electrodes positioned close to the others | iv. Voltage sensors (V) placed 5 cm proximally and 5 cm distally from the centre of injury, and the source and sink electrodes positioned close to the others | iv. Blood flow testing 2.54 cm at 226.8 g pressure (i.e., the cuff was inflated to 200 mmHg to create ischemia), reliability testing: 2.54 cm and 5.08 cm between the probes |
| | iv. Over m. Gastrocnemius; current electrodes placed outer-most and voltage-sensing electrodes 10 mm inside away from them | | iv. Anatomical landmarks were identified by palpation and reference distances as follows: A. Calf: 5 cm (I) and 10 cm (V) distally from the popliteal line and proximal from the posterior intermalleolar line B. Proximal hamstrings: 5 cm (V) proximally and distally to the point of maximum pain and injecting electrodes (I) were positioned adjacent to the others | In vastus intermedius where the muscle is anatomically deeper, voltage sensors (V) placed 10 cm proximally and 10 cm distally from the centre of the injury and source and sink electrodes (I) were placed close to the others In adductors where the injury is close to the groin, voltage sensors (V) placed 5 cm medially and 5 cm laterally from the | In vastus intermedius where the muscle is anatomically deeper, voltage sensors (V) placed 10 cm proximally and 10 cm distally from the centre of the injury and source and sink electrodes (I) were placed close to the others Centre of the injury was determined by ultrasound | Injury testing: 2.54 cm separation with 2.2 N pressure |
| | S2 | | | | | |
| | i. Tetrapolar | | | | | |
| | ii. 44 mm × 22 mm | | | | | |
| | iii. Ag/AgCl (Ambu Blue Sensor N) + integrated gel | | | | | |
| | iv. Over m. Gastrocnemius | | | | | |
| | S3 | | | | | |
| | i. Tetrapolar | | | | | |
| | ii. 49 mm × 33 mm | | | | | |

| | | | | | | | |
|--------------------------|---|--------------------------------------|--|--|--|---|--|
| | iii. Ag/AgCl (Ambu Blue Sensor SU) + conductance paste (Ten20) | | | centre of the injury and current source and sink (I) close to the others | | | |
| | iv. Over m. Gastrocnemius | | | Centre of the injury was determined by ultrasound | | | |
| Stance Parameters | Standing, supine, sitting – feet free on floor, sitting – feet touching floor | Supine | Supine for 15 min before BIA measurement – room temp 22°-24° | Supine for 15 min before BIA measurement – room temp 22°-24° | Supine for 15 min before BIA measurement – room temp 22°-24° | Sitting with knees extended, allowing easy access to feet | |
| BIA Parameters | $Z, R, X_C, \varphi, f_C, R_e, M_C, R_i$ | Z | R, X_C, φ | R, X_C, φ | R, X_C, φ | μA | |
| Repeated | 6 times with a 1 sec interval | 1 time for injured and uninjured leg | S1 24h post trauma 13 days post-surgery 16 days post-surgery 30 days post-surgery 75 days RTP S2 | | | Opposite limb | |

| | | | | | | |
|------------------------|---|--|--|--|--|--|
| | | | 24h post trauma | | | |
| | | | 13 days | | | |
| | | | 20 days | | | |
| | | | 30 days RTP | | | |
| | | | S3 | | | |
| | | | 24h post trauma | | | |
| | | | 5 days | | | |
| | | | 9 days RTP | | | |
| Reference Point | Area Circumference Method | Area Circumference Method, Area Photograph Method, Volume Displacement Method | MRI | MRI | MRI | |
| Conclusion | 1. Ag/AgCl electrodes showed reduction in BIA parameters (Z , R , X_C and φ), SU type + conductance paste found to be the least effective | 1. Injured group: Z was lower in the injured leg compared to uninjured leg 2. BIA correlated best with the water volume displacement method followed by | 1. The greater the severity of muscle injury the greater the R , X_C and φ 2. R , X_C and φ do not reach same levels as prior to injury | 1. R indicates the ECF and electrolyte composition, X_C indicates the cell membrane mass and function and φ the cell membrane vitality | 1. Increase in severity predicted greater decrease in L-BIA measurements 2. Increase in X_C indicates epidermal | 1. Blood flow response to five minutes of occlusion, after occlusion blood flow increases by at least fifty-fold showed a slight decrease in μA and did not change significantly for 30 |

| | | | | | |
|---|---|---|--|---|--|
| <p>2. Changing subjects position relating to stance parameters, BIA results increased (Z, R, X_C and φ)</p> <p>3. φ adapted being independent of body mass and size</p> <p>4. Through circumference measurements injured legs for subjects #1 and #2 were slightly atrophied</p> <p>5. Low R in relation to Z indicates oedema</p> | <p>circumference and photographic cross-sectional methods</p> <p>3. Unable to demonstrate correlations between the fracture mechanism, classification, or time from injury and any of the measurements of swelling, possibly because of the small sample size</p> <p>4. Lower Z implies oedema</p> | <p>3. Subject #1, R reduced 24 h post injury then 13 days post-surgery returned to normal due to the fluid drainage</p> <p>4. Decrease in X_C related to damage to integrity of muscle structures; decrease in R related to fluid accumulation</p> | <p>2. Reduction on the three parameters due to injury X_C and φ - the more severe the injury the greater the reduction, although for R, grade II injuries showed a greater reduction to grade I, yet grade III showed less reduction to grade II although $n=2$ for grade III; GIII.I had a 20.6% decrease and the GIII.II only had a 7.5% decrease; where GIII.I decreased more than most grade II samples</p> <p>3. Amount of oedema on the MRI indicative of severity of injury is debatable, since oedema has been present at the time of RTP; in contrast, X_C could be a more</p> | <p>proliferation and granulation</p> <p>3. R proportional to the fibrin clot and epithelialization and indicates successful wound healing</p> <p>4. The greater the φ the healthier the cell membranes</p> <p>5. Significant changes in X_C more important to muscle injury than R and φ</p> | <p>seconds after cuff was deflated; little change observed in the short period of time of occlusion and after blood flow was restored</p> <p>2. Probe separation created insignificant differences</p> <p>3. Measurements over injured areas decreased</p> <p>4. μA independent from blood flow</p> <p>5. Increase in R in ischemia tissue due to hypoxia from increased inflammation from increased metabolic activity and decreased blood supply; not due to oedema</p> |
|---|---|---|--|---|--|

**s-subject*

sensitive and specific
indicator

6. Increase in pressure
of probes altered
results

7. Some factors that
influence this current
flow were the DC
current which may not
overcome the
resistance of the skin

Table 2.6 BIA diagnosis for wounds

| Author | Lukaski, Moore [45] | Kekonen, Bergelin, Eriksson, Kaartinen, Viik [37] | Kekonen, Bergelin, Eriksson, Vaalasti, Ylanen, Viik [38] | Kenworthy, Phillips, Grisbrook, Gibson, Wood, Edgar [43] | Kenworthy, Grisbrook, Phillips, Gittings, Wood, Gibson, Edgar [42] |
|--|---|---|--|---|---|
| Hypothesis | BIA to monitor cellular processes involved in wound healing | Z ratio of control and wound to monitor wounds, as wound heals Z ratio approaches 100% | Z ratio of control and wound to monitor wounds, as wound heals Z ratio approaches 100% | R and ρ will increase with oedema related to burn wound healing | |
| Subjects | | | | | |
| i. n | i. 3 | i. 1 | i. 4 | i. 28 | i. 28 |
| ii. Subject Description | ii. Human | ii. Human | ii. Human | ii. Human | ii. Human |
| iii. Wound Type | iii. S1 Chronic Wound; S2 Post-surgical wound and skin graft; S3 Infected wound (methicillin-resistant Staphylococcus aureus (MRSA) | iii. Post-surgical wound after breast reconstruction – horizontal wound extending from surface to deep fascia | iii. S1 Needle puncture; S2 Epidermal scratch; S3 Epidermal scratch; S4 Post-traumatic wound | iii. Minor limb burns (<5% TBSA) | iii. Minor limb burns (<5% TBSA) |
| iv. Wound Size; | | iv. | iv. S1 DM 0.35, D 5; S2 DM 0.3, D dermis; S3 DM 0.3, D dermis; S4: L:W:D 70:20:dermis/subcutis | iv. Superficial partial thickness (n=9), mid dermal (n=11), deep partial thickness (n=6) and full thickness (n=2) | iv. Superficial partial thickness (n=9), mid dermal (n=11), deep partial thickness (n=6) and full thickness (n=2) |
| L-length, W-width, D-depth, DM-diameter; mm | iv. L:W:D S1 19:17:2; S2 25:25:100; S3 25:25:4 | | | | |

| | | | | | |
|--|--|--|--|---------------------|---------------------------------------|
| Reference Point | | Healthy skin close to wound | Healthy skin | | |
| Equipment | Quantum IV, RJL Systems | Solartron 1294A, 1260 FRA | Solartron 1294A, 1260 FRA | SFB7 | SFB7 |
| Current | i. AC | i. AC | i. AC | i. AC | i. AC |
| i. Current Source | ii. 800 μ ARMS | ii. 0.4 VRMS | ii. 0.4 VRMS | ii. 250 μ ARMS | ii. 250 μ ARMS |
| ii. Current Supply | | | | | |
| Frequency | i. sfBIA | i. 1 Hz – 1 MHz | i. 10, 100, 1 k, 2.5 k, 6.3 k, 10 k, 25 k, 40 k, 63 k, 100 k | i. sfBIA | i. sfBIA |
| i. sfBIA / mfBIA | ii. 50 kHz | ii. | ii. | ii. 3 kHz -1000 kHz | ii. 3 kHz -1000 kHz |
| ii. Frequency / Frequency Range | | | | | |
| Electrodes | i. Tetrapolar | i. Tetrapolar | i. Dipolar | i. Not mentioned | i. Tetrapolar |
| i. Poles | ii. | ii. | ii. 16 x 19 mm | ii. | ii. |
| ii. Size | iii. | iii. | iii. Ag/AgCl | iii. Ag/AgCl | iii. Ag/AgCl |
| iii. Material | iv. Outer distal current source and sink placed | iv. 4 cm apart – one pair (V source and V sensor) on | iv. Local – measurements not specified | iv | iv. a. whole body electrode placement |
| iv. Placement | 10mm adjacent to inner distal voltage sensors that | both sides of wound | | | |

| | | | | | |
|--------------------------|---|---|---|---|--|
| | are located on the edge of the wound | | | | b. whole limb segmental placement c. voltage sensors localised on longitudinal axis and current source and sink (drive electrodes) on foot and hand |
| Stance Parameters | Supine | Supine | Not specified | Supine | Supine |
| BIA Parameters | R, X_C, φ | Z ratio between wound and control | Z ratio between wound and control | R_0, R_{inf}, R_i | R_0, R_{inf}, R_i |
| Follow Up | 24 hrs S1 – 40 days S2 – 80 days, placement of graph about day 18 S3 – 125 days | 5 measurement points per decade - every 3 days over a 9-day period, starting from first postoperative day | S1 – 1 day S2 – 6 days S3 – 23 days S4 – 93 days (147 control) | | Initial measurements within 96h of injury, within 14 days |
| Reference Point | | | Visual assessment (photography) | Limb segment volume | Limb segment volume |
| Conclusion | 1. S1 serial changes in parameters. General pattern longitudinal increase in R, X_C and φ | 1. Ratio adapted for this analysis approaches 100% as the wound heals | 1. S1 Needle puncture: lowest frequency results in | 1. φ and R_i not significantly associated with wounds | 1. Localised electrode positioning most valid |

related to uncomplicated healing. Relative to increased cell mass, epithelialization and decreased ECF.

2. S2 Serial changes in parameters. Short term decreases following skin graft followed by increase.

3. Serial changes in parameters. Infections increases ECF and decreases cell numbers.

4. R is inversely proportional to ECF and directly proportional to cell mass.

5. X_c increases through proliferation and granulation while decreasing with infection.

6. φ proportional to cell membranes integrity.

difference of Z from ratio (10 Hz)

2. S2 – S3 Epidermal scratch: initial stages of wound healing (days 2-3) frequencies above 1 kHz indicated variance

3. On completely healed wound, ratio approaches 100%

2. R_{inf} , R_0 increase as wounds heals

2. R_0 , R_{inf} decreased over time, R_i did not change

2.3.6 Summary

A general correlation between the primary BIA parameters (R , X_C , Z , φ) and the healing process of soft tissue has been identified. It has been observed that Z and R are closely related to the inflammation of a region where low Z and R values are indicative of oedema and an early stage of wound healing. R , X_C and φ are commonly grouped together given that an increase in the φ corresponds to an increase in R and X_C signifying a reduction in oedema [38,142]. Moreover, φ has been associated with chronic wounds and diseases [43,45]. An increase in R_e and R_i with a decrease of M_C denotes cellular repair of the tissue fibres.

2.4 Adaption of electrodes for BIA systems

2.4.1 BIA systems

A BIA system is composed of differential amplifiers [171,172] connected to coupled biopotential electrodes. It sends an electric charge penetrating the skin enabling impedance analysis of soft tissue. Thus, the electrodes link the skin to the BIA system by creating an interface. The measurements of the biosignal are influenced by the electrode-skin impedance. A difference in electrode-skin impedance reduces the common mode rejection ratio (CMRR) of the system resulting in excessive noise [49]. In addition, high skin electrode impedances (Z_{es}) can cause signal attenuation and distortion. A difference in Z_{es} between the coupled electrodes causes an electrode mismatch referred to as 'hook artefact' and occurs at high frequencies. This can be visualised on the Cole-Cole for mfBIA. A hook artefact can influence the smooth contour fit of the BIA algorithm resulting in flawed measurements [50,173–175] (Figure 2.7).

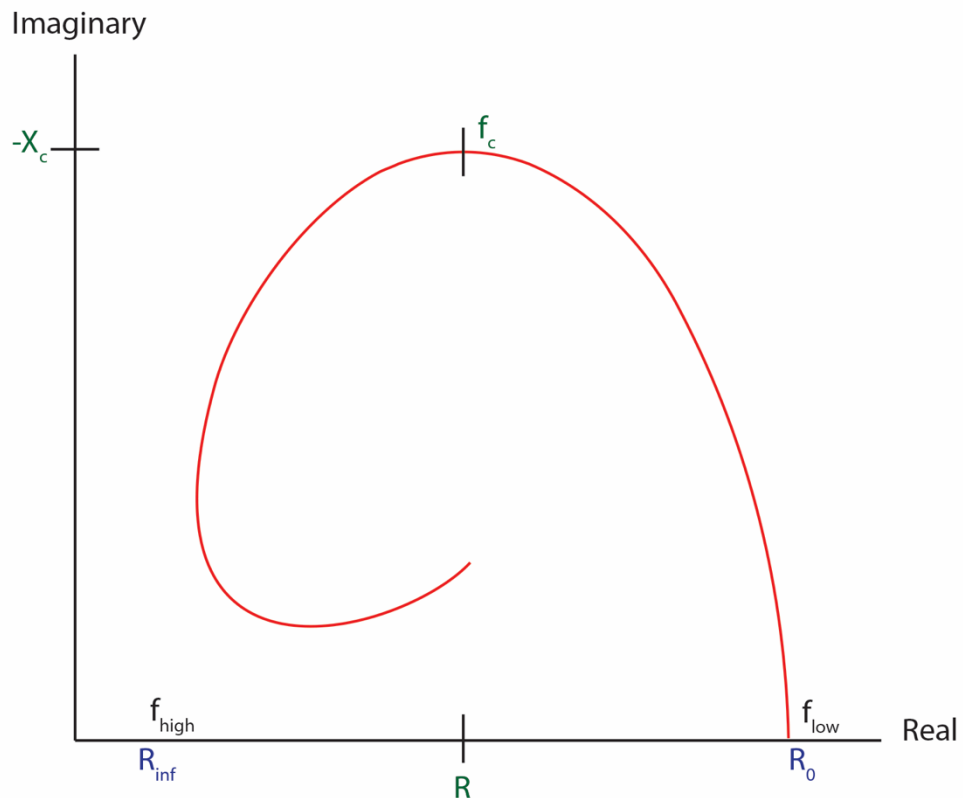


Figure 2.7 Cole Cole plot with hook artefact.

The positioning of the electrodes is another variable that has yet to be standardised in local BIA measurements. Smirnov et al. [176] specifies the spacing between the distal and proximal current injecting electrodes influences the penetration depth of the current into the body. Therefore, by varying this distance it is hypothesised that there is a possibility that a different BUS is measured. However, an inconsistency in electrode positioning is common in previous research.

In addition, it is important to identify that commercial BIA systems have been designed for to measure total body weight (TBW). Thus, the electrodes are explicitly positioned to allow for whole body measurements. Manufacturers of the equipment suggest the electrodes are positioned at a great distance on the body, for example one set close to the wrist and the other close to the ankle. To measure limbs researchers have adapted segmental positioning where the electrodes are proximally and distally placed on the limb under study. However, in order to measure targeted areas on the body, local BIA positioning is used where there is a minimal space between the electrodes. Thus, this variation from the manufacturer's suggestions could influence the electrode mismatch in the experimental protocol.

2.4.2 Electrodes

An electrode is a conductor used for electricity to enter or leave the BUS. For BIA measurements, the electrodes act as current injecting electrodes and voltage sensors. The former can be classified as current carrying electrodes (CC) and the latter, pick up electrodes (PU). These current-carrying electrodes (CC) transmit an exogenic signal and the biopotential difference generates an endogenic signal received from the pick-up electrodes (PU). The CC electrodes consist of a current source (I+) and current sink (I-) required to supply and receive the charge while the PU electrodes are considered voltage sensors that measure the potential difference. Local BIA requires the electrodes to be positioned locally at two contact sites surrounding the BUS and as the current penetrates through the skin, it passes through the ICF and ECF depending on the frequency range. The electrical activity of the BUS is monitored through the biopotential difference.

2.4.3 Electrode configuration

There are two common types of coupled electrode configurations, tetrapolar and dipolar (Figure 2.8). In a tetrapolar configuration, a pair of electrodes act as the current source (I+) and current sink (I-) and a separate pair of voltage sensors are positioned adjacent to and in between the source and sink. This configuration is common in whole body analysis such as measuring TBW and has been accepted in various local BIA applications including monitoring of wounds, muscle injuries and inflammation [35,40,44,45,137–139,163]. However, some researchers have simplified this into a dipolar configuration [36]. For a dual electrode setup, one electrode acts as a current source (I+) and voltage sensor while the other acts as a current sink (I-) and voltage sensor [177]. The electrodes adapted for BIA are wet electrodes commonly used in clinics, while dry electrodes emerged in the last few years.

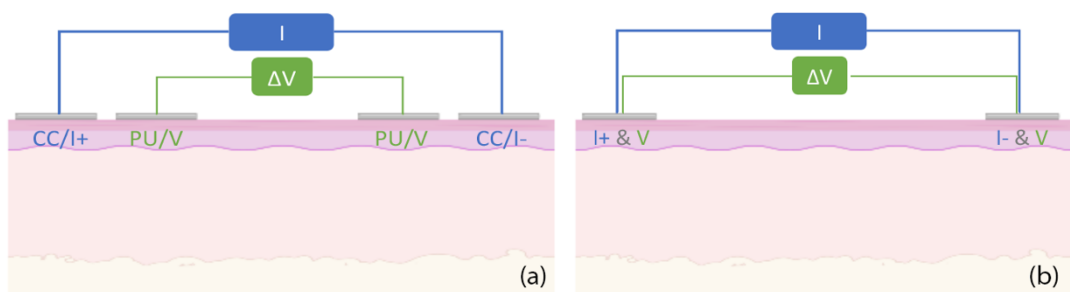


Figure 2.8 Electrode Configurations (a) tetrapolar and (b) dipolar.

2.4.4 Wet and dry electrodes

Electrodes can influence the accuracy of BIA measurements due to the electrode-skin interface. Current clinical electrodes commonly used in clinics, specifically Ag/AgCl, are classified as wet electrodes [47]. These electrodes are produced with an additional layer consisting of an electrolyte 'gel', specifically agarose. This gel allows the electrode a non-polarized attribute [178]. Thus, they are versatile and can be used across all systems regardless of the operating frequency of the system. This 'gel' layer also enhances the performance of the electrophysiological recordings through a redox reaction that switches from an electronic current in the leads to an ionic current that is transmitted through the epidermis to the BUS [179]. The electrolyte layer ensures stable electrical contact while minimising electrode-skin impedance where the electrode-electrolyte interface is negligible [180].

However, these electrodes have certain drawbacks limiting their performance in long term monitoring applications. Firstly, thorough preparation of the skin is required including removal of any hair and grime for the electrodes to adhere to the skin and perform efficiently [181]. In addition, its adhesive layer can irritate the skin [182]. However, its greatest hindrance is due to the drying of the adhesive layer leading the detachment of the electrodes from the subject over a long period [182]. Thus, resulting in an unstable redox reaction leading to unreliable measurements. Therefore, these electrodes are inappropriate for use in long term applications and need to be substituted.

2.4.4.1 Dry Electrodes

Dry electrodes differentiate from wet electrodes as they do not have an electrolyte layer and come into direct contact with the epidermis [51]. Recently, much research has been directed into the fabrication and application of dry electrodes to resolve the common issues of wet electrodes for various biosignal measurements. However, dry electrodes possess a polarization impedance [47,51,52,183,184] that can increase the Z_{es} .

The electrode-skin impedance is a continuous issue relative to biosignal measurements that has yet to be overcome. A large electrode-skin impedance can impact the quality of the biological signal implying low signal amplitude and low signal to noise ratio (SNR) [53,54]. In addition, the BIA measurements at high frequencies can be affected due to Z_{es} mismatch [175,185]. This could be contributed from instrumentation artefacts or uncontrolled electrode parameters [47]. Even though research has been undertaken in examining the degradation of wet electrodes, much interest has motivated the study into fabricating and adapting dry electrodes to replace wet electrodes. The first types of dry electrodes were rigid and were quickly surpassed with flexible and e-textile electrodes. Rigid electrodes are based on the

manufacturing of solid metals. Flexible and e-textile electrodes have various fabrication methods. Their use is common in ECG, EMG, EEG measurements while e-textiles has also been adopted for transcutaneous electrical nerve stimulation (TENS), refer to Figure 2.9. Figure 2.10 presents a mind map for the aspects covered in the research currently conducted for dry electrodes. Figure 2.11 is an analysis of the literature review covered in this thesis on dry electrodes.

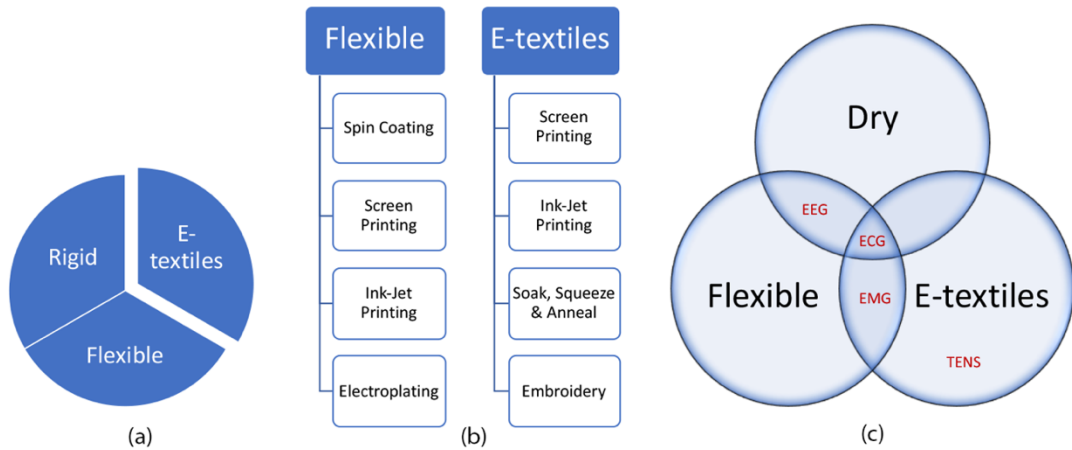


Figure 2.9 Dry electrodes (a) types of dry electrodes, (b) fabrication methods for flexible and e-textile electrodes and (c) uses of dry electrodes.

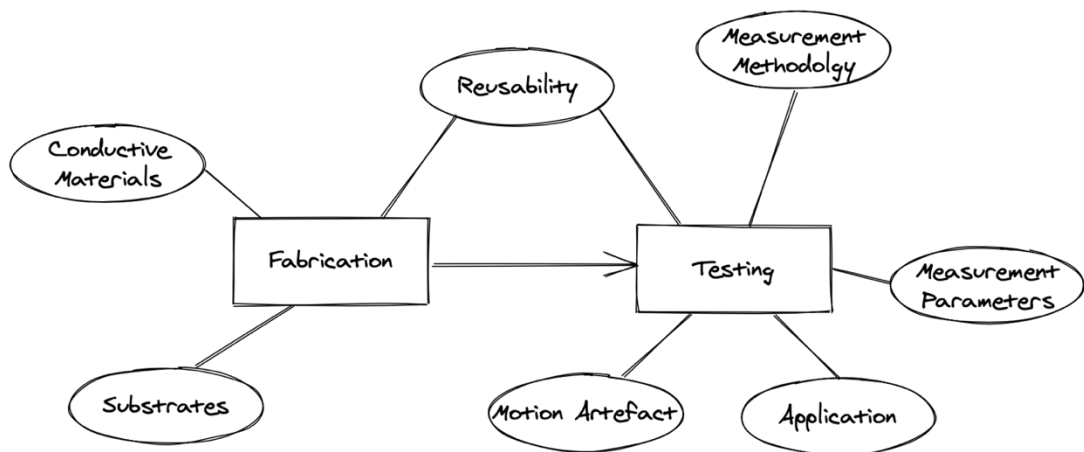


Figure 2.10 Mind map of aspects covered for dry electrodes in literature review.

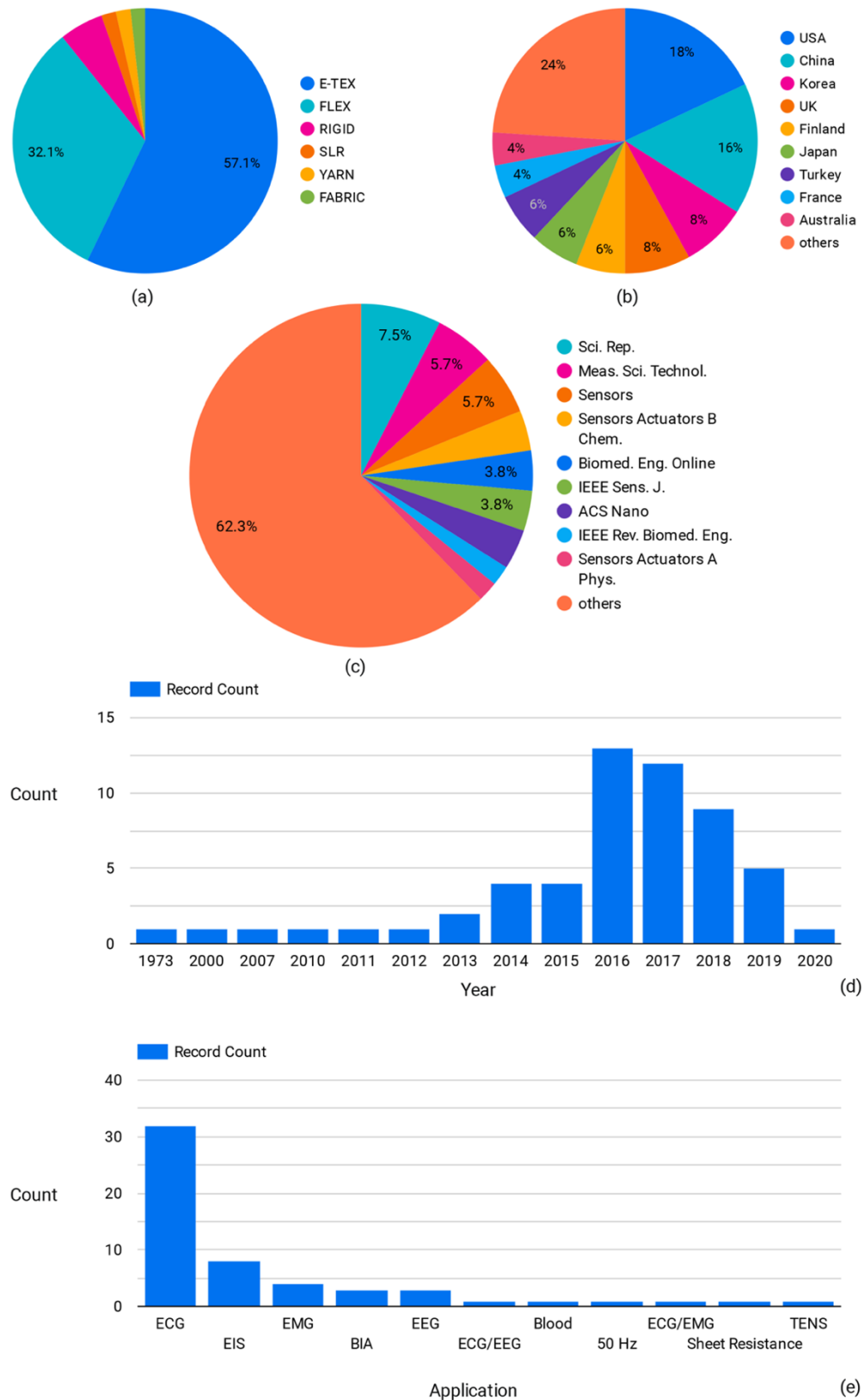


Figure 2.11 Literature review of dry electrodes in thesis, including: (a) type of electrodes, (b) countries conducting research, (c) journals publishing articles, (d) number of articles relative to year of publication and (e) dry textiles testing methods.

2.4.4.2 Rigid electrodes

Wiese et al. [186] compared the relationship between motion artefact and degraded wet electrodes to dry electrodes by defining a protocol and creating an algorithm for ECG applications. Exposing the wet electrodes to high temperatures of air caused the degradation and their behaviour in this state imitated the dry electrodes. The protocol was tested on subjects following specific movements. However, a conclusion was drawn that this was not a viable tool and future research will require a new algorithm that compares the differences in the actual ECG signal. Suggestions on improving motion artefact include the use of accelerometers to measure electrode motion and adaptive filters to cancel motion artefact [187,188].

Albulbul [178] compared commercial pre-gelled Ag/AgCl with dry orbital and stainless steel electrodes for a frequency ranging between 1 Hz and 1 MHz. The coating of the orbital electrode is an alloy of Ag/AgCl, Al, Au/AuCl, Ni and Ti. These selected materials permit it to last longer than the clinical Ag/AgCl electrodes. For stable contact on the skin, the shape is prepared with pins (spikes). Stainless steel is resistant to corrosion thus these types of electrodes are favourable. However, Ag/AgCl electrodes proved to be more efficient having the lowest skin impedance yet providing the highest capacitance between the electrode and skin.

Searle et al. [189] compared pre-gelled Ag/AgCl with dry and insulating electrodes from Ti, Stainless Steel and Al with a diameter of 12 mm at a single frequency of 50 Hz. The Ag/AgCl were analysed without any modifications whilst a buffer was integrated to the dry and insulating electrodes. The purpose of this buffer was to minimise the contact impedance mismatch by lowering the impedance of the electrodes thus forming an 'active' electrode. This contact impedance was referred to and as such comparable to powerline interference. The impedance mismatch for the wet paired electrodes (Ag/AgCl) is negligible contrary to the dry electrodes where it significantly increased. Additionally, by pairing a wet electrode with a dry electrode the powerline interference was substantial implying that the electrodes must be identically paired. To overcome the issue of powerline interference, an additional circuit can manually reduce the mismatched contact impedance [189,190]. It was observed that the contact impedance did not vary significantly between the dry. Although Ag/AgCl initially had the lowest contact impedance, after a 600 second period the contact impedance for the dry electrodes were comparable to the wet electrodes. However, by shielding the electrodes the dry and insulating electrodes performed better than the wet electrodes.

Chi et al. [55] studied non-contact, insulated and dry electrodes by presenting their electrical models. This review focuses on the signal quality relative to noise and motion artefact whilst incorporating the issue of comfort. Chi et al. supporting Searle et al. [189], concluded that with time the motion artefact for dry electrodes is

reduced; this may be due to perspiration hydrating the skin acting as the electrolyte layer of the wet electrodes. Clinically used wet electrodes are convenient as the electrolyte layer permits the fixation of the electrode at the desired location. However, for applications managing continuous monitoring, the gel of the wet electrodes will dehydrate therefore losing its efficiency and causing skin irritation. This research is limited to ECG and EEG applications.

2.4.4.3 Flexible electrodes

Printed electrodes on flexible substrates can perform efficiently due to their form that can adapt to the body shape thus reducing any motion artefact [56–58,191]. In addition, by modifying the surface morphology, dry electrodes can maximise the advantage of skin moisture as substitute to irritant gels [59,192–194].

Imani et al. [195] fabricated a skin-worn Chem-Phys hybrid wearable patch interfaced to a custom-PCB offering concurrent and real-time monitoring of ECG and lactate via wireless transmission. The hybrid patch consisted of biosensors measuring the lactate concentration in addition to electrodes for ECG monitoring. Experiments revealed that the two modalities can be measured simultaneously when co-fabricated on a flexible substrate with negligible cross talk. To validate the electrodes, the ECG signals were compared with commercially available Ag/AgCl electrodes. Screen-printing technology was used to fabricate the Chem-Phys hybrid patch. An arrangement of Ag/AgCl, Prussian blue and insulator inks were printed on a highly flexible transparent polyester substrate by using customized stencils. Interference and shunting effects of the hybrid patch were minimized by printing two vertically orientated hydrophobic layers of Ecoflex next to the biosensor. Through vigorous exercise, the ECG recording was affected by perspiration.

Peng et al. [196] fabricated a flexible dry Ag/AgCl electrode that overcomes the drawbacks of wet and dry electrodes. The intricate process used parylene C as a substrate deposited with a layer of chromium and copper (Cr/Cu); Ag was electroplated onto the Cr/Cu layer. A dry Ag electrode film was fabricated at this stage. In addition to the first electrode, by adding chloride to the Ag layer, a dry Ag/AgCl electrode film was produced. By altering the surface topology, an additional three electrodes were derived of varying in sizes (i.e., E1, E2 and E3); they consisted of Ag/AgCl micro pads protruding from the Ag layer. This raised layer works with the moisture of the skin eliminating the need for a gelled electrolyte. For the three samples, the size of the electrodes was kept constant; however, the radius and distribution of the AgCl pads varied altering the AgCl to Ag area ratio (AR). Comparing the three electrodes, an increase in R and AR showed a reduction in electrode-skin impedance. With an AR of 38.5% and r measuring 50 μm , E3 showed results comparable to commercial electrodes. By testing the two electrodes over a period of 48 hours at 100 Hz, the skin-electrode impedance of E3 decreased after 1 hour and

remained relatively stable for the remaining period proving to be more efficient than the commercial electrode. However, for this first hour the commercial electrode generated a lower skin-impedance which increased substantially thereafter. These electrodes were used for ECG and EEG measurements.

Khan et al. [197] developed mechanically flexible electrode arrays on free standing flaps. This complies better to wounds where the electrodes need to conform to a surface with cuts. A gold compound was deposited onto a PEN substrate encapsulated with a hydrophobic thin layer of Crypto to avoid interference from bodily fluids. O₂ plasma etching was used to expose the 31 electrodes then CO₂ laser cutting was used to cut and create electrode flaps. The spacing between the electrodes ranged from 2 to 7 mm. Gold was selected due to its stability and inertness when it comes into contact with biological fluids or living tissue. The nanoparticle ink was deposited onto the PEN substrate and sintered at 200 °C. Sheet resistance of the electrodes were low range from 0.28 to 0.36 Ω sq⁻¹. Furthermore, the change in resistance was negligible when the electrodes were placed under stress and strain.

2.4.4.4 E-textiles electrodes

The advancement of wearable technology has placed focus on the development of e-textile electrodes [55,198,199] for various applications. There are various methods in the production of e-textile electrodes. Conducting polymers deposited onto textiles have been developed by dip-coating, screen and inkjet printing. These methods are simple and cost effective. In addition, technological advancements in the textile industry introducing conductive yarns has led to the fabrication of woven and embroidered e-textile electrodes.

The advantage of textile electrodes is that they maintain conformal contact with the human body. However, the application of conducting polymers on textiles may give rise to dermatological issues such as skin irritation when in contact with the skin for a long period of time [63]. Contrary to this, embroidered electrodes are entirely based on yarn. In addition, they are convenient and allow for onsite fabrication and can be tailored to the patient's ailment.

Takamatsu et al. [60] presented a method for depositing a conducting polymer on thick knitted textiles for ECG applications. A polydimethylsiloxane (PDMS) stencil was laser cut to create the pattern, in turn this was placed onto the knitted textile and the stencil was filled with the conducting polymer poly(3,4-ethylenedioxythiophene)-poly(styrenesulfonate) PEDOT:PSS forming the electrode. An ionic liquid (IL) gel was added acting as an electrolyte for the electrode. PDMS was selected as a stencil due to its hydrophobic properties confining the PEDOT:PSS solution. PEDOT:PSS was selected due to its efficiency in cutaneous applications and biocompatibility. PEDOT:PSS electrodes of 1 cm² were patterned on knitted polyester 300 μm with a

stretch of 50% in the knit direction. The measured sheet resistance was 230 Ω/sq . The prototype was tested on a wristband and the results were compared to the clinical Ag/AgCl electrodes on three subjects. A comparison of the electrodes indicates the textile electrode to be superior by producing a lower electrode-skin impedance with an equal SNR. In addition, the combination of PEDOT:PSS/IL gel with the conformable support provided by the knitted textile showed to mitigate motion artefacts. This was used for ECG measurements.

Bihar et al. [61] fabricated fully printed PEDOT:PSS/IL gel electrodes on commercially available pantyhose (100% wt, polyamide) using inkjet technology and tested with ECG recordings. Pantyhose was chosen as a substrate offering great stretchability; PEDOT:PSS was chosen as the conductive layer due to its high conductance and biocompatibility [200]. ECG recordings were taken from one subject. Initially the number of printed layers required for efficiency was determined by evaluating the resistance of the electrodes. This resulted in a printed electrode of eight layers of PEDOT:PSS. Although the printing increased the rigidity of the textile, it could still be stretched up to 200%. Cyclic strain tests were performed in order to evaluate durability; it was concluded after 50 cycles the electrode showed stability at 30% strain. By adding five layers of IL gel, the electrode displayed an impedance spectrum comparable to a commercial wet Ag/AgCl. Moreover, the stretchability improved showing a decrease in the change in electrical resistance at large elongations. The SNR remained constant for the first 24 hours although after 40 days slight degradation was observed. However, the commercial electrode did not record any signal after a period of 12 hours.

Jin et al. [62] studied the efficiency of inks applicable to printing on a PU stretchable substrate and a 30-denier tricot knit nylon textile. Initially drawing attention to the two substrates, it was concluded that the ink stabilizes more efficiently on the textile showing cracks on the PU substrate under strain. A control of the ink permeation resulted in the fabrication of the stretchable textile electrode with a sheet resistance of 0.06 $\Omega \text{ sq}^{-1}$. This increase about 70 times when the textile was stretched to 450% strain. Moreover, the resistance changes to the textile were negligible under vertical pressure, twisting and folding. The conductive ink is comprised of a fluoroelastomer (PVDF-HFP), butyl carbitol acetate (BCA) and silver flakes. PVDF-HFP contributes to the softness of the composite; whilst BCA has a high boiling point (247) and low vapour pressure (0.01 mmHg) resulting in a penetration depth of 231 μm reaching the junction points of fibre bundles. Electrical and mechanical properties of the textile were stable even after 220 days in air which is promising for long term monitoring. A demonstration of the stretchable printed textile showed its potential as electrodes for an EMG monitoring system. Using the conductive ink, transmission lines and electrodes were printed onto the compression garment; thereafter, thermoplastic polyurethane (TPU) layers were laminated on both sides of the

transmission lines preventing any contact. By comparing the e-textile with commercial Ag/AgCl electrodes, the e-textile shows promising for EMG recordings.

Contrary, Karim et al. [63] evaluated a nanoparticle synthesis substrate (NP1) as a base printed onto a woven cotton textile for Ag and rGO electrodes thus preventing permeability. Surface pre-treatment of NP1 was found to be optimum with 12 layers whereas the conductive compounds only required 6 layers. For the pre-treated textile, a sheet resistance for Ag was found to be $1.18 \Omega \text{ sq}^{-1}$ whilst for rGO the resistance was $1.09 \times 10^3 \Omega \text{ sq}^{-1}$. These electrodes were adapted for ECG recordings and shown to have a lifespan of 10 laundry washing cycles.

Paul et al. [64] presented a wearable patch of an array of networked dry passive electrodes fabricated via screen and stencil printing. To ensure stable contact pressure, the patch was sewn onto a vest with a silicon foam insertion in between. It was tested against commercial Ag/AgCl for ECG recordings. Screen printing was used to fabricate the electrode pads and tracks onto a woven textile. The process required a polyurethane (PU) interface layer of $30 \mu\text{m}$ on the textile in which a $5 \mu\text{m}$ layer of silver conducting ink was printed; a final layer of PU encapsulated the tracks. Electrode pads were stencil printed with carbon black loaded silicone rubber. This material was selected due to its flexibility, being water resistant whilst having a low surface energy. In comparison to commercial electrodes, the ECG recordings of the vest were comparable to those with using Ag/AgCl electrodes.

Sinha et al. [201] tested screen printed PEDOT:PSS electrodes onto a t-shirt composed of 85% polyester. PEDOT:PSS was selected due its ability to function as an ionic and electronic conductor making it suitable as a dry electrode. However, the signal improved with the onset of perspiration or by applying a lotion. Moreover, an elastic strap was required to increase the skin contact with the electrodes in order to minimise motion impedance. A sheet resistance of $0.5 \Omega \text{ sq}^{-1}$ was found. By testing the t-shirt with ECG recordings, it was observed to have a higher amplitude compared to the Ag/AgCl electrodes. This could be due to the increase in motion artefact from the t-shirt that is alleviated by the Ag/AgCl electrodes.

Pani et al. [65] fabricated PEDOT:PSS electrodes via a soak, squeeze and anneal method using woven cotton and polyester swatches. A snap fastener was sewn onto the swatches using conductive thread. The swatches were then sewn onto non-conductive foam in order to alleviate any influence on the biopotential reading from the skin. Polyester showed to be more promising as an electrode and was used to test under dry and wet conditions; the latter moistened with 0.9% saline solution. By sending a current of 1.0 mA for a frequency range of 20 to 250 Hz with a 5 min delay, an ECG reading of the two electrodes was compared to commercial Ag/AgCl electrodes. Testing was conducted with the subject in a state of rest, deep breathing and exercise. At rest, the dry electrode performed as well as the wet and Ag/AgCl;

however, when the subject was in motion the dry electrodes failed to perform due to motion artefact. To conclude the wet electrode performed slightly better than the Ag/AgCl, although after a few hours the saline evaporated thus performing as a dry electrode.

Kannaian et al. [53] embroidered electrodes for ECG measurements. A 100% polyester woven textile was used for the embroidery of stainless-steel electrodes measuring 11 mm x 11 mm. By using a constant satin stitch, the stitch densities were tested. To measure the electrode efficiency, the embroidered electrodes were tested relative to clinical Ag/AgCl electrodes on human skin using a multimeter. An impedance of 1.4 M Ω was measured. By adapting the electrodes for ECG recordings, a SNR of 31.46 db was observed; this was identical for the two densities. Thus, the measurement remains efficient in terms of SNR despite reducing the conductive thread used in the embroidery process by 50%.

Shafti et al. [202] employed embroidered electrodes for sEMG (surface EMG). By varying the area, iteration and density of the electrodes, the resistance was measured using a multimeter. It was observed that an electrode with a 2 cm diameter, 2 iterations and 2 mm, 5 mm or full spacing (density) showed the lowest mean impedance. This research demonstrates by increasing the area, decreasing the iterations and increasing the density a lower resistance is achieved. The EMG measurements using the embroidered electrodes were comparable to the common clinical electrodes.

Weder et al.'s [203] ECG electrodes were embroidered from polyethylene terephthalate yarn plasma-coated with silver and a titanium layer on top for passivation. Electrode pads measuring 2 x 7 cm were embroidered into an ECG belt. ECG measurements were carried out for Ag coated and Ag/Ti coated dry and wet electrodes. Dampening the dry electrode with water vapour combined with silver and titanium resulted in optimum ECG electrodes. A flexible water tank was added to the belt to provide continuous vapour. However, this system is complicated and requires a constant supply of water.

Berk et al. [204] tested embroidered electrodes for TENS application. A 100% polyester textile was used to embroider the electrodes using silver conductive fibre Shieldex 235/34 dtex. By maintaining a constant size for the electrodes (i.e., a circle of diameter 3 cm), the stitch type and density varied. Four stitch types were tested, such as fill, satin, star and zigzag with high and low densities. To measure the electrode efficiency, the resistance of 16 points on the electrode surface were recorded using a multimeter before investigating the SNR of the TENS electrodes. Based on the results, the low-density star stitch electrodes showed the lowest resistance of 0.42 Ω whilst the highest was measured for the satin stitch. Moreover, it was observed that the stitch density is relative to the resistance, specifically, the

lower the stitch density, the lower the resistance. However, when testing the electrodes with a TENS system, the satin stitch showed higher SNR. Pertaining to low resistances, low stitch densities demonstrated higher SNR.

Trindade et al. [205] embedded embroidered textiles for ECG recordings in fitted t-shirts with compression bands to support the electrodes. The electrodes were embroidered with Ag coated PA66 thread in a circular shape of 16 mm in diameter. It was observed that when the subject was not in motion, the ECG recordings were efficient with a low SNR; however, when the subject was in motion, the readings were greatly affected. It was also shown that by laundering the t-shirts 30 times the electrode resistance and ECG SNR did not alter significantly.

This was also observed by Cho et al. [206] when adapting various e-textile electrodes for ECG recordings in a t-shirt. A knitted e-textile electrode from a 50/50% stainless steel/cotton forming a single jersey textile (Type B) was compared to an embroidered electrode in a labyrinth shape on this jersey e-textile electrode as a substrate (Type C) and on a cotton substrate (Type C). It was observed that Type A and Type C were comparable to the ECG recording, while Type B did not perform as well. However, it was concluded that due to inconsistent pressure across the t-shirt there was an inconsistency in ECG recordings. Moreover, the signal can be influenced by motion and any changes in posture.

2.4.4.5 Summary and limitations

Research into dry electrodes for ECG, EMG, EEG and TENS applications has shown promising long-term medical applications. Even though for some dry electrodes, an electrolyte layer has been incorporated into the design to assist the redox reaction. Various measuring methodologies have been employed testing the efficiency of the dry electrodes resulting in an inconsistency of parameters. Sheet resistance is often applied to measure 2D materials, while multimeters used provide resistance and impedance measurements.

However, incompatible observations are reported when the electrodes are tested on a subject. Testing the electrodes on a subject can be influenced by changes in certain properties of skin including skin temperature and perspiration. Provided that these properties differ for each subject it is difficult to identify how the electrodes perform autonomously. Although, the research undertaken showed a consistency in the comparison of dry electrodes and wet electrodes over a long period. Initially, wet electrodes performed better; however, over a period of time the performance of the dry were comparable and in some instances performed better. In addition, e-textile electrodes have the advantage of being washable and reusable signifying cost efficiency and are environmentally friendly. The limitations of research associated with e-textile electrodes are presented in Table 2.7.

Table 2.7 Limitations and potential research

| Limitations | Reason | Potential Research |
|--|--|--|
| Measurements on e-textile electrodes - parameters (R, sheet resistance) | Methods adapted to measure dry electrodes only apply for 2D structures E-textile electrodes are 3D in structure | Dry electrodes possess a reactance and resistance influencing Z_p |
| ECG, EEG, TENS, EMG measurements | Systems operate at a low frequency (0.5 – 1000 Hz) – negligible effect on Z_p dry electrodes | BIA applications use larger frequency (50 kHz) |
| E-textile electrodes with no electrolyte layer | No comparison of e-textile electrodes in dry form and wet form | Comparing Z_p of dry electrodes to dry electrodes with an electrolyte layer |
| Independent influence of embroidery characteristics | No analysis on all possible embroidery characteristics | Influence of combined embroidery characteristics on Z_p |
| Skin temperature and perspiration | No analysis of isolating the influence of skin properties on Z_p of e-textile electrodes | Influence of skin temperature and perspiration on Z_p |
| Influence of elliptical vs rectangular shape for BIA | Comparison of shape on e-textile electrodes and influence on Z_p | Does shape influence Z_p |
| Efficacy of e-textile electrodes compared to wet electrodes for studies adapted to monitoring wound healing using BIA over a time period | Comparison of e-textile electrodes to Ag/AgCl electrodes has not been completed in-vivo or ex-vivo | Are the parameters adapted to monitor wounds influenced by Z_p of the e-textile electrodes (i.e., Z , R , X_C , ϕ , R_0 and R_{int}) |

Chapter 3

Equipment, Materials and Methodology

3.1 E-textile electrode fabrication and testing

3.1.1 Embroidery Machines

3.1.1.1 Singer Future XL 550

The SINGER Futura XL 550 (Singer Corporation, Tennessee, United States) is an electronic computerised embroidery machine featuring a 210 x 120 mm embroidery area. Its primary electronic onboard feature used for this study was the thread tension setting while the bobbin thread tension was manually adjusted. It has a USB port where a USB key storing the embroidery design can be inserted directly or permitting direct connection to a computer where the design can be transferred from any supporting software to the embroidery machine.



Figure 3.1 Singer Futura XL 550

3.1.1.2 Brother F440E Embroidery Machine

The Brother F440E Embroidery Machine (Brother Australia, New South Wales, Australia) is an electronic computerised embroidery machine featuring a 130 x 180 mm embroidery area. It features a touch panel and touch sensor stitch select display screen displaying all embroidery information. Its USB port allows for all embroidery designs to be easily transferred using a USB. This equipment does not connect to a computer and designs must be saved to a USB device and transferred through the USB port.



Figure 3.2 Brother F440E Embroidery Machine

3.1.1.3 Software EasyDesign EX and Embrilliance

The EasyDesign EX (Elna International Crop. SA, Geneve, Switzerland) software was adapted to design the electrodes for the Singer machine while the Embrilliance (BriTon Leap, Inc, Albuquerque, New Mexico, United States) was used for the Brother machine. Both software packages have built in designs allowing users to select the shape and with the package features a user can alter the stitch characteristics of the electrodes. The primary characteristics associated with the e-textiles are: (i) the size (surface area), (ii) stitch type, (iii) stitch length and (iv) stitch density (stitch spacing). Due to the basic design of the electrodes, the two software packages provided the same functionality for this research.

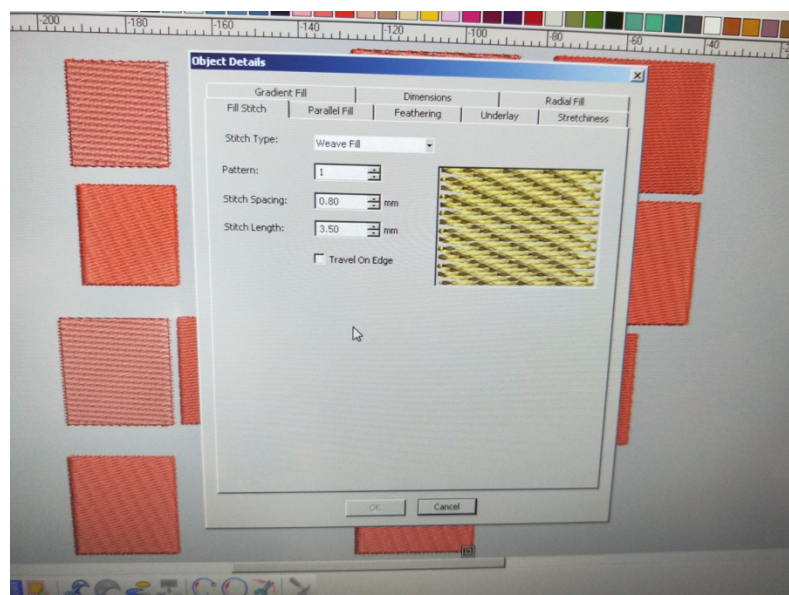


Figure 3.3 EasyDesign EX with the weave stitch settings on display

3.1.2 Electrical Impedance Measurements Equipment for Embroidered E-Textiles (Voltage Drive)

3.1.2.1 HM8118 LCR Meter (Rohde & Schwarz, Munich, Germany)

The HM8118 LCR Meter with four terminals connected to a set of Kelvin probes. It has the capability of measuring the common impedance parameters, specifically impedance (Z), resistance (R) and reactance (X_C) for frequencies ranging between 20 Hz to 200 kHz. The accuracy according to its specifications is 0.05%. It features an option of setting an equivalent circuit of the measured test, this was set to automatic. The AC test signal level is 50 mVrms to 1.5 Vrms with a resolution of 10 mVrms.



Figure 3.4 HM8118 LCR Meter

3.1.2.2 PM 6306 LCR Meter (Fluke Australia Pty Ltd, New South Wales, Australia)

For the PM 6306 LCR Meter with four terminals, two plug-in adapters were used creating the same effect as the Kelvin probes. Its test frequency ranges from 50 Hz to 1 MHz. Its AC test signal level is 50 mVrms to 2 Vrms with a resolution of 10 mVrms.



Figure 3.5 PM 6306 LCR Meter

3.1.3 Materials for E-Textiles

3.1.3.1 Substrates - Textiles

For this study the most common textiles in the textile industry were selected to evaluate their suitability as substrates for e-textile electrodes. The substrates were purchased commercially. The selected substrates include a polyester non-woven felt and cotton substrates of various structures: plain weave, poplin and velvet.

3.1.3.2 Shieldex 117/17 dtex 2ply Thread

The Shieldex Conductive Yarn is a polyamide 6.6 filament plated with 99% pure silver. Silver Plated Nylon (Ag/PA66) 2x117/17 dtex (Shieldex U.S., Palmyra, NY, United States and Statex Produktions and Vertriebs GmbH, Bremen, Germany). The linear resistance of this thread provided by the manufacturer is about 1,500 Ω /m for a specified linear density of $28.0 \pm 3\%$ tex (refer to Appendix I for textile units). It has a linear density of about 35,000 m/kg with a tenacity of about 44 cN/tex $\pm 5\%$. It possesses high electrical performance with a linear resistance of about $< 1,500 \Omega$ /m. Another advantage is that the thread is composed of silver which is known to have anti-fungal, antimicrobial and anti-inflammatory properties [207]. Thus, it can be adapted for long-term monitoring without causing irritation to the skin which is a major concern with current Ag/AgCl electrodes.



Figure 3.6 Shieldex 117/17 dtex 2ply Thread

3.1.4 Methodology E-Textiles

3.1.4.1 E-textile electrode fabrication

The fundamental material providing conductivity to the e-textile electrode was the Shieldex Conductive Yarn. To account for efficient e-textile electrode functionality, the silver thread needs to touch the skin thus this forms the inner-side of the e-textile electrode. In addition, by encapsulating the conductive thread in the electrode-skin contact, the electrode is less susceptible to noise. Due to the stitching structure (Figure 2, Appendix I), if the conductive thread was used on the outer-side of the e-textile any noise from the external environment would be transmitted to the inner-side resulting in unreliable measurements. Thus, a non-conductive polyester (PES) thread was selected for the outer-side of the electrode. Adapting a PES thread results in a reduction in manufacturing costs without compromising its performance. It is more cost efficient compared to the silver plated nylon thread and it reduces the fabrication time by improving the tension parameters on the embroidery machine.

To select a PES thread, its linear density must be relatively close to the linear density of the conductive thread.

A denier count wrap reel was used to measure the actual linear density of the conductive yarn. The measurement was in accordance with specification, measuring 29.5 tex. This was matched with a strong 100% PES non-conductive thread with a measured linear density of 39.8 tex (refer to Appendix I for textile units). To begin the fabrication process, the embroidery machine had to be adjusted and set to create e-textile electrodes that correspond to the standards ISO 4915:1991 301 implying an equivalent stitch is created on both sides of the textile (i.e., top and bottom) [208].

Due to the coarseness of the conductive thread, it was threaded through the bobbin compartment forming the inner-side of the electrode, while the polyester thread was threaded through the needle to create the outer-side of the electrode. For the e-textile electrodes to perform efficiently, the importance of having a non-conductive outer-side and a conductive inner-side was reported. However, it is also important that the conductive thread does not loop on the outer-side as this may result in noise. Thus, it is vital that: (i) the linear density of the two threads are relatively close and (ii) the bobbin and needle thread tensions are balanced. The relatively close linear densities of the threads assisted in the tension balance between the bobbin and needle thread settings and set-up of the embroidery machine. It is important to ensure an ideal balance so neither thread pulls the other thread through the substrate and all interlocks occur within the substrate, refer to Figure 2 in Appendix I, resulting in an ideal fabricated e-textile electrode.

To resolve the small tolerance error associated with the embroidery machine, a 'trial and error' approach was taken to set up the required tension balances (to calibrate the embroidery machine) by embroidering a rectangle of dimension 4 x 3.3 cm (surface area of 13.2 mm²) based on standard clinical Ag/AgCl electrode size [48]. The elliptical electrodes were fabricated with an equal surface area. For simplicity, the default stitch settings of the software were used (i.e., stitch type, length and density: weave, 3.5 mm, 0.4 mm) which were later adapted in Chapter 4. Provided the Ag/PA66 is a coarser thread in comparison to the PES, it is expected for the bobbin to have more of a pull on the thread; thus, the initial e-electrodes stitch interlocks occurred on the conductive side of the electrode. To balance the tension, a trial and error approach was taken by continually increasing the tension of the needle thread from the electronic settings of the embroidery machine while mechanically loosening the tension of the bobbin thread manually (this can only be done manually and there is no relative measurement of tension provided by the machine) resulting in an increase in the mechanical pull of the needle thread. For the Brother F440E, this was achieved with the functionality of the embroidery machine. Regarding the Singer Future XL 550, by setting the needle tension thread to a maximum and reaching the

minimal tension of the bobbin thread, a slight improvement was profound. However, the interlocks were still occurring on the conductive interface indicating the tensions were still unbalanced. To resolve this issue, it was obvious that more tension was required for the needle thread. Thus, an additional thread tensioner was built for the needle thread consisting of tension discs with added weights to increase the tension. The ideal balance was found through trial and error resulted in an additional 42.12×10^{-3} kg to these tension discs. In order to maintain this balance, it was observed that the amount of thread spooled onto the bobbin needed to remain relatively consistent. Thus, prior to embroidering each electrode a full bobbin was inserted into the bobbin compartment to maintain the ideal tension settings.



Figure 3.7 Shieldex 117/17 dtex 2ply Thread

To enable the connection of probes to the e-textile electrodes for measurements, commercially available snap-fasteners with a 9 mm diameter were mechanically attached in the centre of the e-textile in accordance with standard clinical Ag/AgCl electrodes. The snap fasteners constituted of a ball part and a ring with spikes stabilising the ball part. A single snap fastener was added to the e-textile electrodes by fixing the ball part on the outer-side (non-conductive) allowing connectivity to measuring systems while the smooth side of the ring was located on the inner-side. For comparable measurements, the size of the snap-fasteners was consistent across all e-textile electrodes. In addition, practical measurements and use of e-textile electrodes require a connector. Thus, the snap fasteners conform the electrodes and must always be incorporated into the measurements.

3.1.4.2 Methodology for measuring polarization impedance

To conduct measurements, the electrodes were paired together in a wafer method [48] interfaced with a suitable material avoiding a short circuit. The leads of the LCR Meter were stabilised to reduce any motion artefact. In addition, this also reduced the possibility of a change in Z_p when changing the e-textile electrodes for testing. For the dry configuration, mini wooden craft pegs were chosen to secure the e-textiles in the wafer method. Dry wood is an insulator and was selected as it will not influence any polarization measurements [47]. The pegs were carefully positioned at the edges of the four corners of the substrate making sure they did not come into contact with the embroidered region avoiding any pressure distribution across the electrodes. Kelvin test leads were connected to the ball part of the snaps to enable measurements.

3.2 Comparison of Electrodes

3.2.1 Electrical Impedance Measurements Equipment for BIA (Current Drive) SFB7

The SFB7 (ImpediMed, Queensland, Australia) consists of a control unit with four test probes. The device is current driven and can operate in discrete frequency mode or frequency sweep mode measuring the electrical impedance in less than 1 second. The display is equipped with a touch screen where results can be viewed immediately. In frequency sweep mode the device scans 256 frequencies between 3 kHz and 1000 kHz based on a logarithmic scale. Discrete frequency measurements are also measured, for the frequencies of 5, 50, 100 and 200 kHz. The device was set in interval mode to collect the measurements. In interval mode, five measurements were taken at intervals of 3 seconds.

The device has an ethernet port to connect and transfer the data to a computer. Through its supporting software, BioImp, the Cole-Cole model was adopted for the complete frequency sweep and to extract the parameters, Z , R , R_0 and R_{inf} . The rejection limit of the measured data points used to generate the Cole-Cole plot were set to 0 as recommended by ImpediMed. The pre-set discrete frequency measurements are based on (i) the actual measurements and (ii) the fitted Cole-Cole model. For this study the actual measurements were extracted for analysis.

Prior to taking any measurements, the SFB7 was calibrated with its associated test cell where a 'passed' message was displayed on the screen.



Figure 3.8 ImpediMed SFB7

3.2.2 Materials for BIA

3.2.2.1 Ambu WhiteSensor WS Electrodes

Single use Ambu WhiteSensor WS non-polarized biopotential electrodes were used for this study. These sensors feature strong adhesion and a flexible foam backing material. The skin contact area measures 36 x 40 mm. Its sensor material is common Ag/AgCl measuring 79 mm² centred in a highly conductive sold gel area measuring 201 mm².



Figure 3.9 Ambu WhiteSensor WS Electrodes

3.2.2.2 Pork Belly

Pork meat is a common alternative to human skin in the field of biomedical engineering and research associated with sensors. Pig skin immunology has been studied and compared to human skin. It has identical histological and physiological properties [209]. The skin of pig ear is known to be the closest representation to human skin [210]; however, there is a limited surface area to conduct BIA experiments. Hence, pork belly is better suited. In addition, it closely imitates the material properties of the human body with respect to the surface of the skin and underlying soft biotissues.

At the skin surface, human skin has deep sulci, friction ridges and pores that can impact the contact of the electrode and skin. This is vital in dry electrode applications where a gap is present between the electrode and skin thus influencing Z_{es} [211]. In addition, body segments are anisotropic in nature in terms of the underlying structure [212]. The fibre direction of the underlying biotissues vary transversally and longitudinally. This can also have an impact in Z measurements [213]. The two principal characteristics in selecting pork belly (abdominal) for BIA measurements is (i) its close representation of skin thickness and (ii) its relatively close dielectric properties [214]. Human and porcine skin thickness ranges between 0.05 cm to 0.8 cm [70], where the difference between the two types of skin can vary slightly by a factor of 10^{-4} cm. Pig abdominal skin was selected due to its permeability [215] and the available surface area for BIA experiments. The samples weighed about 1.4 kg. All bones were removed from the samples.

3.2.3 Methodology

3.2.3.1 Preparation of the pork belly

Pork belly samples were cut off fresh carcasses at the butcher and transported in cooler bags to the laboratory. The use of icepacks was avoided due to the possibility of inhomogeneous temperature distribution. In the lab, the samples were removed from the cooler bags and placed on individual sheets of bench-roll laid on the bench. The bench-roll is made of 3 layers of paper tissue and lined with 1 layer of soft polyethylene, providing a waterproof and absorbent surface. The samples were thoroughly cleaned twice with isopropyl alcohol swab wipes and left to settle in ambient room temperature (about 20°C with a RH of about 50%) for one hour, prior to placing the electrodes. A preliminary experiment was conducted on the pork belly with the skin in-tact. To compare the wet electrodes with the dry electrodes, an incision was created.

3.2.3.2 Incisions

Incisions were created using commercially available disposable scalpels (Swann-Morton Handle Scalpels No. 15, MedShop, Victoria, Australia). The depth of the incisions was consistent across all experiments, measuring 0.5 cm. This was selected in connection to the depth of melanoma incision considering surgical wounds may vary in depth depending on the surgery while other forms of wounds can vary greatly. The incisions were created in the centre of the skin therefore it would also be centred between the electrodes. The length (l) and width (w) for small incisions were also based on previous studies using BIA for wounds that was within the limitations of the size of the pork belly samples, measuring 2x 2 cm. This incision was simply adapted as a guide to the positioning of the electrodes.

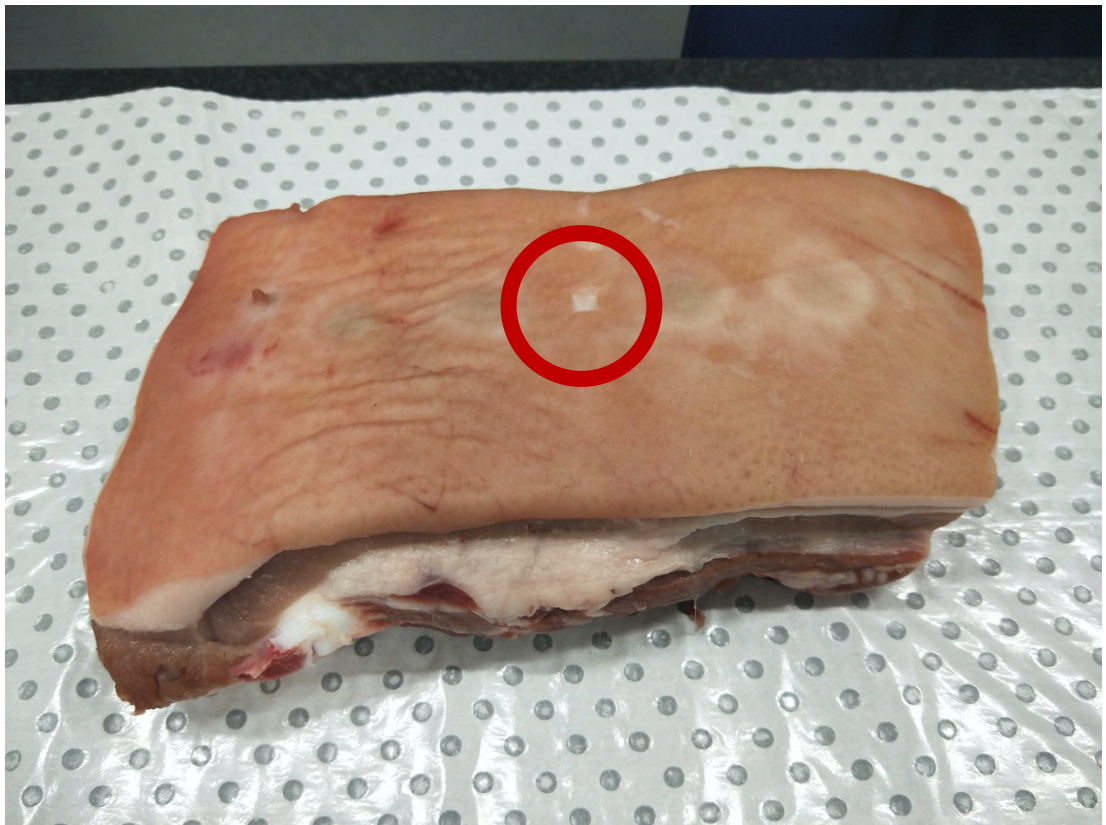


Figure 3.10 Pork belly with incision

3.2.3.3 Storing of the pork belly

To store the pork belly, the refrigerator was set at a temperature of 5 °C. For the preliminary experiments, the pork belly samples were individually wrapped in a fresh sheet of bench roll ensuring no air passed through. However, this method created a moisture build up on the skin. Therefore, the storing method was modified, and the

pork belly samples were individually wrapped in natural calico and placed in airtight polyethylene storage sealable bags. In both cases, the samples were adjacently placed on the grill shelves of the refrigerator.

3.2.3.4 Electrode Configuration

In a tetrapolar mode, the electrodes acting as voltage sensors were positioned at the edge of the wound, at a distance of about 0.5 cm to the incision. Their associated current source and sink electrodes were positioned adjacently on the outside at a distance of 1 cm [45]. In a dipolar mode, the current source lead was connected with the voltage sensor lead on a single electrode while the current sink connected with the voltage sensor lead were connected to the second electrode. However, the main focus of this study is based on a tetrapolar configuration.

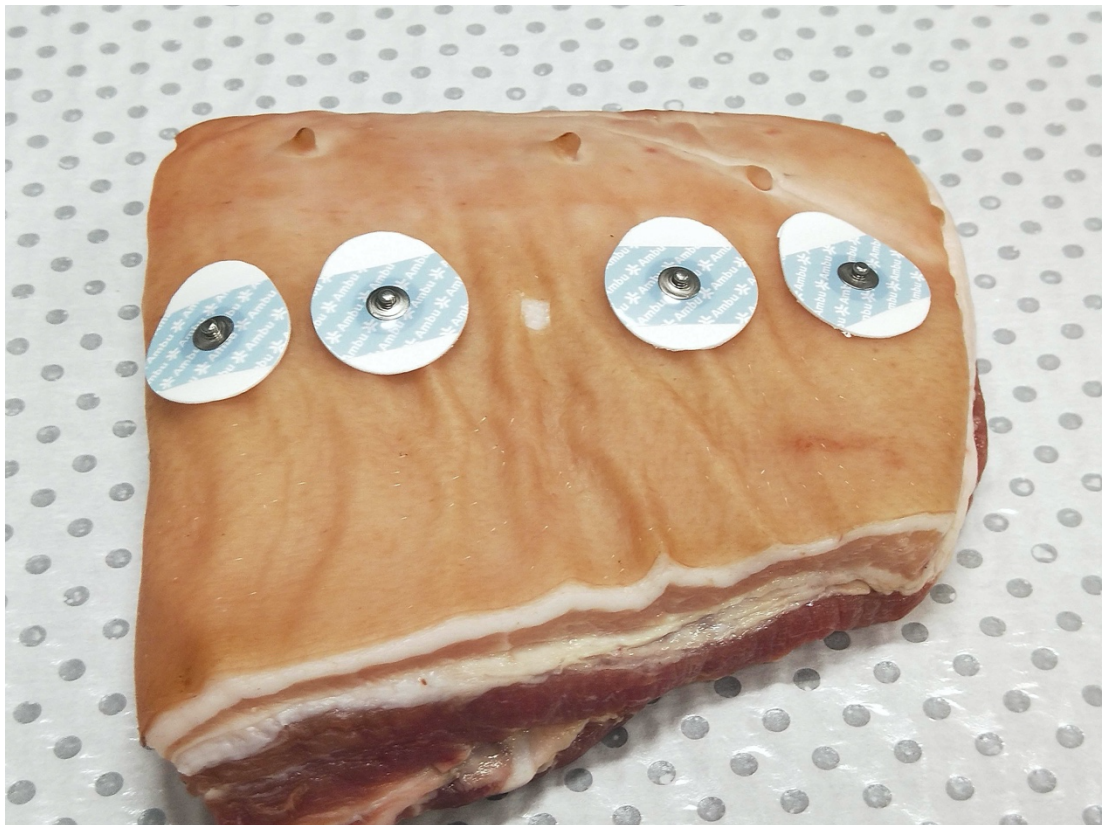


Figure 3.11 Pork belly with a tetrapolar electrode configuration

3.2.3.4 Data collection and trend analysis

This research studies the change in BIA parameters relative to time; thus, a trend was observed and not absolute values. However, the change in impedance is relatively small to plot on a logarithmic scale. This small change in impedance has been previously reported by Yamamoto [216]. Therefore, the data was normalised and plotted as a percentage change in Chapter 6.

Chapter 4

Fabrication process for e-textile electrodes: impact of the characteristics on Z_p for use with BIA

4.1 Introduction

Wet biopotential electrodes are the standardised choice in biomedical applications used with equipment that send an alternating current (AC) with a discrete frequency or frequency sweep. Current applications include: (i) transcutaneous electrical nerve stimulation (TENS); (ii) recording biosignals, such as electromyography (EMG) and electrocardiography (ECG); (iii) iontophoresis and (iv) bioelectrical impedance analyses (BIA) measuring the integrity of biotissues [217,218]. For (i) – (iii), the systems operate at relatively low frequencies, for example: (i) TENS – 1 to 150 Hz; (ii) EMG – 20 to 500 Hz and ECG – 0.5 to 100 Hz; (iii) iontophoresis – 5 to 1000 Hz [219–223]. Measurements using single frequency BIA (sfBIA) commonly use a frequency of 50 kHz. In addition, a vast amount of BIA systems on the market operate only at 50 kHz [139]. Recently, BIA has emerged as a diagnostic tool for monitoring muscle gap and injuries [137–139,165], biotissue abnormalities [74,167–169], inflammation [44], fractures [166] and wounds [45,170].

The system connects to non-invasive surface electrodes that adhere to the skin. The electrodes create a pathway for the charge providing a way to measure the integrity of biotissue under study (BUS). However, the electrode-skin interface can influence the efficacy of measurements. Dry electrodes introduce a polarizing impedance (Z_p) that impacts the electrode-skin impedance (Z_{es}) resulting in unwanted artefacts and attenuation noise in measurements [53,54,178]. Taking accurate BIA measurements, the biosignal should ideally have no artefacts at the preferred frequency. Thus, a low to negligible Z_{es} is desired while maintaining a high signal amplitude in addition to obtaining a high signal-to-noise ratio (SNR) [178]. Moreover, other factors associated with long-term monitoring must be accounted for, such as (i) maintaining a stable biosignal over time and (ii) ensuring the electrodes are safe for use with the skin where improper electrodes can induce abrasions or give rise to skin allergies [57].

4.1.1 Electrode polarization impedance

Dry electrodes are subject to a charge-build-up relative to the electrode material and frequency, known as the polarizing impedance (Z_p). Wet electrodes are ideally non-polarized due to the electrolyte ‘gel’ layer and can be adapted to all equipment irrespective of the system’s frequency [59,192]. However, thorough preparation of the skin is required [58] in addition to the onset of skin irritations [198]. Over a period of time the ‘gel’ layer dries impacting the accuracy of measurements due to the variance that occur in the impedance output; thus, they are not deemed appropriate

for long term use. The purpose of dry electrodes is to resolve these issues. Research has led to the development of membranes [56,60,224,61,63,193–197,199], drying paste membranes [64], tattoos [65,201] and e-textiles [66,202–204,206,225,226].

Embroidered electrodes are an ergonomic, comfortable and low-cost solution for long-term BIA monitoring of biotissue. The fabrication process is convenient and can be done on-site with simple common equipment. It also allows for the electrodes to be tailored specifically to a patient’s ailment [53,202–204]. Another advantage is the feasibility of replicating and customising designs with respect to the design of the electrodes; this includes the geometry, stitch type, stitch length and stitch density (i.e., spacing/distribution) [227]. This allows optimising the design to achieve a reduction in Z_p lowering Z_{es} .

The complex vector Z_p stems from the summation of a real part, i.e., resistance (R) and an imaginary part i.e., reactance (X_C). To calculate the total impedance modulus Z_p refer to Equation 4.1. Where X_C is frequency dependent based on the system used (Equation 4.2). Thus, it is important to consider the frequency when designing and testing Z_p as it must comply to the specified equipment. For example, a different Z_p is expected when tested at frequencies in accordance with the previously mentioned systems (i.e., TENS, EMG, ECG and BIA).

$$|Z_p| = \sqrt{R^2 + X_C^2} \quad \text{Equation 4.1}$$

where

$$X_C = \frac{1}{2\pi f C} \quad \text{Equation 4.2}$$

For the rest of the manuscript Z_p is used as the modulus for simplicity.

4.1.2 Previous research

Researchers have adapted various testing methodologies in studying the efficiency of e-textile electrodes. The two main strategies used to test the electrodes sensors are (i) testing sensors autonomously or (ii) adapting them to medical equipment (i.e., EMG’s and ECG’s). A simple test analysing the electrodes autonomously is conducted by measuring the DC resistance of the conductive surface using a multimeter [53,197,202,204]. However, provided that most medical systems use AC, the actual Z_p is not defined. Another approach is by using a multi-meter to measure to the AC impedance at different points across the surface of the electrode. However, measurements at various points can differ depending on the surface topography of the fabricated electrode and does not measure the impedance relative to the surface area of the electrode. Measurements for Z_p of e-textiles have been studied using agar-agar phantom skin imitating human skin, specifically the curves of the body. The advantage of this method is the e-textile electrodes are measured in an ideal

application by taking the form of the body. However, Z_{es} and Z_p cannot be extrapolated; in addition, agar-agar can be influenced by time. This phantom skin can dehydrate over time thus changing its properties that influence the results. Moreover, it compares one e-textile electrode to an Ag/AgCl electrode as a reference. This is common in many studies; however, this does not present an ideal methodology given that electrodes are coupled when adapted to medical systems. Research measuring the signal-to-noise-ratio (SNR) overlook the measurement of Z_p as a standalone parameter. Although, it is an ideal 'applied' solution there can be many external factors that influence the SNR independent of electrode application.

Electrodes are adapted for AC applications; thus, research measuring the DC R omit the capacitive resistance of the electrode (X_C) that is dependent on the frequency. Neglecting to measure Z_p , Z_{es} is compromised. This could be the cause of a discrepancy in efficiency in Berk et al.'s [204] study on embroidered electrodes. The e-textile electrode possessing a low R , was not efficient in terms of SNR for a TENS system. Shafti et al.'s research demonstrated a correlation between e-textile electrodes and Ag/AgCl electrodes for sEMG (surface EMG) measurements. However, comparable to Berk et al. this study also overlooked X_C .

Kannaian et al. [53] conducted AC measurements adapted for an ECG system. At these low frequencies, Z_p was identified as 1.4 M Ω . By measuring the SNR, it was also observed that this remained consistent when the amount of conductive thread used was reduced by 50%. However, this research was conducted based only on two sets of e-textile electrodes.

Previous research into e-textile electrodes is conducted for use with systems that operate at much lower frequencies than BIA systems. Moreover, all possible variables associated with embroidery electrodes are not addressed thus neglecting possible combinations in the design process. In addition, neglecting Z_p results in inconsistent research on efficiently designed embroidered electrodes. In this study, the aim is to address these limitations by (i) incorporating the possible embroidery variables in order to measure Z_p at a frequency of 50 kHz and (ii) identifying the optimal variables for reducing Z_p of e-textiles. Maintaining a single frequency, possibility of frequency dependency on the material properties is reduced.

Measurements were performed on e-textile electrodes in a dry and wet state, evaluating R and X_C relative to Z_p . In addition, these parameters were associated to the variables of the e-textile electrodes. This study provides a better understanding to the equivalent electrical circuit of embroidered electrodes for BIA systems operating at 50 kHz. It is hypothesised that the fabrication process of dry electrodes requires a large amount of conductive material to reduce Z_p . Thus, the utilization of conductive thread as a fundamental material was evaluated by varying certain

variables associated with the fabrication process including the surface area of the electrodes and the embroidery settings at 50 kHz.

4.2 Materials and methods

The substrate selected for the e-textile electrodes was a polyester non-woven felt commercially purchased with a thickness of about 1 mm. This substrate was preferred due to its strong friction properties; thus, avoiding any issues of the textile slipping in the fabrication process. It has close to zero elasticity and very low drape, allowing for a consistency in embroidery stitches across the surface area. In addition, it is resistant to fraying resulting in a tightly compact e-textile electrode without the risk of the threads pulling apart. These characteristics of the felt assist in the simplicity of the fabrication process and there is less concern over any textile movement while conducting measurements in the experiment. The Shieldex Conductive Twisted Yarn was used to provide conductivity to the electrode with the selected non-conductive thread.

The electrodes were measured in pairs using a wafer method [48] interfaced with a dry and wet material. The dry material was selected based on the criteria of possessing low dielectric properties to minimise any impact on the conductivity of the e-textile electrodes. For the wet material, selection was based on its high ionic properties. To test in a dry configuration, a piece of non-woven polyester was used with dimensions 4.5 x 4 cm. This material was chosen as it is impervious to water thus not absorbing humidity resulting in a consistent dielectric as its electrical properties remain unaltered in time. A commercially available hydrogel pad (Medela) was chosen for the wet configuration with identical dimensions to the non-woven polyester felt used as the dry configuration interface (4.5 x 4 cm). The composition of the hydrogel pad includes water, Sodium AMPS and glycerol. Sodium AMPS possesses high ionic properties providing a conductive pathway for the penetration of charge through the skin. Thus, it can be hypothesised that this will cause a redox reaction reducing Z_p and Z_{es} . This hypothesis is based on the function of the agarose 'gel' layer of Ag/AgCl electrodes causing them to be an ideal non-polarized electrode. However, due to the dehydration issues associated with Ag/AgCl an interface that could potentially delay the onset of drying was selected. The glycerol composite of the Medela hydrogel pad assists in maintaining the moist properties of the pad while moisturising the skin thus preventing any skin irritations. In addition, glycerol has certain skin healing properties [228,229].

4.3 Methodology

4.3.1 Sample Fabrication

The design of the electrodes was based on current clinical electrodes. Nescolarde et al. tested the efficiency of four rectangular shaped Ag/AgCl electrodes in terms of their resistance and reactance [50] using a wafer test method. The method was adopted for this study and provided a base for the surface area of the e-textile electrodes. For the stitch types of the e-textile electrodes the standard embroidery stitches were used, specifically the weave and satin stitches. The stitch length and density were varied from the default settings of the EasyDesign EX software where applicable. Apropos to the satin stitch length, a specified embroidery parameter on the software auto split was set. Satin stitches are limited by the fact that machines do not execute them for areas over 12 mm in width; therefore, to cover the large areas in this research auto split breaks the long satin stitches into shorter ones by distributing the needle penetrations randomly. Contrary to this, weave stitches are preferred for large areas in a design and as such the software provided the option of user control relating to the stitch length. The software EasyDesign EX stitch density settings also differ for the satin and weave stitch; the former is set in terms of percentage (%) coverage of the embroidery area while the latter is in terms of distance (mm) from adjacent interlocks. The correlation between percentage (%) in terms of distance (mm) is calculated through an algorithm which is IP protected by the company; thus, this work is limited in relating the density between a satin and weave stitch in terms of distance. By increasing and decreasing the stich parameters, the electrodes presented in Table 4.1 were fabricated, refer to Table 4.2 for the associated stitch characteristics. The fabrication method and test set-up of the e-textile electrodes is presented in Figure 4.1.

Table 4.1 Electrode types - stitch and size mapped to convention [47] “© IOP Publishing. Reproduced with permission. All rights reserved.”

| Stitch type and electrode convention | Dimensions (cm) | Surface Area (cm²) |
|---|------------------------|--------------------------------------|
| Weave Stitch (W-E1) | 4 × 3.3 | 13.2 |
| Satin Stitch (S-E1) | | |
| Weave Stitch (W-E2) | 3.2 × 3.2 | 10.2 |
| Satin Stitch (S-E2) | | |
| Weave Stitch (W-E3) | 2.7 × 2.9 | 7.8 |
| Satin Stitch (S-E3) | | |
| Weave Stitch (W-E4) | 2.3 × 2.5 | 5.7 |
| Satin Stitch (S-E4) | | |

Table 4.2 Stitch variables [47]. “© IOP Publishing. Reproduced with permission. All rights reserved.”

| Stitch Type | Stitch Type | Stitch Length | Stitch Spacing / Density |
|--------------|-----------------------|---------------|--------------------------|
| FE- <i>n</i> | Base Stitch (-BS) | Weave | 3.5 mm |
| FE- <i>n</i> | Long Stitch (-LS) | Weave | 7.0 mm |
| FE- <i>n</i> | Low Density (-LD) | Weave | 3.5 mm |
| SE- <i>n</i> | 50% Density (-50%D) | Satin | N/A |
| SE- <i>n</i> | 150% Density (-150%D) | Satin | N/A |

**n* refers to electrode size convention in Table 4.1 (1, 2, 3, 4)

**throughout this article the samples are coded, for example, W-E1-BS



Figure 4.1 Fabrication and experimental process: (a) embroidery setup, (b) sample e-textile electrode prepared with snap, i.e., ball and spiked ring components (c) e-textile electrode with hydrogel pad tested as a wet e-electrodes, and (d) LCR meter with frequency setting 50 kHz [47]. “© IOP Publishing. Reproduced with permission. All rights reserved.”

Another important aspect associated with the design of the e-textile electrodes, is the amount of yarn consumed. A textile and fabric weighing scale balance with an accuracy of the nearest 0.01 g and 200 g capacity was used to measure the substrates absent of embroidery and the embroidered substrates acting as the e-textile electrodes. The measurements were recorded accordingly for the various sizes adapted for the e-textile electrode fabrication. The linear mass density equation

(Appendix I) was used for the conductive and polyester threads to determine the amount of the conductive thread that was used to produce the e-textile electrodes.

4.3.2 Experimental methodology

To conduct the tests, the triple-layer wafer methodology was adopted. The interfacing polyester non-woven felt and the samples of hydrogel pads were interposed between a pair of e-textile electrodes coming into contact with the inner-side of the electrodes (the conductive side). This created a wet and dry configuration in addition to preventing the metal components of the e-textiles (i.e., the snap fasteners) causing a short circuit from the rings of the snap fasteners. For the dry configuration, to couple the three layers while maintaining consistency across the measurements external adjoining support was required. Mini wooden craft pegs were chosen as dry wood is an insulator and will not influence any polarization measurements. The pegs were carefully positioned at the edges of the four corners of the substrate making sure they did not come into contact with the embroidered region avoiding any pressure distribution across the electrodes. Pressure is known to have an impact on Z_p and the impact of pressure on e-textile electrodes is outside the scope of this project. Contrary, the hydrogel swatch possesses adhesive properties and no external support was required for the wet configuration.

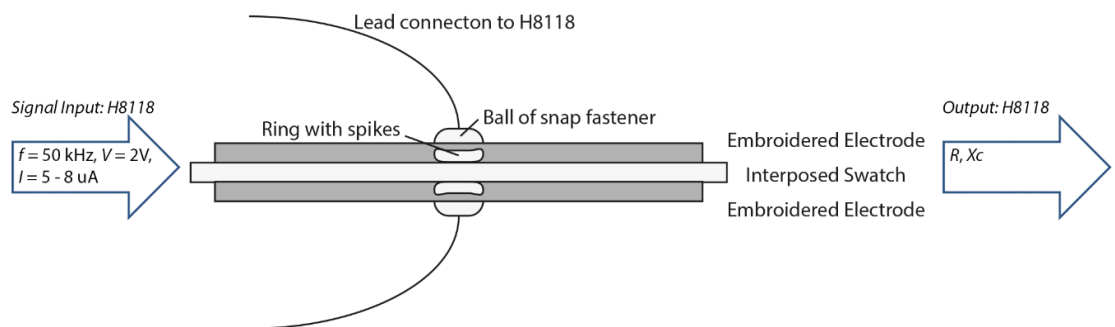


Figure 4.2 Experimental protocol [47]. “© IOP Publishing. Reproduced with permission. All rights reserved.”

To test the efficiency of the e-textile electrodes for BIA applications using AC, its associated parameters, R and X_C were measured using a voltage driven HM8118 LCR Meter. The setup is presented in Figure 4.2. Although BIA is current driven, provided the e-textile electrodes are tested autonomously as a material, voltage driven equipment has been adapted. Given that electrodes are coupled when used with medical equipment, a dipolar electrode was setup by connecting the ball part of the snap-fasteners to the LCR bridge using the Kelvin (4-Wire) test leads as dual contact probes. The HM8118 LCR bridge was calibrated by connecting the two probes in order to obtain a 0 measurement.

The electrode wafer configurations were connected to the LCR bridge over a three-minute period enabling dynamic testing of Z_p . For the dry configuration, this timeframe was sufficient to observe no change in measurements. However, the hydrogel pad displayed unstable measurements. Inconsistent fluctuations of R and X_C were observed. Thus, the experimental protocol was designed to take measurements every 20 seconds for 20 intervals. A period of 20 seconds was selected allowing adequate time to record measurements. To comply with a small error rate (of about 5%), 20 intervals was adequate for the experiment. These measurements were taken over a continuous function of time and are considered dynamic; thus, eliminating the need for analysis in terms of error, such as standard deviation and error bars [47].

4.4 Results

4.4.1 Electrodes in dry and wet form

To analyse the results, the e-textile electrodes were categorised and grouped relative to their stitch type and surface area (the electrode size), respectively, while the various stitch variables are shown within the surface area grouping. By adapting the dynamic measurement protocol over a three-minute period, the dry electrode configuration displayed consistent measurements of R and X_C for all e-textile electrodes, shown in Figure 4.3. However, for the e-textile electrodes in the wet form R and X_C was averaged over the 20 intervals, refer to Figure 4.4, the actual measurements are available in Appendix II.

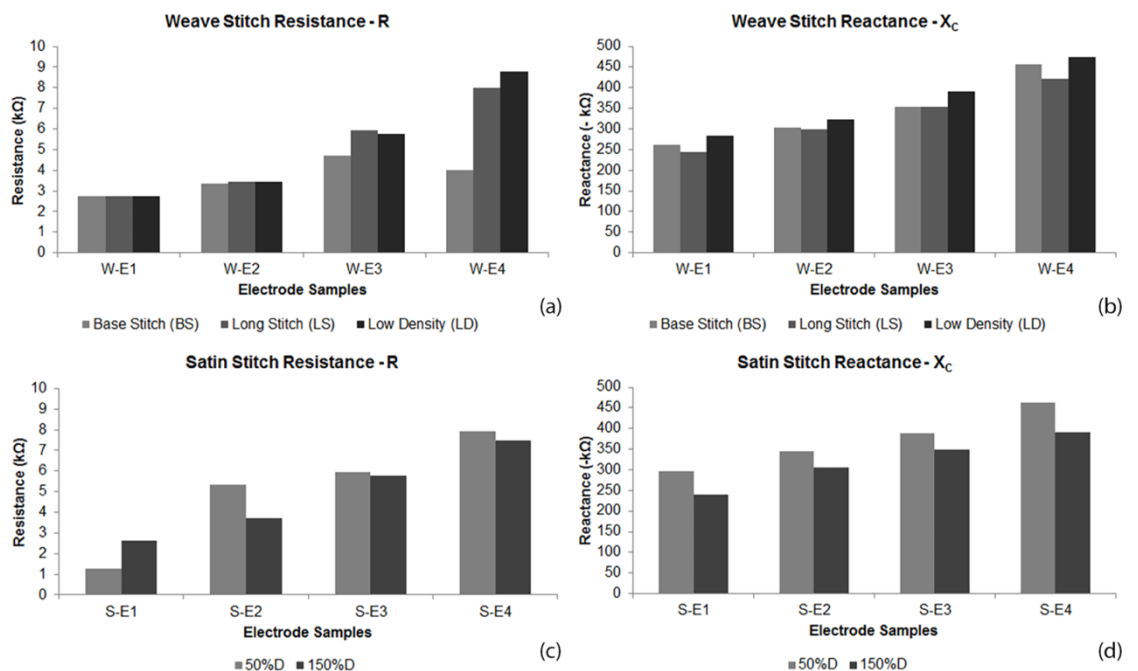


Figure 4.3 Dry wafer measurements of e-textile electrode samples (refer to table 4.2 for conventions) [47]. “© IOP Publishing. Reproduced with permission. All rights reserved.”

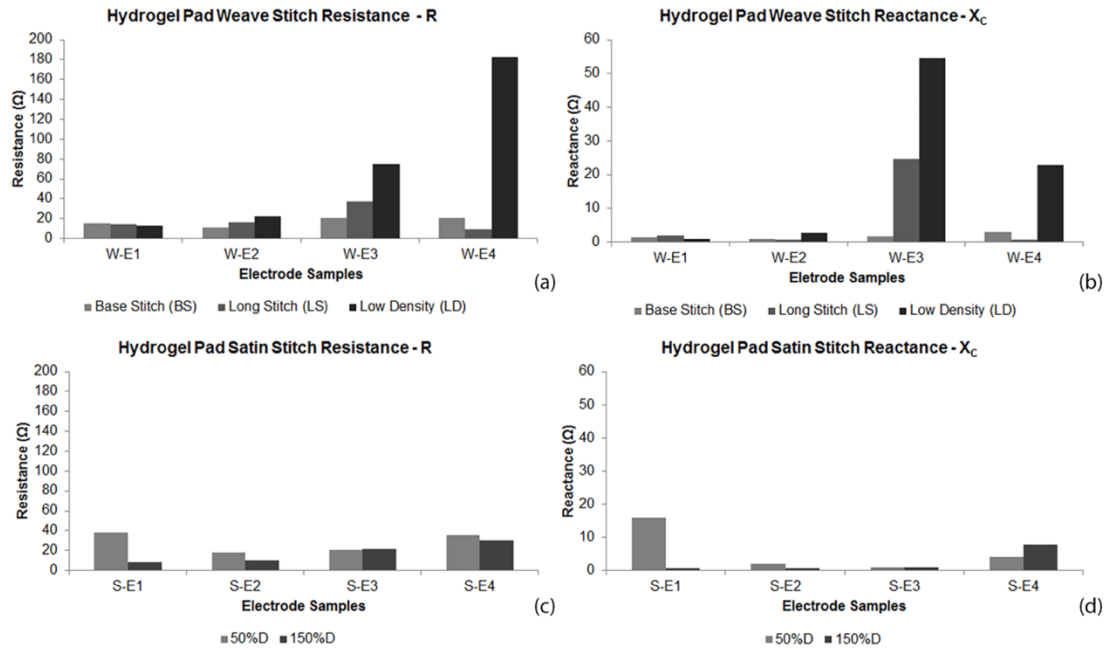


Figure 4.4 Wet wafer measurements of e-textile electrode samples [47]. “© IOP Publishing. Reproduced with permission. All rights reserved.”

It was observed that R and X_C were not relative to a single electrode sample. More precisely, a low R relating to an electrode did not correlate to a low X_C . For the dry electrode configuration, the satin stitched samples with the largest surface area of 13.2 cm^2 (S-E1) possessed the lowest R and X_C . However, these measurements were obtained from electrodes fabricated with two different stitch variables. Sample S-E1-50%, with the lowest satin stitch density resulted in the lowest R of $1.28 \text{ k}\Omega$. Contrary to this, the sample with the largest stitch density (S-E1-150%) possessed the lowest X_C of $240 \text{ k}\Omega$.

Thus, it was observed in the dry state, low R and X_C values are related to a large conductive surface area. This was verified by highlighting the highest R and X_C values obtained. The electrodes with the smallest surface area resulted in large R and X_C values. However, in this case the results were associated with the two different stitch types, although both were from samples with low stitch densities. Sample W-E4-LD with a weave stitch had R of $8.8 \text{ k}\Omega$ indicating a tremendous increase compared to the stitch sample S-E1-50%D, where R is about $1.3 \text{ k}\Omega$. Although this sample presented the lowest R across the electrodes with the smallest surface area, it exhibited one of the largest X_C measurements, with a difference of $11 \text{ k}\Omega$ to the largest X_C measurements across all electrodes.

In contrast to the dry electrodes, the wet electrodes did not demonstrate consistency over time displaying creep where R and X_C of each sample showed an increase over the allocated time period (refer to Appendix II). Thus, the mean of each parameter relative to the samples was analysed, Figure 4.4. In the wet electrode configuration,

the lowest R was observed from the sample set that was fabricated with a large surface area analogous to the wet configuration. However, this sample was fabricated with the largest stitch density, sample S-E1-150% displayed an R as low as 8.3Ω . Contrary to the dry electrode configuration, the lowest X_C value was measured from a sample set belonging to the category of the weave stitch electrodes with the smallest surface area. Sample W-E4-LS with a long stitch had a mean X_C of 0.55Ω . However, sample W-E4-LD belonging to the same category (W-E4) with the lowest density presented the largest R of 182Ω . The largest X_C measurement was sporadic and was not related to the categories of largest or smallest surface area although it was fabricated with a reduced stitch density setting. Sample W-E3-LD showed a X_C of 55Ω .

It was observed that the efficiency of the dry electrode cannot be analysed through R and X_C independently and are not identically influenced relative to the configuration (wet or dry) or to changes relating to the electrode variables. Therefore, Z_p was calculated for the electrodes comprising of R and X_C , refer to Figure 4.5. For the dry configuration, the electrodes possess a higher X_C relative to R ; hence, X_C dominantly contributes to Z_p . For example, observing sample W-E1-LS, where R has a value of $2.75 \text{ k}\Omega$ while X_C is much larger measured at $244 \text{ k}\Omega$. Z_p was calculated to have a value identical to X_C , $244 \text{ k}\Omega$. However, for the wet configuration the measured R is much greater than X_C resulting in a significant contributing to Z_p . One example is sample W-E1-LS where R is 14.84Ω , while X_C is as low as 1.9Ω resulting in Z_p of 14.84 .

In the wet electrode configuration, the tests resulted in supporting the hypothesis of a reduction in R and X_C by a magnitude of $\text{k}\Omega$. However, this specific hydrogel was selected for its glycerol properties preserving the moisture content of the wet pad that would provide stability in measurements over time. This study indicated that there is no consistency in Z_p across the electrodes relative to their variables, refer to Figure 5.5. In addition, the creep observed in each electrode sample (Appendix II) indicates dehydration of the gel pads. The dry electrode configuration displayed consistency in measurements across the samples; thus, the remainder of this study focused on the variables influencing the parameters associate to the dry electrode configuration.

The individual measured parameters, R and X_C are presented in Table 4.3. Z_p was also calculated for all samples. In addition, the volume impedance was identified to quantify the ability for charge to travel along the electrodes. Sheet resistance is commonly adapted for conductive 2D materials. However, studying e-textile electrodes, the mechanics of stitching and the embroidered structure need to be accounted. The conductive thread forms a 3D plane and Z_p occurs along and perpendicular to the electrode plane. Thus, sheet resistance cannot be applied to

isolate Z_p from the size and shape of the electrodes. Therefore, the 3D properties of the electrodes were taken into consideration to calculate the volume impedance ($Z_{p/v}$) measuring Z_p per cm^3 using equation 4.3.

$$Z_{p/v} = \frac{Z_p}{V} \quad \text{Equation 4.3}$$

where the volume (V) is

$$V = \frac{l \times w \times h}{2}, \quad \text{Equation 4.4}$$

and is calculated by measuring the length (l), width (w) and height (h) of the e-textile electrodes.

For accurate calculations, it is important to note that the conductive section of the electrode is of importance (i.e., the inner-side). To ensure accuracy, the thread tension of the embroidery machine must be balanced where the interlocking of the conductive and non-conductive threads occur across the centre plane of the substrate (Appendix I). Thus, the total height of the electrode was measured and divided by two eliminating the height of the non-conductive thread. This standardised method allows comparisons between various shaped e-textile electrodes based on efficiency. $Z_{p/v}$ was included in Table 4.3.

Table 4.3 R , X_C , Z_p and $Z_{p/v}$ for dry e-textile electrode samples [47]. “© IOP Publishing. Reproduced with permission. All rights reserved.”

| Electrode set | Surface area (cm^2) | Quantity of conductive thread (m) | R (k Ω) | X_C (k Ω) | Z_p (k Ω) | $Z_{p/v}$ (k Ω) / cm^3 |
|---------------|--------------------------------|-----------------------------------|-------------------|---------------------|---------------------|---|
| W-E1-BS | 13.2 | 8.61 | 2.75 | 261 | 261 | 186 |
| W-E1-LS | | 8.04 | 2.75 | 244 | 244 | 153 |
| W-E1-LD | | 4.33 | 2.75 | 284 | 284 | 237 |
| S-E1-50%D | 10.2 | 4.22 | 1.28 | 296 | 296 | 211 |
| S-E1-150%D | | 12.56 | 2.61 | 240 | 240 | 150 |
| W-E2-BS | | 5.7 | 3.35 | 303 | 303 | 303 |
| W-E2-LS | 7.8 | 5.33 | 3.45 | 299 | 299 | 249 |
| W-E2-LD | | 2.99 | 3.45 | 322 | 322 | 358 |
| S-E2-50%D | | 2.86 | 5.35 | 345 | 345 | 345 |
| S-E2-150%D | 5.7 | 8.82 | 3.72 | 305 | 305 | 235 |
| W-E3-BS | | 4.04 | 4.73 | 354 | 354 | 443 |
| W-E3-LS | | 3.56 | 5.94 | 353 | 353 | 392 |
| W-E3-LD | 5.7 | 0.93 | 5.76 | 390 | 390 | 557 |
| S-E3-50%D | | 1.41 | 5.94 | 389 | 389 | 486 |
| S-E3-150%D | | 5.67 | 5.77 | 349 | 349 | 349 |
| W-E4-BS | 5.7 | 1.87 | 3.99 | 457 | 457 | 762 |
| W-E4-LS | | 1.62 | 8.01 | 421 | 421 | 601 |
| W-E4-LD | | 0.05 | 8.80 | 473 | 473 | 946 |
| S-E4-50%D | 5.7 | 0.08 | 7.93 | 462 | 462 | 770 |
| S-E4-150%D | | 3.56 | 7.50 | 390 | 390 | 557 |

4.4.2 Surface area

The lowest R and X_C measurements obtained across the electrodes was studied. It was observed that for the dry configuration both instances were related to the electrodes having the largest surface area. An inverse relationship was observed for R and X_C relative to the surface area. An increase in the surface area resulted in a decrease in R and X_C . However, this was not consistent for all electrodes. The weave stitch electrode with base stitch variables (i.e., stitch length and density 3.5 mm and 0.4 mm, respectively) defied this trend at one instance. Specifically, comparing sample the two samples W-E4-BS and W-E3-BS with surface areas of 5.7 cm² and 7.8 cm² respectively an increase in surface area displayed a decrease in R , from 4.73 to 3.99 k Ω respectively. Therefore, X_C accounts for R in Z_p decreasing relative to the increase of surface area; where Z_p for W-E4-BS and W-E3-BS were calculated to be 457 and 354 k Ω . On closer inspection of the results in Table 4.3, it is obvious that in the dry state X_C associated with the capacitance of the e-textile electrodes is closely related to the overall Z_p ; where for all electrodes $Z_p = X_C$.

Relating Z_p to the surface area of the e-textiles, it can be noted that an increase in the surface area of the electrodes while maintaining the stitch variables consistent resulted in a reduction in Z_p , refer to Figure 4.5. Thus, the electrodes with the greatest surface area measuring 13.2 cm² possessed the least Z_p indicating the most efficient group in terms of size. In contrast, the electrodes with the lowest surface area of 5.7 cm² demonstrated the lowest Z_p ; thus, these electrodes are the least suitable. The e-textile electrodes in the largest electrode grouping for each category (i.e., weave and sating stitch): W-E1-BS, W-E1-LS, W-E1-LD, S-E1-50%D and S-E1-150%D, resulted in Z_p of 261, 244, 284, 296 and 240 k Ω respectively. Contrary to this, the electrodes in smallest surface area groups: W-E4-BS, W-E4-LS, W-E4-LD, S-E4-50%D and S-E4-150%D resulted in Z_p of 475, 421, 473, 472 and 390 k Ω respectively. This indicates a difference close to 50% in Z_p implying a preference for larger surface areas where more conductive yarn is consumed in the fabricating process of the e-textile electrodes. A larger surface area implies more silver thread thus higher conductivity reducing the impedance. However, a threshold on the amount of conductive thread used was identified.

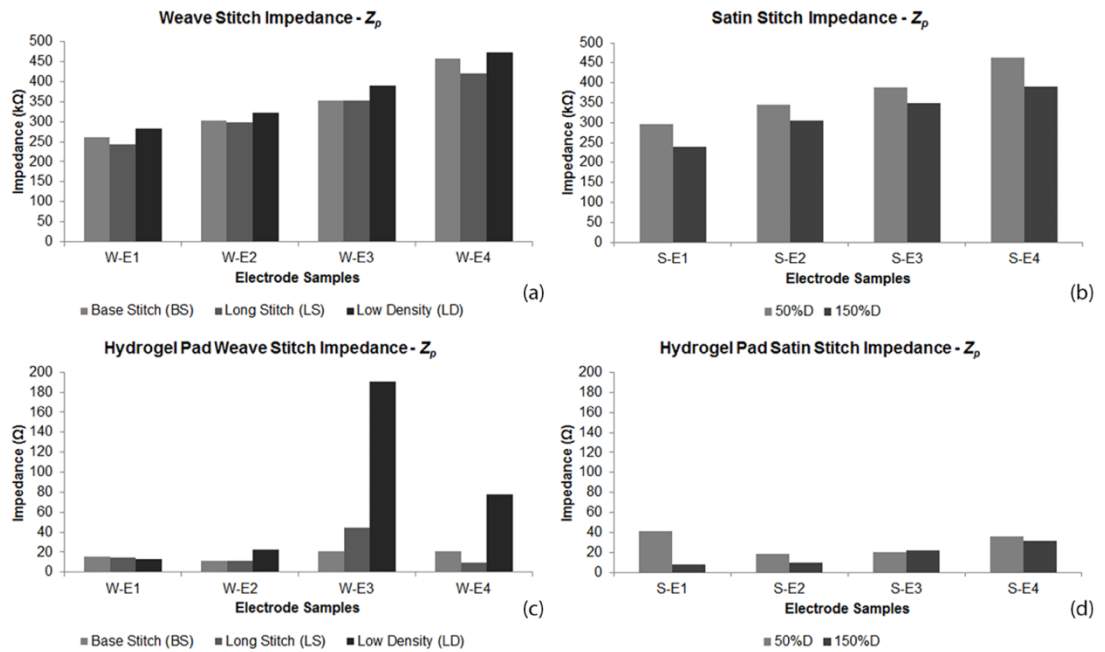


Figure 4.5 Z_p for e-textile electrode samples (a) weave and (b) satin stitch dry wafer measurements; (c) weave and (d) satin stitch wet wafer measurements [47]. “© IOP Publishing. Reproduced with permission. All rights reserved.”

4.4.3 Stitch parameters

The two stitch parameters varied in this study pertaining to both stitch types were (i) the stitch length and (ii) stitch density. For the weave stitch, the stitch density is measured in mm while the satin stitch density is measured in %. An increase in stitch density for the satin stitch means the spacing between the stitches decreases contrary to a weave stitch where an increase in stitch density results in an increase in stitch spacing. By reducing the stitch spacing there is an increase in conductive yarn used for the electrodes. Given that a significant capacitance behaviour of the electrodes was observed, it is expected to have a decrease in Z_p by increasing the stitch density due to an increase in conductivity. Tripling the stitch density from 50% to 150% for sample set S-E1 resulted in Z_p decreasing from 296 to 240 k Ω . Comparing the weave samples W-E1, increasing the stitch spacing resulted in a reduction of conductive thread used on the sample thus Z_p also increased. For example, W-E1-BS resulted in a Z_p of 261 k Ω while a 50% decrease in stitch spacing for the W-E1-LD electrode demonstrated Z_p of 284 k Ω .

Provided there is control over the stitch length variable for the weave stitch, the stitch length was increased while maintaining the denser stitch spacing. A slight improvement was observed for Z_p , decreasing to 244 k Ω . The stitch length was doubled from the base stitch, where the base stitch length default setting of the embroidery machine is 3.5 mm and the new stitch length was 7.0 mm. This could be attributed to the number of interlocks in the embroidery process.

To understand this, a basic concept of the embroidery process is required (Figure 2, Appendix I). Embroidery machines create stitches using a mechanical lockstitch method. A lockstitch is defined by the interlocking of the needle thread and bobbin thread. The needle thread is passed through the bobbin compartment forming an eyelet passing around the bobbin thread. When the threads form an interlock, they have a mechanical pull on one another forming the stitch. Therefore, the needle thread creates a tension force on the underlying bobbin thread. Thus, the polyester thread creates extra resistance to the conductance of the conductive bobbin thread of the e-textile electrodes. Thus, increasing the stitch length by 50% should theoretically result in a 50% reduction of interlocks implying there is a reduction of tension force applied to the conductive thread. Therefore, a reduction in Z_p is expected. In this study, an increase in stitch length of 50% resulted in a 6.5% reduction of Z_p . Although, a relatively small decrease is anticipated compared to the influence of the surface area and stitch density.

4.4.4 Quantity of conductive thread

By measuring the amount of conductive yarn consumed for the electrodes, the influence of the conductive component of the electrode can be determined. Figure 4.6 presents the amount of conductive thread consumed against Z_p across all electrodes. It was observed that this is a non-linear dependant variable. Although, the predicted trend whereby an increase in conductive thread results in a reduction in Z_p is profound

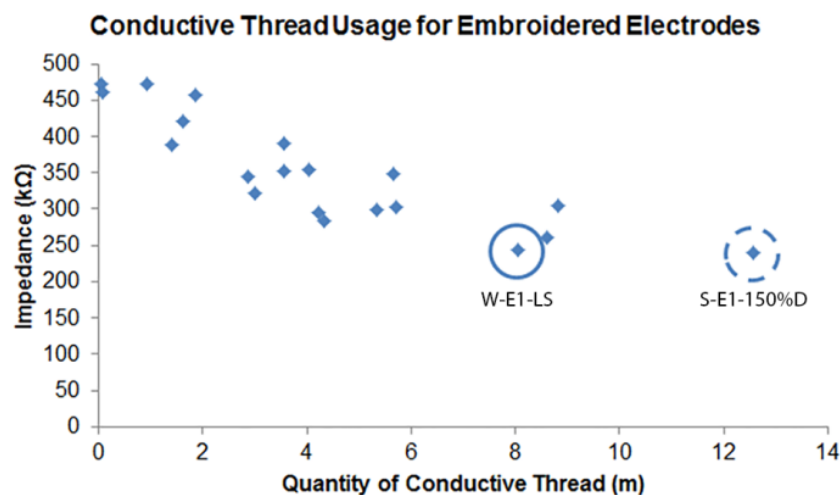


Figure 4.6 Influence of length of conductive thread on Z_p for the e-textile electrodes [47]. “© IOP Publishing. Reproduced with permission. All rights reserved.”

From Figure 4.3, it can be observed that the sample electrodes W-E1-LS and S-E1-150%D possessed a similar Z_p , with as little as 2% difference. However, when analysing the length of conductive yarn in each electrode, W-E1-LS used 40% less than S-E1-150%D, refer to Figure 4.6. This could potentially present a threshold

relating to the amount of conductive yarn consumed whereby Z_p is not influenced by the stitch type. By comparing the two electrodes, the satin stitch does perform better than the weave stitch; however, the latter is preferable due to the large reduction in consumed conductive thread. This reduction decreases the rigidity of the electrode providing a better contour when worn on the body while reducing the manufacturing costs.

4.5 Equivalent Circuit Theory

The circuit equivalent for the experimental setup can be expressed as two parallel RC circuits in series. To identify the capacitive and the resistive components for each of the e-textiles. The following equations for the resistance – R (Equation 4.9) and capacitance – C (Equation 4.10) can be applied to determine the circuit equivalent. This can be adopted for various frequencies.

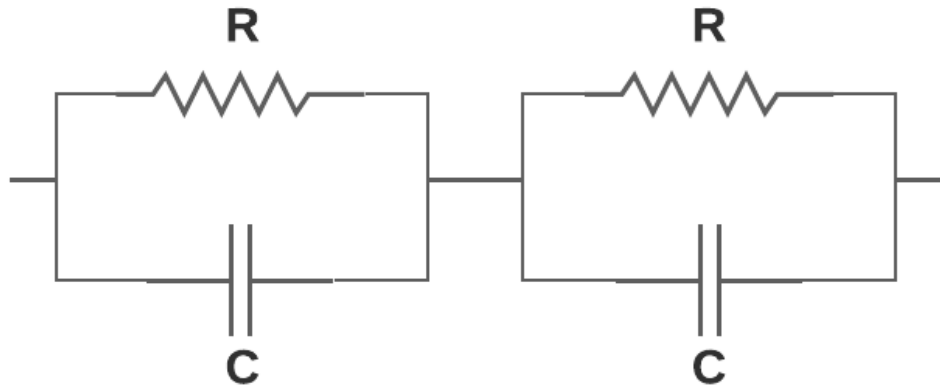


Figure 4.7 Equivalent circuit.

$$Z = Z_1 + Z_2$$

$$Z_2 = Z_1 = \frac{R \times X_c}{R + X_c} = \frac{\frac{R}{j\omega C}}{R + \frac{R}{j\omega C}} = \frac{R}{1 + j\omega RC}$$

$$Z = \frac{2R}{1 + j\omega RC} \times \frac{1 - j\omega RC}{1 - j\omega RC}$$

$$Z = \frac{2R(1 - j\omega RC)}{1 - j\omega RC^2}$$

$$Z = \frac{2R(1 - j\omega RC)}{1 + \omega^2 R^2 C^2}$$

$$Re = \frac{2R}{1 + \omega^2 R^2 C^2}$$

$$Im = \frac{-2j\omega R^2 C}{1 + \omega^2 R^2 C^2}$$

$$\begin{aligned}
Re &= \frac{2R}{1+\omega^2 R^2 C^2} \\
Re(1 + \omega^2 R^2 C^2) &= 2R \\
Re + Re\omega^2 R^2 C^2 - 2R &= 0
\end{aligned}
\tag{Equation 4.5}$$

$$\begin{aligned}
Im &= \frac{-2\omega R^2 C}{1+\omega^2 R^2 C^2} \\
Im(1 + \omega^2 R^2 C^2) &= -2\omega R^2 C \\
Im + Im\omega^2 R^2 C^2 + 2\omega R^2 C &= 0
\end{aligned}
\tag{Equation 4.6}$$

$$\begin{aligned}
Re + Re\omega^2 R^2 C^2 - 2R &= 0 && \text{Equation 4.5} \\
1 + \omega^2 R^2 C^2 - \frac{2R}{Re} &= 0 && (\div Re)
\end{aligned}$$

$$\begin{aligned}
Im \left(1 + \omega^2 R^2 C^2 - \frac{2R}{Re} \right) &= 0 && (\times Im) \\
Im + Im\omega^2 R^2 C^2 - \frac{2RIm}{Re} &= 0 && \text{Equation 4.7}
\end{aligned}$$

$$Im + Im\omega^2 R^2 C^2 + 2\omega R^2 C = Im + Im\omega^2 R^2 C^2 - \frac{2RIm}{Re} \tag{2)=(3)}$$

$$\begin{aligned}
R \left(2\omega RC + \frac{2Im}{Re} \right) &= 0 \\
2\omega RC &= \frac{2Im}{Re} \\
RC &= \frac{2Im}{Re2\omega}
\end{aligned}
\tag{Equation 4.8}$$

$$\begin{aligned}
Re + Re\omega^2 (RC)^2 - 2R &= 0 \\
Re + Re\omega^2 \left(\frac{2Im}{Re2\omega} \right)^2 &= 2R
\end{aligned}$$

$$R = \left(\frac{1}{2} \right) Re + Re\omega^2 \left(\frac{2Im}{Re2\omega} \right)^2 \tag{Equation 4.9}$$

$$C = \frac{2Im}{RRe2\omega} \tag{Equation 4.10}$$

4.6 Discussion

This research identified that dry e-textile electrodes for AC measurements act as conductors composed of resistive and capacitive components. An electrode can be represented as an equivalent electrical circuit, specifically an RC in parallel circuit. For a predefined frequency of 50 kHz, R has a negligible influence on Z_p , where Z_p is identical to X_c . Much research into measuring the efficiency of dry electrodes only account for R or the sheet resistance (RS), the resistance per square. This study shows the importance of incorporating X_c into the measurements. Studying Z_p for dry electrodes results in an accurate insight into the efficiency of dry electrodes. This is evident in the results of this study where the lowest R and X_c values were not associated to a single electrode with specific parameters indicating no correlation of R and X_c . Thus, it is critical to measure Z_p .

The influence of the embroidery variables on Z_p was also presented. To reduce Z_p , an increase in the conductivity is required. This can be achieved by increasing the electrodes surface area and stitch density to increase the amount of yarn of the e-textile electrodes thus increasing the conductivity of the e-textile electrodes causing a reduction in the Z_p . However, observing the amount of conductive yarn used for the electrodes (in terms of length) it is safe to assume that there is a threshold relating to the type of stitch used in the fabrication process. By achieving this threshold, the amount of conductive yarn used does not influence Z_p . Although, Berk et al. [204] suggested that decreasing the amount of yarn used by reducing the stitch density resulted in a decrease in resistance across all stitch types presented using a similar yarn to this research. Antithesis, the findings presented here are measured in terms of Z_p taking into account X_c . Thus, indicating that for an efficient e-textile electrode a reduction in Z_p can be achieved by: (i) increasing the surface area and (ii) increasing the stitch length and density. In addition, the threshold observed indicates that Z_p is not impacted by the amount of yarn used for the e-textile electrode.

4.7 Conclusion

In this study, it was determined that the most efficient e-textile electrode had a surface area of 13.2 cm². It was fabricated with a weave stitch with a stitch length of 7 mm and a density of 0.4 mm. Z_p was measured to be 244 k Ω , representing close to a 50% reduction compared to the various electrodes evaluated in this study. For this e-textile electrode, 8 m of conductive thread was used, making it ergonomic in addition to efficiency in manufacturing costs. This study presents the importance of measuring Z_p of dry electrodes to adapt to BIA systems and the influence of embroidery variables of the electrode design.

Chapter 5

Evaluating e-textiles for usability with BIA application

5.1 Introduction

Adapting Bioelectrical Impedance Analysis (BIA) as a diagnostic tool [44,45,168–170,74,134,137–139,163,166,167] to monitor electrophysiological activities can potentially improve the quality of life for patients while reducing costs and efficiency in the health system. An ideal application would be to develop a diagnostic system permitting patient self-monitoring in home settings resulting in a reduction in the length of hospital stays, visits to emergency departments and number of hospital readmissions [230]. Recent research into further development of internet applications, has given rise to the Internet of Things improving telemedicine. However, telemedicine today is still based on the traditional patient-doctor interaction. To improve this current situation, technology has the potential to collect objective diagnostic data using BIA from the patient in the comfort of their surroundings and transmit this data to a practitioner in real time. In order to not restrict the patient's daily activities, a wearable system should be designed for long-term monitoring while accounting for the patient's physiological comfort. Recently, research into conductive yarns have given rise to the fabrication of e-textiles. This has given an opportunity to replace wet electrodes with e-textile electrodes for BIA systems.

E-textile electrodes fabricated with embroidery techniques are advantageous for long term monitoring due to its simple fabrication process, and versatility allowing customisation of the electrodes relating to a patient's ailment [53,202–204]. Although, e-textile electrodes are have been researched and tested with ECG, EEG and EMG biosignal analysis [60,61,206,219–221,225,226,231,63–65,199,201–203,205], its polarization impedance (Z_p) has been disregarded. A low Z_p is associated with clear and concise measurements reducing any signal attenuation and distortion [47].

Chapter 4 showed the influence of certain embroidery characteristics of e-textile electrodes relative to Z_p for use with single frequency BIA (sfBIA) of 50 kHz [47]. Using a triple layer wafer experimental methodology, the electrodes were tested autonomously. It was observed that an increasing the e-textile electrodes surface area resulted in Z_p being reduced significantly. This could be attributed to the amount of conductive yarn consumed in the fabrication of the e-textiles. Small changes to Z_p were also noticeable when varying specific stitch variables, specifically regarding the stitch properties (i) type (ii) length and (iii) spacing (density).

This set the foundation in adapting e-textile electrodes for BIA systems. However, practically e-textile electrodes form the link between the system to the biotissue under study (BUS). Non-invasive contact electrodes adhere to the skin forming an electrode-skin interface. It is common for skin conditions to change, specifically the skin temperature and perspiration. Research into the physiological comfort of textiles focus on their properties relative to environmental temperature, moisture regain and breathability. Thus, adapting textiles as substrates for e-textile electrodes it is safe to hypothesis that skin temperature and perspiration relating to environmental temperature and moisture regain of textiles will influence Z_p . In addition, breathability is important in selecting a substrate to improve the microclimate between the e-textile electrodes and skin. Air passing through the e-textile electrodes reduces the possibility of the skin temperature increasing while allowing perspiration vapor to be transported to the outside atmosphere. Thus, the study of the e-textile electrode based on practical conditions of the electrode-skin interface is important.

This interface gives rise to an additional impedance, specifically the electrode-skin impedance (Z_{es}) [51,184,232,233] and is influenced by the electrodes Z_p . When using the BIA for diagnostics attached to paired e-textile electrodes, the system measures the impedance (Z_m) of the BUS in addition to the Z_{es} and can be expressed as:

$$Z_m = Z_{BUS} + Z_{es} + N,$$

$$\text{thus } Z_{BUS} = Z_m - Z_{es} - N,$$

where Z_m refers to the impedance measurement resulting deduced from the BIA system, Z_{BUS} is the actual BUS impedance while the electrode-skin impedance is represented by Z_{es} . This equation has also taken into account any unwanted noise N , this could be due to any motion or pressure artefacts [191,211,234,235]. However, the focus of this study is to understand the characterisation of Z_p relating to e-textile electrodes.

Isolating and resolving Z_{es} is an ongoing problem in the field of electrophysiological activity measurements. Ag/AgCl are commonly used in clinical settings and have a layer of electrolyte 'gel' making the electrode non-polarized [179]. This results in a low Z_{es} ; however, electrode mismatch between the coupled electrodes continues to disrupt measurements. In addition, when this 'gel' layer dries and loses its adhesiveness an unstable Z_m occurs leading to inaccurate analysis of the BUS. In addition, Z_{es} is significantly affected. This gives rise to powerline interference thus contributing to N [49].

The 'gel' and 'adhesive' properties of wet electrodes give rise to degradation of the functioning electrodes reducing the ability of controlling changes in skin properties

over an extensive period of time. However, these issues can be resolved with the use of e-textile electrodes. By making use of textile properties, such as its permeability, changes in Z_p associated with e-textile electrodes relative to skin properties can be identified, i.e., perspiration and temperature. Adapting a methodology to characterise this relationship can potentially lead to consistent and accurate system measurements (Z_m). In addition, by characterising Z_p relative to changes in skin properties, it can contribute to determining Z_{es} which can facilitate in identifying Z_{BUS} from Z_m . Thus, it is important to select an appropriate substrate for the fabrication of e-textiles. It is preferable for the substrate to contribute to a reduced Z_p in conjunction with a small change in Z_p relative to changes in skin properties.

5.1.1 Skin temperature and perspiration

Body temperature refers to skin and core temperature; it is also the cause of perspiration. Skin is the largest sensory organ of the human body comprising of thermoreceptors that detect differences in temperature triggering the appropriate defence responses. Research has yet to identify whether skin acts as a feedforward or feedback control in thermoregulation. Feedback describes the skin temperature influence on the thermoregulation process. Contrary to this, feedforward implies the influence of the thermoregulation process on skin temperature [98].

It is understandable that skin temperature is dependent on environmental temperature in addition to body core temperature. However, it is also subject to skin properties such as skin thickness and its underlying structure. This results in varied skin temperatures associated to various parts of the human body.

Skin temperature is also associated with a patient's medical conditions. Regular bodily structure and function is disturbed due to any illness or ailment resulting in changes in skin temperature [101]. An increase in body temperature is caused by the body's immune response acting to fight off any infections including viruses and bacteria. This gives rise to the production of perspiration from the sweat glands in order to reduce the skin temperature and maintain its thermophysiological temperature. Skin temperature is also affected by administered anaesthesia during surgical procedures. General anaesthesia causes a decrease in the body's temperature [96] while local anaesthesia decreases the temperature of the region.

Thermophysiological skin temperature is defined as the temperature where the body feels comfortable. However, a defined threshold for the thermophysiological skin temperature has yet to be determined, although suggested thresholds in previous research demonstrate relatively close variances. Research conducted in 1936 presented a threshold of 33.5 and 36.9°C for skin temperature [99]. However, with the advancement of technology it is expected that research conducted recently would reveal different thresholds, indicating a variation between 30-34°C [102–104].

A correlation between skin temperature, skin wetness and relative humidity (RH) was demonstrated by Mole et al. [236]. It associates skin wetness to an increase in RH defining a low boundary at 40% RH for a temperature threshold of 30-34°C [236]. Given the research conducted in the area of skin temperature and skin wetness, these boundary conditions provide a foundation to test the influence of skin changes on Z_p of e-textile electrodes.

To reduce the influence of skin changes, the breathability of the e-textile electrode should be tested. This is associated with the comfort of the wearing the electrodes and the microclimate induced between the electrodes and skin. Fabricating e-textile electrodes that possess low air permeability can potentially cause the skin temperature to increase giving rise to perspiration [237]. Refer to Appendix III for information on air permeability relating to textiles. Therefore, it is important to consider an e-textile electrode possessing a relatively large air permeability to maintain the skin's thermoregulation.

This study considers the impact of skin temperature and perspiration on Z_p of the e-textile electrodes. The current body of knowledge in skin properties was acquired to form an experimental protocol characterizing Z_p of the e-textile electrodes fabricated on various substrates. An initial test was conducted in an ambient environment identical to the method in Chapter 4 [47] to verify the impact of substrate selection on Z_p . To follow, the electrodes were placed in a climatic chamber and the temperature and RH were set to the boundary conditions emulating human skin temperature and perspiration; thus, Z_p was measured accordingly. To conclude the selection of the substrate, it was important to consider the electrode-skin microclimate associated with the physiological comfort of the e-textile electrodes, thus the air permeability was evaluated across all fabricated e-textile electrodes. By choosing an appropriate substrate, the influence of the shape of the electrodes was also considered. The shape of the electrode can have an impact on the polarization impedance due to the charge distribution and flux fringing. This is commonly associated with wearable antennae's that operate at significantly higher frequencies.

5.2 Method

The process involved in fabricating the e-textile electrodes was presented in Chapter 4. However, for this study the substrate of the e-textile electrodes varied in order to observe the impact of skin temperature and perspiration on Z_p . It is important to select a substrate supporting a relatively low and stable Z_p of the e-textile electrode across these changes in skin properties for accurate diagnostic measurements. Thus, the most common textiles in the textile industry were selected to evaluate their suitability as substrates for e-textile electrodes. The selected substrates include the polyester non-woven felt (as presented in Chapter 4), and cotton substrates with various structures including plain weave, poplin and velvet. This ability to tailor e-

textile electrodes potentially provides a fundamental approach into creating a diagnostic tool based on BIA measurements to monitor electrophysiological activity long-term. Referring to Figure 5.1a, the e-textile electrodes can be used with the BIA system in order to collect the electrophysiological measurements from the patient. However, the patient presents physiological properties that can influence the performance of the e-textile electrode. These physiological influences need to be considered in the design process of the e-textile electrode, Figure 5.1b.

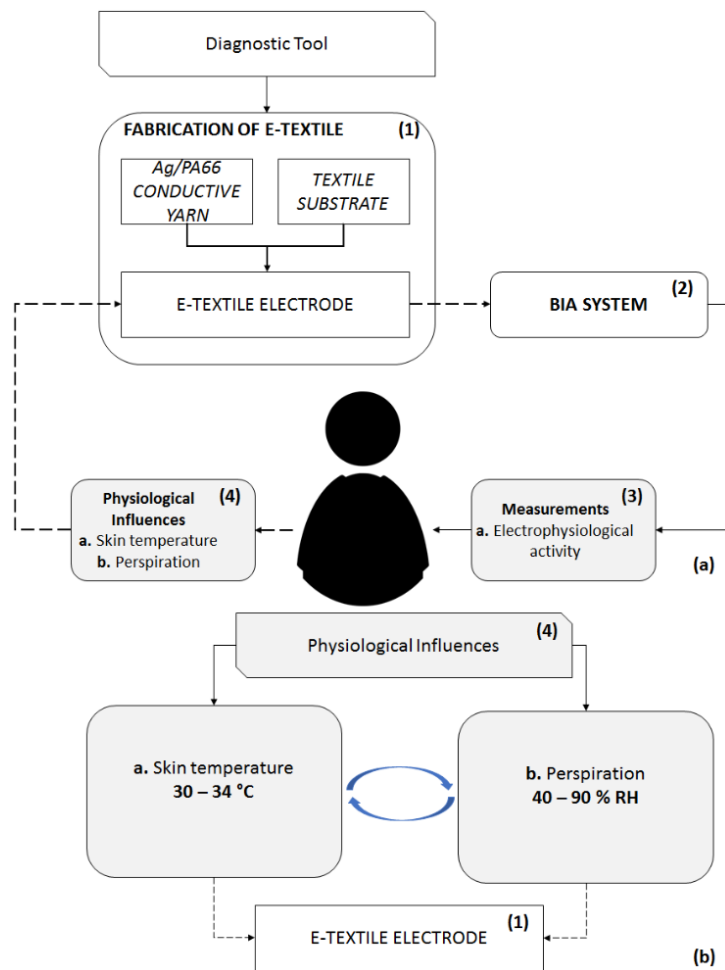


Figure 5.1 Relation of a BIA diagnostic system and associated components with patient: (a) system relating to the monitoring the patient, (b) patient's physiological parameters that can impact the e-textile electrodes [238]. "© IOP Publishing. Reproduced with permission. All rights reserved."

5.2.1 The fabrication process

The embroidery methodology reported in Chapter 4 [47] was used with different substrates to fabricate the e-textile electrodes. The substrates for this study were purchased commercially. They were selected based on their distinct properties in terms of (i) thread composition, (ii) textile structure, (iii) weight, (iv) thickness and (v) relative permittivity, refer to Table 5.1. Variables (i)-(iii) are provided by the

manufacturer while the other variables were measured with: (iv) a fabric thickness gauge and (v) a split post dielectric resonator. For an explanation on relative permittivity please refer to Appendix III. In addition to these properties, the substrates possessed a low drape resulting in relatively rigid textiles. To distinguish the structure of the substrates Scanning Electron Microscopy (SEM) was used, with the SEM images shown in Figure 5.2 (for a standard photo of the studied substrates refer to Figure 1 in Appendix III). This assists in the stability of the e-textile electrodes when conducting measurements. For the purpose of this study, an appropriate substrate for the fabrication of e-textile electrodes was selected based in the characteristics of Z_p . The characteristics of the substrates are provided as a guideline and the correlation of Z_p on the substrates properties is outside the scope of this study. For further information on the substrates, please refer to Appendix III. Future research will study the impact of the textile structures on Z_p (refer to Chapter 7). This study adapted commercially available substrates emphasising the simplicity of the in-house fabrication process.

Table 5.1 Characteristics of selected substrates as a base for the e-textile electrodes [238]. “© IOP Publishing. Reproduced with permission. All rights reserved.”

| | Substrate 1 (for e-textile electrodes 1 - E1) | Substrate 2 (for e-textile electrodes 2 - E2) | Substrate 3 (for e-textile electrodes 3 - E3) | Substrate 4 (for e-textile electrodes 4 - E4) |
|---------------------------------|--|--|--|--|
| <i>Description</i> | Cotton Plain Weave | Cotton Poplin | Cotton Velvet | Polyester Non-Woven Felt |
| <i>Composition</i> | Co 100% | Co 100% | Co 100% | PES 100% |
| <i>Structure</i> | Plain Weave | Poplin | Velvet | Non-Woven |
| <i>Weight (g/m²)</i> | 200 | 100 | 300 | 200 |
| <i>Thickness (mm)</i> | 0.65 | 0.4 | 1 | 1.5 |
| ϵ_r | 1.12 | 1.14 | 1.33 | 1.20 |

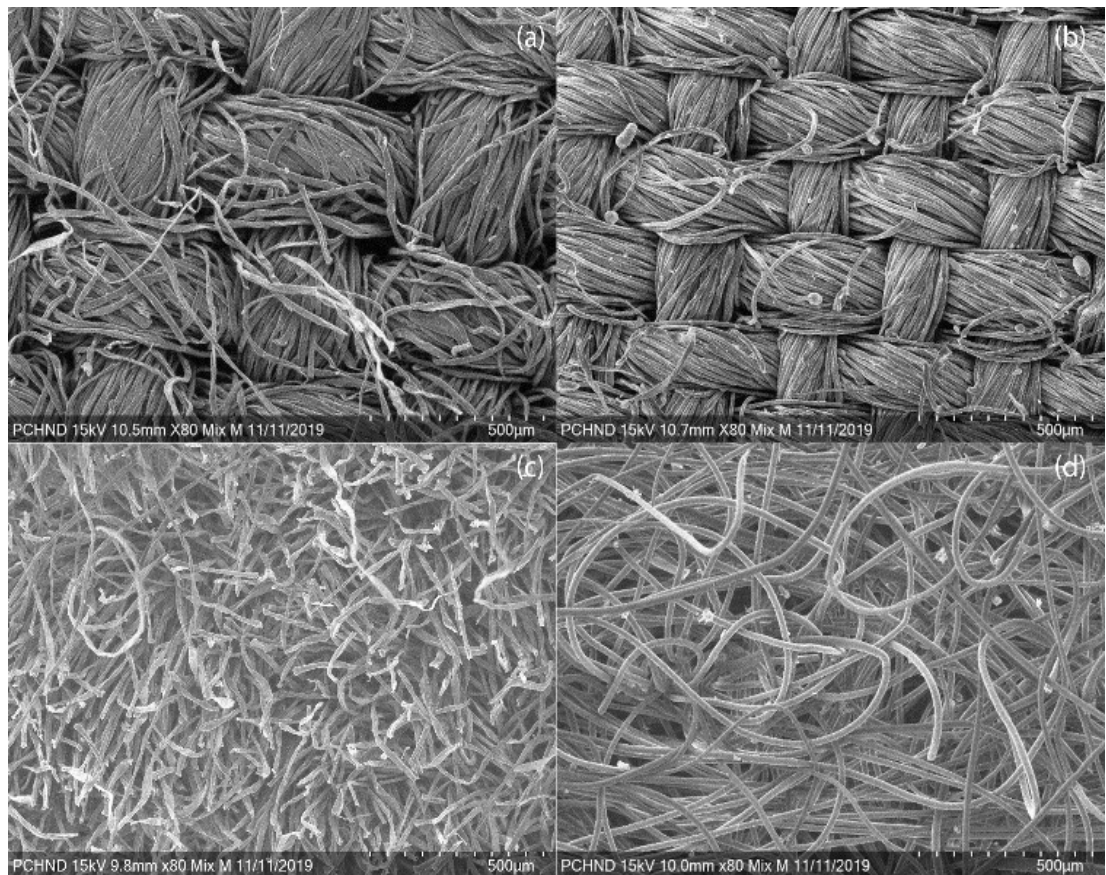


Figure 5.2 SEM representation of the selected textile substrates: (a) S1 (b) S2 (c) S3 and (d) S4 [238]. “© IOP Publishing. Reproduced with permission. All rights reserved.”

The fundamental material providing conductivity to the e-textile electrode was the Shieldex Conductive Yarn which was used with the polyester non-conductive yarn. The electrodes were designed based on the findings in Chapter 4. E-textile electrodes rectangular in shape with a surface area of 13.2 cm² demonstrated a reduction in Z_p for the weave and satin stitch demonstrating comparable results. However, the weave stitch consumed less thread. The e-textile electrodes were reproduced for this study with the embroidery settings of stitch length and density of 7 mm and 0.4 mm respective. This embroidery design was created using the EasyDesign EX software that was connected to the Singer Futura XL-550 embroidery machine.

The e-textile electrodes fabricated on the selected substrates (refer to Table 5.1) are shown in Figure 5.3. The samples were weighed in order to calculate the length of conductive thread used relative to the substrate using the textile units formula (Appendix I). The length of conductive thread measured in the sample sets were relatively close: E1 = 7.9 m; E2 = 7.3 m; E3 = 7.7 m and E4 = 7.6 m. Considering the electrodes as a whole, they were all fabricated with consistent embroidery settings

and thus they only differ in terms of the substrate. This difference in Z_p can be due to the different substrate structures in terms of density, thickness or surface roughness. However, the selection of the substrate is based on its efficiency as an e-textile electrode as a whole. By selecting the most suitable substrate, 12 sets (2 samples per set) of rectangular and elliptical e-textile electrodes of the same surface area (i.e., 13.2 cm²) were fabricated.

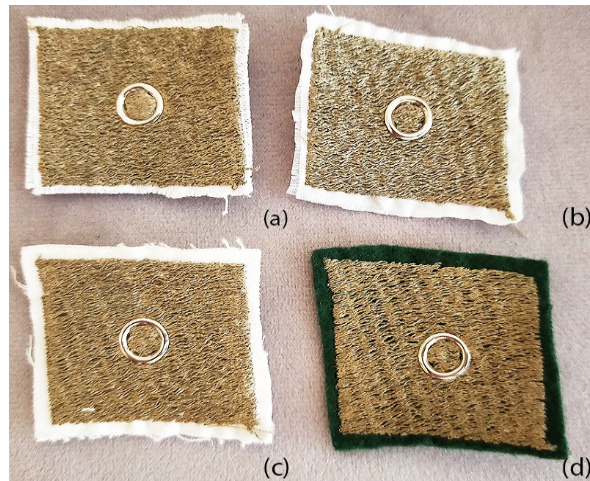


Figure 5.3 Fabricated e-textile electrodes with selected substrates: (a) cotton plain weave (E1), (b) cotton poplin (E2), (c) cotton velvet (E3) and (d) polyester non-woven felt (E4) [238]. “© IOP Publishing. Reproduced with permission. All rights reserved.”

5.2.2 Experimental protocol

To measure Z_p of the various electrodes, the triple-layer wafer testing method [47] was adopted. This wafer method was prepared by having the inner-sides of the top and bottom electrodes interfaced with a polyester swatch measuring 45 x 40 mm. Polyester was selected due to its hydrophobic properties resulting in consistent electrical properties over time. The swatch was cut large enough to cover the conductive surface area of the electrodes to avoid any short circuit. Non-conductive wooden craft pegs were positioned at the corners of the electrodes stabilising the wafer configuration. These were clipped to the outer-edge of the embroidered surface and were only in contact with the substrates. Thus, preventing the cause of inaccurate measurements due to any pressure impacting the electrodes surface area.

The HM8118 Meter was used to measure Z_p . To test the electrodes in ambient temperature, the HM8118 was connected to the electrodes with Kelvin clip test leads attached to the ball-parts of the snap fasteners on the top and bottom electrodes (refer to Chapter 4).

To emulate skin properties, the climatic chamber used for this study was the CCK-25/48 (Dycometal, Spain). To test the rectangular electrodes in a climatic chamber,

care was taken into placing the electrodes to avoid any electrical interference. The craft pegs held the electrode at a distance from the grill of the chamber. The Kelvin clip test leads were passed through an aperture of the climatic chamber and connected to the electrodes by the ball-part of the snaps and the aperture was sealed with a rubber plug, that also stabilised the leads.

Measuring the resistance (R) and reactance (X_C) of the electrodes, the Z_p was calculated for the e-textiles using the following equation:

$$|Z_p| = \sqrt{R^2 + X_C^2}, \quad \text{Equation 5.1}$$

$$\text{where } X_C = \frac{1}{2\pi f C}. \quad \text{Equation 5.2}$$

For simplicity Z_p is used as the modulus.

Previous studies on the properties of textiles indicate a consistent resistance of a substrate across various samples showing that textiles are associated with a well-defined resistance [239]. The electrodes were measured as a continuous function of time, as conducted in Chapter 4. Chapter 4 presented a consistent Z_p over three minutes thus eliminating the use of standard deviation and error bars [47].

The electrodes were first tested in ambient room conditions with a temperature of 25°C before being placed into the climatic chamber. To emulate skin properties, the temperature and RH of the climatic chamber was varied with the thresholds identified in previous research, refer to Figure 5.4. The electrodes were tested for temperatures between 30 and 34°C by 1°C increments while RH ranged from 40 to 90% incremented by 10%.

By setting the climatic chamber to these RH boundaries defined by Mole et al. [236], skin wetness causes the textile to become wetter. This is dependent on the moisture regain of the substrate. After each experiment the electrodes were removed from the climatic chamber and let out to dry. Lastly, the PROWHITE AIRTEST II (PROWHITE, Istanbul, Turkey) was used and set at 200 Pa to test the air permeability of the electrodes. Measurements were recorded for the substrates and e-textile electrodes. By selecting the most appropriate textile as a substrate, a new set of rectangle electrodes were fabricated in addition to elliptical electrodes where Z_p was tested in ambient conditions using the wafer method.

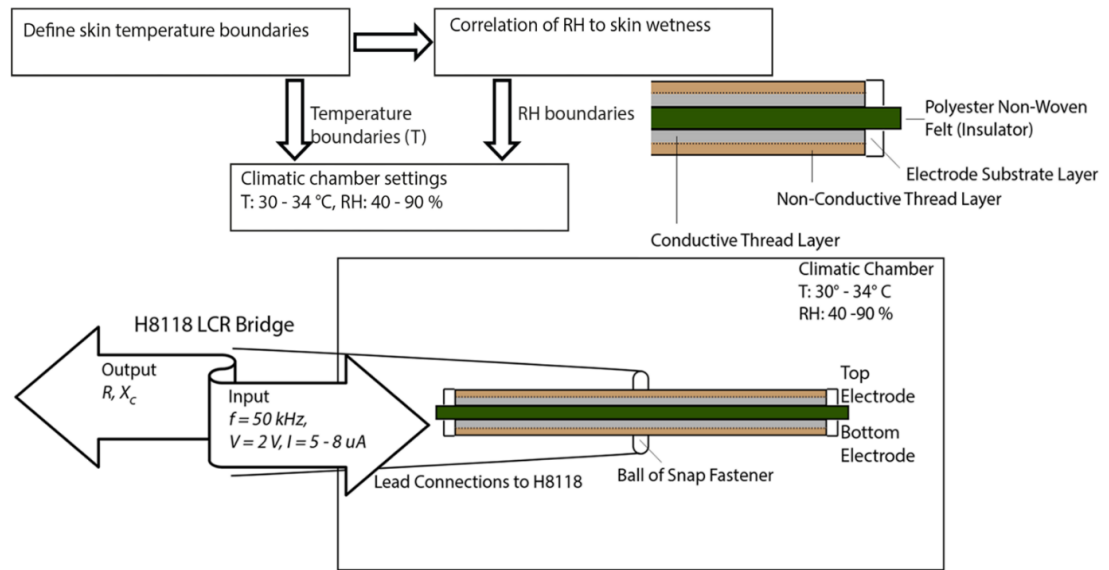


Figure 5.4 Experimental protocol using climatic chamber [238]. “© IOP Publishing. Reproduced with permission. All rights reserved.”

5.3 Results

5.3.1 Testing in ambient conditions

The different substrates used to fabricate the e-textile electrodes, resulted in a variance in Z_p , refer to Figure 5.5. Due to its capacitive properties, as demonstrated in Chapter 4, the difference in ϵ_r of the various substrates impacted the overall impedance. Testing of the e-textile electrodes resulted in Z_p for the sets: E1 - 269, E2 - 284, E3 - 258 and E4 - 244 k Ω . Thus, it is observed that the polyester non-woven substrate demonstrated the lowest Z_p with a 15% difference to the cotton poplin e-textile electrodes which possessed the largest Z_p in ambient conditions. Further study into the substrate's properties showed no relationship to the substrate's properties presented in Table 5.1. The set of electrodes with the lowest Z_p were E4, followed by E3 then E1 while E2 presented the highest Z_p . Their associated substrates: (i) ϵ_r – 1.2, 1.33, 1.12 and 1.14; (ii) thickness (mm) – 1.5, 1, 0.4, 0.65; (iii) weight (g/m²) – 200, 300, 200 and 100. The textile variables that can possibly influence Z_p include: the structure of the textiles, the linear density of the thread used in the substrates or any finishing applied to the textile [55]. However, these variables are outside of the scope of this research. Nevertheless, given the application of e-textiles the impact of temperature and wetness on Z_p was examined.

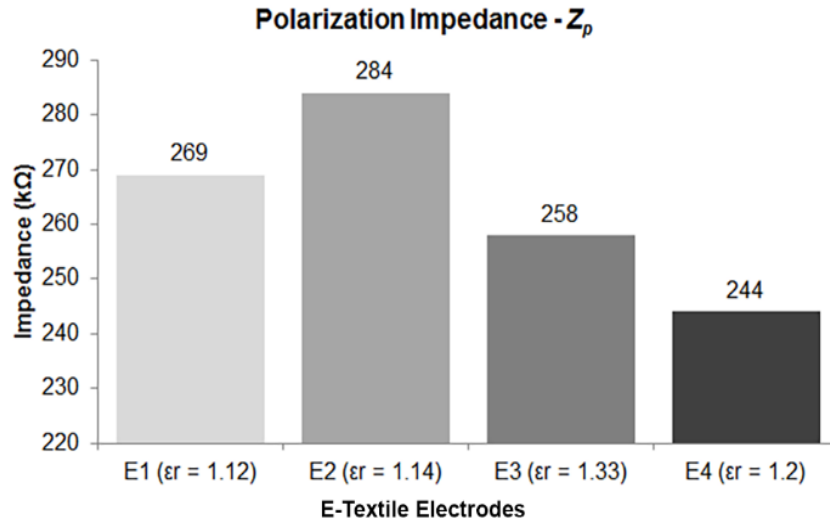


Figure 5.5 Ambient measurements of Z_p relative to ϵ_r of substrate [238]. “© IOP Publishing. Reproduced with permission. All rights reserved.”

5.3.2 Testing using climatic chamber

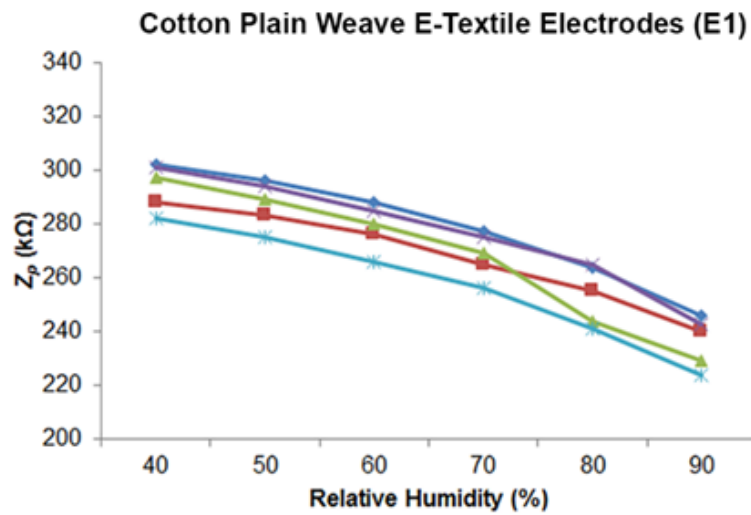
For each set of electrodes, the results of Z_p relative to temperature and RH were plotted in Figure 5.6. It was observed that temperature does influence Z_p . Absolute values of Z_p are presented in Table 5.1 (Appendix IV). However, no direct correlation can be realized for the electrodes autonomously or across the various electrodes. To gain a better understanding of the temperature influence, Figure 5.7 presents the behaviour of Z_p relative to a single unit of temperature increments. It is observed that the impact of temperature is relatively small; however, it is inconsistent displaying unpredictable fluctuations of Z_p . This is evident across all sample sets for all RH settings. Sample set E1 demonstrated the largest changes relative to all the sample sets. Contrary to sample set E4 which was relatively stable and, in some instances, demonstrated no change in Z_p . The greatest change in samples E4 were observed close to the boundaries for all RH settings, specifically increases in temperature from 30°C-31°C and 33°C-34°C, with the least changes occurring between 31°C-33°C. The relative difference between $Z_{p(max)}$ and $Z_{p(min)}$ was calculated for the defined skin temperatures (30-34°C) relative to the RH. The relative difference was found using Equation 5.3 and is presented in Table 5.2. It is evident that RH had a greater influence on Z_p . Figure 5.8 presents the change in Z_p corresponding to the 10% RH increments for all the temperature settings.

$$\Delta Z_p(\%) = \frac{Z_{p(Tmax)} - Z_{p(Tmin)}}{Z_{p(Tmin)}} \times 100 \quad \text{Equation 5.3}$$

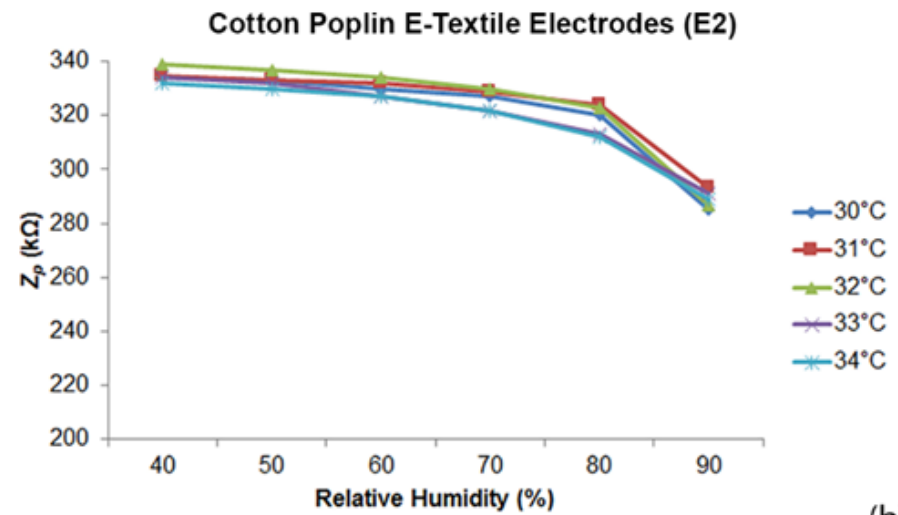
Table 5.2 Relative difference of Z_p associated to skin properties (Equation 5.3) [238]. “© IOP Publishing. Reproduced with permission. All rights reserved.”

| | 40% | 50% | 60% | 70% | 80% | 90% | 40% | 50% | 60% | 70% | 80% | 90% |
|--------------------|-----|-----|-----|-----|-----|-----|-----|-----|-----|-----|-----|-----|
| | E1 | | | | | | E2 | | | | | |
| ΔZ_p^* (%) | 7.6 | 7.6 | 8.2 | 9.9 | 9.9 | 9.8 | 2.1 | 2.1 | 2.1 | 2.4 | 3.8 | 2.8 |
| | E3 | | | | | | E4 | | | | | |
| ΔZ_p^* (%) | 2.4 | 1.4 | 1.4 | 0.4 | 2.6 | 9.0 | 2.5 | 2.9 | 3.3 | 3.8 | 5.0 | 6.5 |

*Relative difference in Z_p for temperature

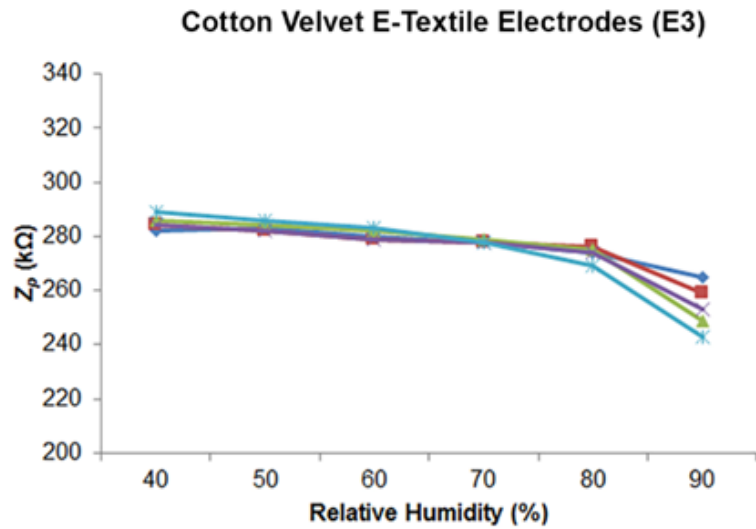


(a)

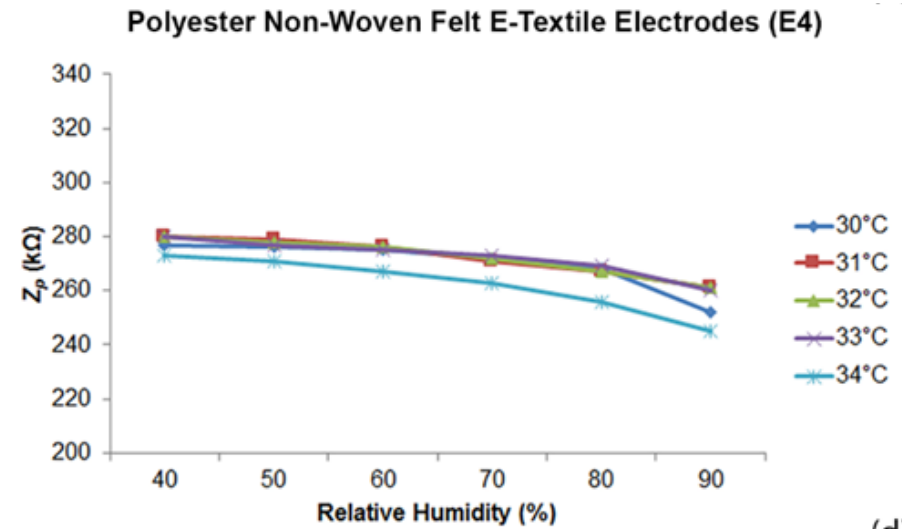


(b)

Figure 5.6a-b Impact of temperature and wetness (RH) on Z_p : (a) E1 and (b) E2 [238]. "© IOP Publishing. Reproduced with permission. All rights reserved."



(c)



(d)

Figure 5.7c-d Impact of temperature and wetness (RH) on Z_p : (c) E3 and (d) E4 [238]. "© IOP Publishing. Reproduced with permission. All rights reserved."

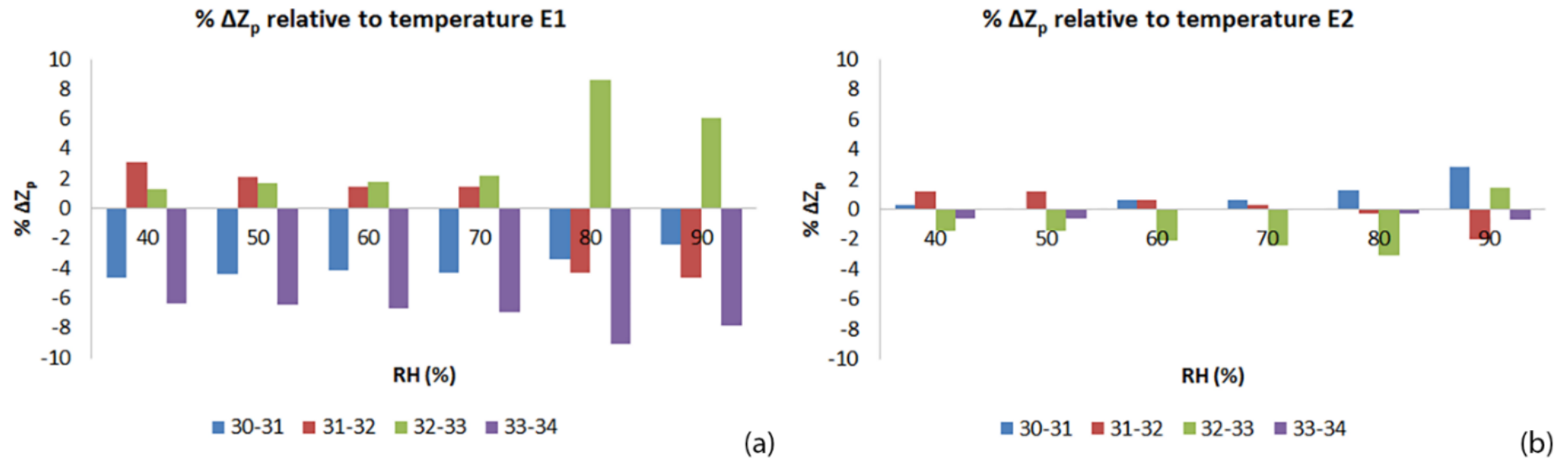


Figure 5.8a-b Relative change in Z_p associated with temperature: (a) E1 and (b) E2 [238]. "© IOP Publishing. Reproduced with permission. All rights reserved."

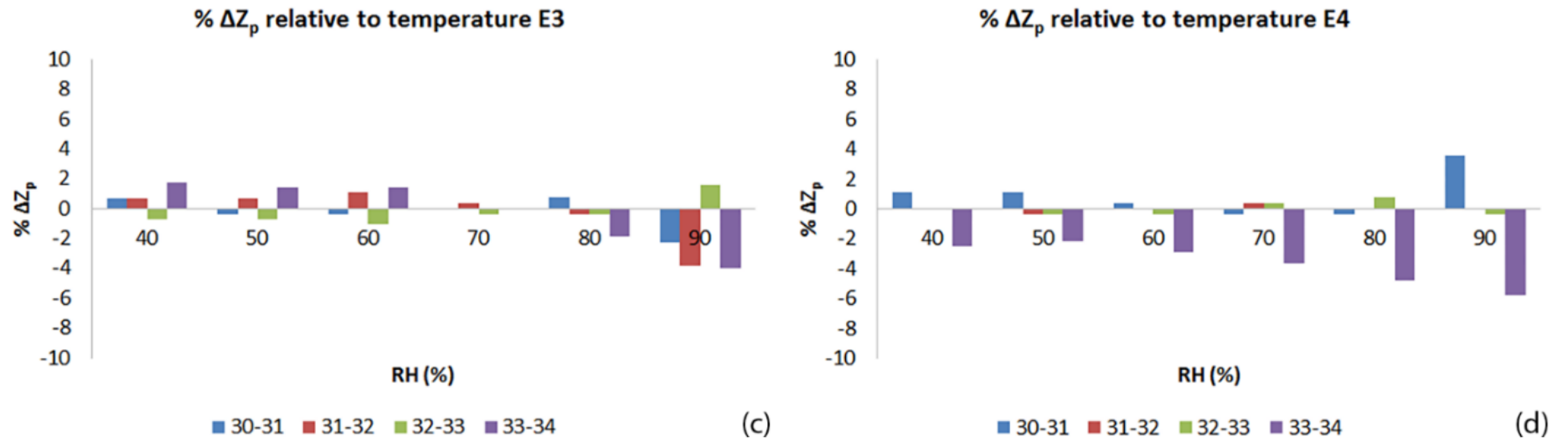


Figure 5.9c-d Relative change in Z_p associated with temperature: (c) E3 and (d) E4 [238]. “© IOP Publishing. Reproduced with permission. All rights reserved.”

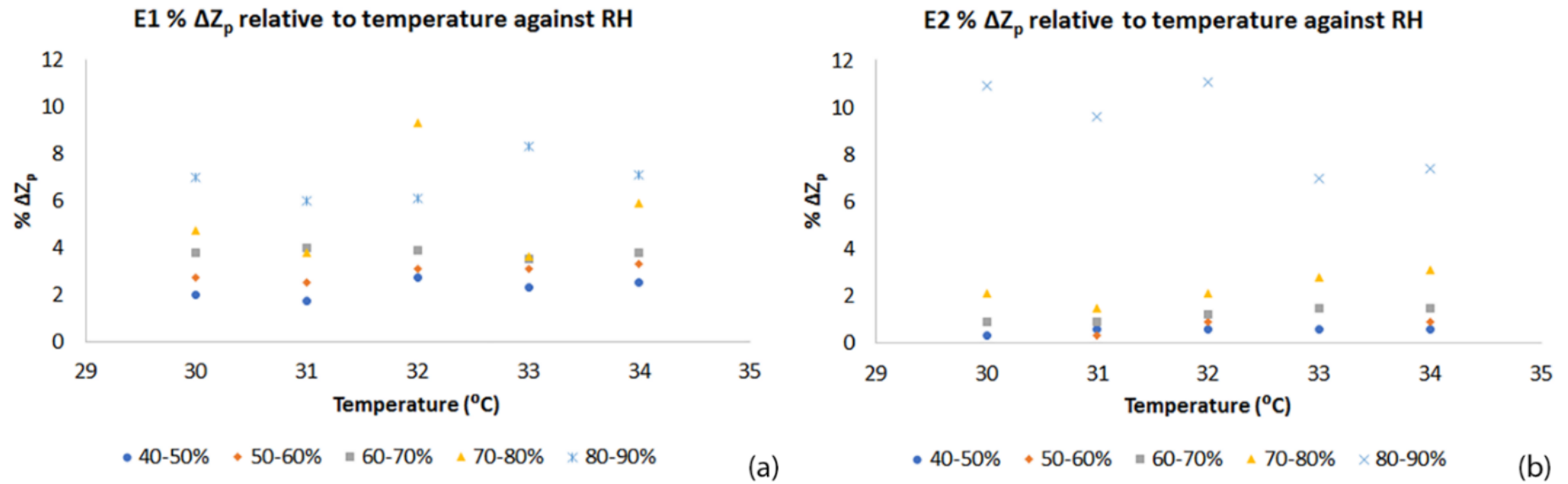


Figure 5.10a-b Relative change in Z_p associated to increments of RH: (a) E1 and (b) E2 [238]. "© IOP Publishing. Reproduced with permission. All rights reserved."

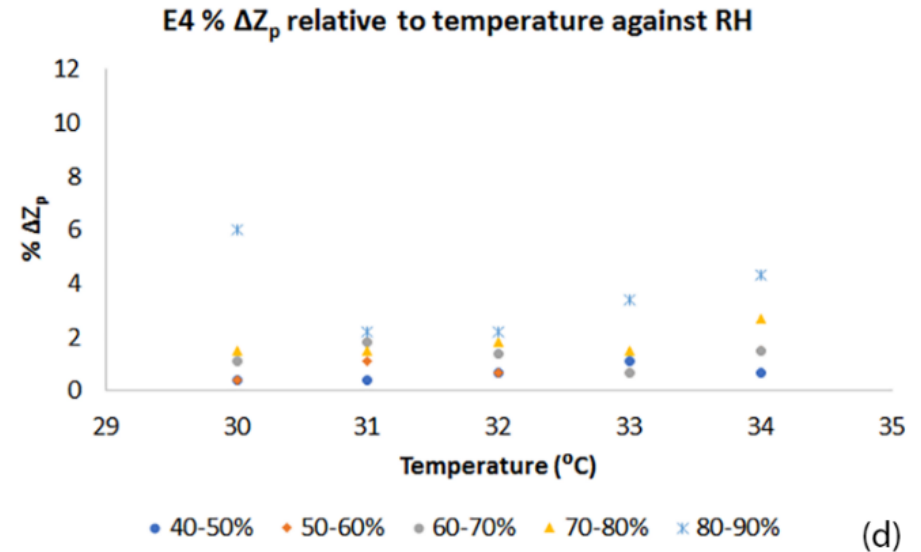
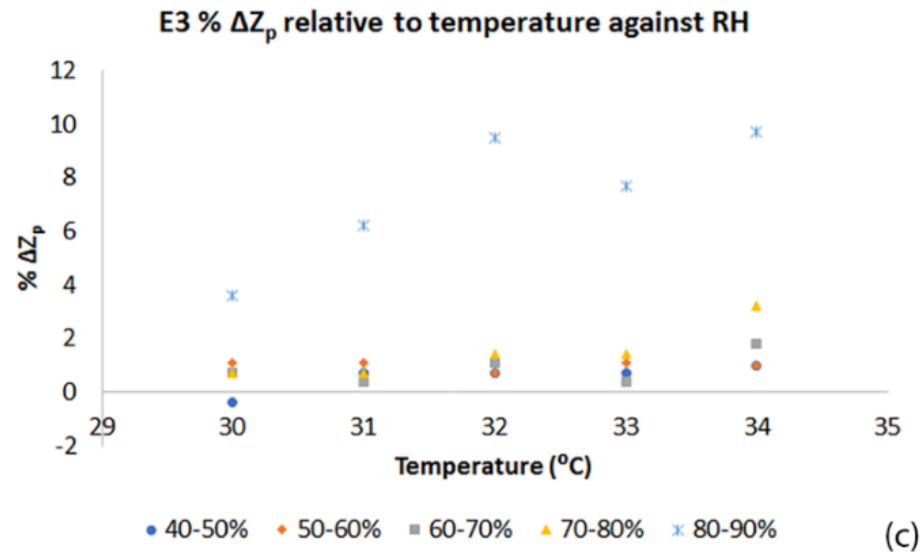


Figure 5.11c-d Relative change in Z_p associated to increments of RH: (c) E3 and (d) E4 [238]. “© IOP Publishing. Reproduced with permission. All rights reserved.”

Referring to Figure 5.8, it is observed that a greater change in Z_p occurs relative to an increase in RH compared to a change in temperature. However, an inconsistency in Z_p is evident across RH relative to temperature increments. When applying a polynomial trend $R^2 < 0.5$, with samples E1 showing the weakest R^2 . Although sample sets E2, E3 and E4 are presented with a stronger correlation, no mathematical correlation is observed between the equations. This is observed by the parabolas alternating between positive and negative values and varies in width. Therefore, no relation was observed across the various temperatures (Table 2, Appendix IV).

It is suggested that the temperature is dependent on RH for changes in Z_p . Figure 5.8 indicates a large decrease in Z_p at a RH of 90% across for all electrode samples. Taking into consideration that textiles begin to dampen at about 80% RH, it is expected that at 90% RH substrate is considered wet due to the moisture content resulting in a significant drop in Z_p . Therefore, the effect of RH on Z_p within the range of 40-80% was analysed. By applying linear regression to the plots in Figure 5.6, the change in Z_p relating to RH was observed, refer to Figure 5.9. The linear regression equations ($y = mx + c$) are presented in Table 5.3. Referring to Figure 5.9 and Table 5.3, samples E3 and E4 were observed to be impacted the least by changes in the applied temperatures and RH ranges with a close to 'zero slope' indicating small variation. However, samples E4 are preferred as they are indicative of possessing a lower Z_p due to its lower y intercept value. This shows that any changes due to skin temperature and perspiration will not significantly impact Z_p while maintaining a relatively low Z_p . For electrophysiological measurements, this is an ideal substrate as any changes to the skin relating to the temperature and humidity from perspiration can result in the BIA measurements being unstable. Moreover, this study has determined the trends relating to skin temperature and perspiration across various substrates that can potentially be applied to BIA systems. This trend indicates the scale of interference; this, this can be taken into consideration when calibrating the design of the system.

Table 5.3 Linear regressions associated to skin temperature relative to RH (40 - 80%): $y = mx + c$ [238]. “© IOP Publishing. Reproduced with permission. All rights reserved.”

| | 30°C | R^2 | 31°C | R^2 | 32°C | R^2 | 33°C | R^2 | 34°C | R^2 |
|-----------|---------------|-------|---------------|-------|---------------|-------|---------------|-------|---------------|-------|
| <i>E1</i> | $-1.0x + 342$ | 0.98 | $-0.8x + 234$ | 0.98 | $-1.3x + 351$ | 0.93 | $-0.9x + 339$ | 0.99 | $-1.0x + 325$ | 0.98 |
| <i>E2</i> | $-0.3x + 349$ | 0.91 | $-0.3x + 346$ | 0.92 | $-0.4x + 356$ | 0.94 | $-0.5x + 357$ | 0.95 | $-0.5x + 297$ | 0.90 |
| <i>E3</i> | $-0.2x + 292$ | 0.86 | $-0.2x + 292$ | 0.98 | $-0.3x + 297$ | 0.97 | $-0.2x + 293$ | 0.97 | $-0.5x + 310$ | 0.94 |
| <i>E4</i> | $-0.2x + 287$ | 0.91 | $-0.3x + 295$ | 0.95 | $-0.3x + 294$ | 0.96 | $-0.2x + 290$ | 0.98 | $-0.4x + 291$ | 0.96 |

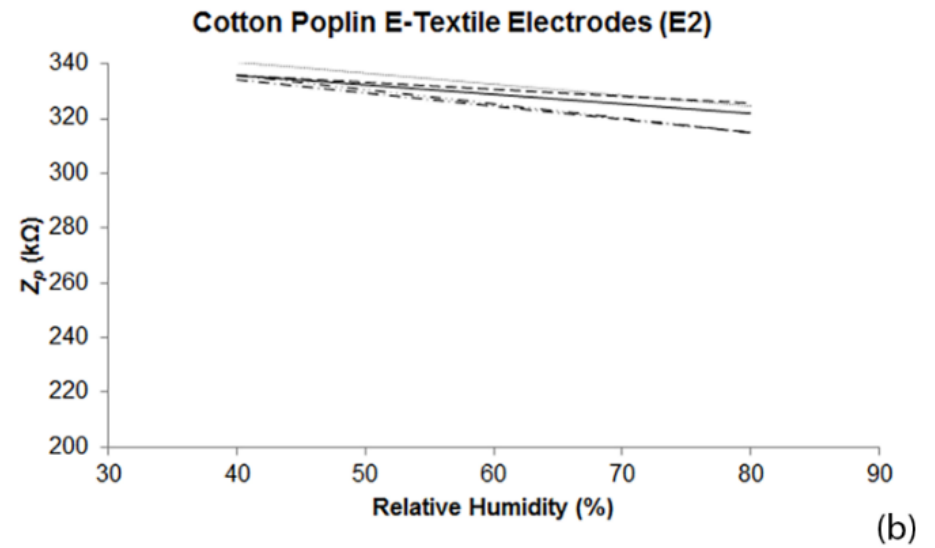
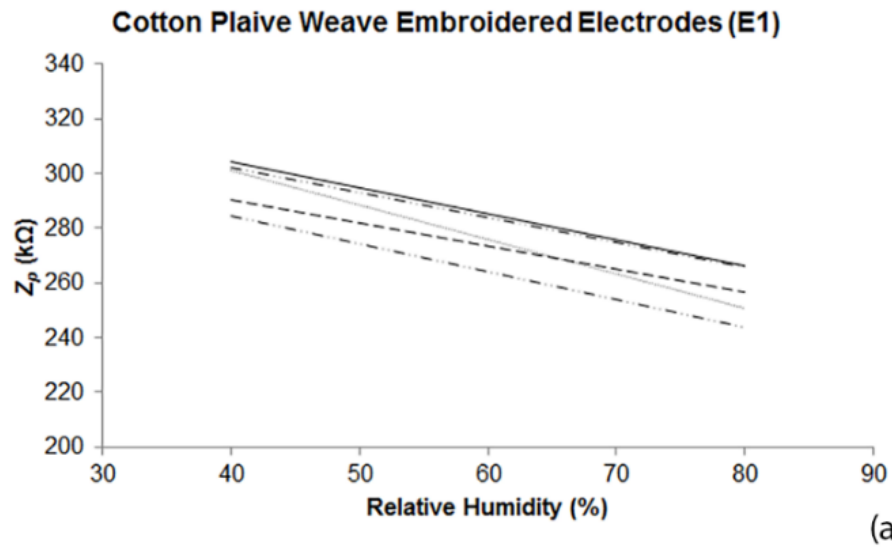


Figure 5.12a-b Z_p linear regressions associated with skin properties - temperature and wetness RH (40 - 80%): (a) E1 and (b) E2 [238]. "© IOP Publishing. Reproduced with permission. All rights reserved."

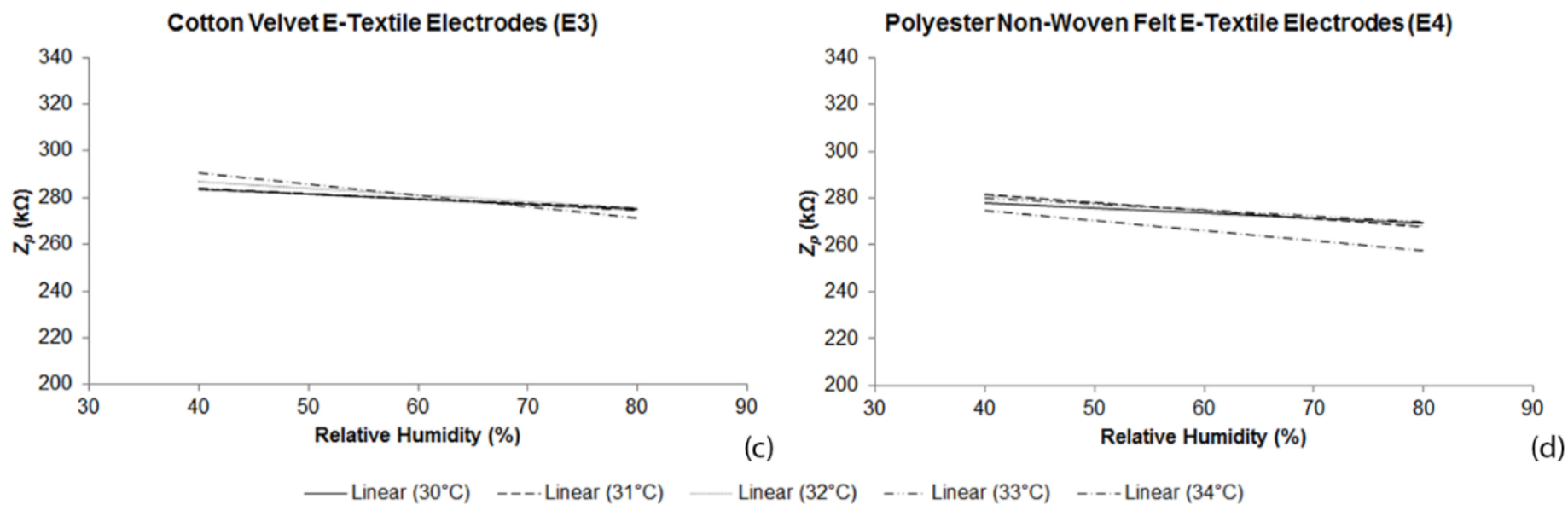


Figure 5.13c-d Z_p linear regressions associated with skin properties - temperature and wetness RH (40 - 80%): (c) E3 and (d) E4 [238]. “© IOP Publishing. Reproduced with permission. All rights reserved.”

5.3.3 Comfort in terms of air permeability

From the previous section, E4 demonstrated to perform the most efficient from all samples. However, it is vital to consider the physiological comfort of the electrodes. To ensure the consistency across the samples, SEM images of the conductive side of the e-textiles are shown in Figure 5.10. Air permeability tests were conducted on all substrates and e-textile electrodes, refer to Figure 5.11. It can be expected that the substrates have a higher permeability than the fabricated electrodes. This is due to the additional Ag/PA66 and PES stitched layers. The polyester non-woven substrate demonstrated the largest air permeability. This can be associated to it being non-woven thus is more porous as a substrate. The embroidery process transforming the substrates into electrodes resulted in a reduction of air permeability for samples E1, E2 and E4 with a drop of 71%, 61% and 64%, respectively. However, sample E3 demonstrated an increase in air permeability by 57%. Sample E3 is a dense substrate thus the needle penetration through the substrate could have created additional pores thus allowing more air to pass through the textile; although, its air permeability remains very low. Thus, comparing the electrode samples, E4 results in the highest air permeability due it's non-woven structure with the needle penetration creating additional pores; thus, exhibiting an overall practical electrode that can be worn by patients.

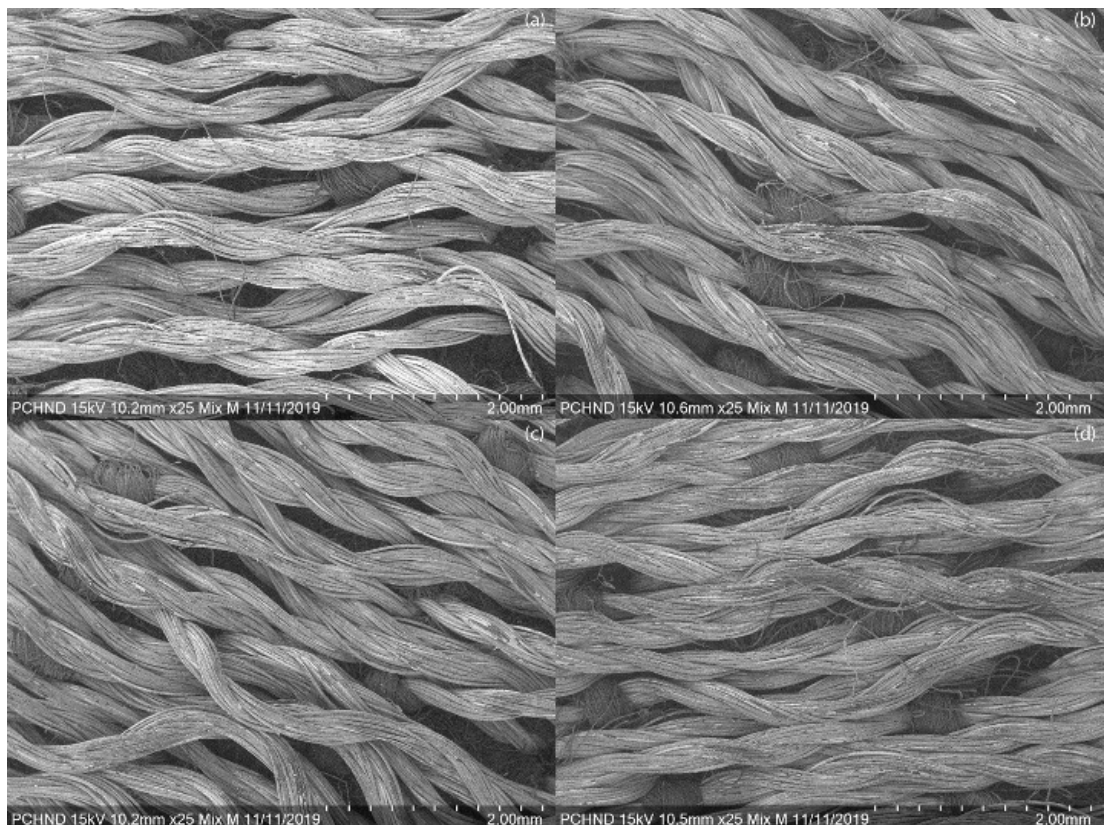


Figure 5.14 SEM representations of the e-textile electrodes with various substrates: (a) E1, (b) E2, (c) E3 and (d) E4 [238]. “© IOP Publishing. Reproduced with permission. All rights reserved.”

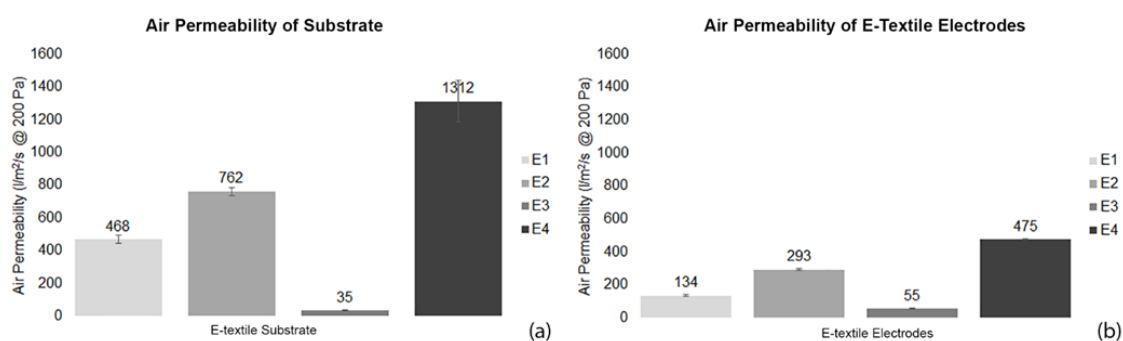


Figure 5.15 Measuring air permeability for the: (a) substrates and (b) e-textile electrode samples [238]. “© IOP Publishing. Reproduced with permission. All rights reserved.”

5.3.4 Evaluation of shape on Z_p

By fabricating new rectangular electrodes (Samples Rectangular S-R1 to S-R12) with the elliptical electrodes (Samples Elliptical S-E1 to S-E12) on the non-woven polyester substrates, Z_p was measured as shown in Figure 5.12. By testing the 12 sets for each shape, an average Z_p of 235.4 and 205.8 k Ω was observed for the rectangular and elliptical e-textile electrodes, respectively. The range between the sample sets was relatively low, close to 4% for both shapes. There is a 13.5% difference in Z_p due to the shape of the electrode. φ is indicative of a pure capacitive effect that is consistent across both shapes. The elliptical shape has an even charge distribution across the surface area, while the charge on the rectangular e-textile electrodes potentially stray to the edges.

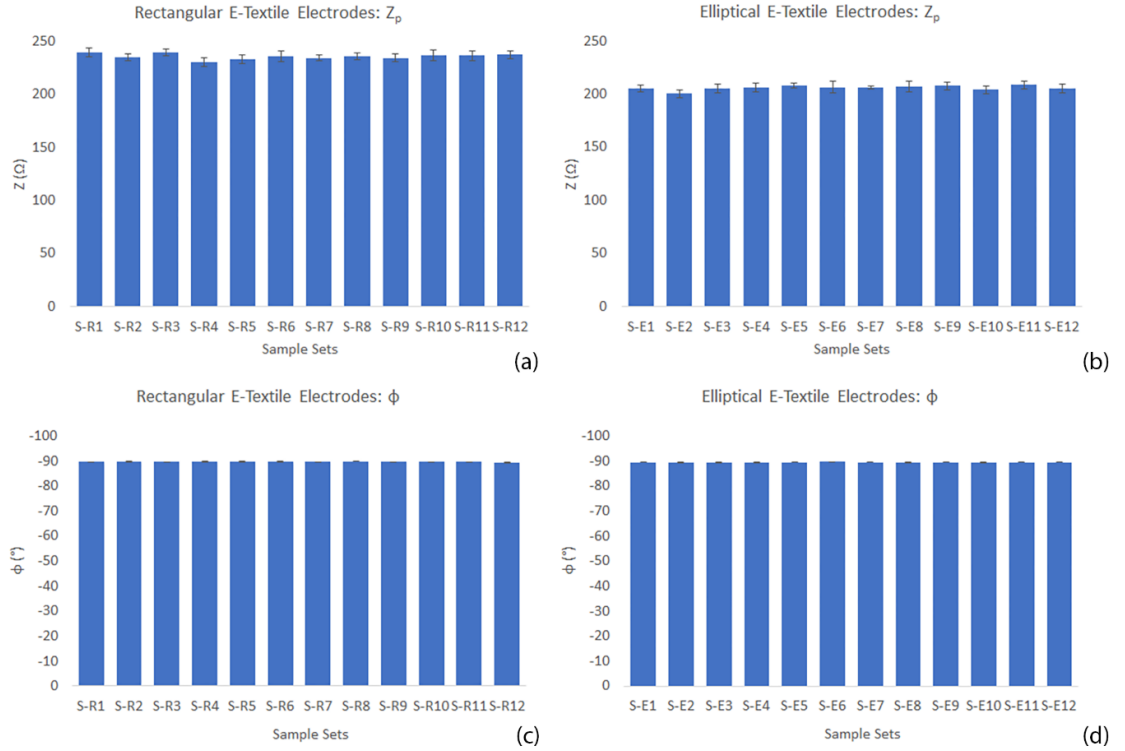


Figure 5.16 Comparison of rectangular and elliptical electrodes.

5.4 Discussion

The fabrication of e-textile electrodes heavily depends on the properties relating to the three materials used, specifically: (i) the substrate, (ii) Ag/PA66 and (iii) PES thread. The embroidery settings were maintained the same for all samples; thus, it is safe to assume that there is a consistent amount of PES and Ag/PA66 thread. Ag/PA66 is highly conductive and responsible for Z_p due to the presence of silver. Contrary to this, the cotton and polyester substrates as well as the PES thread are insulators. However, a large difference in Z_p was observed across the various substrates despite a comparable amount of yarn present in each electrode. In the results section, no correlation between Z_p was identified and the properties of the substrates. It is recommended for future research the textiles are designed and fabricated for use as substrates to identify a correlation, refer to Chapter 7.

In this chapter it was evident that a moisture regain associated with the substrates significantly impacted Z_p . This is demonstrated where an increase in RH resulting in more moisture content present in the textile causes a reduction in Z_p . However, this decrease is inconsistent across the samples. A study conducted by Murphy et al. [239] demonstrated that an increase in temperature and moisture content of the textile resulted in a decrease in resistance. Moreover, for settings where RH is greater than 80% causing the textile to dampen, polarization of the textile occurs resulting in a substantial increase in conductance. This is also true for polyester. Shahzad et al. studied the conductivity of a hybrid polyester and stainless-steel (PSS) fibre-based

thread. Various samples were produced by increasing the amount of polyester in the yarn resulting an increase in linear electrical resistance of the thread. By testing the conductivity of these samples relative to an increase in RH when adapting a climatic chamber, the PSS thread demonstrated a stable resistance up to 80% with a predominant decrease above 80%. However, these two studies conducted by Murphy et al. and Shahzad et al. [239,240] measured the resistance in DC. The research conducted in this study uses AC at a frequency of 50 kHz to measure Z_p , composed of a R and X_c which also demonstrated a decrease in Z_p with an increase in RH.

The change in Z_p relative to temperature for a RH between 40-80% is relatively small. E2, E3 and E4 presented a change between -1% to 3%. However, it is clear that when the textile is dampened (RH increases from 80%-90%) this also affects the temperature. Thus, it is evident that RH has a dominant influence on Z_p due to the moisture regain.

The findings of Z_p relative to RH in this study is comparable to the studies conducted by Murphy et al. and Shahzad et al. [239,240]. The conductive thread used in this study (AgPA66) has a linear resistance of about 1,500 Ω /m and is comparable to the PSS thread produced by Shahzad et al., [240] with a linear resistance of about 1,350 Ω /m. Thus, its behaviour to an increase in RH is expected to be identical. Shahzad et al. [240] demonstrated a constant resistivity of up to about 80% RH decreasing as RH increases above 80% RH. The investigation presented in this chapter shows a gradual reduction in Z_p for the ranges of 40-80% RH. This is possibly associated with the reaction of the electrolyte impurities found in distilled water, the substrates and PES thread. The moisture regain of polyester and cotton is about 0.4% and 8.5% respectively. Thus, a gradient closely representing a 'zero-slope' is expected for the polyester non-woven felt e-textile electrode. The significant decrease in Z_p at 90% can be related to any reactions of the Ag/PA66 electrolytic conductivity.

This study identifies the influence of skin properties on Z_p , specifically skin temperature and perspiration. Although water is the main component of sweat, it also consists of minerals, urea and lactic acid. The chemical elements of minerals include calcium, potassium, sodium and magnesium and can be found in salt form as ions; thus, acting as electrolytes in sweat and possessing conductive properties. Lactic acid is also known to have a slight conductivity while urea is considered an insulator. Therefore, to gain a better understanding of Z_p relative to perspiration, a solution resembling human perspiration can be used to supply the climatic chamber. This will add further complexity to the experimental protocol as there is a mixture of conductive and insulating elements in addition to the electrodes. Thus, tests will be conducted on a regular basis to gain an understanding of the practicality of the electrodes for long-term monitoring.

Research in the area of e-textile electrodes focus on the influence of stitch characteristics and analyse the SNR compared to Ag/AgCl electrodes for specific applications, such as ECG and EMG [53,202]. However, the research conducted neglect to study the complexity associated with the changes in skin physiology and the impact of the textile substrates selection criteria. In this investigation, the importance of the e-textile substrate and its influence on Z_p was identified relative to changes in skin properties relating to a patient's medical conditions. In addition, it is important to take into consideration the air permeability of e-textiles associated with the physiological comfort for long-term monitoring. Moreover, an elliptical shape reduces Z_p ; thus, it is safe to assume that this will assist in reducing Z_{es} .

5.5 Conclusion

This study identified the dependence of Z_p associated with e-textile electrodes to the electrode's substrate. There was also a strong correlation between Z_p and RH. This could be from the substrates potential to reduce or increase the exposure of the electrodes to the electrolytes in the moisture absorbed. In addition, by forming an experimental protocol relating skin temperature and perspiration to climatic chamber settings the implications of variances in these variables attributing to changes in Z_p of the electrodes was identified. Although, Z_p relative to temperature displayed an irregular trend, a steady trend was associated with RH. It was observed that an increase in RH resulted in a decrease in Z_p across all electrodes. The polyester non-woven felt was realised as a fitting substrate for e-textiles that can be used to monitor electrophysiological activities with BIA systems. Its trend displayed negligible variances due to changes in temperature and RH and maintained a lower Z_p compared to the other substrates. This in addition to its high air permeability results in an e-textile electrode suitable for long-term monitoring. By fabricating elliptical e-textile electrodes, a slight improvement in Z_p was observed which can improve the efficacy of adapting e-textile electrodes to BIA measurements. The emergence of conductive yarn gives rise to the fabrication of e-textile electrodes that can be adapted for long-term electrophysiological monitoring. However, this presents a complex study of the electrode-skin interface in addition to the electrode's material characteristics. This study will progress to its compatibility in BIA applications.

Chapter 6

Comparison of e-textile and Ag/AgCl electrodes for BIA

6.1 Introduction

Clinical wound management is a growing problem and concern [1–4]. It is currently performed by practitioners and nurses in accordance with standards for wound prevention and management [106]. This methodology relies heavily on visual assessment leading to misinterpretation of the healing progress [5–9]. In addition, wound management is completed with the aid of multiple measuring tools which can be time consuming for the patient and medical professionals [241]. These shortcomings result in a growing cost of dealing with wounds, specifically with infections and ulcer treatments from premature withdrawal of treatments.

Bioimpedance analysis (BIA) measures the resisting electric current flow of the tissue where the biological tissue responds to an external electric current [160,181,242–245]. It is a safe, non-invasive and simple methodology that is commonly associated with measuring Total Body Water (TBW) [74,134,166,246]. This methodology was recently adapted to muscle injuries focusing on relating a change in soft tissue to a change in measured physiological parameters, such as impedance (Z), resistance (R), reactance (X_C) and phase angle (φ) [137–139,163]. By placing the electrodes in a segmental or local tetrapolar configuration, researchers observed a change in these physiological parameters relative to a healing tissue under study (BUS) over a number of days [45]. It was only until recently that researchers adapted these methods to monitor wounds objectively observing trends in changes relative to the wound healing process [39,42,43].

6.1.1 Electrodes

Research into BIA adapt clinical electrodes, specifically Ag/AgCl. With the recent advances of wearable technology [247–249], current methodologies into monitoring wounds can be developed into a wearable device by adapting e-textile electrodes. Wet electrodes, such as Ag/AgCl, are considered ideally nonpolarized where the electrode-electrolyte layer does not have a charge build up due to the injected current [178]. However, wet electrodes are not perfect nonpolarized electrodes with the presence of some polarization [180,250]. Contrarily, dry electrodes are classified as polarized electrodes where there is a charge build up on the surface [47,51,52,183,184]. This polarization phenomenon can impact the electrode-skin impedance (Z_{es}) influencing the measurements. Madison et al. studies Z_{es} of wet and dry electrodes for low frequencies ranging from 6 Hz to 1 kHz [251]. For this low frequency range, it is evident that wet electrodes have a significantly lower Z_{es} impedance compared to dry electrodes [251]. These frequency ranges associated

with ECG measurements result in unwanted noise [252]. In addition, Z_{es} varies depending on the electrode positioning on the body. Rosell et al. [253] studied Z_{es} for frequencies ranging from 1 kHz to 1 MHz. The electrodes were placed on various sites of the body which were flat or convex in nature. It was observed that for frequencies ranging between 100 kHz and 1 MHz, Z is relatively close regardless of the electrode location or volunteer. While between 1 and 100 kHz, there is a difference in Z . These frequency ranges relate to BIA.

Previous studies into e-textile electrodes measure the polarization impedance Z_p or resistance R autonomously relating to the electrodes at a single time point [53,61,194,197,202,204]. Chapter 4 indicates that measuring the electrodes Z_p independently and not in contact with skin results in Z_p being comparable to X_C . Moreover, various applications indicate that e-textile electrodes can be adapted to monitor biosignals such as ECG, EEG and EMG [33,201,254–260]. These signals operate at a significantly lower frequency ranges compared to BIA and measurements are completed over a short time period.

6.1.2 Methods adapted for monitoring wounds

Lukaski et al. [45] observes the impact of wound healing based on various types of wounds. In addition, this study indicates a relation of R , X_C and φ measurements to the wound healing process over a period of days. A frequency of 50 kHz was applied for this study with a tetrapolar electrode configuration. The electrodes were placed locally adjacent to the wounds with 1 cm distance between the current injecting electrodes and associated voltage sensors. Given the various wound types and sizes, the intermediate distances between the inner voltage sources positioned on the edge of the wounds varied. The studied wound types include (i) an uncomplicated wound, (ii) a surgical wound and (iii) an infected wound. Observing the trend associated with the studied parameters for an uncomplicated wound, an increase in trend was depicted across all parameters as the wound healed. The surgical wound included several interventions during the healing phase. This included debridement and grafting. For this type of wound, a fluctuation in the trends of the parameters was observed relative to the interventions. The infected wound demonstrated various changes in magnitude and direction of the trend across all parameters. To conclude, it is suggested that R can be adapted to monitor successful wound healing; however, X_C and φ are indicative of neuropathy.

A study completed by Muller et al. [46] focused on lower limb ulcers of 20 diabetic patients. The sizes of the ulcers were not reported. Measurements of the wounds were collected over a period of days, in addition to measurements of the opposite limb. Adapting the SFB7, a frequency sweep was performed with the electrodes in a local tetrapolar configuration. The pair of voltage sensors were positioned at the edge of the wound with the current injecting electrodes adjacently positioned at a

distance of 1 cm. For the data analyses, the Cole-Cole model was adapted with the frequency range setting of 3 -1000 kHz. The analysis was performed for R and X_c associated to the centre frequency (f_c) from the Cole-Cole plot with a focus on the resulting Z . By comparing Z of the wounded area to that of the healthy area of the opposite limb, the results were comparable to Lukaski et al. [45]. Z of the wounded area was significantly smaller than the healed area. For the control group, Z of the two limbs were relatively close; thus, indicating that Z is expected to increase during the healing process.

In addition to acute and chronic wounds, Kenworthy et al. [41–43] adapted the SFB7 to monitor burn wounds with a tetrapolar electrode configuration. A frequency sweep was performed for the range of the SFB7 (i.e., 3-1000 kHz), and the data analysed was based on the Cole-Cole model. The burns varied in size and depth. Several studies were performed including: (i) validation of the reliability of the equipment [42], (ii) electrode positioning [41,42] and (iii) a correlation between BIA and the healing phase [43]. For (i)-(ii), statistical analysis was conducted on R_o , R_{inf} and R_i , and for study (iii) φ was included. The tests were conducted on a significant number of volunteers, more than 30. It was concluded that the SFB7 was a reliable instrument to monitor the resistance of the wounds regardless of the wound type, and electrode positioning. Further analysis of the electrode positioning included three various configurations, specifically whole body, segmental and local placements. It was concluded that local positioning of the electrodes was the most sensitive. However, the manufacturer's specification suggests positioning the electrodes in a whole body configuration; thus, to overcome errors of BIA measurements for a local configuration, it was suggested that strict placement protocols must be followed for consistency in observations [42]. Further research was conducted to identify the parameters associated with the wound healing process based on the Cole-Cole model, specifically the open circuit resistance (R_o), the short circuit resistance (R_{inf}) and the intracellular resistance (R_i), the phase angle was also assessed (φ). The electrodes were positioned longitudinally at a distance of 3cm on either side of the burn wound. This study indicated that R_o and R_{inf} are strongly related to the wound healing process contrary to R_i and φ . During the healing phase, an increase in R_o and R_{inf} is noticeable [43].

Kekonen et al. has a series of studies focusing on an ideal methodology using BIA to measure the wound healing process on various types of wounds [35–40]. This research was conducted using the Solartron 1260A Frequency Response Analyzer and Solartron 1294A Impedance Interface using a frequency sweep. However, the Cole-Cole plot was not adapted, and Z measurements were recorded at discrete frequency ranges varying from 10 Hz to 100 kHz. Measurements were recorded over numerous days. The methodological approach adapted initially, measured Z in a dipolar and tetrapolar electrode configuration [36,39]. For the dipolar configuration, one

electrode was placed on the wound with the second electrode acting as a reference on the undamaged skin surrounding the wound. This concept was also adapted for the tetrapolar configuration, where two electrodes were positioned on the wound and another two on the undamaged skin [37]. It was observed that for both configurations an increase in Z was observed as the wound healed. This study indicates that at low frequencies, less than 1 kHz, Z is associated with the stratum corneum, while frequencies greater than 1 kHz are recommended for monitoring the wound healing process [39]. Proceeding studies adapted the tetrapolar configuration transitioning from positioning the electrodes onto the wound to surrounding the wound with reference electrodes at a short distance from the wound [37]. This analysis is based on the normalisation ratio of the wound Z relative to the reference point and indicates a healthy wound healing process as the ratio approaches 100% [35,38].

Inflammation is another factor associated with wounds [261]. King et al. associates BIA with the inflammation of ankle swelling due to acute ankle fractures [44]. Although, this study is not directly correlated to wounds it does provide a general insight into the relation between inflammation and BIA. This study was conducted on 14 injured patients with a control group of 17 healthy subjects. A segmental tetrapolar electrode configuration was adapted for the frequencies of 5 kHz and 200 kHz. Measurements based on Z were recorded from the injured limb and compared to the uninjured limb. To follow, the results were compared to the volume of the limbs using a water displacement methodology. This was repeated for the healthy subjects. The control group presented similar measurements. For the injured group, a significant decrease in Z was observed in the injured limb compared to the healthy limb. Moreover, the results were relatively close at the discrete frequencies of 5 kHz and 200 kHz.

Previous research is indicative of the methodologies and analysis adapted for BIA measurements associated with the wound healing process. A tetrapolar electrode configuration positioned locally adjacent to the wound has been shown to be the most accurate method of measuring BIA parameters associated with the wound healing process. Research has adapted the Cole-Cole plot with frequencies ranging between 3 – 1000 kHz, or alternatively using discrete frequencies specifically 50 kHz. To monitor the wound healing process, emphasis is placed on the trend of the measurements [262], specifically relating to Z and R . Contrary, it has been suggested that X_c and φ are associated with complicated wounds.

The application of BIA to monitor wounds is not based on absolute values and is a comparative study. A reference point is always considered when measuring the state of a wound. Several reference points are taken into consideration, such as a healthy point of measurement (i.e. an uninjured limb) and time [37,45]. Moreover, the

observation of a wound healing is based on trend analysis of several parameters [262]; specifically, Z , R , R_0 , R_{inf} while X_c and φ have been associated with infected wounds and neuropathy [45]. These parameters are measured by using (i) discrete frequencies (i.e. 5 kHz, 50 kHz), (ii) a frequency sweep or (iii) by adapting the Cole-Cole model [35–43,46]. This study takes into consideration these factors to compare the behaviour of e-textile electrodes to wet electrodes, specifically Ag/AgCl, that are currently used for BIA. To create a BIA system for short-term and long-term monitoring, it is important to test the e-textiles electrodes over a period of time.

6.2 Materials and Methodology

6.2.1 Materials

For this experiment, pork belly was used due to its identical dielectric properties to human skin and refrigerated overnight, refer to Chapter 3. Ambu WhiteSensor WS electrodes were used possessing a highly conductive solid gel, large surface area with strong adhesion and foam backing. The elliptical e-textile electrodes were adapted from Chapter 5. An Elastocrepe Heavy Weight Crepe Bandage which was commercially purchased and sewn to create the compression sleeve used in Part B of the experiment in this chapter.

6.2.2 Methodology

6.2.2.1 Part A Preliminary Study of Z on Biotissue Under Study (BUS)

A preliminary study was undertaken to measure Z of the pork belly BUS in a tetrapolar configuration of a distance of 10 cm between the electrodes [163]. A dipolar configuration was also tested as a comparison, refer to Appendix V; however, a tetrapolar configuration common to studies in monitoring wound healing was adapted. Clinical Ag/AgCl electrodes were conventionally placed onto the pork belly, relying on the adhesiveness of the electrodes to create the electrode-skin contact. The properties of this test sample are presented in Table 1.

Table 6.1 Pork belly sample for preliminary experiment

| Pork Belly Sample | Configuration | Weight (kg) | Size (cm) (l x w x h) | Electrodes |
|-------------------|---------------|-------------|-----------------------|------------|
| ST1 | Tetrapolar | 1.5 | 20 x 18 x 4 | Ag/AgCl |

6.2.2.2 Part B Comparison of Ag/AgCl and Ag/PA66 e-textile electrodes

The focus of this study was to compare the behaviour of e-textile electrodes to Ag/AgCl electrodes in terms of parameters that are adapted to local BIA configurations to monitor wounds. Three samples of pork belly were used for the wet electrodes and three samples of pork belly were used for the dry electrodes over two

days. The weight and measurements of the pork belly were recorded and presented in Table 6.2 with their associated electrodes. The Z_p of the elliptical electrodes were measured in pairs and the actual values are presented in Chapter 5. To prepare the pork belly for measurements, a 2 x 2 cm excision was created in the centre of the BUS sample as a guide for the positioning of the electrodes. The skin was cleansed with Isopropyl Alcohol swab wipes and let to dry prior to placing the electrodes with the aid of a compression sleeve.

Table 6.2 Pork belly samples for final experiment

| Pork Belly Sample | Weight (kg) | Size (cm) (l x w x h) | Electrodes |
|-------------------|-------------|-----------------------|------------|
| S1 | 1.5 | 20 x 17 x 4 | Ag/AgCl |
| S2 | 1.5 | 21 x 17 x 4 | Ag/AgCl |
| S3 | 1.5 | 21 x 17 x 4 | Ag/AgCl |
| S4 | 1.5 | 20 x 18 x 4 | S-E1, S-E2 |
| S5 | 1.5 | 21 x 18 x 4 | S-E3, S-E4 |
| S6 | 1.5 | 20 x 17 x 4 | S-E5, S-E6 |

6.2.2.2.1 Compression Sleeve

Various commercially available materials were trialled and tested to conform the e-textile electrodes to the BUS samples. These were purchased from haberdashery stores and chemists. To be able to compare the e-textile electrodes to the standard Ag/AgCl electrodes, the e-textile electrodes were placed onto the skin using sports strapping tape. However, this did not provide strong adherence and the e-textile electrodes would detach and become prone to motion artefact. This was also an issue with Micropore Paper Tape and Surgical Tape. It is possible that this will work on human skin; however, it was not a suitable solution for the BUS samples used in this study. The velcro was able to secure the e-textile electrodes in position. However, the e-textile electrodes did not conform to the deep sulci or shape of the pork belly sample due to rigidity of the velcro. This could potentially make the e-textile electrode susceptible to noise due to the air gap between the electrode and the skin [51,211]. A medium weight crepe bandage had too much stretch resulting in the same issue with the velcro. Moreover, the pressure was not consistent and difficult to control. The Elastocrepe Heavy Weight Crepe Bandage was then trialled which was commercially purchased from the chemist. The bandage has a stretch of 60%. This was cut to half the width of the BUS samples and sewn at the edges to form a small compression sleeve. For 'real-life' applications, velcro would be sewn onto both edges of the compression bandage allowing for the sleeve to be strapped on and removed with ease.

No modifications were made to the sleeves used with the Ag/AgCl electrodes. The e-textile electrodes were hand-sewn onto the sleeve avoiding any possible damage to their conductive side from the sewing machine. The electrodes acting as the voltage

sensors were positioned at the edge of the bandage with the current injecting electrodes at a distance of 1 cm from the voltage sensors. The pork belly was rolled up imitating the concave shape of a limb [263] and passed through the compression sleeve with the voltage sensing electrodes positioned relatively close to the edge of the excision (i.e. about 0.5 cm). For the Ag/AgCl electrodes, the pork belly was first passed through the sleeve holding the pork belly into shape at its edges prior to adhering the electrodes to the skin in the same configuration to the e-textile electrodes, refer to Figure 1. The sleeve was then passed over the Ag/AgCl electrodes. Ag/AgCl electrodes are designed to adhere to the skin; however, the sleeve was used providing relatively consistent pressure across the Ag/AgCl electrodes and e-textile electrodes as this can impact their performance [211]. The snaps were then passed through an opening of sleeve allowing for a connection to the SFB7.

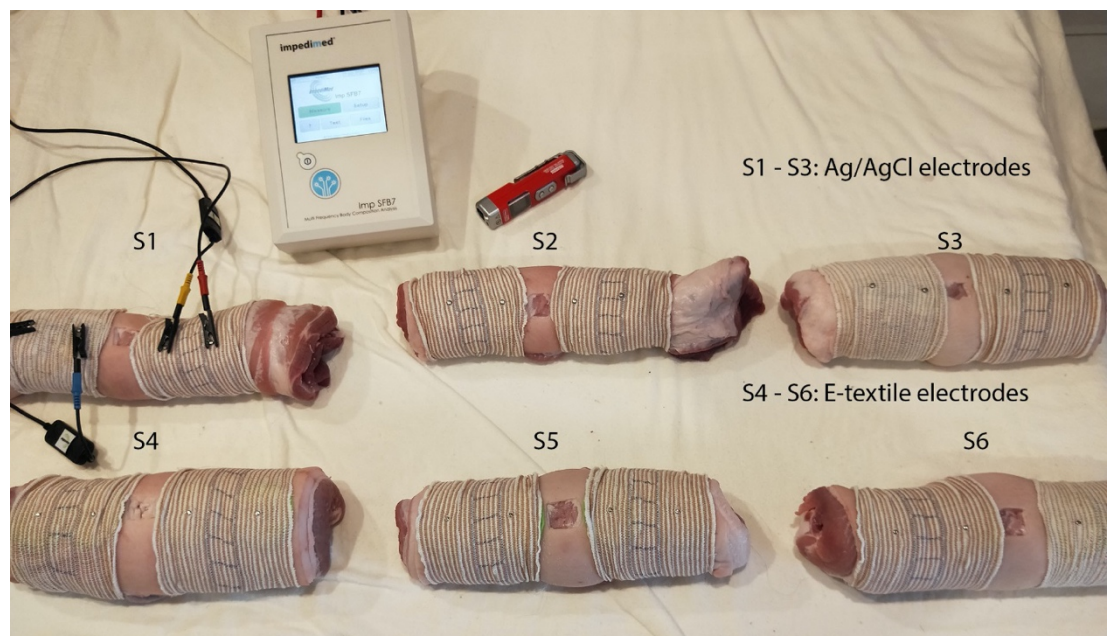


Figure 6.1 Experimental set-up.

6.2.3 Measurements

Measurements were taken in ambient room temperature, 20°C with a RH of 60%. The use of a necrotic BUS has certain limitations in these room settings, specifically time. Therefore, Part A was to determine the time period to complete the final experiments.

6.2.3.1 Part A

The first experiments were conducted every 30 minutes over a period of 180 minutes. This was repeated over a two-day period forming a basis of this study. The purpose of this study was to identify the performance of the necrotic BUS. The temperature was collected at each time point.

6.2.3.2 Part B

The method adapted in the final study comparing the Ag/AgCl and e-textile electrodes was based on the observations of the BUS in Part A. For this experiment, the measuring time was reduced to 15 minutes over a 60-minute period for each sample. The time period of 60 minutes provides enough time to collect data before changes to the pork belly samples occur that can influence the measurements, such as bacterial growth. The measurement time interval was reduced to 15 minutes in order to have more data points between shorter time periods. Provided that there are 6 samples, this is substantial time to collect and verify the measurements. At each time point, the skin temperature was measured. The SFB7 was set to complete a frequency sweep with discrete frequency readings, collecting 5 measurements every three seconds for the individual data collection times. This experiment was repeated over two days. At the end of day 1, the sleeves were washed on a delicate cycle setting, cold water with a spin cycle of 300, and let to dry overnight. The primary reason for washing the sleeves was to test the repeatability of the e-textile electrodes. In order to account for any changes in shape to the sleeve due to the wash, all sleeves were washed including those used with the Ag/AgCl electrodes.

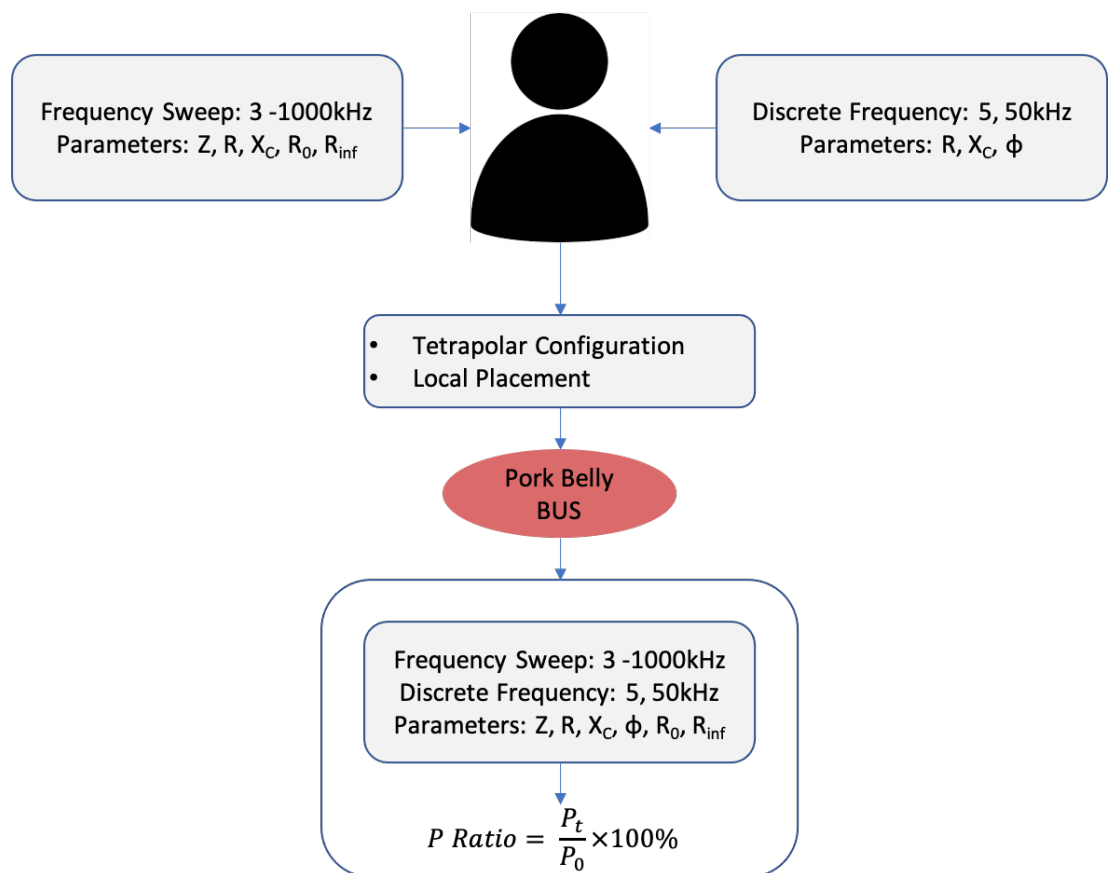


Figure 6.2 Adaption of BIA configuration and parameters for monitoring wounds in previous research for the experimental protocol

6.2.4 Analysis

Provided the performance of the e-textile electrodes over time is studied, the absolute value was used taking the parameter of interest at time 0 as a reference point for each sample. Normalisation was adapted for all the studied parameters, refer to Equation 6.1. Provided that the rate of change of these parameters in relation to time is relatively small for the necrotic BUS, a percentage ratio was adopted. This small rate of change is also true of healthy tissue [216].

$$P \text{ Ratio} = \frac{P_t}{P_0} \times 100\%, \quad \text{Equation 6.1}$$

6.1

where P refers to the parameter of interest, P_t is the absolute value of the parameter at time t , while P_0 is the absolute value of the parameter at time 0. For example, analysing Z at 30 minutes, the equation is expressed as:

$$Z \text{ Ratio} = \frac{Z_{30}}{Z_0} \times 100\%, \quad \text{Equation 6.2}$$

Therefore, the 100% line is with reference to the value at time 0. Thus, at time 0 all parameters are located on the 100%, as time passes it indicates the deviation from this reference point.

6.2.4.1 Part A

The data was analysed for the preliminary experiments for a frequency sweep of 3-1000 kHz and for various discrete frequencies, including: 5, 50, 100 and 200 kHz. Analysis was completed for the common BIA parameters, Z , R , X_C and φ .

6.2.4.2 Part B

For this main experiment, the focus was on the frequencies and parameters that have been adapted from previous research into monitoring wound healing using BIA. Although, Z and R (including R_0 and R_{inf}) have been closely associated with wounds X_C and φ were also incorporated for this study. Z , R , X_C and φ were analysed for the specified discrete frequencies and for the sweep associated with the Cole-Cole model. R_0 and R_{inf} are parameters associated specifically with the Cole-Cole model.

6.3 Results

6.3.1 Temperature

The skin temperature of the BUS samples was recorded prior to each measurement. The study undertaken in Chapter 5 indicated that a change in temperature ranging between 30-34°C [47,68,96], did not influence the Z_p of the electrodes compared to the wetness. However, to raise the temperature of the pork belly to imitate human

skin would cause changes to its properties that cannot be controlled across all samples. The BUS sample in part A had a large temperature change over the 180-minute period, averaging about 3°C. For part B, the change in skin temperature over a 60-minute period was as low as 1°C.

6.3.2 Error of uncertainty

The absolute values of Z , R , R_0 and R_{inf} were extracted from the BiImp software while X_C and φ were calculated from Z and R . From the five measurements collected at each time point, the average was taken, and the error of uncertainty calculated. It was observed that the error of uncertainty across all experiments were consistent for all parameters measured using the Ag/AgCl and e-textile electrodes. Z , R was low, ranging between 0 and 0.4%, contrary to X_C and φ that had an uncertainty range of 0.3 to 5%. R_0 and R_{inf} also demonstrated a low level of uncertainty comparable to Z and R , ranging between 0 and 0.4%.

6.3.3 Part A

The dipolar method (refer to Appendix V) has previously been adapted to measure Z of necrotic pork tissue in the food and technology field. For such studies, a dipolar method is common. Bai et al. [213] measured Z across a range of frequencies. Referring to this study, about 650 Ω was measured on day 1 at 50 kHz. This is comparable to the value of Z measured in the dipolar mode, with a value of about 600 Ω at time 0 minutes for sample ST2 (refer to Appendix V for BUS properties and trend analysis). Therefore, this supports the method adapted to measure BIA on the pork BUS. This provided a basis to conduct the experiments in a tetrapolar configuration common to BIA measurements on human beings. Z was measured to be about 70 Ω in a tetrapolar configuration. This is comparable to measurements on human beings in a tetrapolar configuration [137]; therefore, confirming the dielectric properties of pork belly skin. Referring to Figure 6.3a and 6.3b, an exponential decay for Z and R is observed over the 180-minute period for the frequency sweep and the discrete frequencies over two days. This decay settles between 60 and 90 minutes and is observed over the two-day period. An identical trend can be observed for the dipolar configuration, refer to Appendix V. However, referring to Figure 6.3b-e, no trend associated with X_C and φ is discernible. This could be the cause of capacitive artefacts [264]. Although, it does not appear to affect the trends associated to Z and R . Moreover, it is distinct at the higher frequencies, specifically 100 and 200 kHz. This capacitive leakage is commonly associated with the dipolar configuration [265]; however, recent research has suggested it can also impact a tetrapolar configuration [266]. This leakage could potentially be related to an unstable electrode-skin interface. Research has indicated that the performance of electrodes significantly improved when a pressure is applied [211,256,258]. Thus, from Part A for a tetrapolar

configuration a significant exponential decay occurs in the pork belly BUS within 60 minutes. In addition, this trend is identical when repeated over a two-day.

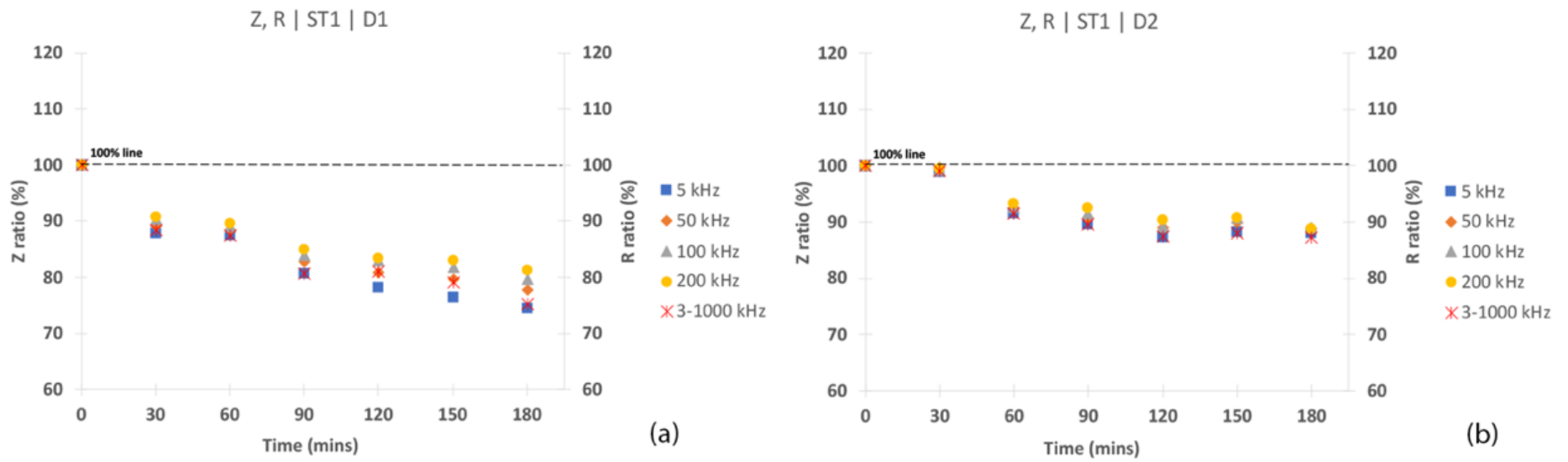


Figure 6.3a-b Trends in intact BUS sample using Ag/AgCl in tetrapolar configuration for (a) Z and R day 1 and (b) Z and R day 2.

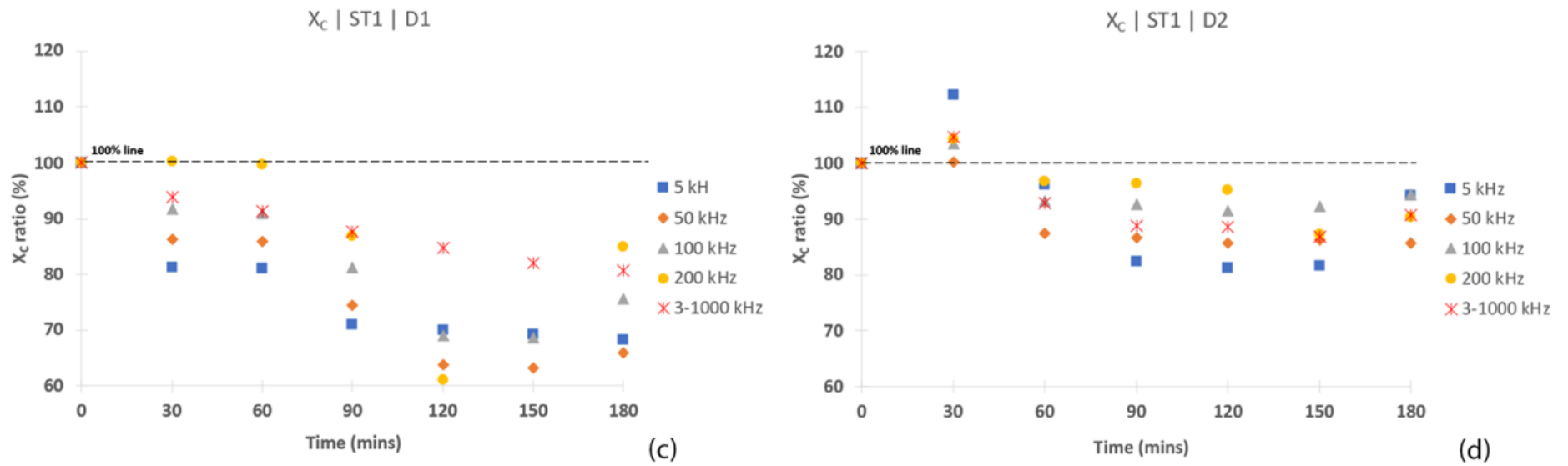


Figure 6.4c-d Trends in intact BUS sample using Ag/AgCl in tetrapolar configuration for (c) X_c day 1 and (d) X_c day 2.

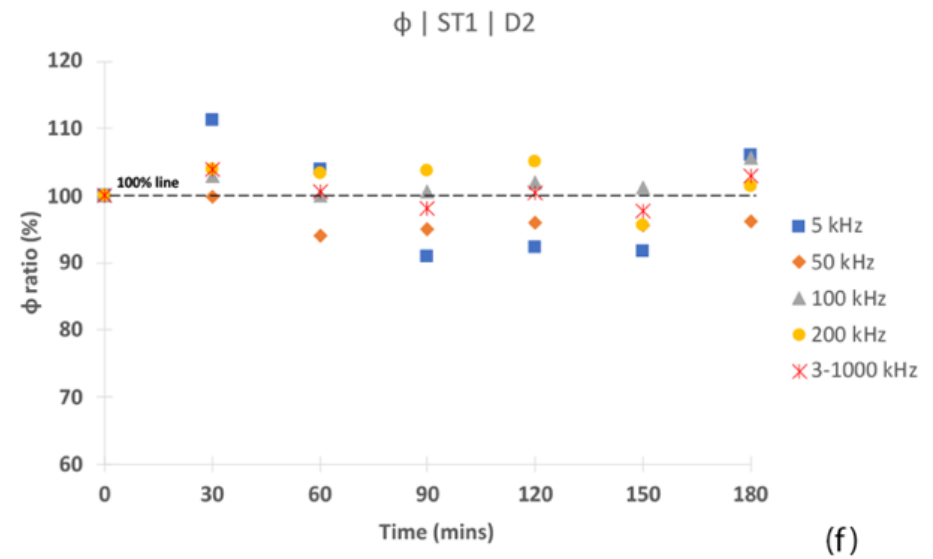
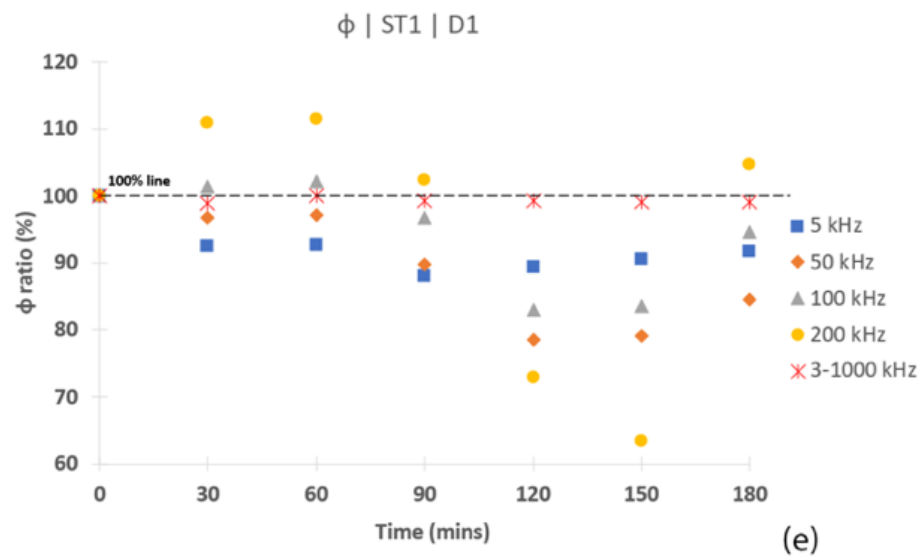


Figure 6.5e-f Trends in intact BUS sample using Ag/AgCl in tetrapolar configuration for (e) φ day 1 and (f) φ day 2.

6.3.4 Part B

6.3.4.1 Electrode Mismatch

Chapter 5 indicated that the Z_p of the e-textile electrodes demonstrated slight variances between the sample sets. However, this did not cause an electrode-mismatch and the Cole-Cole model was not impacted. A Cole-Cole plot for the e-textile electrodes is presented in Figure 4. Therefore, a frequency sweep of 3-1000 kHz was acceptable for analysis.

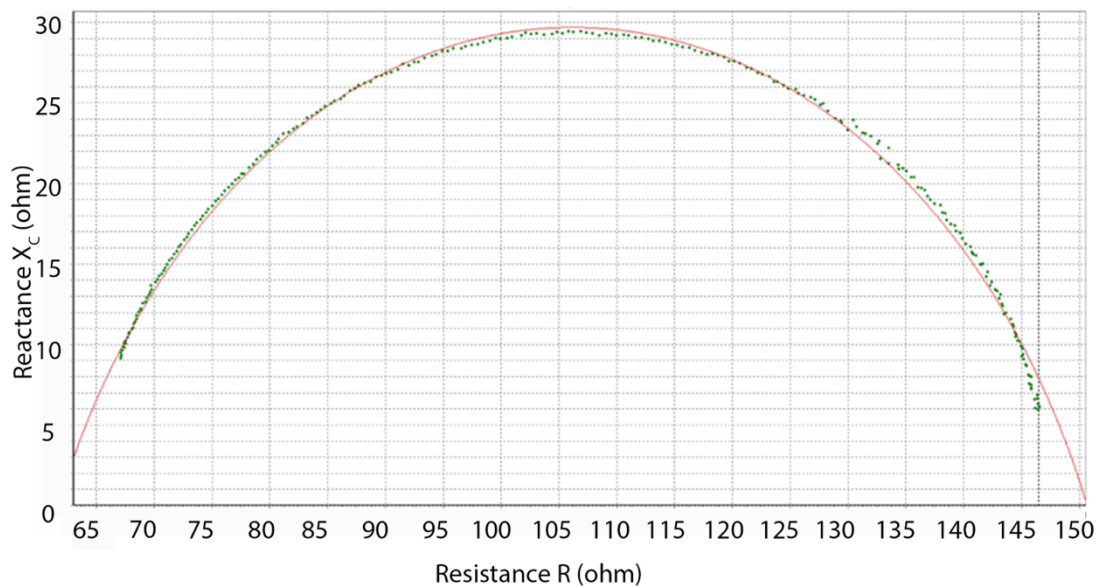


Figure 6.6 Cole-Cole plot for e-textile electrodes as presented by SFB7.

6.3.4.2 Evaluation of Z and R between Ag/Cl and e-textiles

The rate of change in Z and R for the Ag/AgCl and e-textile electrodes over the two-day period is presented in Figure 6.5a - d. Normalisation ratios for Z and R were plotted on the same graph. For the Ag/AgCl electrodes, the maximum ratio difference between Z and R was as low as 0.1%. The e-textile electrodes had a slight difference, with a ratio difference of 0.4%. However, these differences have a negligible effect on the trend. An exponential decrease of Z over time is expected and has been associated with the electrode-skin contact impedance. Searle et al. indicates that at low frequencies (i.e., 50 Hz) Z_{es} for stainless steel dry electrodes is significantly greater than the Ag/AgCl electrodes [69].

For BIA applications to monitor wounds, the frequency range is significantly larger. While there is a difference in absolute values across the samples for Z and R , the rate of change is identical. On day 1, time 0 and at 50 kHz, BUS samples S1, S2 and S3 resulted in Z of 152, 115 and 100 Ω respectively. For S4, S5 and S6, Z was 85, 115 and

110 Ω . 50 kHz is commonly associated with BIA measurements [69]. The pressure from the compression sleeve potentially influences a relatively small decrease in the impedance [267]. However, the range of these values are indicative of the difference in impedance measurements across various subjects where absolute Z measurements are subject dependent due to changes in skin thickness, moisture or hair. A percentage difference of 42% is observed from the sample with the lowest and highest Z for the Ag/AgCl electrodes. This falls within the range of measuring Z in vivo [138]. While for the e-textile electrodes, the variance was 25%. These differences in initial Z measurements did not impact the trend observed over time which was identical across all samples for the frequency sweep, and discrete frequencies associated with Ag/AgCl and the e-textile electrodes, for the frequency sweep refer to Figures 6.5; while Figures 6.6 and 6.7 show the discrete frequencies 5 and 50 kHz, respectively. Therefore, this indicates that the e-textile electrodes performance is comparable to the Ag/AgCl regardless of whether a frequency sweep is performed, or measurements are taken at the discrete frequencies of 5 and 50 kHz. Moreover, washing the e-textile electrodes did not affect their performance, refer to Figures 6.5-6.7 c-d.

Moreover, it is evident that R is a dominant factor of Z in Z_{es} for both type of electrodes. Thus, it is safe to assume that the polarization impedance of the e-textile electrodes did not influence Z . The results in this study ex-vivo indicate a 6-7% decrease over 60 minutes on day 1, and about 16-17% decrease on day 2 for the Ag/AgCl and e-textile electrodes. Analysing the exponential regression of the plots, the equations were comparable across all samples. Thus, no significant difference was observed between the samples measured with the Ag/AgCl electrodes to those measured with the e-textile electrodes. Moreover, a strong correlation was observed for all frequency settings over the two-day period. For S1-S3, R^2 ranged from 0.87-0.98 and S4-S6 was from 0.82-0.99, refer to Table 1 in Appendix VI.

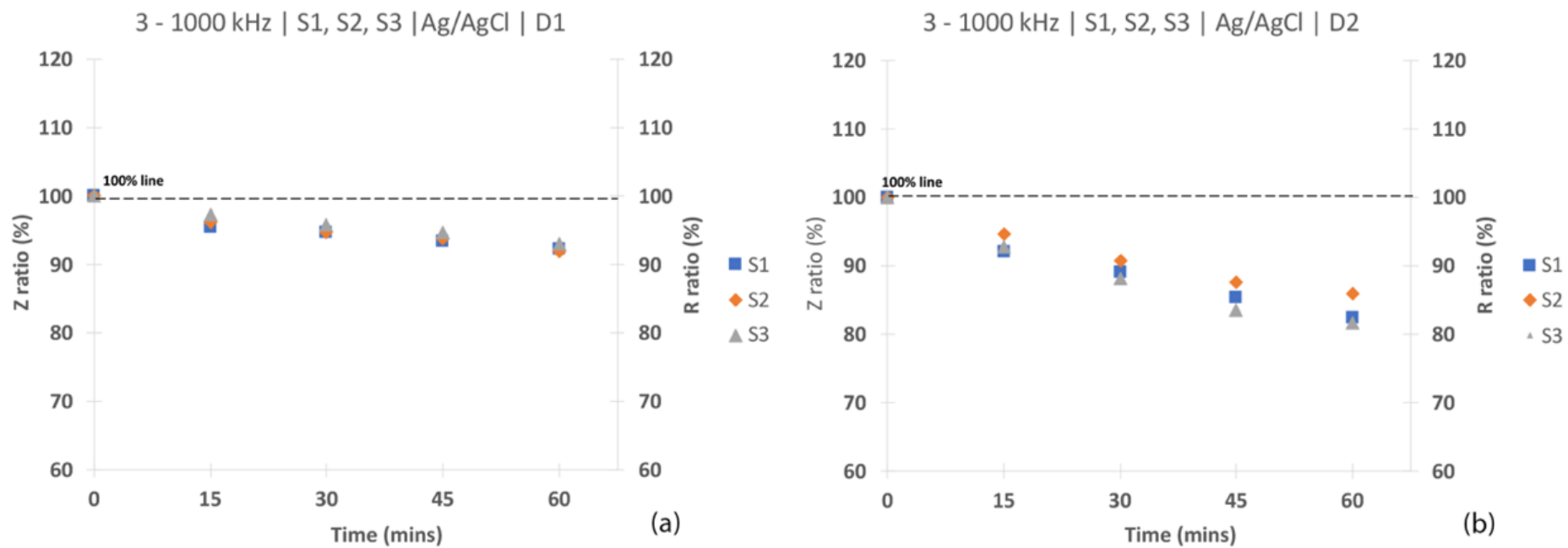


Figure 6.7a-b Z and R ratio relative to time at 3-1000 kHz sweep for electrodes: (a) Ag/AgCl day 1 and (b) day 2.

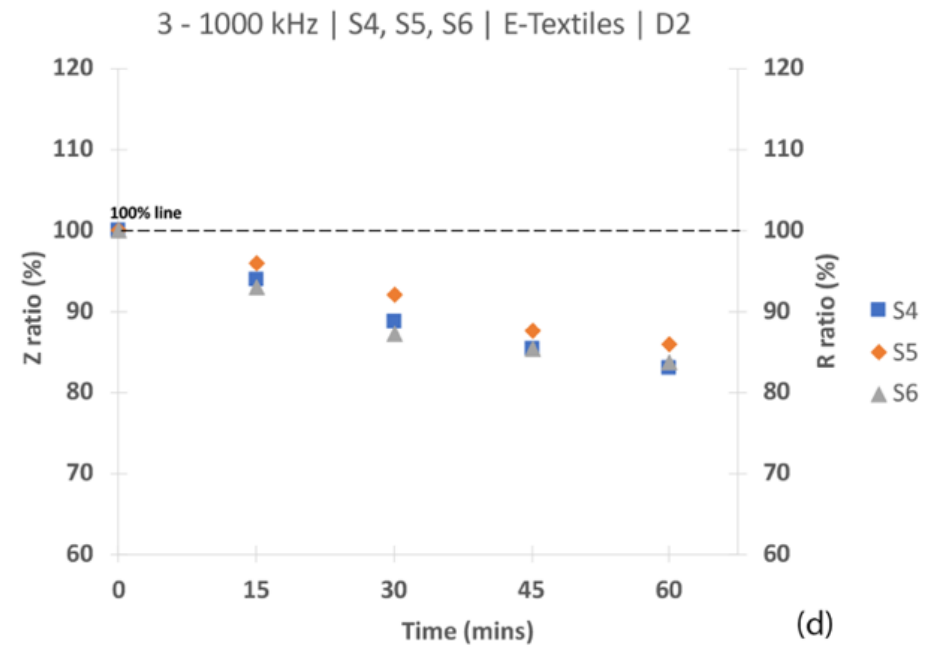
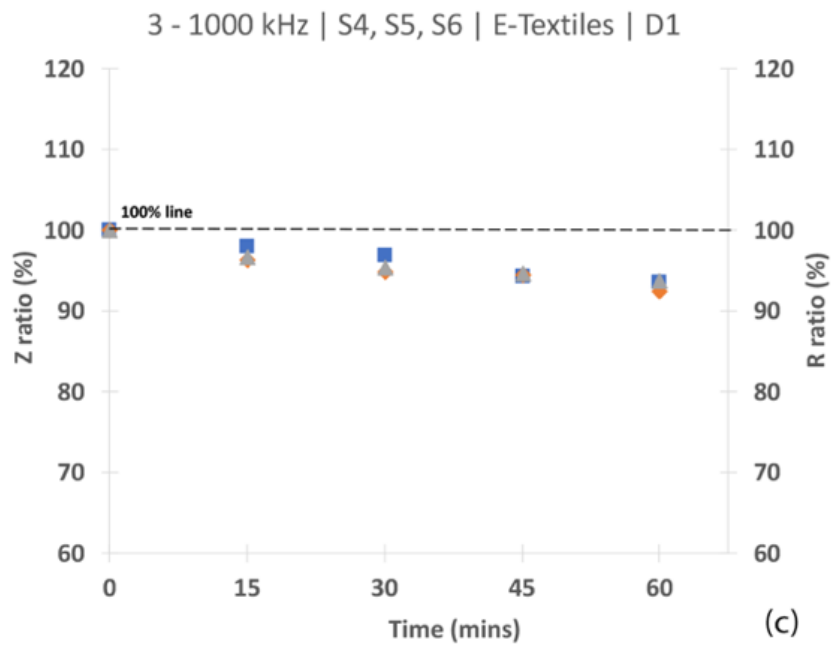


Figure 6.8c-d Z and R ratio relative to time at 3-1000 kHz sweep for electrodes: (c) e-textiles day 1 and (d) day 2

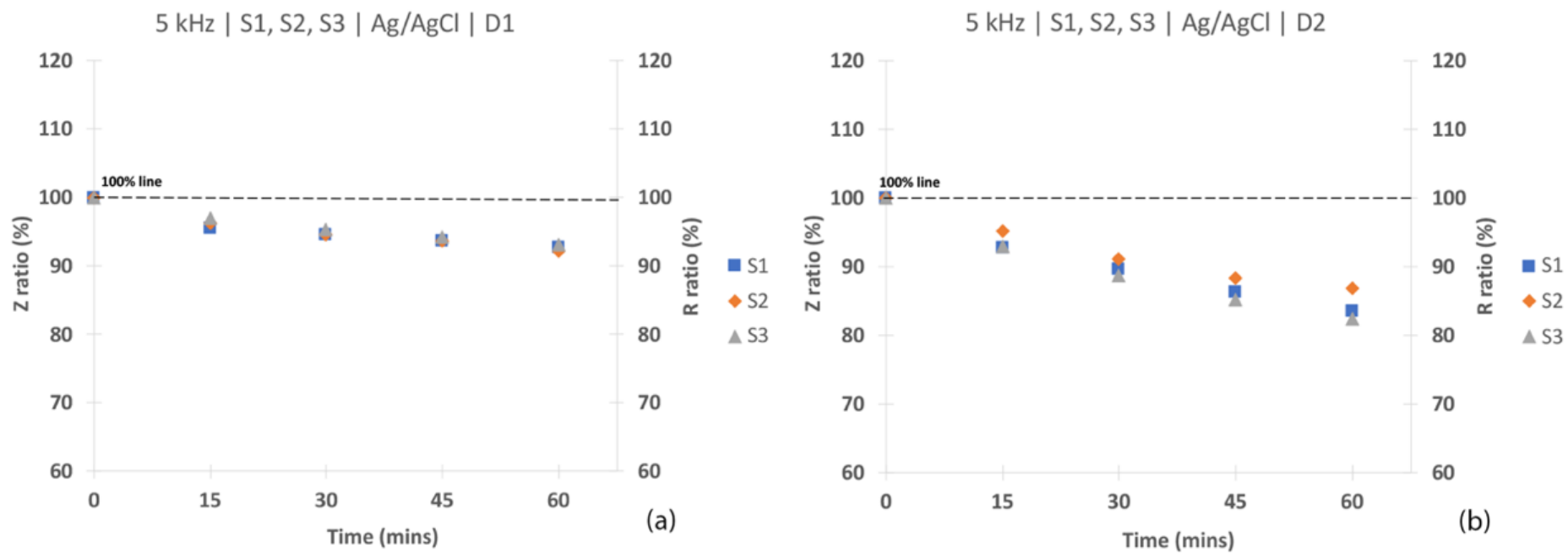


Figure 6.9a-b Z and R ratio relative to time at 5 kHz for electrodes: (a) Ag/AgCl day 1 and (b) day 2.

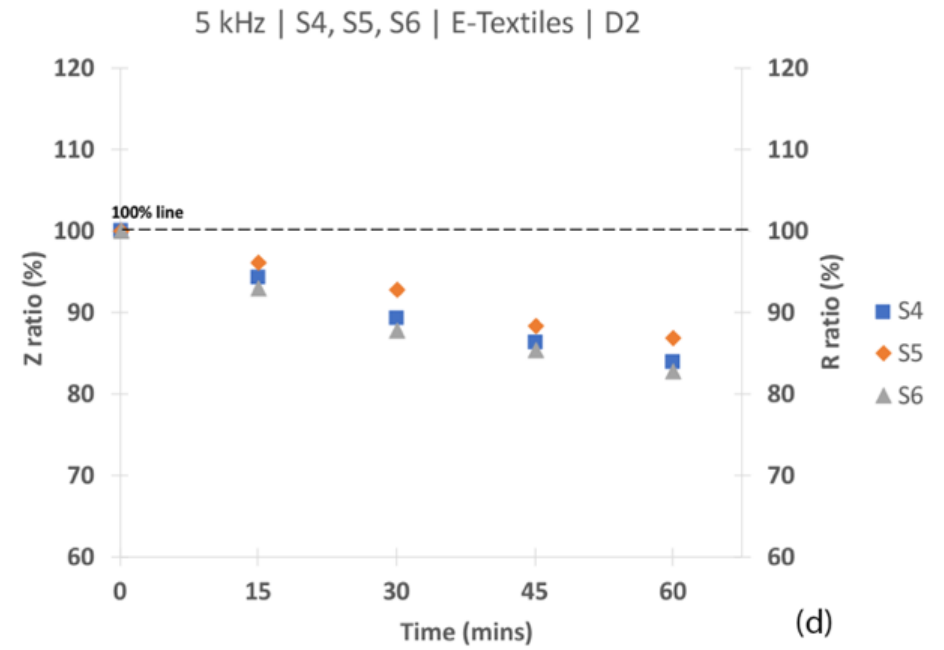
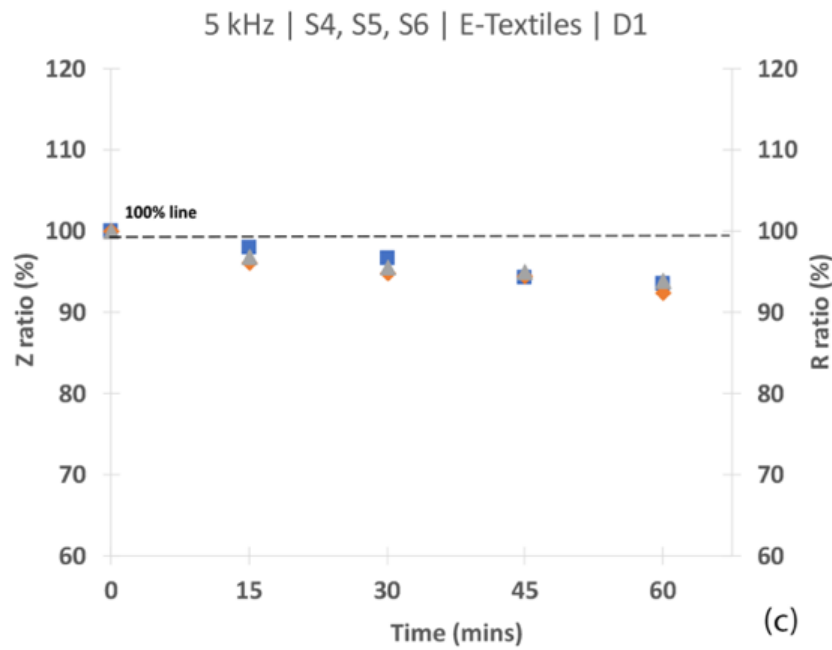


Figure 6.10c-d Z and R ratio relative to time at 5 kHz for electrodes: (c) e-textiles day 1 and (d) day 2.

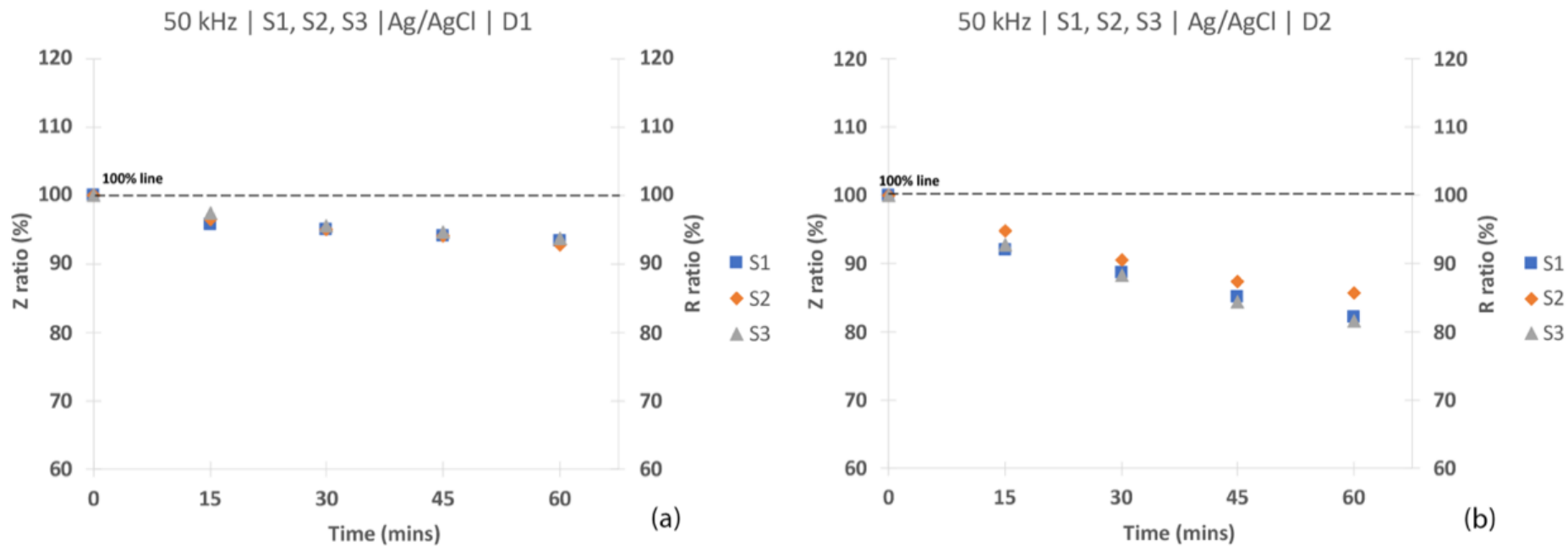


Figure 6.11a-b Z and R ratio relative to time at 50 kHz for electrodes: (a) Ag/AgCl day 1 and (b) day 2.

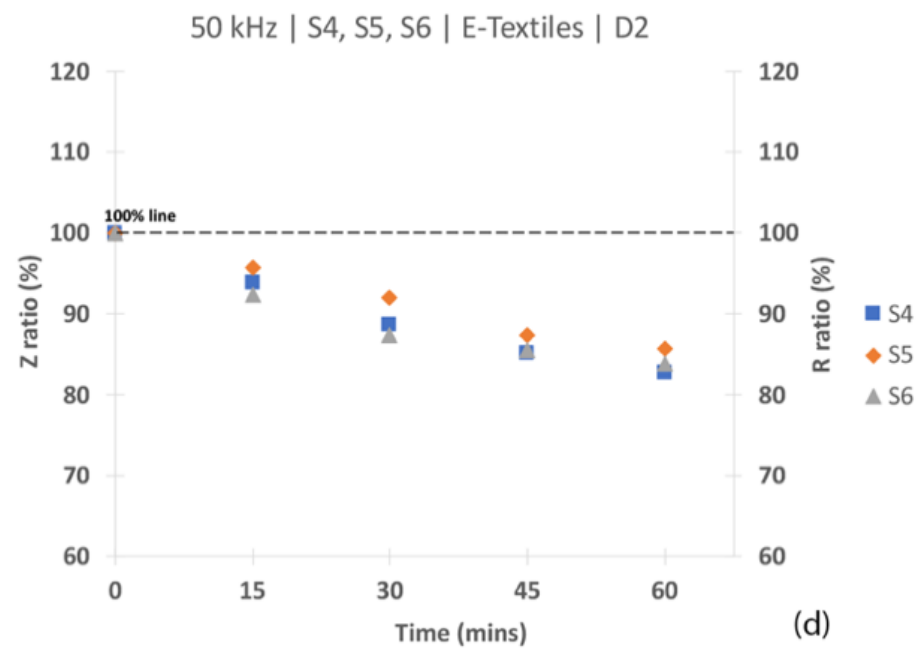
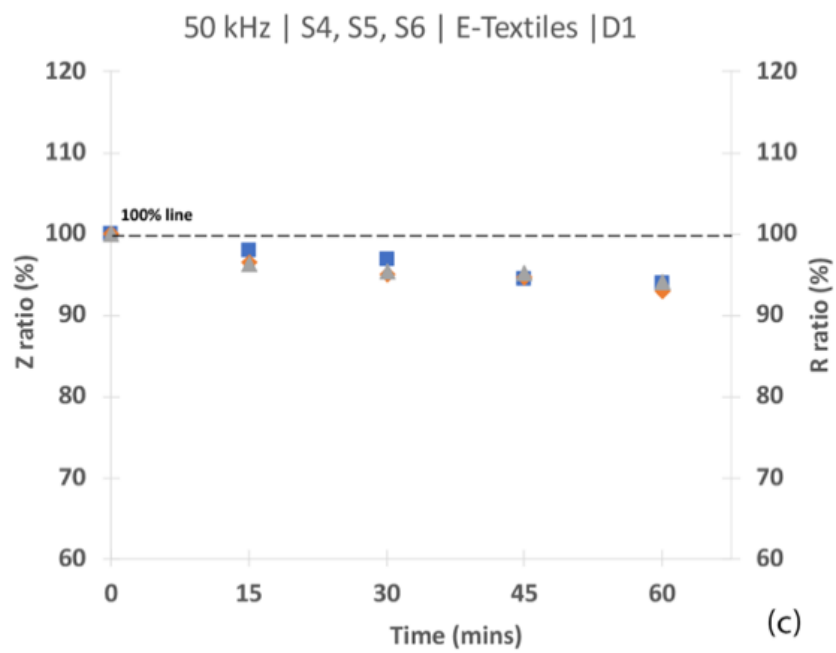


Figure 6.12c-d Z and R ratio relative to time at 50 kHz for electrodes: (c) e-textiles day 1 and (d) day 2.

6.3.4.3 Evaluation of X_c between Ag/Cl and e-textiles

The absolute values measured for X_c on day 1 using the Ag/AgCl electrodes were: 35, 30 and 25 Ω for samples S1, S2 and S3 respectively; with an equivalent capacitance of about 90, 105, 125 nF. While the measured X_c range for the samples using the e-textiles were: 9, 30 and 28 Ω associated with S1, S2 and S3 respectively. An equivalent capacitance of 0.35 μ F, 105 and 115 μ F.

For the standard Ag/AgCl electrodes, the trend of a gradual exponential decay is observed for the frequency sweep, following the trend of the Z and R on day 1 (Figure 6.8a). In this case $R^2 > 0.85$ (refer to Table 2, Appendix VI). However, S1 and S3 do not display this trend on day 2 where $R^2 = 0.33$, refer to Figure 6.8b and Table 2 Appendix VI. At 5 kHz and 50 kHz a clear decay was not observed on day 1, refer to figure 6.9a and 6.10a. While for day 2 at 5 kHz, a decay is observed across all samples (i.e., S1-S3) and at 50 kHz only for S3, refer to figure 6.9b and 6.10b. Thus, there is inconsistency across the replicates over the two days. For day 1, at 50 kHz a similar trend equation was observed comparable to the frequency sweep and $R^2 > 0.72$. However, at 5 kHz although the trend equations were comparable to the frequency sweep and 50 kHz; for S1 and S2 R^2 was as relatively low, with values of 0.21 and 0.14 respectively. On day 2 for 5 kHz, S1-S3 demonstrated a decrease with a strong correlation where $R^2 > 0.96$; at 50 kHz this decrease was repeated by S3 and $R^2 = 0.97$, refer to Figure 11-12b. However, a S1-S2 demonstrated a weak correlation and $R^2 < 0.14$. Therefore, the Ag/AgCl electrodes displayed an inconsistency in behaviour relating to X_c across the various samples over the two-day period.

For the e-textile electrodes this trend dispersion is predominant across all replicates and repeats. It is observed for the frequency sweep, in addition to the discrete frequencies, 5 and 50 kHz, refer to Figure 6.8-6.10c-d. Due to the data fitting an ideal Cole-Cole plot for the Ag/AgCl and e-textile electrodes, this change is not associated with Z_{es} mismatch. A consistent trend was not observed for the Ag/AgCl electrodes, however, the performance of the e-textile electrodes in terms of the measured X_c were significantly impacted. Provided this change in trend is observed in both cases it could potentially be associated with noise, in which case it would be likely for the e-textile electrodes to be significantly influenced. Moreover, provided such a discrepancy in trends is observed over the two-day period for the e-textile electrodes it is indicative that this was not associated with washing the e-textiles electrodes. Refer to Table 2 Appendix VI for the associated equations and R^2 values.

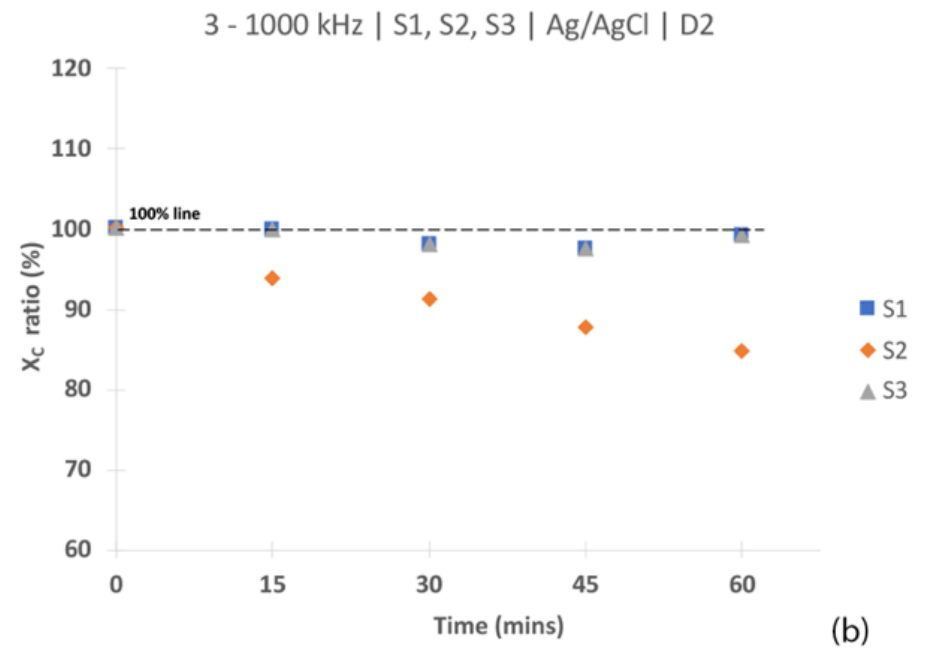
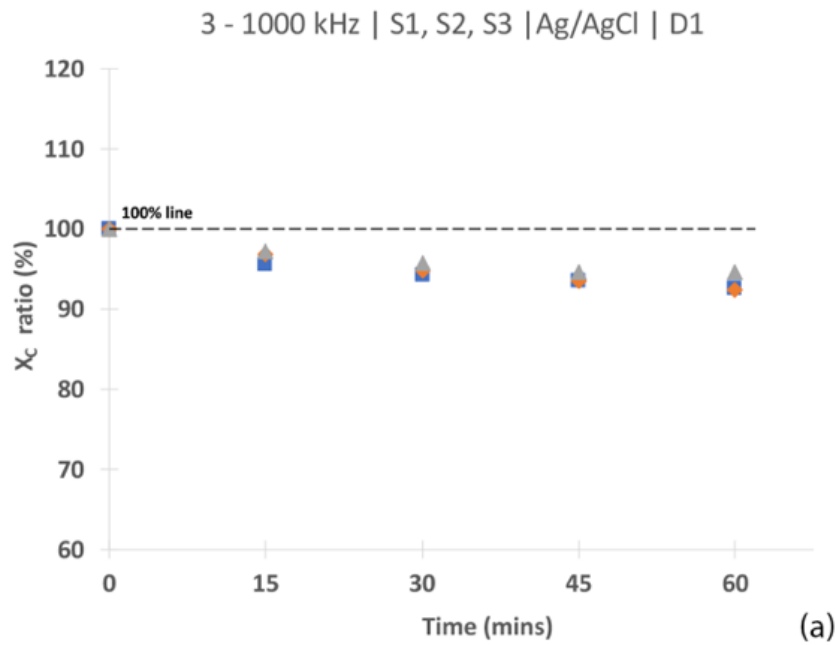


Figure 6.13a-b X_c ratio relative to time at 3-1000 kHz sweep for electrodes: (a) Ag/AgCl day 1 and (b) day 2.

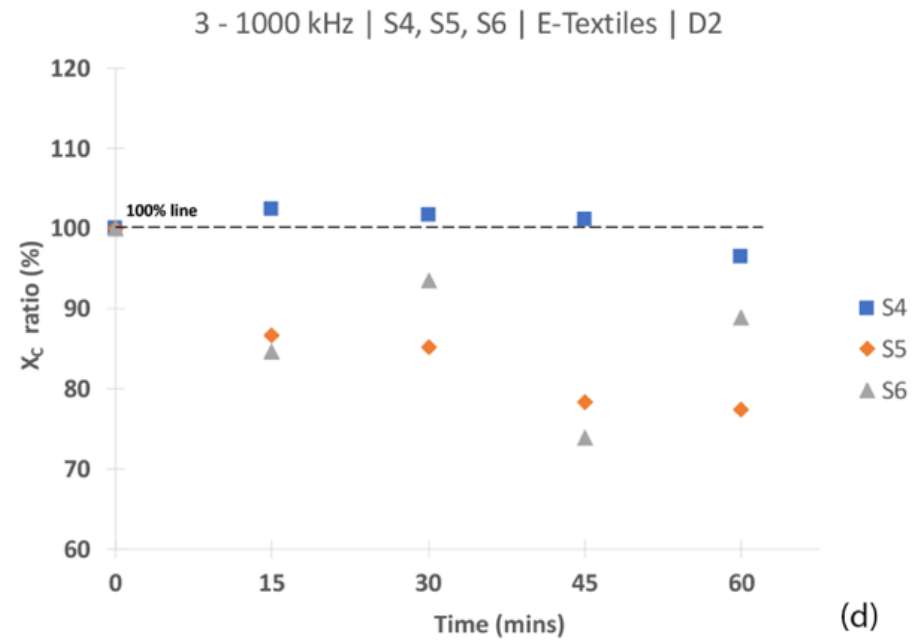
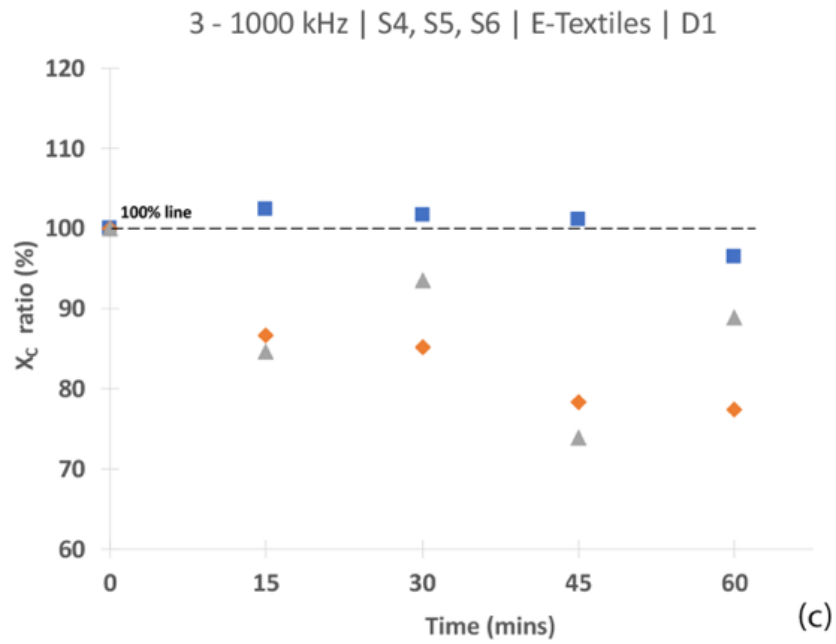


Figure 6.14c-d X_c ratio relative to time at 3-1000 kHz sweep for electrodes: (c) e-textiles day 1 and (d) day 2.

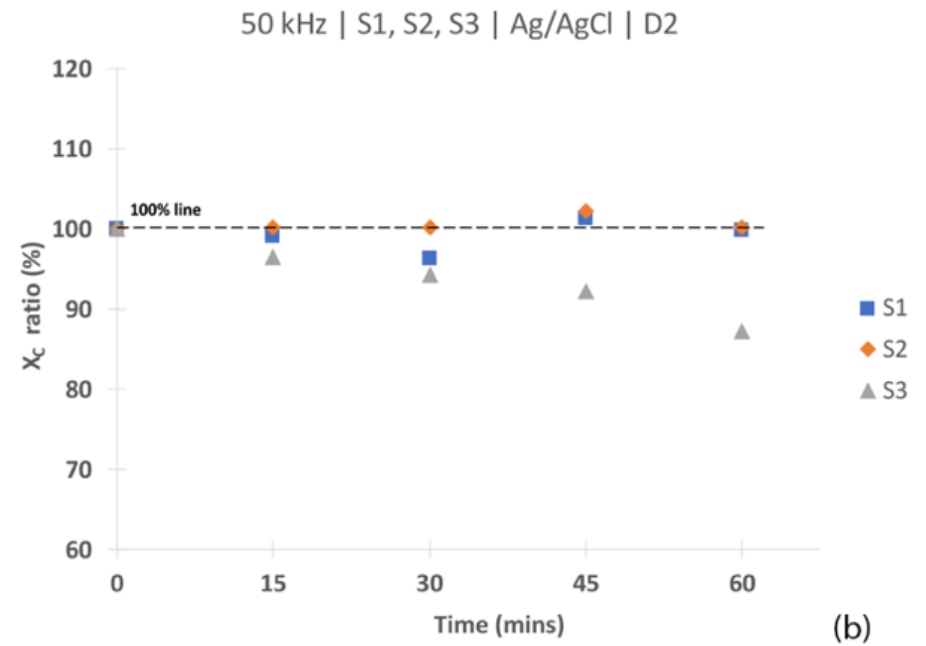
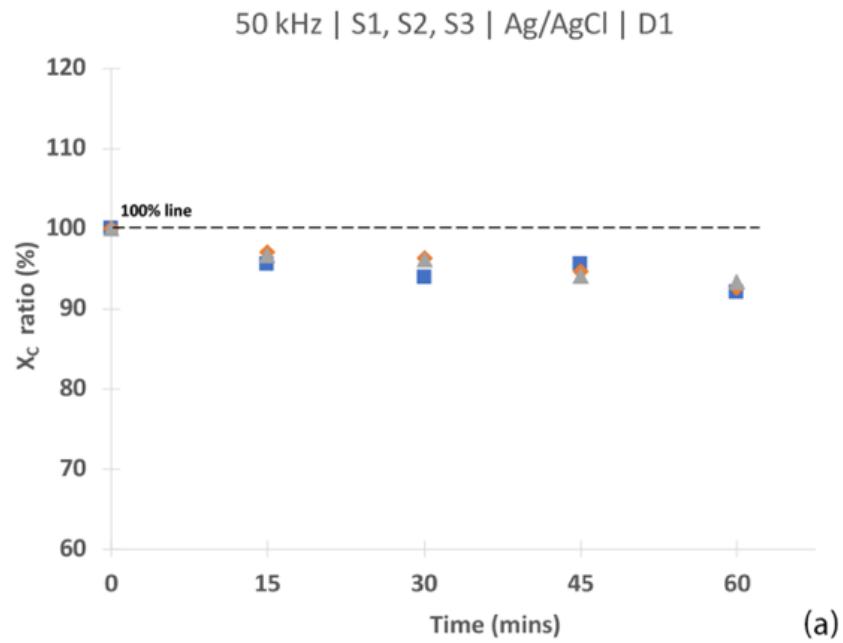


Figure 6.15a-b X_c ratio relative to time at 5 kHz for electrodes: (a) Ag/AgCl day 1 and (b) day 2.

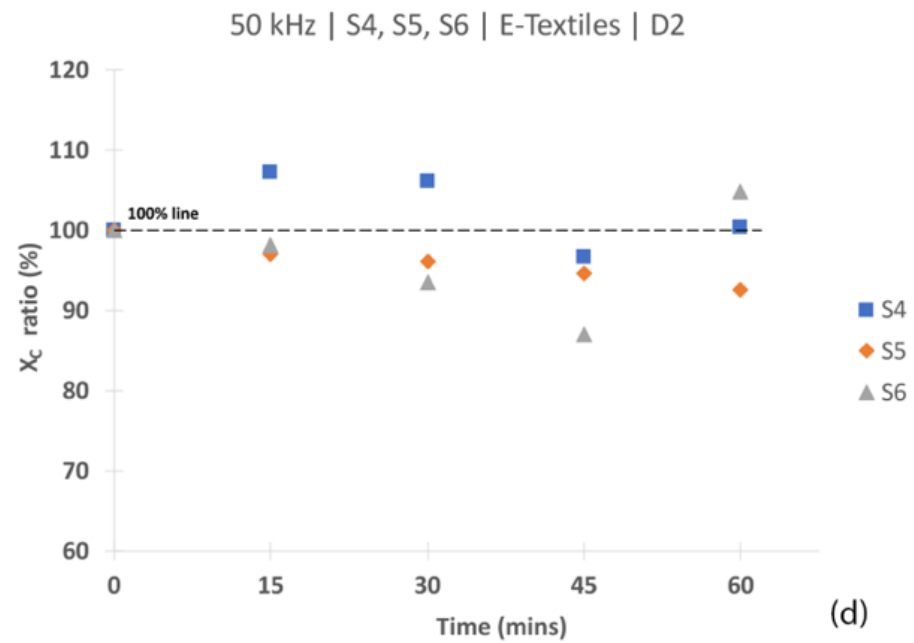
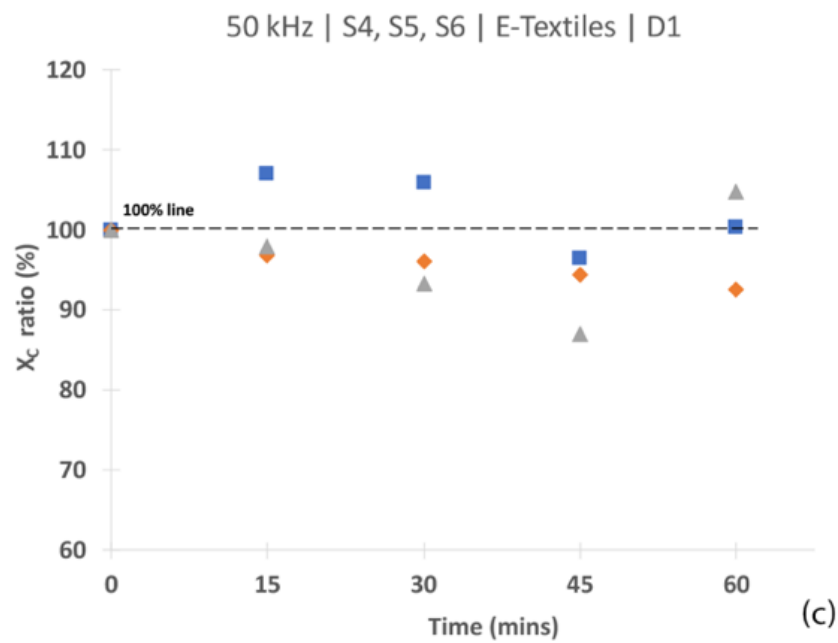


Figure 6.16c-d X_c ratio relative to time at 5 kHz for electrodes: (a) Ag/AgCl day 1, (b) day 2; (c) e-textiles day 1 and (d) day 2.

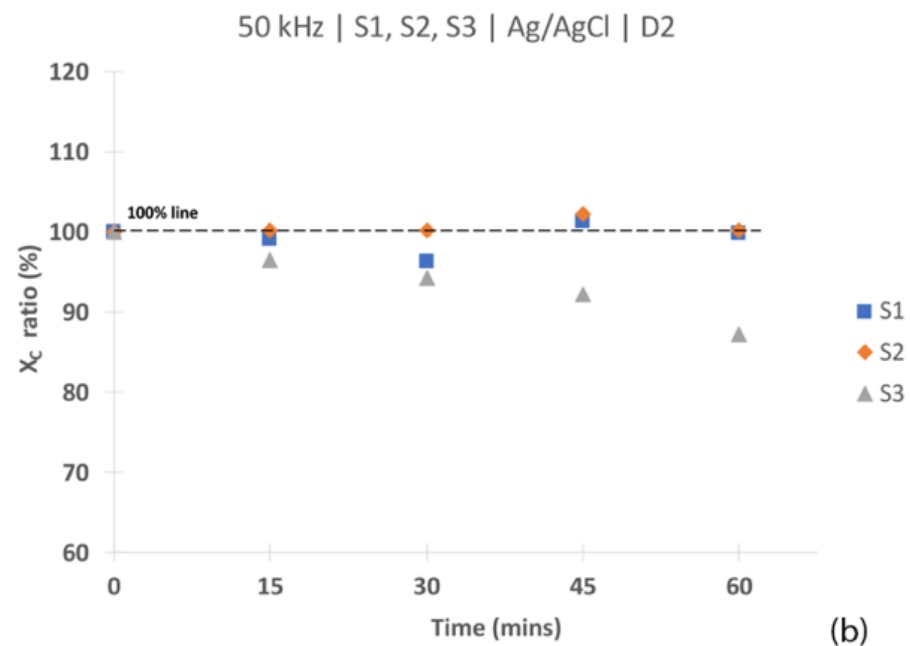
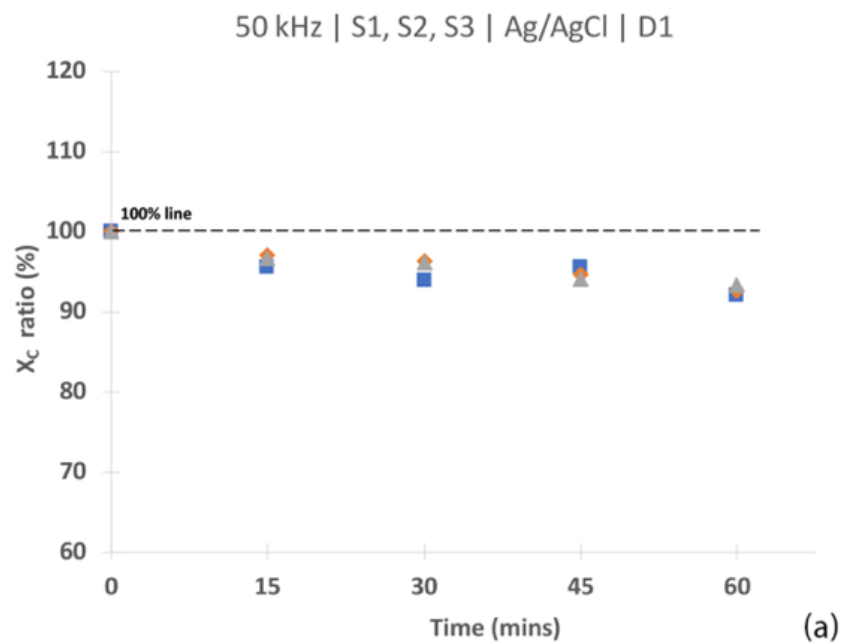


Figure 6.17a-b X_c ratio relative to time at 50 kHz for electrodes: (a) Ag/AgCl day 1 and (b) day 2.

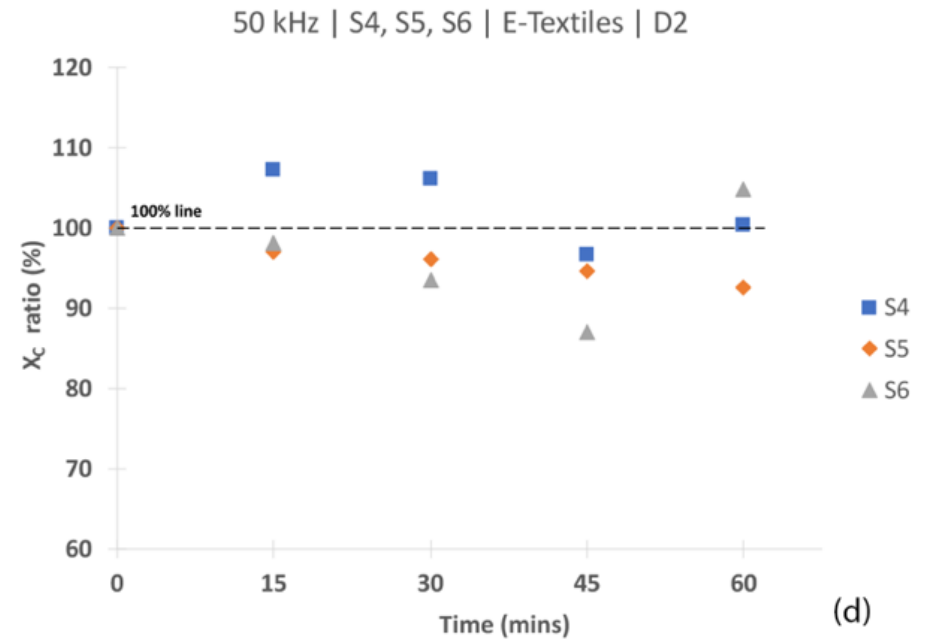
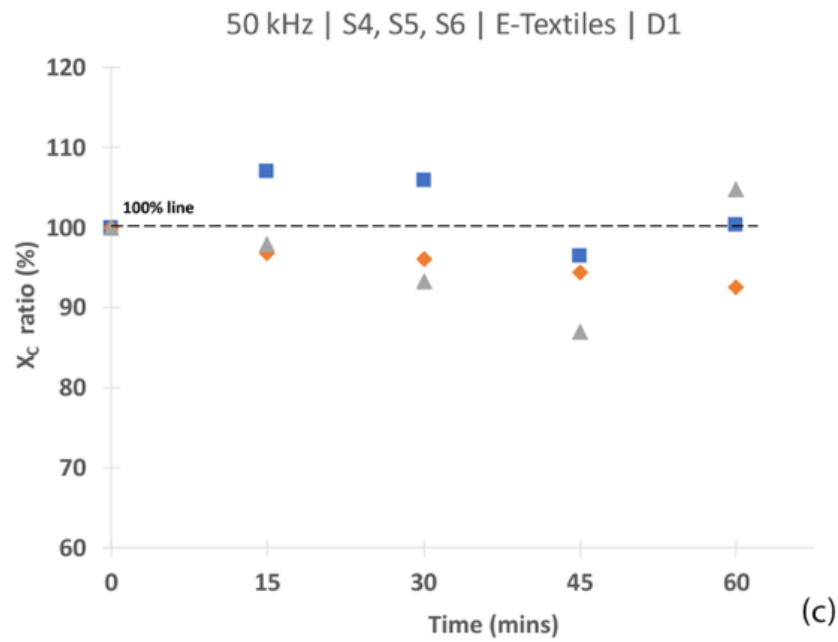


Figure 6.18c-d X_c ratio relative to time at 50 kHz for electrodes: (c) e-textiles day 1 and (d) day 2

6.3.4.4 Evaluation of φ between Ag/Cl and e-textiles

φ appears to be consistent for the Ag/AgCl electrodes for the frequency sweep on day 1 and 2, refer to Figure 6.11a-b. However, at 5 and 50 kHz there is a deviation from the 100 % line, refer to Figures 6.12a-b and 6.13a-b. For the BUS samples tested with the e-textile electrodes, an inconsistency is observed across the samples and for the frequency sweep and discrete frequencies. For the frequency sweep, all samples deviated from the 100% line on day 1 (Figure 6.10c); however, on day 2 samples S5 and S6 showed stability, refer to Figure 6.11d. For the discrete frequency of 5 kHz, the e-textile electrodes and measurements did not display stability nor any identifiable decay trend where dispersion of the signal was observed over the two days, refer to Figure 6.12c-d. However, at 50 kHz, S5 displayed stability on day 1 and day 2 while S6 showed stability only on day 2 (Figure 6.13c-d). Therefore, due to this inconsistency it is safe to assume that the washing of the e-textile electrodes did not influence their performance. Thus, for all samples either measured with the Ag/AgCl or e-textile electrodes, it can be possible that any noise influencing X_C has also impacted φ . As discussed for X_C , this noise is predominant in the e-textile electrodes and the measurements deviate greatly from the 100% line, refer to figures 6.11-6.13c-d. Thus, no comparison is observed. The trends associated to φ across the samples and frequency settings presented inconsistent R^2 , refer to table 3, Appendix VI.

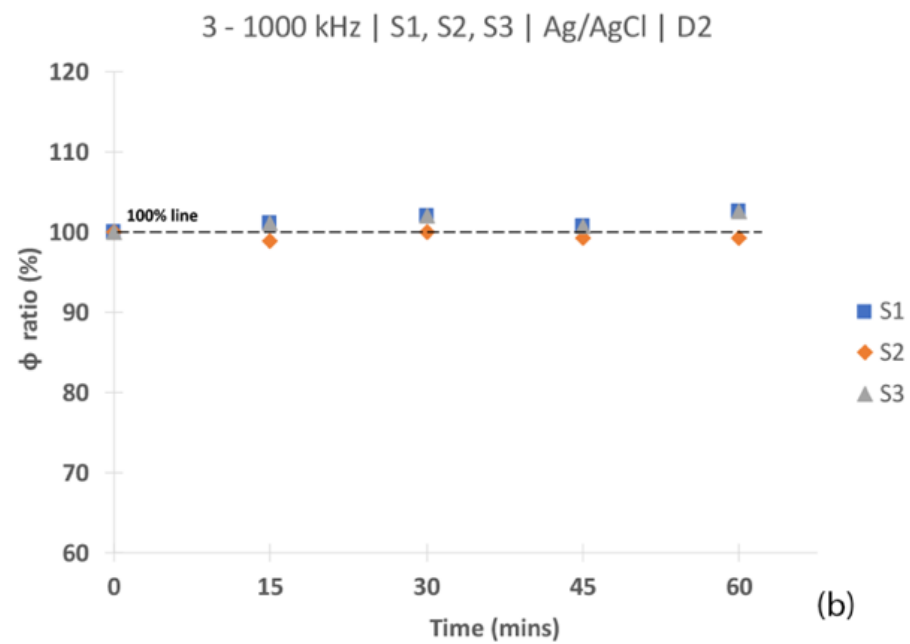
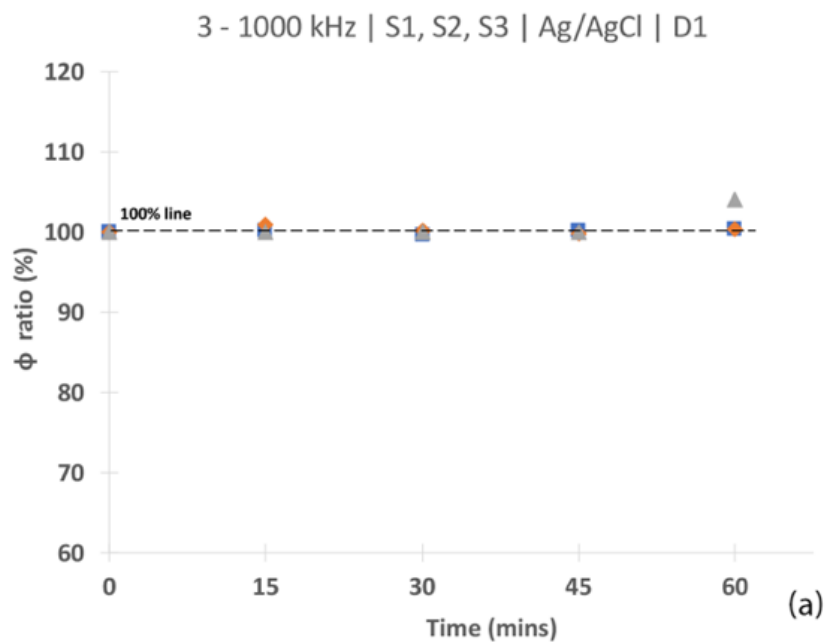


Figure 6.19a-b ϕ ratio relative to time at 3-1000 kHz sweep for electrodes: (a) Ag/AgCl day 1 and (b) day 2.

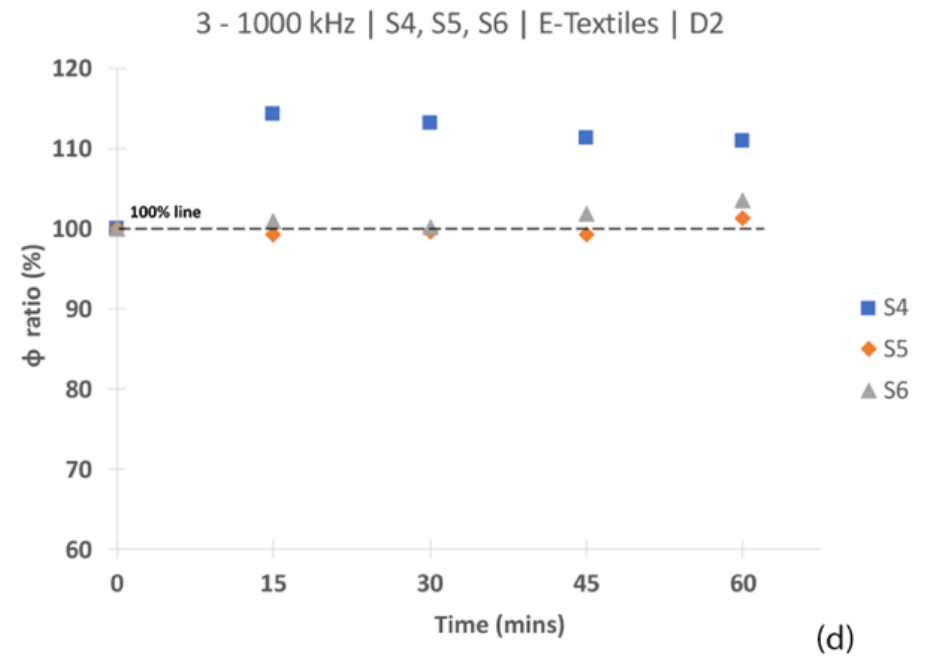
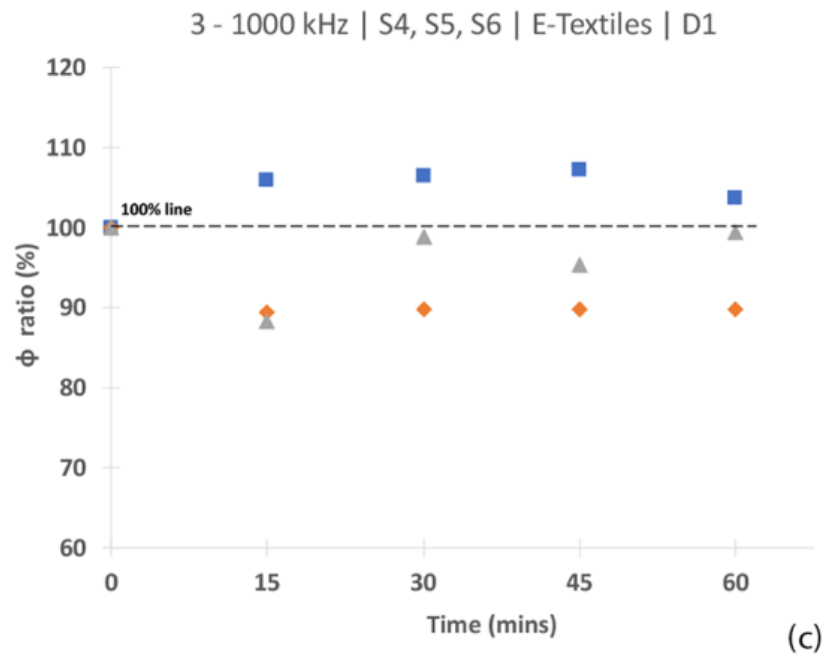


Figure 6.20c-d ϕ ratio relative to time at 3-1000 kHz sweep for electrodes: (c) e-textiles day 1 and (d) day 2.

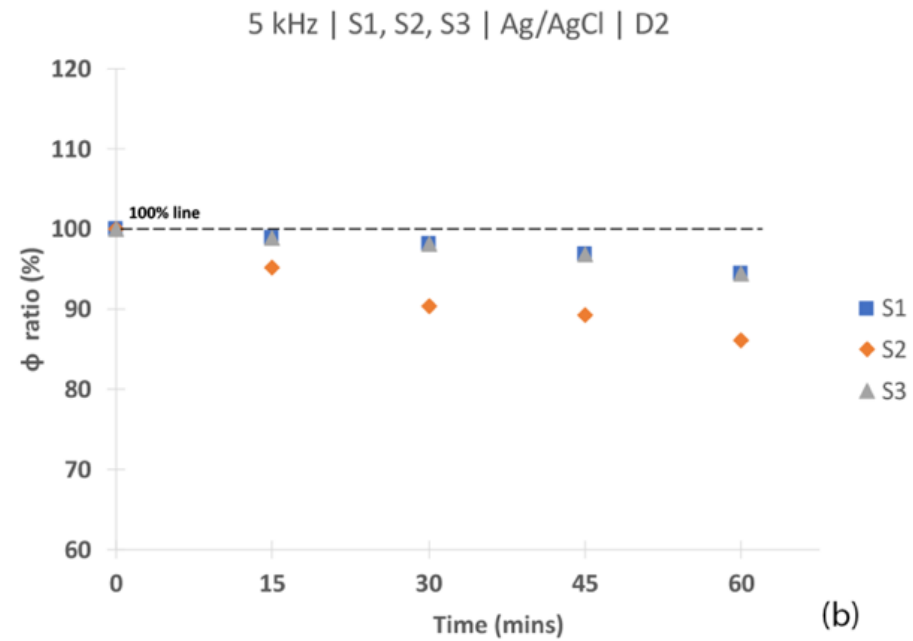
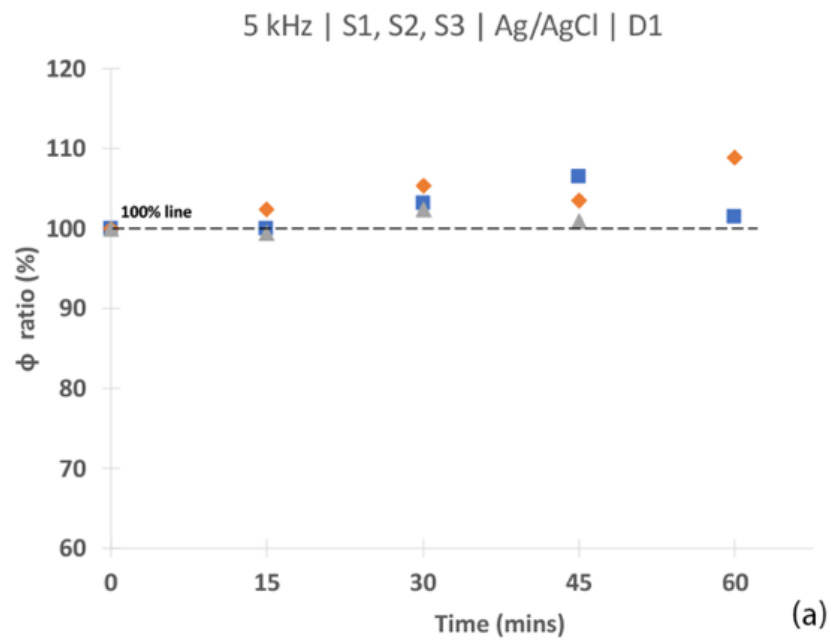


Figure 6.21a-b ϕ ratio relative to time at 5 kHz for electrodes: (a) Ag/AgCl day 1 and (b) day 2.

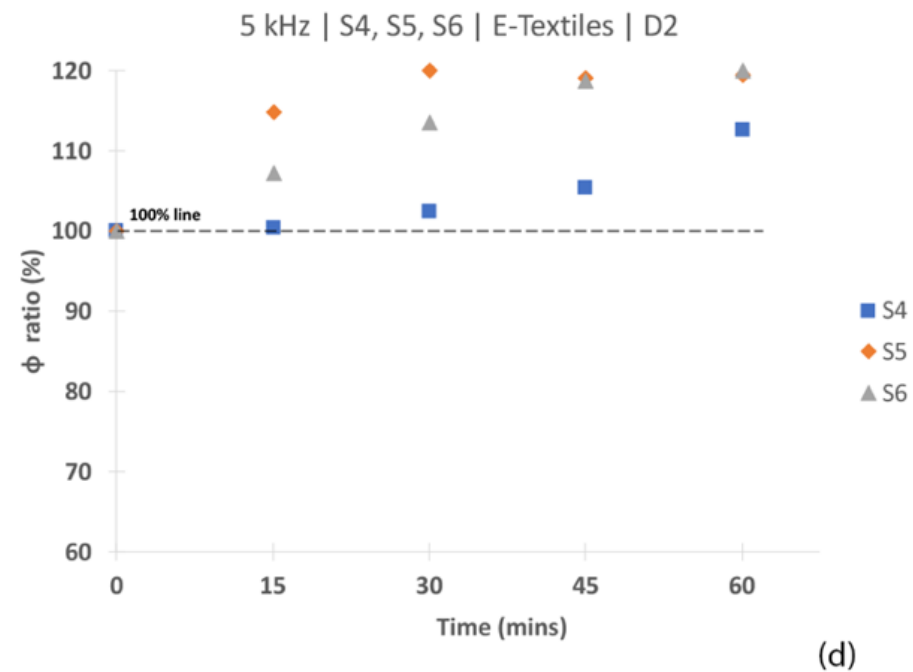
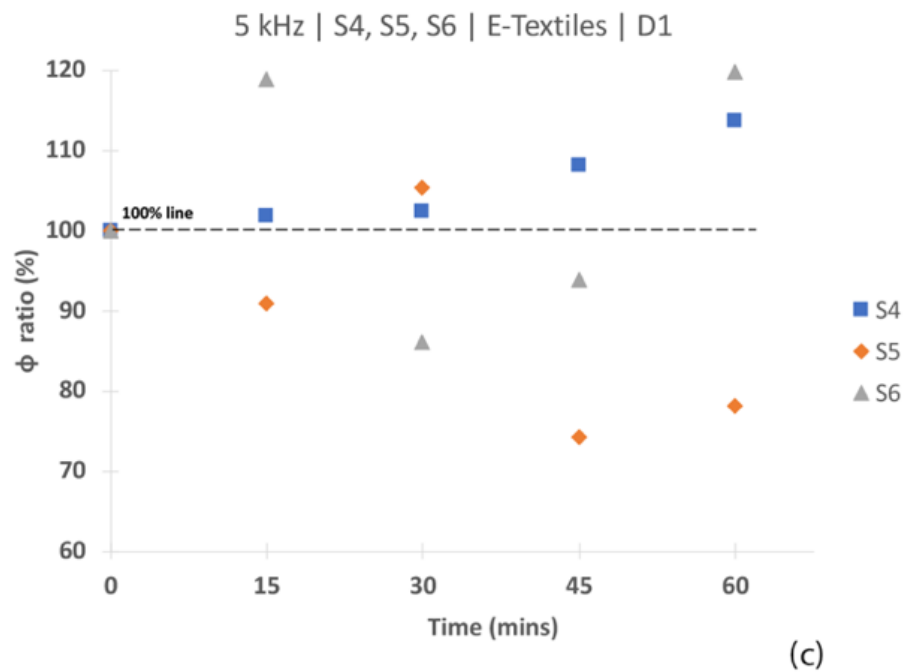


Figure 6.22c-d ϕ ratio relative to time at 5 kHz for electrodes: (c) e-textiles day 1 and (d) day 2.

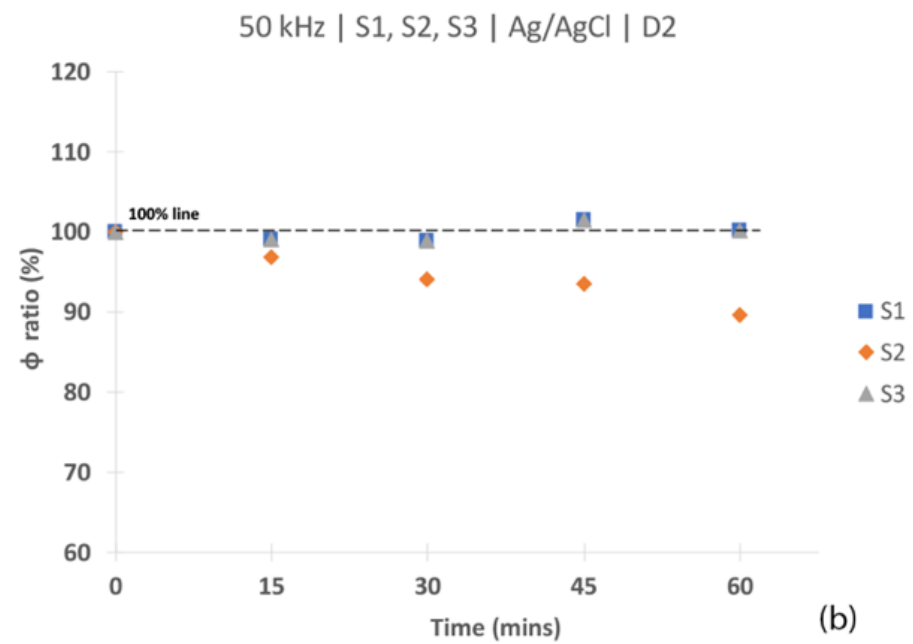
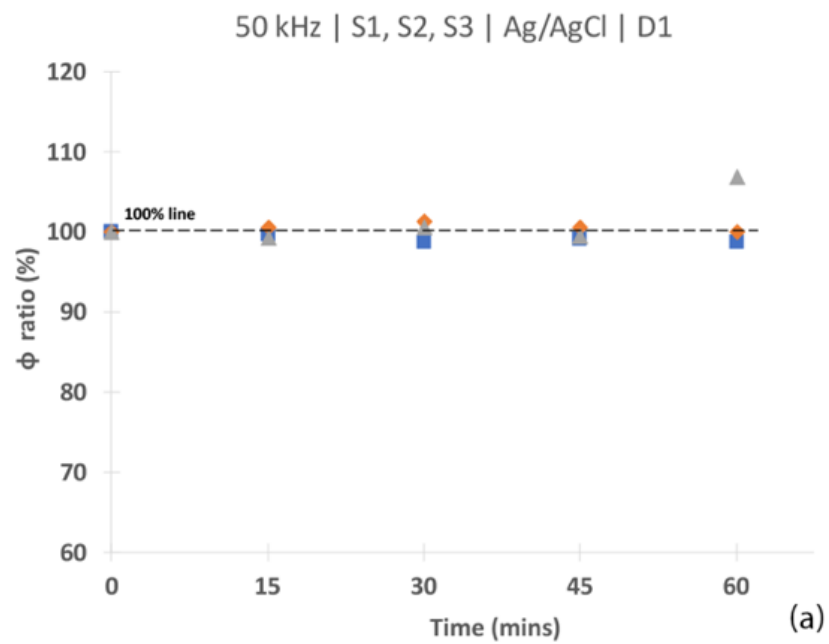


Figure 6.23a-b ϕ ratio relative to time at 50 kHz for electrodes: (a) Ag/AgCl day 1 and (b) day 2.

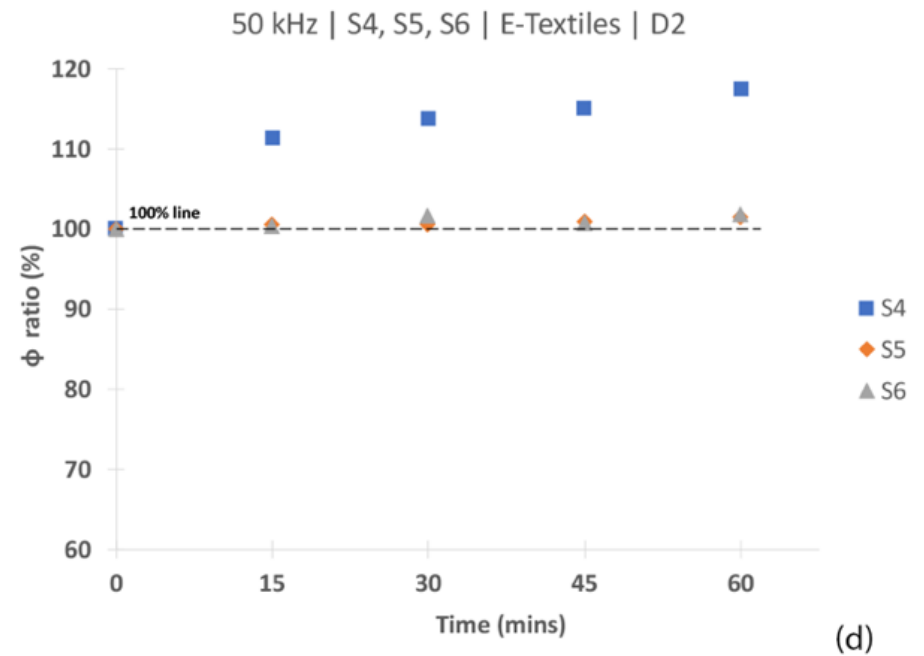
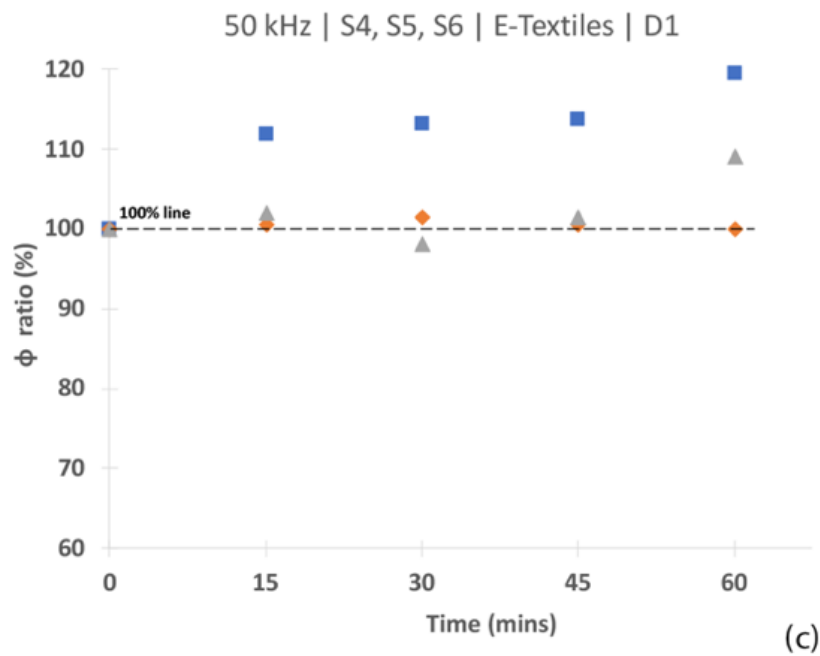


Figure 6.24c-d ϕ ratio relative to time at 50 kHz for electrodes: (c) e-textiles day 1 and (d) day 2.

6.3.4.5 Evaluation of R_0 between R_{inf} and e-textiles

R_0 and R_{inf} replicate the trend of Z and R for the samples using the Ag/AgCl electrodes, implying an exponential decay, refer to figures 14-15a-b. By observing the exponential trend, a strong correlation was observed where $R^2 > 0.85$. However, this exponential decay is not visible using the e-textile electrodes for R_0 , refer to figure 14c-d. This was also demonstrated in the exponential trend correlation coefficient. Day 1, indicated R^2 ranged between 0.47 – 0.62 while for day 2, R^2 ranged between 0.42 – 0.81 across the samples, refer to Table 4, Appendix VI. R_{inf} is indicative of a decay (Figure 15c-d) comparable to the Ag/AgCl electrodes. A strong correlation was indicative across all samples and $R^2 > 0.88$, refer to Table 5, Appendix VI. It is important to note that R_0 and R_{inf} are calculated based on the Cole-Cole model. Provided that the presence of noise interfering with X_C is more prevalent to the e-textile electrode measurements, this could potentially influence R_0 and R_{inf} associated with the model.

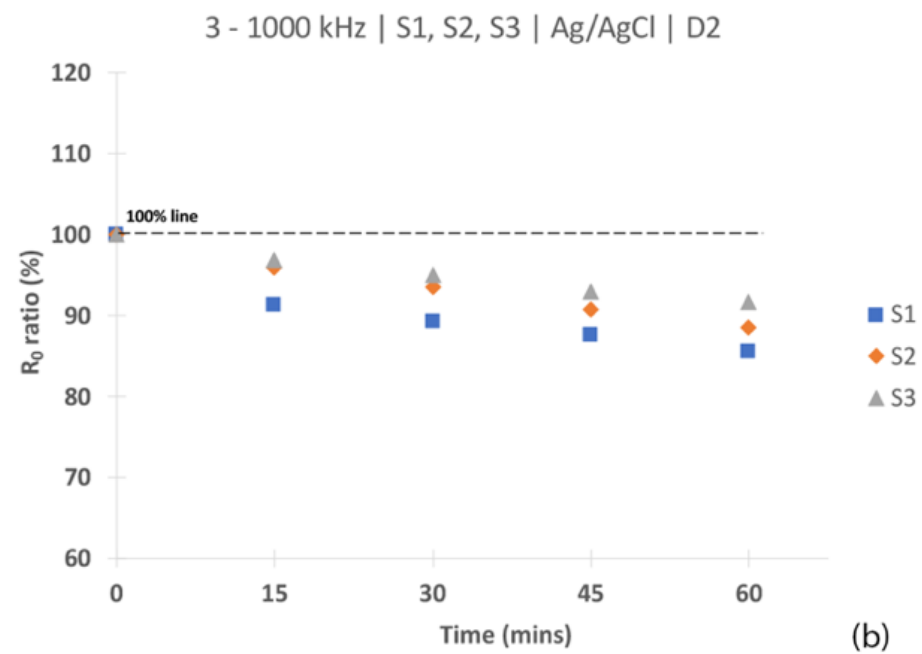
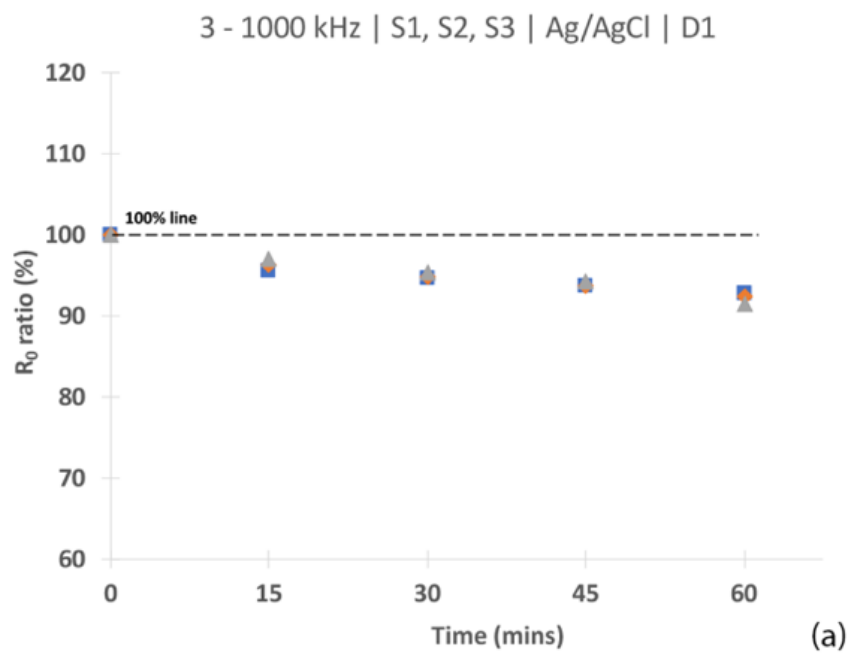


Figure 6.25a-b R_0 ratio relative to time at 3-1000 kHz sweep for electrodes: (a) Ag/AgCl day 1 and (b) day 2.

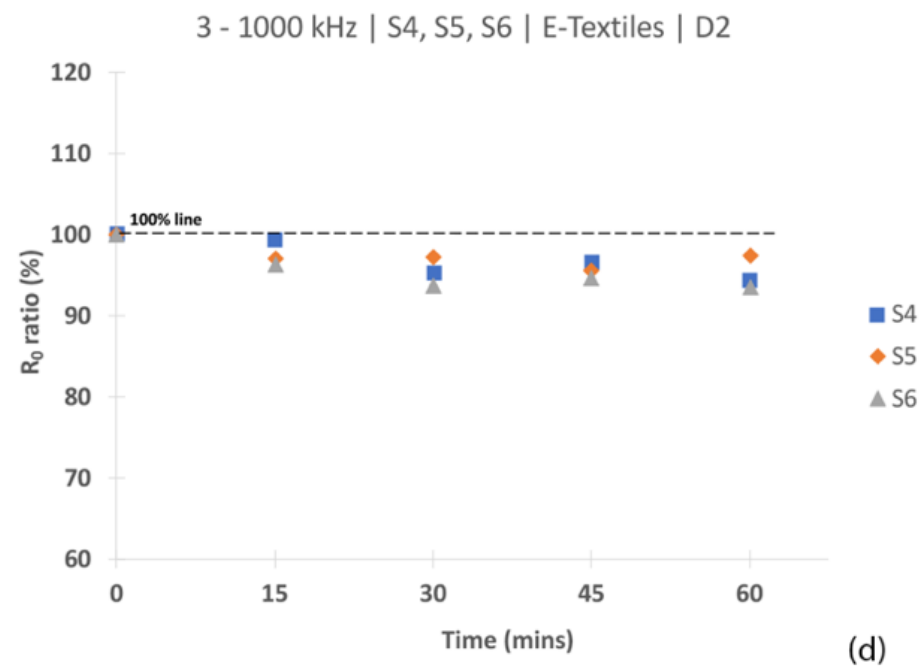
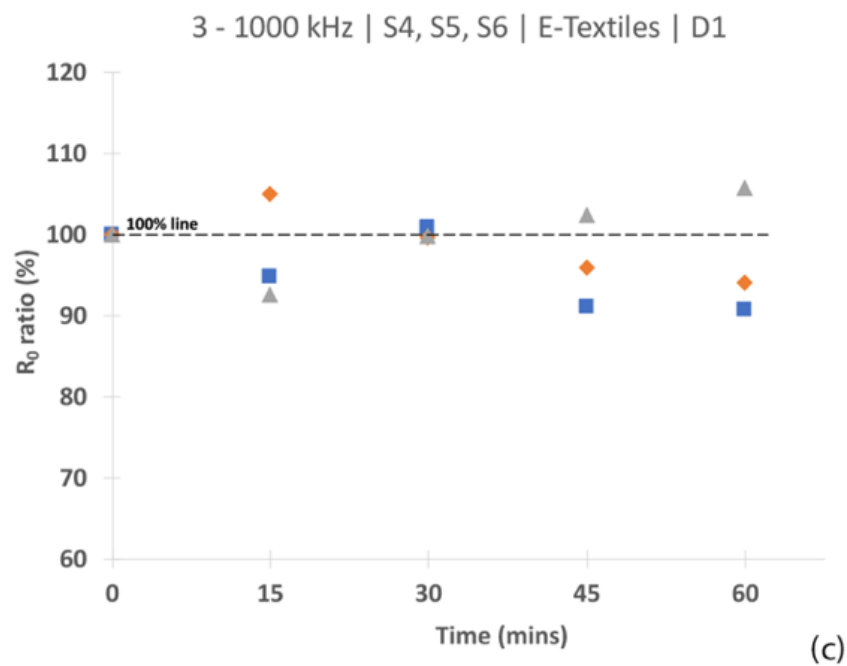


Figure 6.26c-d R_0 ratio relative to time at 3-1000 kHz sweep for electrodes: (c) e-textiles day 1 and (d) day 2.

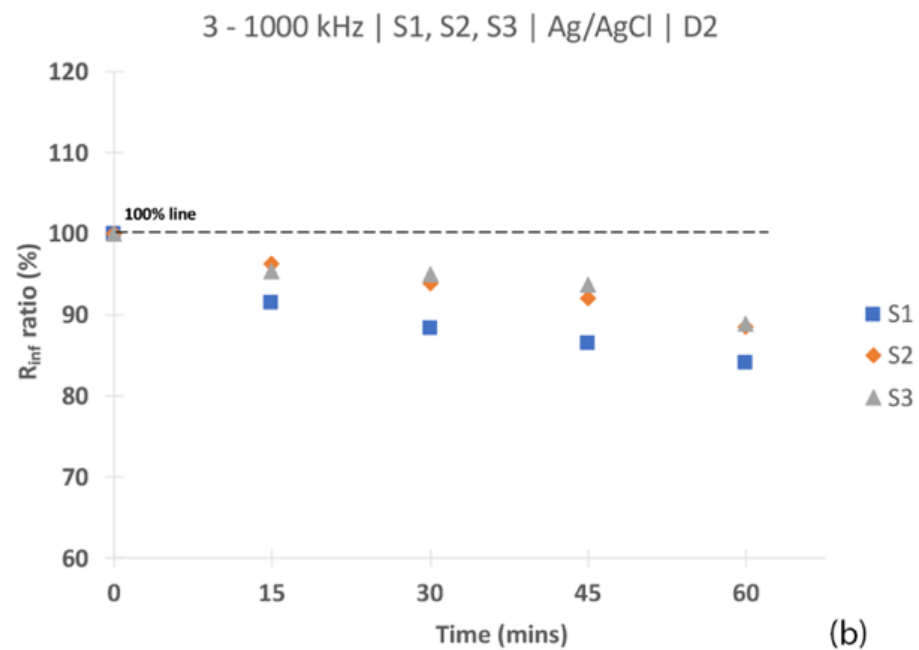
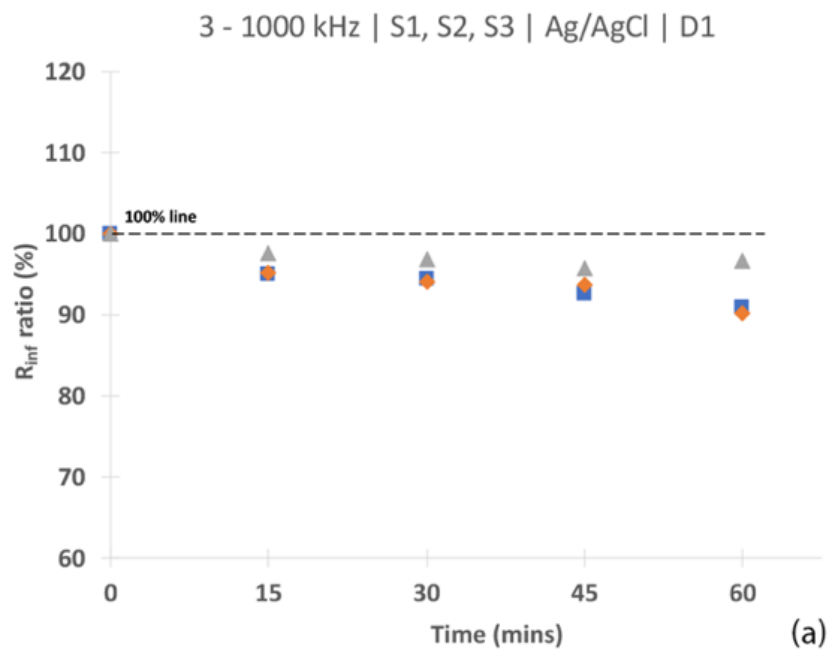


Figure 6.27a-b R_{inf} ratio relative to time at 3-1000 kHz sweep for electrodes: (a) Ag/AgCl day 1 and (b) day 2.

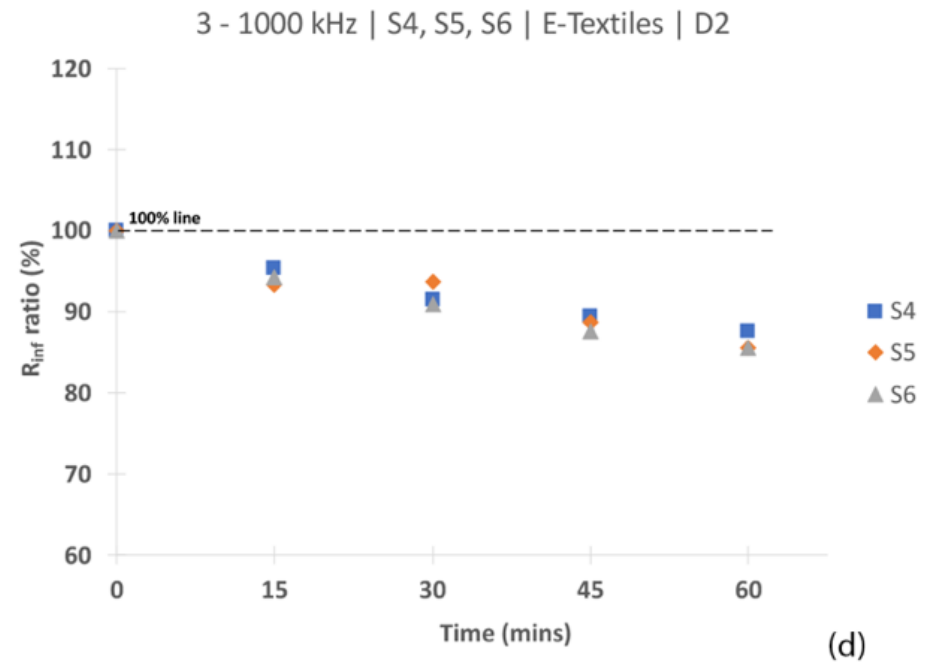
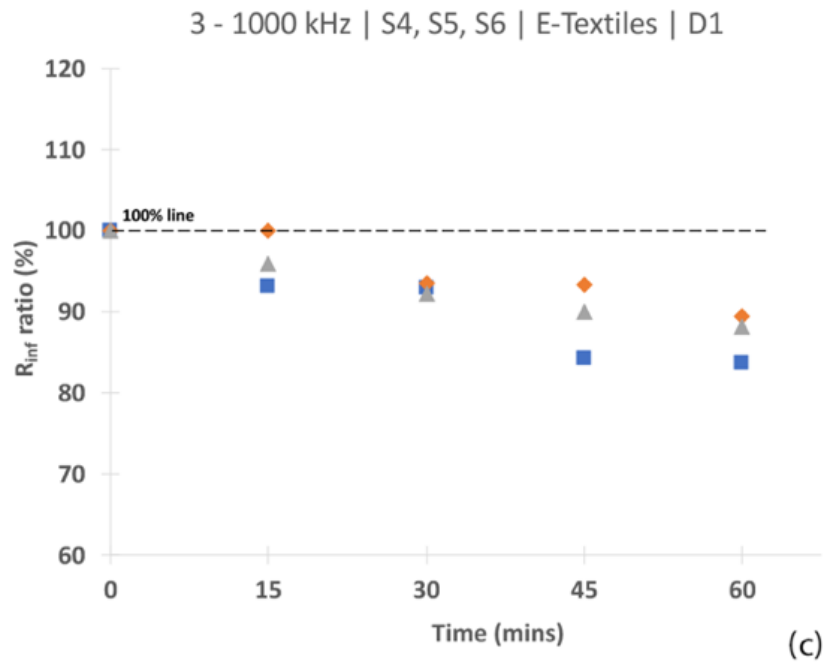


Figure 6.28c-d R_{inf} ratio relative to time at 3-1000 kHz sweep for electrodes: (c) e-textiles day 1 and (d) day 2.

6.4 Discussion

It was observed that the e-textile electrodes indicate an identical trend for Z and R comparable to the Ag/AgCl electrodes for a frequency sweep of 3 – 1000 kHz and for discrete frequencies of 5 kHz and 50 kHz. This was based on positioning the electrodes adjacent to an open excision relative to the size of measured wounds, with a 1 cm distance between the voltage sensors and injecting electrodes. Washing the electrodes indicated that the performance of e-textile electrodes were again comparable to the Ag/AgCl electrodes on day 2. An exponential decay was observed over time; this could potentially be associated with the decay of necrotic tissue. However, previous research into Z_{es} in-vivo has indicated a continuous exponential decay over various time periods before a settling period [189,268–270] is reached. This research is not completed as a continuous function of time; however, injecting a small charge through the necrotic tissue potentially causes a change to the necrotic tissue which requires time to settle. This time may be significantly greater for the necrotic tissue (in vitro) compared to in vivo. However, for this study a simple comparison of the efficacy of the e-textile electrodes for use with BIA systems was made. Chapter 7 discusses the potential for research in the relaxation period associated in-vivo.

Although dry electrodes have been reported to have a higher Z_{es} impedance [271], this could be due to an inappropriate method of application. For example, due to lead connections or the applied method of securing the e-textile electrodes to the body. Provided that e-textile electrodes do not possess an adhesive layer, an air gap between the skin and the electrode creates a dielectric layer resulting in an increase in Z . The method used in this study provides a relatively controlled compression for the e-textile electrodes and the Ag/AgCl electrodes resulting in relatively low impedance values. The additional pressure of all types of electrodes (i.e., wet and dry) have been known to improve the quality of the signal.

In the case of X_C and φ , a similar trend was not clearly depicted between the Ag/AgCl and e-textile electrodes. However, an exponential decay was not clearly observed for X_C with the Ag/AgCl electrodes. This was more dominant with the e-textile electrodes. These fluctuations in X_C potentially influenced the Cole-Cole model resulting in a disruption in R_0 and R_{inf} trends. R_0 is greatly impacted with the e-textile electrodes with no observed trend relative to time. Although, R_{inf} indicates a decay for both types of electrodes, there is a slight difference. This could potentially be due to the different samples, although provided that for a frequency sweep R is identical, it is likely that is influenced by the irregularity occurring with X_C . Moreover, a trend was not distinguishable for φ . This could be due to the noise impacting X_C or it could be due to the anisotropic nature of skin, in which it has been suggested that the φ should

not be adapted to the Cole-Cole model [272]. This also occurred at 5 and 50 kHz. It is safe to assume that X_C was influenced by an external noise.

E-textile electrodes have capacitive properties contrary to Ag/AgCl electrodes [264]. It was observed that for the frequencies adapted for BIA measurements of wounds ex-vivo indicates that X_C is relatively small to Z and the coupling capacitance of Z_{es} possesses a magnitude of μF . Thus, it has shown not to significantly contribute to Z and is more susceptible to noise in comparison to R . This is also true of the Ag/AgCl electrodes [273] in-vivo. It has been shown that for e-textiles, the trend over time associated with the capacitive properties of Z_{es} is not consistent compared to its resistive properties [109].

Noise influencing wet and dry electrodes is commonly associated with (i) motion artefact, (ii) equipment and (iii) ambient environment [273,274]. In this study there is no motion; thus, the fluctuation of direction in X_C could potentially be noise derived from the equipment, resulting in an unstable signal. This possibly explains why the trend is irregular for the Ag/AgCl and e-textile electrodes. Another possibility is from ambient noise due to electromagnetic interference [275]. These issues are common in ECG measurements where the frequency range is significantly lower than BIA systems. Spinelli et al. [276] proposes a front end for insulating electrodes. By analysing the noise at low frequencies, modifications were made to the bias current. In addition, to reduce the input capacitance effects methods such as: (i) guarding to avoid any leakage current, (ii) neutralization and (iii) boot strapping were applied. Moreover, the common-mode rejection ratio was adjusted to reduce power line interferences. Thus, additional hardware could be designed and built to improve the performance of e-textile electrodes with BIA systems.

Another importance factor to consider are the variables associated with the electrodes that can potentially influence the performance of e-textile electrodes. For example, the microclimate formed by the bandage can impact the performance of wet and dry electrodes [277]. This microclimate can be unstable thus affecting X_C , specifically relating to relative humidity [278]. It was observed that the relative humidity has a significant impact on the e-textile electrodes [47,68]. The gel layer could possibly be less susceptible to changes of relative humidity.

In addition, the electrode-skin contact could also interfere with the signal. This could be from the lipids found on skin, and the inhomogeneity of the skin and electrode surface. The surface of the skin contains various lipid bilayers that possess capacitance properties and act as a barrier to the penetration of charge [271]. It is possible that the electrolyte gel layer of the Ag/AgCl electrodes that is used to enhance the redox reaction results in counteracting this barrier [278]. In contrast, there is no wet layer to the dry electrodes. Taking this into consideration, the uneven nature of the conductive interface of the e-textile electrodes could result in a non-

uniform current density occurring on the e-textile electrode surface. Moreover, the skin is also non-uniform in nature. Therefore, there will be some loss between the two contact sites, i.e., the skin and electrode. The adhesiveness of Ag/AgCl potentially reduces this barrier improving the charge dispersion.

This research indicates the e-textile electrodes can be used to measure Z and R associated with BIA to monitor the wound healing process; they can also be washed and not impacted. The electrodes can be positioned locally surrounding the wound. Their trend relative to time is comparable to Ag/AgCl electrodes. However, there are shortcomings of measuring X_C , φ , R_0 and R_{inf} . To improve this shortcoming, a BIA system with improved hardware could potentially assist the use of e-textiles to measure these parameters.

6.5 Conclusion

Currently, research primarily focuses on the trend of BIA parameters (i.e., Z , R , X_C , φ , R_0 and R_{inf}) associated with wounds based on a single measurement on a day to day basis. The use of e-textile electrodes can potentially be applied for long-term monitoring, greater than 1 hour. However, research in vivo needs to be conducted due to the limitations associated with pork belly. Research to monitor the wound healing process as a continue function of time (dynamically) has yet to be conducted. The performance of the e-textile electrodes ex-vivo indicate that they are comparable to Ag/AgCl when measuring Z and R . Future research into continuous monitoring of wounds can be conducted comparing Ag/AgCl to e-textile electrodes based on these parameters. Moreover, with the development of appropriate hardware for continuous monitoring of wounds as a function of time, calibration for e-textile electrodes should be taken into consideration. The design of this hardware must increase the common mode rejection ratio (CMRR) via an AC coupling network with the appropriate filters [279]. This will reduce the noise providing a more accurate device and improving measurements for X_C , φ , R_0 and R_{inf} . Thus, it is possible to monitor the dynamic wound healing process and detect any disturbances to the process at an early stage. This will allow for any complications of the wound healing process to be detected and treated early reducing the risk of the patient suffering from severe wound complications.

Chapter 7

Conclusion and Future Work

Monitoring of the wound healing process is currently performed by medical professionals guided by the standards set by Wounds Australia. This is based on visual assessment and is prone to misdiagnosis leading to poor treatment of the wound. Bioelectrical impedance analysis (BIA) is a standard measurement that has been applied to various research fields. It is only recently that it has been adapted to measure physiological properties, such as the wound healing process. There is potential to transition this methodology for long-term monitoring of wounds. Adapting this technology provides an opportunity for patients to be monitored in remotely and in-home settings resulting in an improved quality of life. By continuously monitoring wounds, it is possible to detect a disruption in the wound healing process and treatment can be administered resulting in a reduction in complications.

Currently, research into monitoring wounds using BIA is conducted using a frequency sweep, or a discrete frequency of 50 kHz. The parameters monitored are Z , R , X_C , φ associated with the Cole-Cole model for a frequency sweep or with the discrete frequency measurements. R_0 and R_{inf} are associated with the Cole-Cole plot. Thus far, research has been conducted with the use of wet electrodes, specifically Ag/AgCl.

However, these are associated with several shortcomings. To apply wet electrodes, it is essential that the skin is prepared. Moreover, for long-term use, the adhesive layer can cause skin irritation. A significant drawback is that the gel and adhesive layer can dehydrate causing unstable measurements. Much research has focused into improving dry electrodes for use with ECG, EEG and EMG devices that operate at relatively low frequencies. The use of BIA to monitor wounds is a recent area of interest; however, research in the area of e-textile electrodes for such application is limited.

E-textile electrodes are considered a type of dry electrode; thus, they possess a polarization impedance (Z_p). The fabrication of e-textile electrodes through an embroidery process allows for on-site fabrication with a simple embroidery machine. This method of fabrication permits customisation of the embroidery variables to reduce the Z_p associated with e-textile electrodes for BIA measurements. Moreover, the broad option of substrate selection allows testing of the influence of changes in skin properties commonly associated with wounds, such as its temperature and perspiration while also maintaining a low Z_p . It is also important to take into consideration the physiological comfort of the e-textile electrodes. The studies conducted herein resulted in the understanding of suitable e-textile electrodes using

BIA in comparison with current methodologies adapted for Ag/AgCl electrodes in monitoring wounds.

Chapter 4 was based on the variables associated with the embroidery fabrication of the e-textile electrodes and their impact on Z_p at a frequency of 50 kHz. This frequency was adapted as it is the basis of BIA. This study included varying the following characteristics: (i) electrode surface area, (ii) stitch type, (iii) length and (iv) density. By varying the size of the electrodes based on the size of common clinical electrodes, the conductive surface area of the e-textile electrodes was modified. It was observed that an increase in the electrode surface area resulted in a reduction in Z_p . The largest and smallest e-textile electrodes with surface areas of 13.2 and 5.7 cm², respectively resulted in a 50% difference in Z_p . An increase in stitch spacing, indicating a higher stitch density, improved the Z_p . Thus, an increase in the amount of conductive yarn present in the e-textile electrodes reduced Z_p . By increasing the stitch length, the number of interlocks were reduced resulting in a potential decrease on the overall strain on the conductive thread. This assisted in reducing Z_p . Regarding the stitch type, it was observed that the satin stitch consumed more conductive thread than the weave stitch. However, a similar Z_p was observed thus indicating that there may potentially be a threshold relating to the amount of conductive thread utilised where Z_p is not impacted.

The second study was based on selecting a substrate that can be adapted for long-term monitoring. This selection was based on Z_p relative to a change in skin properties, specifically perspiration and relative humidity. Four commercially purchased substrates adapted to fabricate the e-textile electrodes: polyester non-woven felt and cotton in the form of plain weave, poplin and velvet. In ambient room conditions, the polyester non-woven felt resulted in the lowest Z_p . A climatic chamber was used to imitate the skin properties, with temperature settings associated to skin temperature between 30-34°C and a relative humidity (RH) range between 40-90% for perspiration. It was observed that there is no direct correlation between Z_p and changes in temperature for any of the e-textile electrodes. The influence of Z_p relative to temperature was inconsistent across the different RH settings. Moreover, for RH ranging between 40-90% inclusive the percentage change relating to a 1 °C was relatively low. The greatest change was observed for the cotton plain weave e-textile electrodes with an 8% change in Z_p observed at a change in the higher temperature ranges (i.e., 32-34 °C) for RH of 80 and 90%. Contrary, the e-textile electrode fabricated using the polyester non-woven felt was the least influenced by temperature, with a maximum change in Z_p as low as 2%. It was observed that RH significantly influenced the e-textile electrodes at a RH of 90%. At 90% RH, the e-textile electrode has sufficiently dampened the e-textile electrode and there is a significant change in Z_p across all the e-textile electrodes. Therefore, analysis of Z_p was completed for RH ranging between 40-80% using linear regression. The polyester

non-woven felt and cotton velvet e-textile samples presented the smallest change relative to RH, with a close to 'zero slope'. However, the polyester non-woven felt e-textile samples indicated a lower y intercept. Thus, indicating a negligible change due to temperature and humidity (perspiration) while maintaining a lower Z_p in comparison to the other substrates. This section also tested the air permeability of the e-textile electrodes relating to the physiological comfort. A significant reduction in air permeability was observed from the substrate to the fabricated e-textile electrodes, as this is expected. For the e-textile electrodes, the polyester non-woven felt substrate again performed the best with the largest air permeability. Therefore, this substrate was used to fabricate elliptical and rectangular electrodes to identify the influence of shape on Z_p . A 13.5 % difference in Z_p was observed where the elliptical shape reduced the Z_p .

A final study was based on comparing the e-textile electrodes to standard clinical Ag/AgCl electrodes ex-vivo adapting the methodology commonly used in monitoring wounds. This study observed the trend of common parameters used to monitor wounds over 60 minutes, specifically Z , R , X_C , φ , R_0 and R_{inf} . By washing the e-textile electrodes, they were also tested a second day. The performance of e-textile electrodes were comparable to the Ag/AgCl electrodes in terms of Z and R . The ex-vivo tests indicated that Z and R were identical on day 1 and day 2 after washing the e-textile electrodes. However, the e-textile electrodes were not comparable to the Ag/AgCl electrodes for X_C , φ , R_0 and R_{inf} . This could potentially be due to the Z_p being influenced by parasitic capacitance. By impacting X_C , it influenced φ . Moreover, this potentially affected the Cole-Cole model resulting in unreliable R_0 and R_{inf} measurements.

To further analyse e-textile electrodes, there are various studies that must be undertaken before adopting to wearable devices. An initial stage into future research would be to explore Chapter 4 further by analysing Z_p relative to the fibre and textile structure of various substrates. Textiles are known accumulate a charge that can influence the relative permittivity [280]. This relative permittivity also varies for synthetic and natural fibres [281]. Thus, future research is required into analysing the impact of selecting synthetic, natural or hybrid fibres as a substrate based on the e-textile electrodes Z_p . There is also the thickness of the textile that can potentially change its properties. For this study, silver thread was adopted and is considered a healing material. Recently, it has been shown that silk also has wound healing properties [282]; thus, by adopting silk as a substrate research can be conducted to identify the healing properties of the e-textile electrodes and any impacts it may have on the Z_p . For future research it is suggested that the textiles used as substrates are designed and fabricated maintaining consistency in terms of: (i) thickness, (ii) weight and (iii) textile structure. Thus, a comparison can be made based on the different relative permittivity of the textile. In addition, varying these variables can provide a

correlation to Z_p . Moreover, further research into the threshold observed for the amount of conductive thread used in the fabrication process is required. Research into the impact of an extended amount of shapes should also be evaluated.

Further studies to improve usability (Chapter 6) would include integrating e-textile electrodes into pressure bandages requires analysis into the impact of shear strain on the polarization impedance. Stretching conductive textiles causes a change in resistance [283]; thus, observing the change in Z_p relative to the surface area of the electrode is required. Further research into the reusability of e-textile electrodes is required. This includes various factors, such as (i) washability, (ii) hysteresis and (iii) fouling. These studies are important in improving the reliability of the e-textile electrodes and their sustainability, as these electrodes are currently 'single-use'. It is then that these e-textile electrodes will be adopted widely into a wearable device for wound monitoring. Chapter 6 presented the current issues associated with adapting e-textiles to current equipment in terms of noise. Thus, the implementation of a wearable device needs to improve the common mode rejection ratio (CMRR) to reduce the level of noise to improve accuracy [279]. To test this device, there is also a lot of research required into understanding the wound healing process.

There is much potential in the future research of long-term monitoring of wounds and a substantial amount of future work needs to be carried out *in-vivo* to gain a better understanding of the physiology of wounds relating to Z . Current research adopt BIA to measure the healing process of wounds by taking a single measurement at specific time points over a defined time period [35,38,39,45]. However, to adapt BIA for long-term monitoring continuous measurements associated with the wound healing process should be performed. This is due to the continuous changes occurring during the healing phase [83]. It is important to measure wounds over a continuous time period to detect a trend associated with the healing process; thus, Z would be relative to time during each phase. These identified trends associated to the four stages of the wound healing phase should form a baseline as a reference. This is the limitations of current research as measurements associated with the wound healing process are compared to an opposite healthy limb or healthy skin adjacent to the wound. However, several variables can cause discrepancies between the unhealthy and healthy skin measurements. For example, Z is based on the resistance and capacitance of the limb (refer to Chapter 2) and the two limbs may differ in terms of the amount of fluid present and the skin thickness which impact the equations associated to resistance and capacitance (Equations 2.3 and 2.4) implying in incomparable Z [168,284]. Therefore, work in this area needs to stem from the underlying complexity of measuring Z on living matter (*in-vivo*). Living material continuously changes. Thus, it is important to gain a better understanding of Z *in-vivo* on healthy skin and its trend relative to the functioning of a healthy body before analysing the trends associated to the wound healing process. This would provide

insight into whether there is a relaxation period associated to in-vivo measurements that can potentially influence dynamic measurements [167]. Therefore, by identifying this relaxation period it can form a basis as to Z as a function of time. Thus, determining whether it has an impact on the dynamic measurements of wounds.

Monitoring the wound healing process dynamically relative to Z also requires a study of how Z is influenced by skin temperature as this is commonly associated with Z_{es} and has yet to be extrapolated [285]. This can also influence Z and depending on the location of the wound in addition to the type of wound, this could potentially influence the trend. Therefore, temperature is an additional variable that needs to be taken into consideration. Thus, understanding Z relative to temperature and the relaxation period can assist in finding the trends of Z during the haemostasis, inflammation, proliferation and regeneration phase.

By identifying the trends associated with the wound healing stages, e-textile electrodes can be adapted for comparison. Provided that wet electrodes cannot be adapted for long-term monitoring [47], a study is required to compare the e-textile electrodes to wet electrodes on healthy skin for a short period of time. By observing their performance on healthy skin, the discrepancies between the two electrode types can be accounted for when they are used to monitor the wound healing process. This is required as the e-textile electrodes are capacitive in nature [47] and can be influenced differently relative to the various stages of the wound healing process. By gaining a deeper understanding into the physiology of wounds relative to Z and the efficacy of e-textile electrodes, a wearable BIA can be designed and developed enabling continuous long-term monitoring of the healing wounds. This permits patients to self-monitor in home settings, thus reducing the length of hospital stays, visits to emergency departments and number of hospital readmissions and improving the quality of life.

References

- [1] Drew P, Posnett J and Rusling L 2007 The cost of wound care for a local population in England *Int. Wound J.* **4** 149–55
- [2] Mcisaac C 2005 Managing wound care outcomes *Ostomy. Wound. Manage.* **51** 54–9
- [3] Hjort A and Gottrup F 2010 Cost of wound treatment to increase significantly in Denmark over the next decade *J. Wound Care* **19** 173-174,176,178,180,182,184
- [4] Fife C, Carter M, Walker D and Thomson B 2012 Wound care outcomes and associated cost among patients treated in US outpatient wound centers: Data from the US wound registry *Wounds* **24** 10–7
- [5] Sood A, Granick M S, Trial C, Lano J, Palmier S, Ribal E and Téot L 2016 The role of telemedicine in wound care: A review and analysis of a database of 5,795 patients from a mobile wound-healing center in Languedoc-Roussillon, France *Plast. Reconstr. Surg.* **138** 248S-256S
- [6] Jayachandran M, Rodriguez S, Solis E, Lei J and Godavarty A 2016 Critical review of noninvasive optical technologies for wound imaging *Adv. Wound Care* **5**
- [7] Kooner S, Sheehan B, Kendal J and Johal H 2018 Development of a simple multidisciplinary arthroplasty wound-assessment instrument: the SMART Wound Tool *Can. J. Surg.* **61** 326–31
- [8] Lucas Y and Treuillet S 2018 Optical imaging technology for wound assessment: A state of the art *Lect. Notes Comput. Vis. Biomech.* **27** 745–53
- [9] Langemo D and Spahn J 2016 A multimodality imaging and software system for combining an anatomical and physiological assessment of skin and underlying tissue conditions *Adv. Skin Wound Care* **29** 155–63
- [10] Gerger A, Hofmann-Wellenhof R, Langsenlehner U, Richtig E, Koller S, Weger W, Ahlgrimm-Siess V, Horn M, Samonigg H and Smolle J 2008 In vivo confocal laser scanning microscopy of melanocytic skin tumours: Diagnostic applicability using unselected tumour images *Br. J. Dermatol.* **158** 329–33
- [11] Flores E, Cordova M, Kose K, Phillips W, Rossi A, Nehal K and Rajadhyaksha M 2015 Intraoperative imaging during Mohs surgery with reflectance confocal microscopy: Initial clinical experience *J. Biomed. Opt.* **20** 61103
- [12] Altintas M, Altintas A, Guggenheim M, Niederbichler A, Knobloch K and Vogt P 2009 In vivo evaluation of histomorphological alterations in first-degree burn injuries by means of confocal-laser-scanning microscopy-more than “virtual histology?” *J. Burn Care Res.* **30** 315–20
- [13] Terhorst D, Maltusch A, Stockfleth E, Lange-Asschenfeldt S, Sterry W, Ulrich M

and Lange-Asschenfeldt B 2011 Reflectance confocal microscopy for the evaluation of acute epidermal wound healing *Wound Repair Regen.* **19** 671–9

- [14] Karunamuni G, Gu S, Ford M, Peterson L, Ma P, Wang Y, Rollins A, Jenkins M and Watanabe M 2014 Capturing structure and function in an embryonic heart with Biophotonic tools *Front. Physiol.* **5** 351
- [15] Banzhaf C, Wind B, Mogensen M, Meesters A, Paasch U, Wolkerstorfer A and Haedersdal M 2015 Spatiotemporal closure of fractional laser-ablated channels imaged by optical coherence tomography and reflectance confocal microscopy *Lasers Surg. Med.* **48**
- [16] Hofmann-Wellenhof R, Wurm E, Ahlgrimm-Siess V, Richtig E, Koller S, Smolle J and Gerger A 2009 Reflectance confocal microscopy-state-of-art and research overview *Semin. Cutan. Med. Surg.* **28** 172–9
- [17] Ud-Din S and Bayat A 2016 Non-invasive objective devices for monitoring the inflammatory, proliferative and remodelling phases of cutaneous wound healing and skin scarring *Exp. Dermatol.* **25**
- [18] Sattler E C E, Poloczek K, Kästle R and Welzel J 2013 Confocal laser scanning microscopy and optical coherence tomography for the evaluation of the kinetics and quantification of wound healing after fractional laser therapy *J. Am. Acad. Dermatol.* **69** e165–73
- [19] Yang Y and Wimpenny I 2016 Image analysis and quantification of tissue scaffolds *Characterisation and Design of Tissue Scaffolds* (Elsevier Inc.) pp 201–23
- [20] Cobb M J, Chen Y, Underwood R A, Usui M L, Olerud J and Li X 2006 Noninvasive assessment of cutaneous wound healing using ultrahigh-resolution optical coherence tomography *J. Biomed. Opt.* **11** 064002
- [21] Mokbul M 2017 Optical coherence tomography: Basic concepts and applications in neuroscience research *J. Med. Eng.* **2017** 1–20
- [22] Meleshina A V., Rogovaya O S, Dudenkova V V., Sirotkina M A, Lukina M M, Bystrova A S, Krut V G, Kuznetsova D S, Kalabusheva E P, Vasiliev A V., Vorotelyak E A and Zagaynova E V. 2018 Multimodal label-free imaging of living dermal equivalents including dermal papilla cells *Stem Cell Res. Ther.* **9** 84
- [23] Glinos G D, Verne S H, Aldahan A S, Liang L, Nouri K, Elliot S, Glassberg M, Cabrera DeBuc D, Koru-Sengul T, Tomic-Canic M and Pastar I 2017 Optical coherence tomography for assessment of epithelialization in a human ex vivo wound model *Wound Repair Regen.* **25** 1017–26
- [24] Israelsen N M, Maria M, Mogensen M, Bojesen S, Jensen M, Haedersdal M, Podoleanu A and Bang O 2018 The value of ultrahigh resolution OCT in dermatology - delineating the dermo-epidermal junction, capillaries in the dermal papillae and vellus hairs *Biomed. Opt. Express* **9** 2240

- [25] Lindert J and Tafazzoli-Lari K 2018 Optical coherence tomography provides an optical biopsy of burn wounds in children - A pilot study *J. Biomed. Opt.* **23** 1
- [26] Hussain A A, Themstrup L, Mogensen M and Jemec G B E 2017 Optical coherence tomography imaging of the skin *Agache's Measuring the Skin: Non-invasive Investigations, Physiology, Normal Constants: Second Edition* (Springer International Publishing) pp 493–502
- [27] Montorfano M A, Pla F, Vera L, Cardillo O, Nigra S G and Montorfano L M 2017 Point-of-care ultrasound and Doppler ultrasound evaluation of vascular injuries in penetrating and blunt trauma *Crit. Ultrasound J.* **9** 5
- [28] Gnyawali S C, Barki K G, Mathew-Steiner S S, Dixith S, Vanzant D, Kim J, Dickerson J L, Datta S, Powell H, Roy S, Bergdall V and Sen C K 2015 High-resolution harmonics ultrasound imaging for non-invasive characterization of wound healing in a pre-clinical swine model ed P McNeil *PLoS One* **10** e0122327
- [29] Mukherjee R, Tewary S and Routray A 2017 Diagnostic and prognostic utility of non-invasive multimodal imaging in chronic wound monitoring: A systematic review *J. Med. Syst.* **41** 1–17
- [30] Paul D W, Ghassemi P, Ramella-Roman J C, Prindeze N J, Moffatt L T, Alkhalil A and Shupp J W 2015 Noninvasive imaging technologies for cutaneous wound assessment: A review *Wound Repair Regen.* **23** 149–62
- [31] Radhakrishnan S, Goldsmith J, Huang D, Westphal V, Dueker D K, Rollins A M, Izatt J A and Smith S D 2005 Comparison of optical coherence tomography and ultrasound biomicroscopy for detection of narrow anterior chamber angles *Arch. Ophthalmol.* **123** 1053–9
- [32] Rajan V, Varghese B, Van Leeuwen T G and Steenbergen W 2009 Review of methodological developments in laser Doppler flowmetry *Lasers Med. Sci.* **24** 269–83
- [33] Ankhili A, Tao X, Cochrane C, Coulon D and Koncar V 2018 Washable and reliable textile electrodes embedded into underwear fabric for electrocardiography (ECG) monitoring *Materials (Basel)*. **11** 256
- [34] Prado-Olivarez J, Arellano-Olivares F, Padilla-Medina A, Diaz-Carmona J, Ramirez-Agundis A, Espinosa-Calderon A, Garcia-Mesita M and Aguilar-Diaz T 2015 Bioimpedance phase angle analysis of foot skin in diabetic patients: An experimental case study *IRBM* **36** 233–9
- [35] Kekonen A, Bergelin M, Eriksson J E, Vesa M, Johansson M and Viik J 2019 Long-term monitoring of acute wound healing from beneath the primary wound dressings *Proceedings of the Biennial Baltic Electronics Conference, BEC* vol 2018-October (IEEE Computer Society)
- [36] Kekonen A, Bergelin M, Eriksson J E, Ylanen H, Kielosto S and Viik J 2016 Bioimpedance measurement system for evaluation of the status of wound

healing *Proceedings of the Biennial Baltic Electronics Conference, BEC* vol 2016-
November (IEEE Computer Society) pp 175–8

- [37] Kekonen A, Bergelin M, Erikssen J E, Kaartinen I and Viik J 2017 Method for evaluation of surgical wound healing: A case study *IFMBE Proceedings* vol 65 (Springer Verlag) pp 446–9
- [38] Kekonen A, Bergelin M, Eriksson J-E, Vaalasti A, Ylänen H and Viik J 2017 Bioimpedance measurement based evaluation of wound healing *Physiol. Meas.* **38** 1373–83
- [39] Kekonen A, Bergelin M, Eriksson J-E, Ylänen H and Viik J 2015 A quantitative method for monitoring wound healing *Int. J. Bioelectromagn.* **17** 36–41
- [40] Kekonen A, Bergelin M, Johansson M, Kumar Joon N, Bobacka J and Viik J 2019 Bioimpedance sensor array for long-term monitoring of wound healing from beneath the primary dressings and controlled formation of H₂O₂ using low-intensity direct current *Sensors* **19** 2505
- [41] Kenworthy P, Grisbrook T, Phillips M, Gibson W, Wood F and Edgar D 2017 Addressing the barriers to bioimpedance spectroscopy use in major burns: Alternate electrode placement *J. Burn Care Res.* **38** 1
- [42] Kenworthy P, Grisbrook T L, Phillips M, Gittings P, Wood F M, Gibson W and Edgar D W 2017 Bioimpedance spectroscopy: A technique to monitor interventions for swelling in minor burns *Burns* **43** 1725–35
- [43] Kenworthy P, Phillips M, Grisbrook T L, Gibson W, Wood F M and Edgar D W 2018 Monitoring wound healing in minor burns - A novel approach *Burns* **44** 70–6
- [44] King R J, Clamp J A, Hutchinson J W and Moran C G 2007 Bioelectrical impedance: A new method for measuring post-traumatic swelling *J. Orthop. Trauma* **21** 462–8
- [45] Lukaski H C and Moore M 2012 Bioelectrical impedance assessment of wound healing *J. Diabetes Sci. Technol.* **6** 209–12
- [46] Muller M, Cristante J, Foote A, Montalibet A, Gharbi S, McAdams E and Pham P 2015 The use of multi-frequency impedimetry for the monitoring of chronic wounds: the BIPPED clinical study *Proceedings of the 5th EAI International Conference on Wireless Mobile Communication and Healthcare - "Transforming healthcare through innovations in mobile and wireless technologies"* (ICST)
- [47] Logothetis I, Fernandez-Garcia R, Troynikov O, Dabnichki P, Pirogova E and Gil I 2019 Embroidered electrodes for bioelectrical impedance analysis: impact of surface area and stitch parameters *Meas. Sci. Technol.* **30** 115103
- [48] Nescolarde L, Lukaski H, De Lorenzo A, De-Mateo-Silleras B, Redondo-Del-Río M P and Camina-Martín M A 2016 Different displacement of bioimpedance

vector due to Ag/AgCl electrode effect *Eur. J. Clin. Nutr.* **70** 1401–7

- [49] Degen T and Jäckel H 2008 Continuous monitoring of electrode - Skin impedance mismatch during bioelectric recordings *IEEE Trans. Biomed. Eng.* **55** 1711–5
- [50] Montalibet A and McAdams E 2018 A practical method to reduce electrode mismatch artefacts during 4-electrode bioImpedance spectroscopy measurements *Conf. Proc. ... Annu. Int. Conf. IEEE Eng. Med. Biol. Soc. IEEE Eng. Med. Biol. Soc. Annu. Conf.* **2018** 5775–9
- [51] Yao S and Zhu Y 2016 Nanomaterial-enabled dry electrodes for electrophysiological sensing: A review *JOM* **68** 1145–55
- [52] Hao L and Xiaoming T 2015 Evaluation methods and instruments of dry biopotential electrodes *Handbook of Smart Textiles* ed T Xiaoming (Springer) pp 775–808
- [53] Kannaian T, Neelaveni R and Thilagavathi G 2013 Design and development of embroidered textile electrodes for continuous measurement of electrocardiogram signals *J. Ind. Text.* **42** 303–18
- [54] Kaappa E S, Joutsen A, Cömert A and Vanhala J 2017 The electrical impedance measurements of dry electrode materials for the ECG measuring after repeated washing *Res. J. Text. Appar.* **21** 59–71
- [55] Chi Y M, Jung T P and Cauwenberghs G 2010 Dry-contact and noncontact biopotential electrodes: Methodological review *IEEE Rev. Biomed. Eng.* **3** 106–19
- [56] Li G, Lyu X, Wang Z, Rong Y, Hu R, Luo Z and Wang Y 2017 All-solid-state carbonate-selective electrode based on screen-printed carbon paste electrode *Meas. Sci. Technol.* **28** 025104
- [57] Kim T, Park J, Sohn J, Cho D and Jeon S 2016 Bioinspired, highly stretchable, and conductive dry adhesives based on 1D-2D hybrid carbon nanocomposites for all-in-one ECG electrodes *ACS Nano* **10** 4770–8
- [58] Liu B, Luo Z, Zhang W, Tu Q and Jin X 2016 Silver nanowire-composite electrodes for long-term electrocardiogram measurements *Sensors Actuators, A Phys.* **247** 459–64
- [59] Liu B, Luo Z, Zhang W, Tu Q and Jin X 2016 Carbon nanotube-based self-adhesive polymer electrodes for wireless long-term recording of electrocardiogram signals *J. Biomater. Sci. Polym. Ed.* **27** 1899–908
- [60] Takamatsu S, Lonjaret T, Crisp D, Badier J M, Malliaras G G and Ismailova E 2015 Direct patterning of organic conductors on knitted textiles for long-term electrocardiography *Sci. Rep.* **5** 1–7
- [61] Bihar E, Roberts T, Ismailova E, Saadaoui M, Isik M, Sanchez-Sanchez A,

Mecerreyes D, Hervé T, De Graaf J B and Malliaras G G 2017 Fully printed electrodes on stretchable textiles for long-term electrophysiology *Adv. Mater. Technol.* **2** 1600251

- [62] Jin H, Matsuhisa N, Lee S, Abbas M, Yokota T and Someya T 2017 Enhancing the performance of stretchable conductors for e-textiles by controlled ink permeation *Adv. Mater.* **29** 1605848
- [63] Karim N, Afroj S, Malandraki A, Butterworth S, Beach C, Rigout M, Novoselov K S, Casson A J and Yeates S G 2017 All inkjet-printed graphene-based conductive patterns for wearable e-textile applications *J. Mater. Chem. C* **5** 11640–8
- [64] Paul G, Torah R, Beeby S and Tudor J 2017 A printed, dry electrode Frank configuration vest for ambulatory vectorcardiographic monitoring *Smart Mater. Struct.* **26** 025029
- [65] Pani D, Dessi A, Saenz-Cogollo J F, Barabino G, Fraboni B and Bonfiglio A 2016 Fully Textile, PEDOT:PSS Based Electrodes for Wearable ECG Monitoring Systems *IEEE Trans. Biomed. Eng.* **63** 540–9
- [66] Beckmann L, Neuhaus C, Medrano G, Jungbecker N, Walter M, Gries T and Leonhardt S 2010 Characterization of textile electrodes and conductors using standardized measurement setups *Physiol. Meas.* **31** 233–47
- [67] Duc C, Malliaras G G, Senez V and Vlandas A 2018 Long-term ageing of PEDOT:PSS: wettability Study *Synth. Met.* **238** 14–21
- [68] Logothetis I, Gil I, Dabnichki P and Pirogova E Australian Biomedical Engineering Conference 2019 (ABEC 2019): Technology & Research in Australian Medical Science - E-textiles for bioelectrical impedance analysis (BIA) (Engineering Collection) - Informit
- [69] Woo E J, Hua P, Webster J, Tompkins W and Pallas-Areny R 1992 Skin impedance measurements using simple and compound electrodes *Med. Biol. Eng. Comput.* **30** 97–102
- [70] Fujita A, Wendler da Rocha R, Escobar A, Nardi A, Bagnato V and Menezes P 2018 Correlation between porcine and human skin models by optical methods
- [71] McGrath J A and Uitto J 2010 Anatomy and organization of human skin *Rook's Textbook of Dermatology* vol 1 (Oxford, UK: Wiley-Blackwell) pp 1–53
- [72] Zaidi Z and Lanigan S W 2010 Skin: Structure and function BT - Dermatology in clinical practice *Dermatology in Clinical Practice* ed S W Lanigan and Z Zaidi (Springer) pp 1–15
- [73] Honari G and Maibach H 2014 Chapter 1 - Skin structure and function *Applied Dermatotoxicology* ed G Honari and H Maibach (Academic Press) pp 1–10
- [74] Kyle U G, Bosaeus I, De Lorenzo A D, Deurenberg P, Elia M, Gómez J M,

Heitmann B L, Kent-Smith L, Melchior J C, Pirlich M, Scharfetter H, Schols A M W J and Pichard C 2004 Bioelectrical impedance analysis - Part I: Review of principles and methods *Clin. Nutr.* **23** 1226–43

- [75] Uzman A 2001 Molecular cell biology (4th edition) *Biochem. Mol. Biol. Educ. - Biochem MOL BIOL EDUC* **29** 126–8
- [76] Roddick J and Higuera V Open wound: Types, treatments, and complications
- [77] Anon Wound types | JOBST USA
- [78] Anon Wound care: A guide to practice for healthcare professionals
- [79] Velnar T, Bailey T and Smrkolj V 2009 The wound healing process: An overview of the cellular and molecular mechanisms *J. Int. Med. Res.* **37** 1528–42
- [80] Prentice W E 2014 *Principles of athletic training: a competency-based approach* (New York, NY: McGraw-Hill)
- [81] Flanagan M 2000 The physiology of wound healing *J. Wound Care* **9** 299–300
- [82] Guo S D and DiPietro L A 2010 Factors affecting wound healing *J. Dent. Res.* **89** 219–29
- [83] Harper D, Young A and McNaught C E 2014 The physiology of wound healing *Surg. (United Kingdom)* **32** 445–50
- [84] Reis e Sousa C 2017 Sensing infection and tissue damage *EMBO Mol. Med.* **9** 285–8
- [85] Watson T 2003 Soft tissue healing *In Touch* **104** 2–9
- [86] Caley M P, Martins V L C and O’Toole E A 2015 Metalloproteinases and wound healing *Adv. Wound Care* **4** 225–34
- [87] Santarlasci V, Cosmi L, Maggi L, Liotta F and Annunziato F 2013 IL-1 and T helper immune responses *Front. Immunol.* **4** 182
- [88] Ogle M E, Segar C E, Sridhar S and Botchwey E A 2016 Monocytes and macrophages in tissue repair: Implications for immunoregenerative biomaterial design *Exp. Biol. Med.* **241** 1084–97
- [89] Silva M T and Correia-Neves M 2012 Neutrophils and macrophages: the main partners of phagocyte cell systems *Front. Immunol.* **3** 174
- [90] Italiani P and Boraschi D 2014 From monocytes to M1/M2 macrophages: Phenotypical vs. functional differentiation *Front. Immunol.* **5** 514
- [91] Gonzalez A C D O, Andrade Z D A, Costa T F and Medrado A R A P 2016 Wound healing - A literature review *An. Bras. Dermatol.* **91** 614–20
- [92] Singh S, Young A and McNaught C E 2017 The physiology of wound healing *Surg. (United Kingdom)* **35** 473–7

- [93] Gurtner G C, Werner S, Barrandon Y and Longaker M T 2008 Wound repair and regeneration *Nature* **453** 314–21
- [94] Van Putte L, De Schrijver S and Moortgat P 2016 The effects of advanced glycation end products (AGEs) on dermal wound healing and scar formation: a systematic review *Scars, Burn. Heal.* **2** 205951311667682
- [95] Xue M and Jackson C J 2015 Extracellular matrix reorganization during wound healing and its impact on abnormal scarring *Adv. Wound Care* **4** 119–36
- [96] Logothetis I, Gkoutzeli D, Kagkas D, Vassiliadis S, Siores E and Pirogova E 2019 Thermoelectric heat patch for clinical and self-management: Melanoma excision wound care *Ann. Biomed. Eng.* **47** 537–48
- [97] Logothetis I, Vassiliadis S, Siores E and Pirogova E Thermoelectric heat patch for clinical and self-management of post melanoma excision wound care
- [98] Romanovsky A A 2014 Skin temperature: Its role in thermoregulation *Acta Physiol.* **210** 498–507
- [99] Bierman W 1936 The temperature of the skin surface *J. Am. Med. Assoc.* **106** 1158–62
- [100] Lavery L A, Higgins K R, Lanctot D R, Constantinides G P, Zamorano R G, Armstrong D G, Athanasiou K A and Agrawal C M 2004 Home monitoring of foot skin temperatures to prevent ulceration *Diabetes Care* **27** 2642–7
- [101] Evans S S, Repasky E A and Fisher D T 2015 Fever and the thermal regulation of immunity: The immune system feels the heat *Nat. Rev. Immunol.* **15** 335–49
- [102] Bach A, Stewart I, Disher A and Costello J 2015 A comparison between conductive and infrared devices for measuring mean skin temperature at rest, during exercise in the heat, and recovery *PLoS One* **10** e0117907
- [103] Choi J K, Miki K, Sagawa S and Shiraki K 1997 Evaluation of mean skin temperature formulas by infrared thermography *Int. J. Biometeorol.* **41** 68–75
- [104] Tyler C J 2011 The effect of skin thermistor fixation method on weighted mean skin temperature *Physiol. Meas.* **32** 1541–7
- [105] Chanmugam A, Langemo D, Thomason K, Haan J, Altenburger E A, Tippett A, Henderson L and Zortman T A 2017 Relative temperature maximum in wound infection and inflammation as compared with a control subject using long-wave infrared thermography *Adv. Skin Wound Care* **30** 406–14
- [106] Anon Standards for wound prevention and management (Third Edition) (2016)
- [107] Nagle S M, Waheed A and Wilbraham S C 2019 *Wound assessment* (McLaren Oakland: StatPearls Publishing, Treasure Island (FL))

- [108] Dowsett C 2019 T.I.M.E. To improve patient outcomes: Use of a clinical decision support tool to optimise wound care *Br. J. Community Nurs.* **24** S6–11
- [109] Olivieri B, Yates T E, Vianna S, Adenikinju O, Beasley R E and Houseworth J 2018 On the cutting edge: Wound care for the endovascular specialist *Seminars in Interventional Radiology* vol 35 (Thieme Medical Publishers, Inc.) pp 406–26
- [110] Joyce P, Moore Z E and Christie J 2018 Organisation of health services for preventing and treating pressure ulcers *Cochrane Database Syst. Rev.* **2018**
- [111] Grey J E, Enoch S and Harding K G 2006 Wound assessment *Br. Med. J.* **332** 285–8
- [112] Benbow M 2016 Best practice in wound assessment *Nurs. Stand.* **30** 40–7
- [113] Oliverio J, Gero E, Whitacre K L and Rankin J 2016 Wound care algorithm *Adv. Skin Wound Care* **29** 65–72
- [114] Demidova-Rice T N, Hamblin M R and Herman I M 2012 Acute and impaired wound healing *Adv. Skin Wound Care* **25** 304–14
- [115] Wynn M and Freeman S 2019 The efficacy of negative pressure wound therapy for diabetic foot ulcers: A systematised review *J. Tissue Viability* **28** 152–60
- [116] Chang M, Yu T, Luo J, Duan K, Tu P, Zhao Y, Nagraj N, Rajiv V, Priebe M, Wood E A and Stachura M 2018 Multimodal sensor system for pressure ulcer wound assessment and care *IEEE Trans. Ind. Informatics* **14** 1186–96
- [117] Yee A, Harmon J and Yi S 2016 Quantitative monitoring wound healing status through three-dimensional imaging on mobile platforms *J. Am. Coll. Clin. Wound Spec.* **8** 21–7
- [118] Siddiqui A R and Bernstein J M 2010 Chronic wound infection: Facts and controversies *Clin. Dermatol.* **28** 519–26
- [119] Heyer K, Herberger K, Protz K, Glaeske G and Augustin M 2016 Epidemiology of chronic wounds in Germany: Analysis of statutory health insurance data *Wound Repair Regen.* **24** 434–42
- [120] Eming S A, Wynn T A and Martin P 2017 Inflammation and metabolism in tissue repair and regeneration *Science (80-.).* **356** 1026–30
- [121] Whitlock E, Morcom J, Spurling G, Janamian T and Ryan S 2014 Wound care costs in general practice: A cross-sectional study *Aust. Fam. Physician* **43** 143–6
- [122] St. Croix C M, Shand S H and Watkins S C 2005 Confocal microscopy: comparisons, applications, and problems *Biotechniques* **39** S2–5
- [123] Jonkman J and Brown C M 2015 Any way you slice it—A comparison of confocal microscopy techniques *J. Biomol. Tech.* **26** 54–65

- [124] Oglat A, Matjafri M, Suardi N, Abdelrahman M, Oqlat M and Oqlat A 2018 A new scatter particle and mixture fluid for preparing blood mimicking fluid for wall-less flow phantom *J. Med. Ultrasound* **26** 134
- [125] Kelechi T J and Michel Y 2007 A descriptive study of skin temperature, tissue perfusion, and tissue oxygen in patients with chronic venous disease *Biol. Res. Nurs.* **9** 70–80
- [126] Iabichella M L, Melillo E and Mosti G 2006 A review of microvascular measurements in wound healing *Int. J. Low. Extrem. Wounds* **5** 181–99
- [127] Hoeksema H, Van de Sijpe K, Tondou T, Hamdi M, Van Landuyt K, Blondeel P and Monstrey S 2009 Accuracy of early burn depth assessment by laser Doppler imaging on different days post burn *Burns* **35** 36–45
- [128] Kairinos N, McKune A, Solomons M, Hudson D A and Kahn D 2014 The flaws of laser Doppler in negative-pressure wound therapy research *Wound Repair Regen.* **22** 424–9
- [129] Martínez-Jiménez M A, Ramirez-García Luna J L, Kolosovas-Machuca E S, Drager J and González F J 2018 Development and validation of an algorithm to predict the treatment modality of burn wounds using thermographic scans: Prospective cohort study ed D M Burmeister *PLoS One* **13** e0206477
- [130] Jaspers M E H, Maltha I, Klaessens J H G M, de Vet H C W, Verdaasdonk R M and van Zuijlen P P M 2016 Insights into the use of thermography to assess burn wound healing potential: a reliable and valid technique when compared to laser Doppler imaging. *J. Biomed. Opt.* **21** 96006
- [131] Prindeze N J, Fathi P, Mino M J, Mauskar N A, Travis T E, Paul D W, Moffatt L T and Shupp J W 2015 Examination of the early diagnostic applicability of active dynamic thermography for burn wound depth assessment and concept analysis *J. Burn Care Res.* **36** 626–35
- [132] Etehadtavakol M and Ng E Y K 2017 Assessment of foot complications in diabetic patients using thermography: A review (Springer, Singapore) pp 33–43
- [133] Oe M, Takehara K, Noguchi H, Ohashi Y, Amemiya A, Sakoda H, Suzuki R, Yamauchi T, Ueki K, Kadowaki T and Sanada H 2017 Thermographic findings in a case of type 2 diabetes with foot ulcer due to callus deterioration *Diabetol. Int.* **8** 328–33
- [134] Khalil S, Mohktar M and Ibrahim F 2014 The theory and fundamentals of bioimpedance analysis in clinical status monitoring and diagnosis of diseases *Sensors* **14** 10895–928
- [135] Grimnes S and Martinsen Ø G 2015 Introduction *Bioimpedance and Bioelectricity Basics* (Elsevier) pp 1–7
- [136] Hui T and Petrofsky J 2013 Injury and inflammation detection by the

application of microcurrent through the skin *Phys. Ther. Rehabil. Sci.* **2**

- [137] Nescolarde L, Yanguas J, Lukaski H, Alomar X, Rosell X and Rodas G 2013 Localized bioimpedance to assess muscle injury *Physiol. Meas.* **34** 237–45
- [138] Nescolarde L, Yanguas J, Lukaski H, Alomar X, Rosell-Ferrer J and Rodas G 2014 Effects of muscle injury severity on localized bioimpedance measurements *Physiol. Meas.* **36** 27–42
- [139] Nescolarde L, Yanguas J, Terricabras J, Lukaski H, Alomar X, Rosell X and Rodas G 2017 Detection of muscle gap by L-BIA in muscle injuries: Clinical prognosis *Physiol. Meas.* **38** L1–9
- [140] Vosika Z B, Lazovic G M, Misevic G N and Simic-Krstic J B 2013 Fractional calculus model of electrical impedance applied to human skin *PLoS One* **8** 59483
- [141] Fricke H and Morse S 1925 The electric resistance and capacity of blood for frequencies between 800 and 41/2 million cycles *J. Gen. Physiol.* **9** 153–67
- [142] Salahuddin S, Porter E, Meaney P M and O'Halloran M 2017 Effect of logarithmic and linear frequency scales on parametric modelling of tissue dielectric data *Biomed. Phys. Eng. Express* **3** 15020
- [143] Holder D 2005 Electrical impedance tomography: Methods, history and applications *Medical Physics - MED PHYS* vol 32
- [144] Schwan H P 1968 Electrode polarization impedance and measurements in biological materials *Ann. N. Y. Acad. Sci.* **148** 191–209
- [145] Ibrahim B, Hall D A and Jafari R 2018 Bio-impedance spectroscopy (BIS) measurement system for wearable devices *2017 IEEE Biomedical Circuits and Systems Conference, BioCAS 2017 - Proceedings* vol 2018-January (Institute of Electrical and Electronics Engineers Inc.) pp 1–4
- [146] Bera T K, Jampana N and Lubineau G 2016 A LabVIEW-based electrical bioimpedance spectroscopic data interpreter (LEBISDI) for biological tissue impedance analysis and equivalent circuit modelling *J. Electr. Bioimpedance* **7** 35–54
- [147] Kim S B, Lee N R, Shin T M and Lee Y H 2014 Development and evaluation of a multi-frequency bioelectrical impedance analysis analyzer for estimating acupoint composition *JAMS J. Acupunct. Meridian Stud.* **7** 33–43
- [148] Gimsa J and Wachner D 1998 A unified resistor-capacitor model for impedance, dielectrophoresis, electrorotation, and induced transmembrane potential *Biophys. J.* **75** 1107–16
- [149] Trung D T, Kien N P, Hung T D, Hieu D C and Vu T A 2016 Electrical impedance measurement for assessment of the pork aging: A preliminary study *BME-HUST 2016 - 3rd International Conference on Biomedical Engineering* (Institute

of Electrical and Electronics Engineers Inc.) pp 95–9

- [150] Amin N, Rayhan S, Anik A A and Jameel R 2017 Modelling and characterization of cell abnormality using electrical impedance spectroscopy (EIS) system for the preliminary analysis to predict breast cancer *Proceedings - 2016 2nd IEEE International Conference on Research in Computational Intelligence and Communication Networks, ICRCICN 2016* (Institute of Electrical and Electronics Engineers Inc.) pp 147–52
- [151] Kapoor R 2015 Electrical bioimpedance: Methods and applications **3** 702–7
- [152] Jalalzadeh M and Hajjesmaeili M 2016 Bio-electrical impedance analysis in patients with critical illnesses *Nephrourol. Mon.* **Inpress**
- [153] Simic M, Babic Z, Risojević V, Stojanovic G and Ramos A 2015 A system for rapid and automated bioimpedance measurement
- [154] Mylott E, Kutschera E and Widenhorn R 2014 Bioelectrical impedance analysis as a laboratory activity: At the interface of physics and the body *Am. J. Phys.* **82**
- [155] Stahn A, Terblanche E and Gunga H-C 2012 Use of bioelectrical impedance: General principles and overview *Handbook of Anthropometry: Physical Measures of Human Form in Health and Disease* pp 49–90
- [156] Macdonald J R and Johnson W B 2005 Fundamentals of impedance spectroscopy *Impedance Spectroscopy* (Wiley) pp 1–26
- [157] Trainito C I, François O and Le Pioufle B 2015 Analysis of pulsed electric field effects on cellular tissue with Cole-Cole model: Monitoring permeabilization under inhomogeneous electrical field with bioimpedance parameter variations *Innov. Food Sci. Emerg. Technol.* **29** 193–200
- [158] Freeborn T, Crenshaw T and Critcher S 2017 Hook artifact correction of localized electrical bioimpedance for improved agreement between different device measurements *Biomed. Phys. Eng. Express* **4**
- [159] Freeborn T J 2018 Bioimpedance analysis using fractional-order equivalent electrical circuits *Fractional Order Systems* (Elsevier) pp 205–37
- [160] Sankar V, Patrick E, Dieme R, Sanchez J C, Prasad A and Nishida T 2014 Electrode impedance analysis of chronic tungsten microwire neural implants: Understanding abiotic vs. biotic contributions *Front. Neuroeng.* **7** 13
- [161] Lafargue A, Cabrales L and Larramendi R 2002 Bioelectrical Parameters of the Whole Human Body Obtained Through Bioelectrical Impedance Analysis *Bioelectromagnetics* **23** 450–4
- [162] Hernandez-Jaimes C, Vazquez-Arenas J, Vernon-Carter J and Alvarez-Ramirez J 2015 A nonlinear Cole–Cole model for large-amplitude electrochemical impedance spectroscopy *Chem. Eng. Sci.* **137** 1–8

- [163] Bartels E M, Sørensen E R and Harrison A P 2015 Multi-frequency bioimpedance in human muscle assessment *Physiol. Rep.* **3** e12354
- [164] Freeborn T J, Milligan A and Esco M R 2018 Evaluation of ImpediMed SFB7 BIS device for low-impedance measurements *Meas. J. Int. Meas. Confed.* **129** 20–30
- [165] Harrison A P, Elbrønd V S, Riis-Olesen K and Bartels E M 2015 Multi-frequency bioimpedance in equine muscle assessment *Physiol. Meas.* **36** 453–64
- [166] Cumming K, Hoyle G E, Hutchison J D and Soiza R L 2014 Bioelectrical impedance analysis is more accurate than clinical examination in determining the volaemic status of elderly patients with fragility fracture and hyponatraemia *J. Nutr. Heal. Aging* **18** 744–50
- [167] Dean D A, Ramanathan T, Machado D and Sundararajan R 2008 Electrical impedance spectroscopy study of biological tissues *J. Electrostat.* **66** 165–77
- [168] Kyle U G, Bosaeus I, De Lorenzo A D, Deurenberg P, Elia M, Gómez J M, Heitmann B L, Kent-Smith L, Melchior J C, Pirlich M, Scharfetter H, Schols A M W J and Pichard C 2004 Bioelectrical impedance analysis - Part II: Utilization in clinical practice *Clin. Nutr.* **23** 1430–53
- [169] Baghbani R, Moradi M H and Shadmehr M B 2018 The development of a four-electrode bio-impedance sensor for identification and localization of deep pulmonary nodules *Ann. Biomed. Eng.* **46** 1079–90
- [170] Swisher S L, Lin M C, Liao A, Leeflang E J, Khan Y, Pavinatto F J, Mann K, Naujokas A, Young D, Roy S, Harrison M R, Arias A C, Subramanian V and Maharbiz M M 2015 Impedance sensing device enables early detection of pressure ulcers in vivo *Nat. Commun.* **6** 1–10
- [171] Conchell J C 2014 *Bio-Impedance circuit design for body worn systems website: www.analog.com/medical Bio-impedance circuit design for body worn systems*
- [172] Noveletto F, Bertemes-Filho P and Dutra D 2016 Analog front-end for the integrated circuit ad5933 used in electrical bioimpedance measurements *IFMBE Proceedings* vol 54 (Springer Verlag) pp 48–51
- [173] Delano M and Sodini C 2018 Evaluating calf bioimpedance measurements for fluid overload management in a controlled environment *Physiol. Meas.* **39** 125009
- [174] Bogónez-Franco P, Nescolarde L, Bragós R, Rosell X and Yandiola I 2009 Measurement errors in multifrequency bioelectrical impedance analyzers with and without impedance electrode mismatch *Physiol. Meas.* **30** 573–87
- [175] Bogónez-Franco P, Pham P, Gehin C, Massot B, Delhomme G, Guillemaud R and McAdams E 2014 *Effect of electrode contact impedance mismatch on 4-electrode measurements of small body segments using commercial BIA devices*

- [176] Smirnov V, Nikolaev V and Rudnev S 2010 Bioelectric impedance analysis *Handbook of Physics in Medicine and Biology* ed R Splinter (CRC press) pp 25.1-25.13
- [177] Grimnes S, Martinsen Ø G, Grimnes S and Martinsen Ø G 2015 Chapter 7 – Electrodes *Bioimpedance and Bioelectricity Basics* (Academic Press) pp 179–254
- [178] Albulbul A 2016 Evaluating major electrode types for idle biological signal measurements for modern medical technology *Bioengineering* **3** 20
- [179] Shinwari M W, Zhitomirsky D, Deen I A, Selvaganapathy P R, Deen M J and Landheer D 2010 Microfabricated reference electrodes and their biosensing applications *Sensors* **10** 1679–715
- [180] McAdams E, Jossinet J, Lacknermeier A and Risacher F 1996 Factors affecting electrode-gel-skin interface impedance in electrical impedance tomography *Med. Biol. Eng. Comput.* **34** 397–408
- [181] Brantlov S, Ward L C, Jødal L, Rittig S and Lange A 2017 Critical factors and their impact on bioelectrical impedance analysis in children: a review *J. Med. Eng. Technol.* **41** 22–35
- [182] Yao S, Myers A, Malhotra A, Lin F, Bozkurt A, Muth J F and Zhu Y 2017 A wearable hydration sensor with conformal nanowire electrodes *Adv. Healthc. Mater.* **6** 1601159
- [183] Kalvøy H 2011 New method for separation of electrode polarization impedance from measured tissue impedance *Open Biomed. Eng. J.* **5** 8–13
- [184] Taji B, Chan A D C and Shirmohammadi S 2018 Effect of pressure on skin-electrode impedance in wearable biomedical measurement devices *IEEE Trans. Instrum. Meas.* **67** 1900–12
- [185] Dodde R E, Kruger G H and Shih A J 2015 Design of bioimpedance spectroscopy instrument with compensation techniques for soft tissue characterization *J. Med. Devices, Trans. ASME* **9** 1–8
- [186] Wiese S R, Anheier P, Connemara R D, Mollner A T, Neils T F, Kahn J A and Webster J G 2005 Electrocardiographic motion artifact versus electrode impedance *IEEE Trans. Biomed. Eng.* **52** 136–9
- [187] Hamilton P S, Curley M G, Aimi R M and Sae-Hau C 2000 Comparison of methods for adaptive removal of motion artifact *Computers in Cardiology* (IEEE) pp 383–6
- [188] Tong D A, Bartels K A and Honeyager K S 2002 Adaptive reduction of motion artifact in the electrocardiogram *Annual International Conference of the IEEE Engineering in Medicine and Biology - Proceedings* vol 2 pp 1403–4
- [189] Searle A and Kirkup L 2000 A direct comparison of wet, dry and insulating

bioelectric recording electrodes *Physiol. Meas.* **21** 271–83

- [190] Adli and Yamamoto Y 1998 Impedance balancing analysis for power-line interference elimination in ECG signal *Conference Record - IEEE Instrumentation and Measurement Technology Conference* vol 1 (IEEE) pp 235–8
- [191] Lee J W and Yun K S 2017 ECG monitoring garment using conductive carbon paste for reduced motion artifacts *Polymers (Basel)*. **9** 439
- [192] Lee S M, Byeon H J, Lee J H, Baek D H, Lee K H, Hong J S and Lee S H 2014 Self-adhesive epidermal carbon nanotube electronics for tether-free long-term continuous recording of biosignals *Sci. Rep.* **4** 1–9
- [193] Kabiri Ameri S, Ho R, Jang H, Tao L, Wang Y, Wang L, Schnyer D M, Akinwande D and Lu N 2017 Graphene electronic tattoo sensors *ACS Nano* **11** 7634–41
- [194] Bareket L, Inzelberg L, Rand D, David-Pur M, Rabinovich D, Brandes B and Hanein Y 2016 Temporary-tattoo for long-term high fidelity biopotential recordings *Sci. Rep.* **6** 25727
- [195] Imani S, Bandodkar A J, Mohan A M V, Kumar R, Yu S, Wang J and Mercier P P 2016 A wearable chemical-electrophysiological hybrid biosensing system for real-time health and fitness monitoring *Nat. Commun.* **7** 1–7
- [196] Peng H L, Liu J Q, Dong Y Z, Yang B, Chen X and Yang C S 2016 Parylene-based flexible dry electrode for biopotential recording *Sensors Actuators, B Chem.* **231** 1–11
- [197] Khan Y, Pavinatto F J, Lin M C, Liao A, Swisher S L, Mann K, Subramanian V, Maharbiz M M and Arias A C 2016 Inkjet-printed flexible gold electrode arrays for bioelectronic interfaces *Adv. Funct. Mater.* **26** 1004–13
- [198] Zhao Y, Cao Y, Liu J, Zhan Z, Li X and Li W 2018 Single-wall carbon nanotube-coated cotton yarn for electrocardiography transmission *Micromachines* **9** 132
- [199] Yapici M K and Alkhidir T E 2017 Intelligent medical garments with graphene-functionalized smart-cloth ECG sensors *Sensors (Switzerland)* **17**
- [200] Carey T, Cacovich S, Divitini G, Ren J, Mansouri A, Kim J M, Wang C, Ducati C, Sordan R and Torrisi F 2017 Fully inkjet-printed two-dimensional material field-effect heterojunctions for wearable and textile electronics *Nat. Commun.* **8** 1–11
- [201] Sinha S K, Noh Y, Reljin N, Treich G M, Hajeb-Mohammadalipour S, Guo Y, Chon K H and Sotzing G A 2017 Screen-printed PEDOT:PSS electrodes on commercial finished textiles for electrocardiography *ACS Appl. Mater. Interfaces* **9** 37524–8
- [202] Shafti A, Manero R B R, Borg A M, Althoefer K and Howard M J 2016 Designing embroidered electrodes for wearable surface electromyography *Proceedings -*

IEEE International Conference on Robotics and Automation vol 2016-June (Institute of Electrical and Electronics Engineers Inc.) pp 172–7

- [203] Weder M, Hegemann D, Amberg M, Hess M, Boesel L, Abächerli R, Meyer V and Rossi R 2015 Embroidered electrode with silver/titanium coating for long-term ECG monitoring *Sensors* **15** 1750–9
- [204] Goncu Berk G 2018 Design of a wearable pain management system with embroidered TENS electrodes *Int. J. Cloth. Sci. Technol.* **30** 38–48
- [205] Trindade I, Machado da Silva J, Miguel R, Pereira M, Lucas J, Oliveira L, Valentim B, Barreto J and Santos Silva M 2016 Design and evaluation of novel textile wearable systems for the surveillance of vital signals *Sensors* **16** 1573
- [206] Cho G, Jeong K, Paik M J, Kwun Y and Sung M 2011 Performance evaluation of textile-based electrodes and motion sensors for smart clothing *IEEE Sens. J.* **11** 3183–93
- [207] Prabhu S and Poulouse E K 2012 Silver nanoparticles: mechanism of antimicrobial action, synthesis, medical applications, and toxicity effects *Int. Nano Lett.* **2** 1–10
- [208] Gil I, Fernández-García R and Tornero J A 2019 Embroidery manufacturing techniques for textile dipole antenna applied to wireless body area network *Text. Res. J.* **89** 1573–81
- [209] DICK I P and SCOTT R C 1992 Pig ear skin as an in-vitro model for human skin permeability *J. Pharm. Pharmacol.* **44** 640–5
- [210] Jacobi U, Kaiser M, Toll R, Mangelsdorf S, Audring H, Otberg N, Sterry W and Lademann J 2007 Porcine ear skin: An in vitro model for human skin *Ski. Res. Technol.* **13** 19–24
- [211] Cömert A, Honkala M and Hyttinen J 2013 Effect of pressure and padding on motion artifact of textile electrodes *Biomed. Eng. Online* **12** 26
- [212] Deeken C R and Lake S P 2017 Mechanical properties of the abdominal wall and biomaterials utilized for hernia repair *J. Mech. Behav. Biomed. Mater.* **74** 411–27
- [213] Bai X, Hou J, Wang L, Wang M, Wang X, Wu C, Yu L, Yang J, Leng Y and Sun Y 2018 Electrical impedance analysis of pork tissues during storage *J. Food Meas. Charact.* **12** 164–72
- [214] Vallejo M, Recas J, del Valle P and Ayala J 2013 Accurate human tissue characterization for energy-efficient wireless on-body communications *Sensors* **13** 7546–69
- [215] Yu M, Guo F, Ling Y, Li N and Tan F 2015 Topical skin targeting effect of penetration modifiers on hairless mouse skin, pig abdominal skin and pig ear skin *Drug Deliv.* **22** 1053–8

- [216] Yamamoto T and Yamamoto Y 1976 Electrical properties of the epidermal stratum corneum *Med. Biol. Eng.* **14** 151–8
- [217] McAdams E 2011 Biomedical electrodes for biopotential monitoring and electrostimulation (Springer, Boston, MA) pp 31–124
- [218] Castizo-Olier J, Irurtia A, Jemni M, Carrasco-Marginet M, Fernández-García R and Rodríguez F A 2018 Bioelectrical impedance vector analysis (BIVA) in sport and exercise: Systematic review and future perspectives ed A Nordez *PLoS One* **13** e0197957
- [219] Kalra A, Lowe A and Al-Jumaily A 2018 Critical review of electrocardiography measurement systems and technology *Meas. Sci. Technol.* **30** 12001
- [220] Estep J R and Christensen J C 2015 Electrode replacement does not affect classification accuracy in dual-session use of a passive brain-computer interface for assessing cognitive workload *Front. Neurosci.* **9** 54
- [221] Liu J, Ying D and Rymer W Z 2015 EMG burst presence probability: A joint time-frequency representation of muscle activity and its application to onset detection *J. Biomech.* **48** 1193–7
- [222] Resende L, Merriwether E, Rampazo É P, Dailey D, Embree J, Deberg J, Liebano R E and Sluka K A 2018 Meta-analysis of transcutaneous electrical nerve stimulation for relief of spinal pain *Eur. J. Pain* **22** 663–78
- [223] Ita K 2016 Transdermal iontophoretic drug delivery: Advances and challenges *J. Drug Target.* **24** 386–91
- [224] Schnitker J, Adly N, Seyock S, Bachmann B, Yakushenko A, Wolfrum B and Offenhäusser A 2018 Rapid prototyping of ultralow-cost, inkjet-printed carbon microelectrodes for flexible bioelectronic devices *Adv. Biosyst.* **2** 1700136
- [225] Trindade I, Spranger P, Martins F, Miguel R and Silva M 2014 Fully integrated embroidery process for smart textiles *Tech. Proc. 2014 NSTI Nanotechnol. Conf. Expo, NSTI-Nanotech 2014* **3** 65–8
- [226] Guo X, Huang Y, Cai X, Liu C and Liu P 2016 Capacitive wearable tactile sensor based on smart textile substrate with carbon black /silicone rubber composite dielectric *Meas. Sci. Technol.* **27** 45105
- [227] Moradi B, Fernández-García R and Gil I 2020 Wearable high-performance meander ring dipole antenna for electronic-textile applications *J. Text. Inst.* **111** 178–82
- [228] Boateng J S, Matthews K H, Stevens H N E and Eccleston G M 2008 Wound healing dressings and drug delivery systems: A review *J. Pharm. Sci.* **97** 2892–923
- [229] Grip J, Engstad R E, Skjæveland I, Škalko-Basnet N and Holsæter A M 2017 Sprayable carbopol hydrogel with soluble beta-1,3/1,6-glucan as an active

ingredient for wound healing – Development and in-vivo evaluation *Eur. J. Pharm. Sci.* **107** 24–31

- [230] Piwek L, Ellis D A, Andrews S and Joinson A 2016 The rise of consumer health wearables: Promises and barriers *PLOS Med.* **13** e1001953
- [231] Yapici M K, Alkhidir T, Samad Y A and Liao K 2015 Graphene-clad textile electrodes for electrocardiogram monitoring *Sensors Actuators, B Chem.* **221** 1469–74
- [232] Li G, Wang S and Duan Y Y 2018 Towards conductive-gel-free electrodes: Understanding the wet electrode, semi-dry electrode and dry electrode-skin interface impedance using electrochemical impedance spectroscopy fitting *Sensors Actuators, B Chem.* **277** 250–60
- [233] Li G, Wang S and Duan Y Y 2017 Towards gel-free electrodes: A systematic study of electrode-skin impedance *Sensors Actuators, B Chem.* **241** 1244–55
- [234] Takeshita T, Yoshida M, Takei Y, Ouchi A, Hinoki A, Uchida H and Kobayashi T 2019 Relationship between contact pressure and motion artifacts in ECG measurement with electrostatic flocked electrodes fabricated on textile *Sci. Rep.* **9** 1–10
- [235] Cömert A and Hyttinen J 2015 Investigating the possible effect of electrode support structure on motion artifact in wearable bioelectric signal monitoring *Biomed. Eng. Online* **14** 44
- [236] Mole R H 1948 The relative humidity of the skin *J. Physiol.* **107** 399–411
- [237] Gidik H, Bedek G and Dupont D 2016 Developing thermophysical sensors with textile auxiliary wall *Smart Textiles and Their Applications* (Elsevier Inc.) pp 423–53
- [238] Logothetis I, Vatansever Bayramol D, Gil I, Dabnichki P and Pirogova E 2020 Evaluating silver-plated nylon (Ag/PA66) e-textiles for bioelectrical impedance analysis (BIA) application *Meas. Sci. Technol.* **31** 75101
- [239] Murphy E J and Walker A C 1928 Electrical conduction in textiles. I: The dependence of the resistivity* of cotton, silk and wool on relative humidity and moisture content *J. Phys. Chem.* **32** 1761–86
- [240] Shahzad A, Rasheed A, Khaliq Z, Qadir M B, Khan M Q, Hamdani S T A, Ali Z, Afzal A, Irfan M, Shafiq M and Kim I S 2019 Processing of metallic fiber hybrid spun yarns for better electrical conductivity *Mater. Manuf. Process.* **34** 1008–15
- [241] Mchugh M J 2016 Wound metrology: Strategies for achieving accuracy in wound measurement *Wounds UK* **12** 20–5
- [242] Prakash S, Karnes M P, Sequin E K, West J D, Hitchcock C L, Nichols S D, Bloomston M, Abdel-Misih S R, Schmidt C R, Martin E W, Pivoski S P and

Subramaniam V V 2015 Ex vivo electrical impedance measurements on excised hepatic tissue from human patients with metastatic colorectal cancer *Physiol. Meas.* **36** 315–28

- [243] Adler A and Boyle A 2017 Electrical impedance tomography: Tissue properties to image measures *IEEE Trans. Biomed. Eng.* **64** 2494–504
- [244] Dowrick T, Blochet C and Holder D 2015 In vivo bioimpedance measurement of healthy and ischaemic rat brain: implications for stroke imaging using electrical impedance tomography *Physiol. Meas.* **36** 1273–82
- [245] Moncada M E and de la Cruz J 2011 La actividad electrodérmica -Revisión *Ing. e Investig.* **31** 143–51
- [246] Mialich M S, Maria J, Sicchieri F, Afonso A and Junior J 2014 Analysis of body composition : A critical review of the use of bioelectrical impedance analysis *Int. J. Clin. Nutr.* 2014, Vol. 2, No. 1, 1-10 **2** 1–10
- [247] Lee J, Kim D, Ryoo H-Y and Shin B-S 2016 Sustainable wearables: Wearable technology for enhancing the quality of human life *Sustainability* **8** 466
- [248] Cheung M L, Chau K Y, Lam M H S, Tse G, Ho K Y, Flint S W, Broom D R, Tso E K H and Lee K Y 2019 Examining consumers' adoption of wearable healthcare technology: The role of health attributes *Int. J. Environ. Res. Public Health* **16** 2257
- [249] Logothetis I, Matsouka D, Vassiliadis S, Vossou C and Siores E 2018 Optimum operating conditions for PZT actuators for vibrotactile wearables *J. Electron. Mater.* **47** 3709–16
- [250] Huigen E, Peper A and Grimbergen C A 2002 Investigation into the origin of the noise of surface electrodes *Med. Biol. Eng. Comput* **40** 332–8
- [251] Spach M S, Barr R C, Havstad J W and Long E C 1966 Skin-electrode impedance and its effect on recording cardiac potentials *Circulation* **34** 649–56
- [252] Berson A S and Pipberger H V. 1968 Skin-electrode impedance problems in electrocardiography *Am. Heart J.* **76** 514–25
- [253] Rosell J, Colominas J, Riu P, Pallas-Areny R and Webster J G 1988 Skin Impedance from 1 Hz to 1 MHz *IEEE Trans. Biomed. Eng.* **35** 649–52
- [254] Löfhede J, Seoane F and Thordstein M 2012 Textile electrodes for EEG recording — A pilot study *Sensors* **12** 16907–19
- [255] An X and Stylios G 2018 A hybrid textile electrode for electrocardiogram (ECG) measurement and motion tracking *Materials (Basel)*. **11** 1887
- [256] Pola T and Vanhala J 2007 Textile electrodes in ECG measurement *Proceedings of the 2007 International Conference on Intelligent Sensors, Sensor Networks and Information Processing, ISSNIP* pp 635–9

- [257] Tsukada Y T, Tokita M, Murata H, Hirasawa Y, Yodogawa K, Iwasaki Y ki, Asai K, Shimizu W, Kasai N, Nakashima H and Tsukada S 2019 Validation of wearable textile electrodes for ECG monitoring *Heart Vessels* **34** 1203–11
- [258] Soroudi A, Hernández N, Wipenmyr J and Nierstrasz V 2019 Surface modification of textile electrodes to improve electrocardiography signals in wearable smart garment *J. Mater. Sci. Mater. Electron.* **30** 16666–75
- [259] Castrillón R, Pérez J J and Andrade-Caicedo H 2018 Electrical performance of PEDOT: PSS-based textile electrodes for wearable ECG monitoring: A comparative study *Biomed. Eng. Online* **17** 38
- [260] Lee S, Kim M O, Kang T, Park J and Choi Y 2018 Knit band sensor for myoelectric control of surface EMG-based prosthetic hand *IEEE Sens. J.* **18** 8578–86
- [261] Landén N X, Li D and Ståhle M 2016 Transition from inflammation to proliferation: a critical step during wound healing *Cell. Mol. Life Sci.* **73** 3861–85
- [262] Gonzalez-Correa C A, Rivera-Garzón R A and Martínez-Táutiva S 2019 Electric impedance and the healing of diabetic foot ulcers *J. Phys. Conf. Ser.* **1272** 12009
- [263] Khodasevych I, Parmar S and Troynikov O 2017 Flexible sensors for pressure therapy: Effect of substrate curvature and stiffness on sensor performance *Sensors* **17** 2399
- [264] Lee S and Kruse J 2008 Biopotential electrode sensors in ECG/EEG/EMG systems *Analog Devices*
- [265] Kobelev A V., Shchukin S I and Leonhardt S 2019 Application of tetrapolar electrode systems in electrical impedance measurements *Biomed. Eng. (NY)*. **52** 383–6
- [266] Areny R P 2018 *Tetrapolar bioimpedance measurements compared to four-wire resistance measurements* vol 9
- [267] Kusche R, Kaufmann S and Ryschka M 2019 Dry electrodes for bioimpedance measurements - Design, characterization and comparison *IOP Biomed. Phys. Eng. Express* **5**
- [268] Bîrlea N M, Bîrlea S I and Toşa V 2009 The skin's electrical asymmetry *J. Phys. Conf. Ser. OPEN ACCESS* **182** 12020
- [269] Shin S C, Lee S, Lee T, Lee K, Lee Y S and Kang H G 2018 Two electrode based healthcare device for continuously monitoring ECG and BIA signals *2018 IEEE EMBS International Conference on Biomedical and Health Informatics, BHI 2018* vol 2018-January (Institute of Electrical and Electronics Engineers Inc.) pp 141–4
- [270] Geddes L A and Valentinuzzi M E 1973 Temporal changes in electrode

impedance while recording the electrocardiogram with “Dry” electrodes *Ann. Biomed. Eng.* **1** 356–67

- [271] Yokus M A and Jur J S 2016 Fabric-based wearable dry electrodes for body surface biopotential recording *IEEE Trans. Biomed. Eng.* **63** 423–30
- [272] Lu F, Wang C, Zhao R, Du L, Fang Z, Guo X and Zhao Z 2018 Review of stratum corneum impedance measurement in non-invasive penetration application *Biosensors* **8** 31
- [273] Cömert A and Hyttinen J 2014 Impedance spectroscopy of changes in skin-electrode impedance induced by motion *Biomed. Eng. Online* **13** 149
- [274] Ravariu C 2011 Contributions to novel methods in electrophysiology aided by electronics devices and circuits pp 123–40
- [275] Tomasini M, Benatti S, Milosevic B, Farella E and Benini L 2016 Power line interference removal for high-quality continuous biosignal monitoring with low-power wearable devices *IEEE Sens. J.* **16** 3887–95
- [276] Spinelli E and Haberman M 2010 Insulating electrodes: A review on biopotential front ends for dielectric skin–electrode interfaces *Physiol. Meas.* **31** S183–98
- [277] Ninagawa T 2012 Measurement of microclimate within clothing using the combination technique of infrared ray absorption method and holographic interferometry *Open Appl. Phys. J.* **5** 54–9
- [278] Bernengo J-C and De Rigal J Physical methods to measure stratum corneum water content in vivo
- [279] Imtiaz U, Bartolomeo L, Lin Z, Sessa S, Ishii H, Saito K, Zecca M and Takanishi A 2013 Design of a wireless miniature low cost EMG sensor using gold plated dry electrodes for biomechanics research *2013 IEEE International Conference on Mechatronics and Automation* pp 957–62
- [280] Alekseeva L V. 2007 Theoretical aspects of predicting the electrostatic properties of textile materials *Fibre Chem.* **39** 225–6
- [281] Bora M N, Baruah G C and Talukdar C L 1993 Studies on the dielectric properties of some natural (plant) and synthetic fibres in audio frequency range and their DC conductivity at elevated temperature *Thermochim. Acta* **218** 435–43
- [282] Wharram S E, Zhang X, Kaplan D L and McCarthy S P 2010 Electrospun Silk Material Systems for Wound Healing *Macromol. Biosci.* **10** 246–57
- [283] Cui H W, Suganuma K and Uchida H 2015 Highly stretchable, electrically conductive textiles fabricated from silver nanowires and cupro fabrics using a simple dipping-drying method *Nano Res.* **8** 1604–14
- [284] Birgersson U, Birgersson E and Ollmar S 2012 Estimating electrical properties

and the thickness of skin with electrical impedance spectroscopy: Mathematical analysis and measurements *J. Electr. Bioimpedance* **3** 51–60

- [285] Smith D C, Tan S and Follett D H 1992 Effects of skin temperature on skin-electrode impedance: measurements at high direct current density *J. Med. Eng. Technol.* **16** 210–3

Appendices

Appendix I

Two-ply twisted yarn

The functional thread, Shieldex Conductive Twisted Yarn (Shieldex U.S., Palmyra, NY, United States), is two-ply twisted. Two-ply twisted yarn is plied by taking two separate yarns that each have a twist to them and twisting them together, refer to Figure 1.

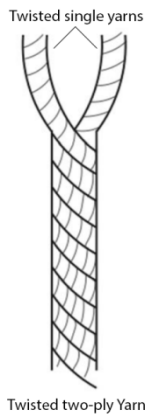


Figure 1. Two-ply twisted yarn [1] “© Gleba et al. 2018. CC BY 4.0.”

Embroidery machines work with two threads, a needle thread and a bobbin thread. The mechanisms of the embroidery machines work to form an interlock of the two threads Figure 2a [2]. To setup the machine, the needle thread runs through the top section of the embroidery machine passing through tension discs and is fed through the needle. The bobbin thread is wound onto a bobbin and inserted into a case that is placed in the lower section of the machine. To make a stitch, the needle is lowered through the cloth into the bobbin area. A rotating hook in the bobbin area catches the needle thread wrapping it around the bobbin thread interlocking the two threads in the middle of the thickness of the textile.

Ideally, for the interlocking to be formed in the middle of the textile, the thread tensions must be balanced. The needle thread tension is adjusted electronically on the upper section of the embroidery machine whilst the bobbin tension thread is manually adjusted on the bobbin case. In addition, the thread tension balance also relates to the equivalence of the needle and bobbin thread mass. This mass is referred to as the linear mass density measured in a textile unit of tex.

Thread Mass

This refers to the linear mass density of thread. It is measured in a textile unit of tex presented below,

$$1 \text{ tex} = 1 \text{ g.km}^{-1}, \text{ and}$$

$$1 \text{ dtex} = 1 \text{ g.10km}^{-1},$$

where g is grams and km is kilometre.

The two principal embroidery stitch types are the weave and satin fill. Satin stitches traverse back and forth over a narrow area, alternating between an angled stitch and a straight stitch. To cover larger areas, embroidery machines have the option of auto split breaking the long satin stitches into shorter ones by distributing needle penetrations randomly. Weave stitches are preferred for large areas in a design. Comprising of straight-line stitches, the stitch penetrations alternate line to line effectively resembling a woven material. Satin and weave stitches can be altered through changing the spacing between the stitch penetrations (i.e., density). The density can be set in terms of percentage coverage of the embroidery area (%) or the distance between adjacent interlocks measured in mm, Figure 2b. In terms of percentage coverage, a low percentage implies a low density and a large percentage implies a high density. However, when the density is measured in distance (mm), a low distance implies a high density while a high distance implies a low density.

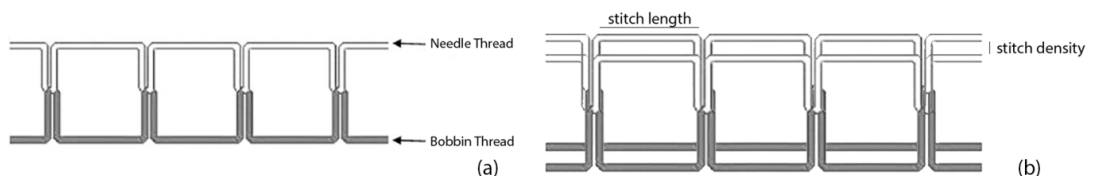


Figure 2. Embroidery stitching: (a) interlocking of needle and bobbin thread [2] “© Wickramasinghe et al.; licensee springer. 2014. CC BY 4.0”, and (b) stitch length and stitch density. “© IOP Publishing. Reproduced with permission. All rights reserved.”

References

- [1] M. Gleba and S. Harris, “The first plant bast fibre technology: identifying splicing in archaeological textiles,” *Archaeol. Anthropol. Sci.*, vol. 11, no. 5, pp. 2329–2346, May 2019, doi: 10.1007/s12520-018-0677-8.
- [2] R. P. Abeysooriya and G. L. D. Wickramasinghe, “Regression model to predict thread consumption incorporating thread-tension constraint: study on lock-stitch 301 and chain-stitch 401,” *Fash. Text.*, vol. 1, no. 1, pp. 1–8, Dec. 2014, doi: 10.1186/s40691-014-0014-5.

Appendix II

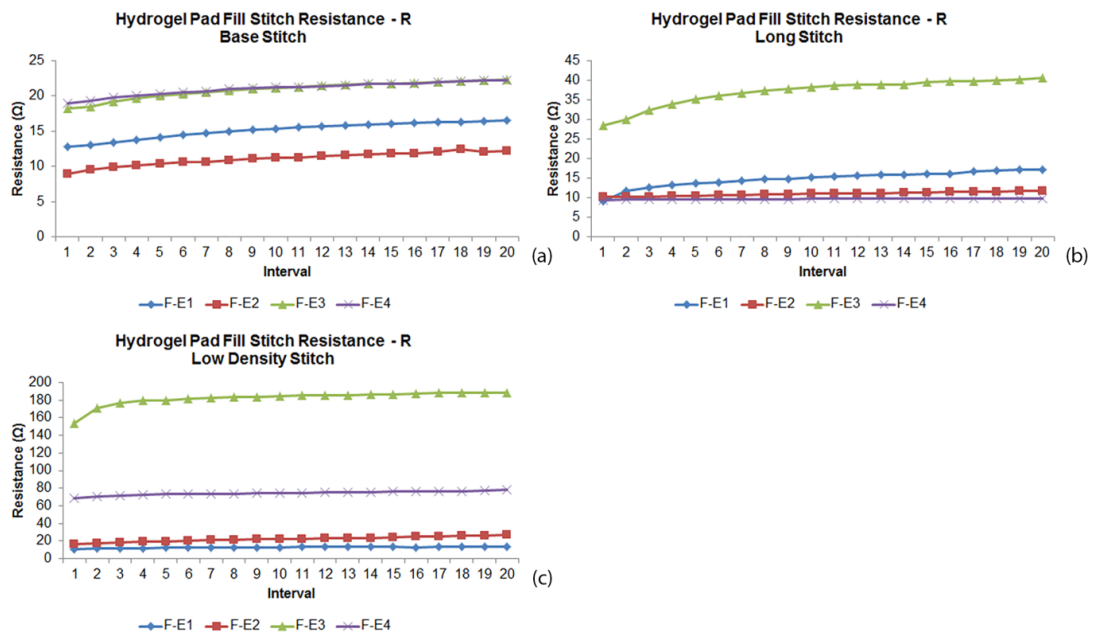


Figure 1. Change in resistance for weave sample electrodes using wet wafer testing method over 20 second intervals. “© IOP Publishing. Reproduced with permission. All rights reserved.”

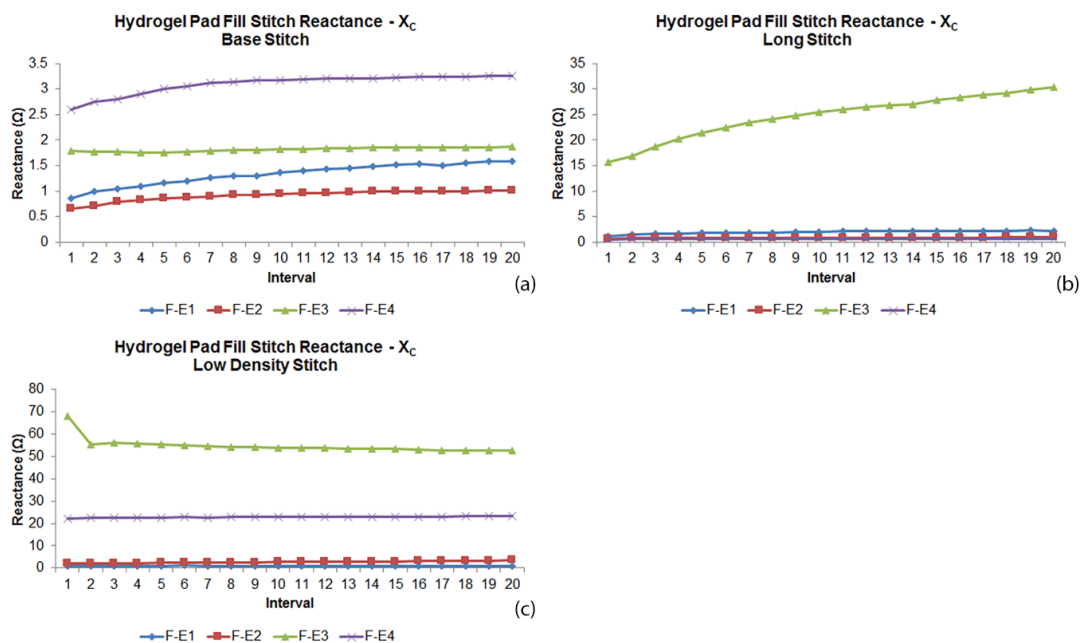


Figure 2. Change in reactance for weave sample electrodes using wet wafer testing method over 20 second intervals. “© IOP Publishing. Reproduced with permission. All rights reserved.”

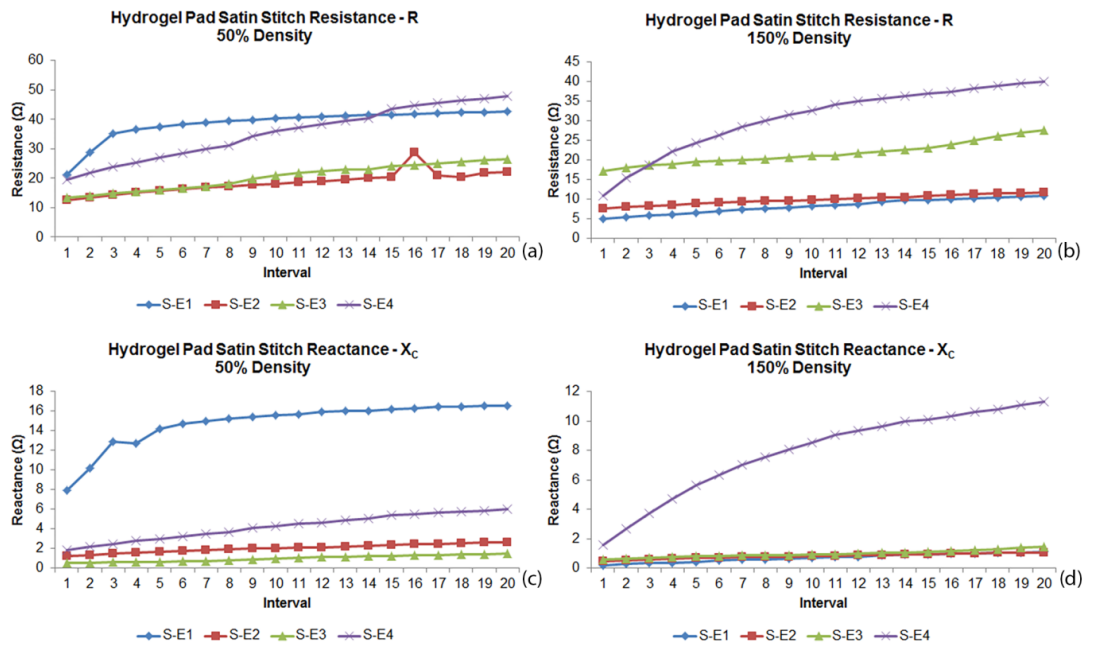


Figure 3. Change in resistance and reactance for satin sample electrodes using wet wafer testing method over 20 second intervals.

Appendix III

Air Permeability

It is important that the textile substrates for embroidered electrodes are efficient and comfortable for long term patient monitoring. Physiological comfort adheres to textiles produced for functional and technical purposes such as embroidered electrodes. One parameter affecting the physiological comfort is the air permeability defined as the ratio of air delivered perpendicularly to a surface of a textile relative to the amount of air passing the surface area. The breathability of the embroidered electrode is determined by testing its air permeability. Factor influencing the permeability characteristics of embroidered electrode are: (i) properties of the raw material of the textile substrate, (ii) structural properties of the textile substrate and (iii) embroidery stitch. It should be noted that not all fabrics are expected to have the same air permeability. This important property of a fabric is one of the critical factors affecting its selection for a particular application. For an extensive read, a number of research articles on permeability properties of textiles and associated influencing factors are accessible in the literature by Zupin et al., Tastan et al., Vimal and Zhu et al. [1]–[4].

Relative Permittivity

Textiles can be electrically characterised by their dielectric constant. The relative permittivity denoted by ϵ_r is frequency dependent and defined as

$$\epsilon_r(\omega) = \frac{\epsilon(\omega)}{\epsilon_0}, \text{ where}$$

$\epsilon(\omega)$ is the complex permittivity of the material and ϵ_0 is the vacuum permittivity.

Textile Structures

The four textile structures of the substrates are (i) plain weave, (ii) poplin, (iii) velvet and (iv) non-woven felt. These are common textiles in the textile engineering field and were commercially purchased for this study. The structure is one of many variables associated with textiles. This research was based on the structure as it is the main feature characterising textiles in their final form visible to the human eye. Figure A1 presents the four textiles adapted as substrates for this study.

Non-woven fabrics are made from bonding fibres through a chemical, mechanical, heat or solvent treatment and are quite pores.

Woven fabrics are often created on a loom interlacing two or more threads at right angles to one another, such as poplin and plain weave. The difference between these two substrates is that the former is much lighter in weight and possess a smooth texture while the latter is somewhat coarser and is slightly thicker.

Velvet fabric is a type of woven tufted fabric with a soft, short dense pile.

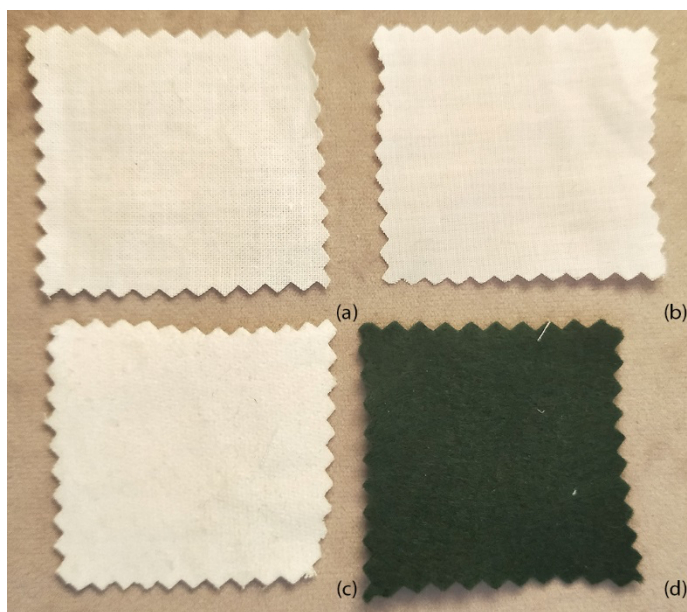


Figure 1. Textiles used as substrates for e-textile electrodes: (a) cotton plain weave, (b) cotton poplin, (c) cotton velvet and (d) polyester non-woven felt. “© IOP Publishing. Reproduced with permission. All rights reserved.”

References

- [1] E. Tastan, M. Akgun, A. Gurarda, and S. Omeroglu, “Investigation of the effect of different structural parameters of cotton woven fabrics on their air permeability,” *IOP Conf. Ser. Mater. Sci. Eng.*, vol. 254, p. 182014, 2017, doi: 10.1088/1757-899x/254/18/182014.
- [2] J. Thanikai Vimal, “Regression model for predicting the air resistance of fabric made from doubled yarns and with different weave structures,” *J. Text. Inst.*, vol. 107, no. 10, pp. 1268–1275, Oct. 2016, doi: 10.1080/00405000.2015.1100819.
- [3] S. Yao and Y. Zhu, “Nanomaterial-enabled dry electrodes for electrophysiological sensing: A review,” *JOM*, vol. 68, no. 4. Minerals, Metals and Materials Society, pp. 1145–1155, 01-Apr-2016, doi: 10.1007/s11837-016-1818-0.
- [4] Ž. Zupin, A. Hladnik, and K. Dimitrovski, “Prediction of one-layer woven fabrics air permeability using porosity parameters,” *Text. Res. J.*, vol. 82, no. 2, pp. 117–128, Jan. 2012, doi: 10.1177/0040517511424529.

Appendix IV

Table 1. Z_p modulus ($k\Omega$) values relating to skin temperature and skin wetness 40 – 90% RH. “© IOP Publishing. Reproduced with permission. All rights reserved.”

| T^* | 40% | 50% | 60% | 70% | 80% | 90% | 40% | 50% | 60% | 70% | 80% | 90% |
|-------|------------|------------|-----|-----|-----|------------|------------|-----|-----|-----|-----|------------|
| | E1 | | | | | | E2 | | | | | |
| 30 | <u>302</u> | 296 | 288 | 277 | 264 | 246 | <u>334</u> | 333 | 330 | 327 | 320 | 285 |
| 31 | <u>288</u> | 283 | 276 | 265 | 255 | 240 | <u>335</u> | 333 | 332 | 329 | 324 | 293 |
| 32 | <u>297</u> | 289 | 280 | 269 | 244 | 229 | <u>339</u> | 337 | 334 | 330 | 323 | 287 |
| 33 | <u>301</u> | 294 | 285 | 275 | 265 | 243 | <u>334</u> | 332 | 327 | 322 | 313 | 291 |
| 34 | <u>282</u> | 275 | 266 | 256 | 241 | 224 | <u>332</u> | 330 | 327 | 322 | 312 | 289 |
| | E3 | | | | | | E4 | | | | | |
| 30 | 282 | <u>283</u> | 280 | 278 | 274 | 265 | <u>277</u> | 276 | 275 | 272 | 268 | 252 |
| 31 | <u>284</u> | 282 | 279 | 278 | 276 | 259 | <u>280</u> | 279 | 276 | 271 | 267 | 261 |
| 32 | <u>286</u> | 284 | 282 | 279 | 275 | 249 | <u>280</u> | 278 | 276 | 272 | 267 | 261 |
| 33 | <u>284</u> | 282 | 279 | 278 | 274 | 253 | <u>280</u> | 277 | 275 | 273 | 269 | 260 |
| 34 | <u>289</u> | 286 | 283 | 278 | 269 | 243 | <u>273</u> | 271 | 267 | 263 | 256 | 245 |

* T Temperature ($^{\circ}\text{C}$)

Table 1 presents the absolute Z_p measurements of the e-textile electrodes relative to the temperature and RH settings of the climatic chamber; the lowest and highest values are underlined and in bold, respectively.

Table 2. Trend equations and correlation coefficient of ΔZ_p relative to temperature against the 10% RH increments. “© IOP Publishing. Reproduced with permission. All rights reserved.”

| | E1 | E2 | E3 | E4 |
|--------|-------------------------------|------------------------------|-------------------------------|------------------------------|
| 40-50% | $y = -0.03x^2 + 1.99x - 32$ | $y = -0.04x^2 + 2.80x - 45$ | $y = -0.11x^2 + 7.59x - 125$ | $y = -0.05x^2 + 3.33x - 55$ |
| R^2 | 0.42 | 0.86 | 0.83 | 0.61 |
| 50-60% | $y = 0.01x^2 + 0.73x - 12$ | $y = 0.12x - 3$ | $y = 0.04x^2 + 2.76x + 45$ | $y = 0.04x^2 + 2.56x - 39$ |
| R^2 | 0.76 | 0.2 | 0.25 | 0.48 |
| 60-70% | $y = -0.01x^2 + 0.41x - 2$ | $y = 0.18x - 5$ | $y = 0.14x^2 - 8.9x + 140$ | $y = -0.01x^2 + 0.43x - 5$ |
| R^2 | 0.18 | 0.9 | 0.55 | 0.01 |
| 70-80% | $y = -0.34x^2 + 22.16x - 352$ | $y = 0.14x^2 - 8.36x - 130$ | $y = 0.21x^2 - 12.69x + 195$ | $y = 0.13x^2 - 7.99x - 126$ |
| R^2 | 0.10 | 0.84 | 0.92 | 0.75 |
| 80-90% | $y = 0.12x^2 - 7.52x + 123$ | $y = -0.16x^2 + 9.10x - 121$ | $y = -0.45x^2 + 30.17x - 496$ | $y = 0.76x^2 - 48.68x + 785$ |
| R^2 | 0.24 | 0.65 | 0.84 | 0.83 |

Appendix V

Dipolar Measurements Day 1 & 2

Table 1. Pork belly properties.

| Pork Belly Sample | Configuration | Weight (kg) | Size (cm) (l × w × h) | Electrodes |
|-------------------|---------------|-------------|--------------------------|------------|
| ST2 | Dipolar | 1.5 | 21 × 18 × 4 | Ag/AgCl |

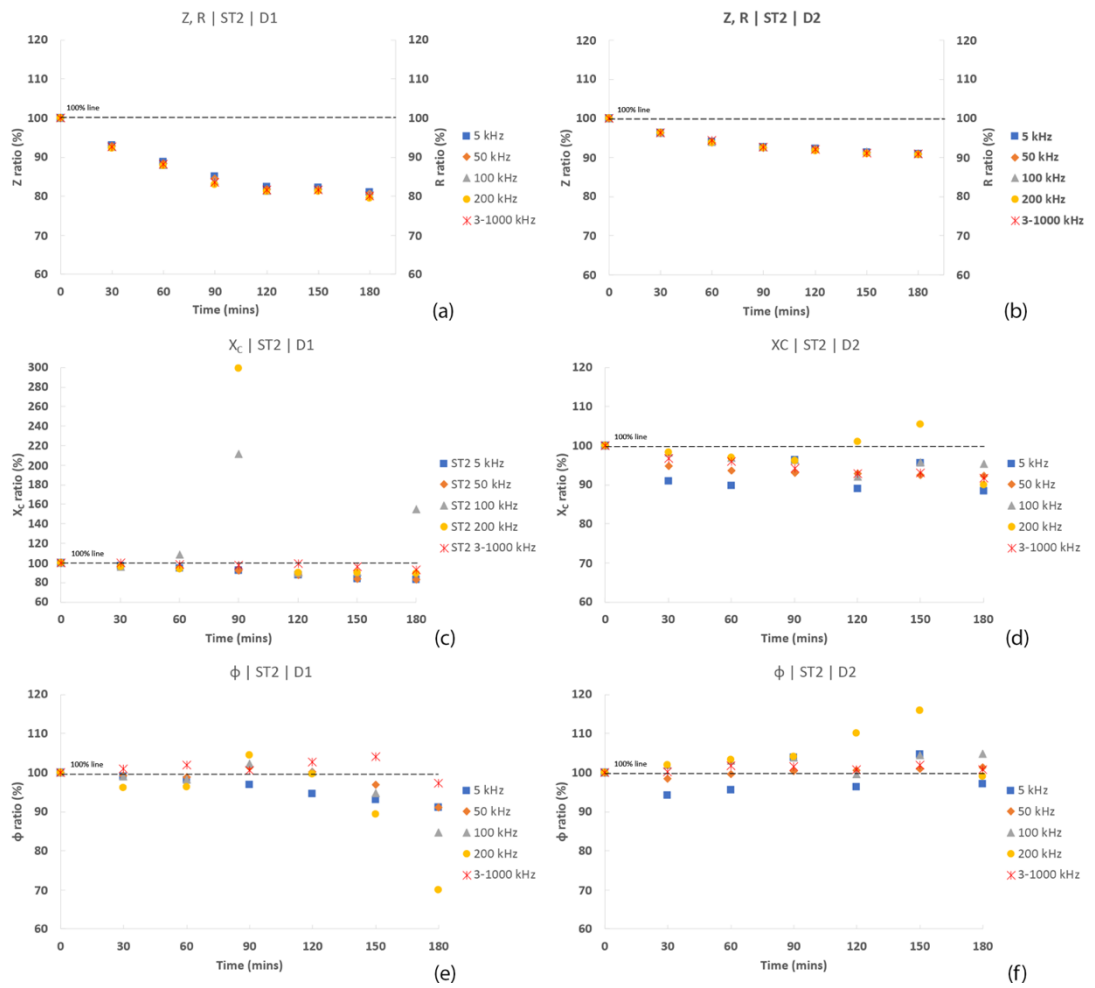


Figure 1. Measurements for intact BUS using Ag/AgCl in tetrapolar configuration: (a) Z and R day 1, (b) Z and R day 2 (c) X_c day 1, (d) X_c day, (e) ϕ day 1, (f) ϕ day 2.

Appendix VI

Table 1. Regression equations (y) and R^2 for Z and R.

| Z, R | | | | | | | |
|-------------------|-------|---------------------|---------------------|---------------------|--------------------|---------------------|---------------------|
| | | Ag/AgCl | | | E-textiles | | |
| 3-1000 kHz | | | | | | | |
| | | S1 | S2 | S3 | S4 | S5 | S6 |
| D1 | y | $98.63e^{-0.001x}$ | $99.02e^{-0.001x}$ | $99.81e^{-0.001x}$ | $99.81e^{-0.001x}$ | $99.03e^{-0.001x}$ | $99.03e^{-0.001x}$ |
| | R^2 | 0.87 | 0.94 | 0.98 | 0.98 | 0.92 | 0.90 |
| D2 | y | $98.204e^{-0.003x}$ | $98.204e^{-0.003x}$ | $98.204e^{-0.003x}$ | $98.81e^{-0.003x}$ | $99.65e^{-0.003x}$ | $97.86e^{-0.003x}$ |
| | R^2 | 0.96 | 0.97 | 0.97 | 0.97 | 0.99 | 0.92 |
| 5 kHz | | | | | | | |
| D1 | y | $98.62e^{-0.001x}$ | $99.03e^{-0.001x}$ | $99.36e^{-0.001x}$ | $99.83e^{-0.001x}$ | $99.00e^{-0.001x}$ | $99.07e^{-1E-03x}$ |
| | R^2 | 0.86 | 0.93 | 0.96 | 0.98 | 0.91 | 0.90 |
| D2 | y | $98.41e^{-0.003x}$ | $98.98e^{-0.002x}$ | $98.63e^{-0.003x}$ | $98.84e^{-0.003x}$ | $99.69e^{-0.002x}$ | $98.23e^{-0.003x}$ |
| | R^2 | 0.97 | 0.97 | 0.98 | 0.97 | 0.99 | 0.95 |
| 50 kHz | | | | | | | |
| D1 | y | $98.62e^{-0.001x}$ | $99.025e^{-0.001x}$ | $99.359e^{-0.001x}$ | $99.77e^{-0.001x}$ | $98.959e^{-0.001x}$ | $98.741e^{-9E-04x}$ |
| | R^2 | 0.86 | 0.93 | 0.96 | 0.98 | 0.90 | 0.82 |
| D2 | y | $98.20e^{-0.003x}$ | $98.94e^{-0.003x}$ | $98.58e^{-0.003x}$ | $98.87e^{-0.003x}$ | $99.68e^{-0.003x}$ | $97.71e^{-0.003x}$ |
| | R^2 | 0.96 | 0.97 | 0.98 | 0.98 | 0.98 | 0.92 |

Table 2. Regression equations (y) and R^2 for X_c .

| X_c | | | | | | | |
|------------|-------|---------------------|--------------------|---------------------|---------------------|---------------------|--------------------|
| | | Ag/AgCl | | | E-textiles | | |
| 3-1000 kHz | | | | | | | |
| | | S1 | S2 | S3 | S4 | S5 | S6 |
| D1 | y | $98.56e^{-0.001x}$ | $99.29e^{-0.001x}$ | $99.33e^{-0.001x}$ | $101.99e^{-6E-04x}$ | $96.24e^{-0.004x}$ | $94.47e^{-0.002x}$ |
| | R^2 | 0.85 | 0.96 | 0.96 | 0.33 | 0.89 | 0.26 |
| D2 | y | $100.12e^{-0.004x}$ | $102.91e^{-0.04x}$ | $100.12e^{-0.004x}$ | $102.85e^{-0.008x}$ | $102.34e^{-0.061x}$ | $98.03e^{-0.037x}$ |
| | R^2 | 0.33 | 0.98 | 0.33 | 0.33 | 0.89 | 0.26 |
| 5 kHz | | | | | | | |
| D1 | y | $98.94e^{-5E-04x}$ | $98.36e^{-3E-04x}$ | $99.37e^{-9E-04x}$ | $97.76e^{0.001x}$ | $102.25e^{-0.007x}$ | $98.80e^{-8E-04x}$ |
| | R^2 | 0.21 | 0.14 | 0.84 | 0.53 | 0.71 | 0.01 |
| D2 | y | $101.94e^{-0.018x}$ | $105.5e^{-0.068x}$ | $103.36e^{-0.032x}$ | $96.34e^{0.0146x}$ | $114.19e^{-0.111x}$ | $99.98e^{-0.012x}$ |
| | R^2 | 0.96 | 0.98 | 0.97 | 0.53 | 0.70 | 0.01 |
| 50 kHz | | | | | | | |
| D1 | y | $98.56e^{-0.001x}$ | $99.52e^{-0.001x}$ | $99.20e^{-0.001x}$ | $103.95e^{-6E-04x}$ | $99.52e^{-0.001x}$ | $96.98e^{-2E-04x}$ |
| | R^2 | 0.72 | 0.97 | 0.93 | 0.12 | 0.97 | 0.003 |
| D2 | y | $98.72e^{0.0019x}$ | $99.87e^{0.0022x}$ | $103.36e^{-0.032x}$ | $104.96e^{-0.01x}$ | $101.31e^{-0.018x}$ | $97.22e^{-0.003x}$ |
| | R^2 | 0.03 | 0.14 | 0.97 | 0.12 | 0.97 | 0.003 |

Table 3. Regression equations (y) and R^2 for φ .

| φ | | | | | | | |
|-------------------|-------|---------------------|---------------------|---------------------|---------------------|---------------------|---------------------|
| Ag/AgCl | | | | E-textiles | | | |
| 3-1000 kHz | | | | | | | |
| | | S1 | S2 | S3 | S4 | S5 | S6 |
| D1 | y | $99.93e^{4E-05x}$ | $100.27e^{-1E-05x}$ | $99.18e^{0.0005x}$ | $102.87e^{0.0006x}$ | $95.646e^{-0.001x}$ | $95.12e^{0.0004x}$ |
| | R^2 | 0.10 | 0.05 | 0.48 | 0.22 | 0.47 | 0.04 |
| D2 | y | $99.80e^{0.0048x}$ | $99.89e^{-0.001x}$ | $99.80e^{0.0048x}$ | $103.96e^{0.0182x}$ | $99.104e^{0.0025x}$ | $98.948e^{0.0076x}$ |
| | R^2 | 0.59 | 0.18 | 0.55 | 0.29 | 0.23 | 0.78 |
| 5 kHz | | | | | | | |
| D1 | y | $100.32e^{0.0006x}$ | $100.28e^{0.0012x}$ | $99.725e^{0.0005x}$ | $98.63e^{0.0021x}$ | $102.17e^{-0.005x}$ | $100.3e^{0.0008x}$ |
| | R^2 | 0.30 | 0.80 | 0.62 | 0.90 | 0.53 | 0.02 |
| D2 | y | $101.7e^{-0.013x}$ | $102.62e^{-0.036x}$ | $101.7e^{-0.013x}$ | $95.528e^{0.0286x}$ | $99.372e^{0.0507x}$ | $96.765e^{0.0482x}$ |
| | R^2 | 0.95 | 0.96 | 0.94 | 0.86 | 0.82 | 0.96 |
| 50 kHz | | | | | | | |
| D1 | y | $99.886e^{-2E-04x}$ | $100.52e^{-2E-05x}$ | $99.424e^{0.0003x}$ | $103.46e^{0.0025x}$ | $100.52e^{-2E-05x}$ | $98.654e^{0.0011x}$ |
| | R^2 | 0.80 | 0.01 | 0.36 | 0.80 | 0.01 | 0.44 |
| D2 | y | $99.132e^{0.0026x}$ | $102.24e^{-0.025x}$ | $99.132e^{0.0026x}$ | $100.1e^{0.0355x}$ | $99.745e^{0.0032x}$ | $99.632e^{0.0042x}$ |
| | R^2 | 0.17 | 0.96 | 0.17 | 0.79 | 0.90 | 0.68 |

Table 4. Regression equations (y) and R^2 for R_0 .

| R_0 | | | | | | | |
|------------|-------|---------------------|--------------------|---------------------|---------------------|---------------------|---------------------|
| Ag/AgCl | | | | E-textiles | | | |
| 3-1000 kHz | | | | | | | |
| | | S1 | S2 | S3 | S4 | S5 | S6 |
| D1 | y | $100.29e^{-0.017x}$ | $100.9e^{-0.019x}$ | $101.72e^{-0.021x}$ | $102.36e^{-0.023x}$ | $105.38e^{-0.021x}$ | $93.81e^{0.0213x}$ |
| | R^2 | 0.85 | 0.94 | 0.98 | 0.54 | 0.62 | 0.47 |
| D2 | y | $100.74e^{-0.035x}$ | $102.39e^{-0.03x}$ | $101.59e^{-0.022x}$ | $101.41e^{-0.015x}$ | $99.428e^{-0.007x}$ | $100.09e^{-0.015x}$ |
| | R^2 | 0.86 | 0.99 | 0.98 | 0.81 | 0.42 | 0.75 |

Table 5. Regression equations (y) and R^2 for R_{inf} .

| R_{inf} | | | | | | | |
|------------|-------|---------------------|---------------------|---------------------|---------------------|---------------------|---------------------|
| Ag/AgCl | | | | E-textiles | | | |
| 3-1000 kHz | | | | | | | |
| | | S1 | S2 | S3 | S4 | S5 | S6 |
| D1 | y | $100.9e^{-0.022x}$ | $101.12e^{-0.022x}$ | $100.27e^{-0.01x}$ | $103.87e^{-0.046x}$ | $103.93e^{-0.029x}$ | $102.5e^{-0.032x}$ |
| | R^2 | 0.91 | 0.90 | 0.88 | 0.92 | 0.94 | 0.98 |
| D2 | y | $102.66e^{-0.029x}$ | $102.66e^{-0.029x}$ | $101.94e^{-0.025x}$ | $102.31e^{-0.033x}$ | $102.79e^{-0.037x}$ | $102.81e^{-0.039x}$ |
| | R^2 | 0.91 | 0.99 | 0.89 | 0.96 | 0.94 | 0.98 |